Abstract of "Human Thermal-Work Strain Performance Optimization from Wearable Physiological Sensors" by Mark J. Buller, Ph.D., Brown University, May 2015.

Hot environments pose a risk of heat illness for many emergency workers, athletes, and other professions especially when heavy workloads or protective clothing are necessary. Modern wearable physiological monitors may be able to mitigate risk of heat illness and improve performance if they are able to track health state and provide feedback to the user. However, effective algorithms and models to make use of wearable sensor information are lacking. We present two contributions: 1) a method for health state estimation of the latent human body core temperature from physiological sensors, and 2) models for policy estimation to provide automated advice to reduce thermal-work strain and improve physiological performance over a course of prescribed work.

Continuous measurement of core body temperature, a requisite of thermal-work strain health state, has been an open physiology problem in the field. We show that the physiological dependencies of the human thermo-regulatory system can be cast into a dynamic Bayesian network model that allows us to estimate core body temperature from wearable physiological sensors. We effectively simplify this model to use only an input of heart rate which is collected by many commercial wearable sensor systems. This approach is validated across different combinations of temperature, hydration, clothing, and acclimation states, and shows similar comparison accuracy to accepted laboratory measures. We finally demonstrate the use and effectiveness of the algorithm from experimental trials during a first responder live training event.

We also present a Markov decision process that uses health state estimates to optimize individual pacing strategies to reduce the overall level of thermal-work strain. We describe the estimation of real world activity objectives and thermal-work strain constraints as a reinforcement learning problem. Using a dynamical simulation of physiology, pacing estimates from this model are shown to reduce overall thermal-work strain.

Our health state and policy estimation contributions were evaluated in the context of an implementation to compare human self-guided pace and policy guided pace. The results show that the policy allowed individuals to complete the task with meaningfully lower thermal-work strain. We demonstrate that real-time feedback from our model was able to match the thermo-regulatory efficiency of a well-trained athlete.

We envision the work in this dissertation will enable practical real-time monitoring systems that can improve human health through preventing thermal injury and use reinforcement learning to improve the physical performance of novice athletes and regular individuals.

Human Thermal-Work Strain Performance Optimization from Wearable Physiological Sensors

by

Mark J. Buller

A dissertation submitted in partial fulfillment of the requirements for the Degree of Doctor of Philosophy in the Department of Computer Science at Brown University

Providence, Rhode Island

May 2015

This dissertation by Mark J. Buller is accepted in its present form
by the Department of Computer Science as satisfying the
dissertation requirement for the degree of Doctor of Philosophy.

Date_________________ ___________________________________

Odest Chadwicke Jenkins, Director

Recommended to the Graduate Council

Date_________________ ___________________________________

Michael Littman, Reader
(Brown University)

Date_________________ ___________________________________

David Williams, Reader
(Brown University)

Date_________________ ___________________________________

Reed Hoyt, Reader
(US Army Research Institute of
Environmental Medicine)

Date_________________ ___________________________________

Peter Weyand, Reader
(Southern Methodist University)

Approved by the Graduate Council

Date_________________ ___________________________________

Peter Weber
Dean of the Graduate School

Acknowledgments

And I gave my heart to seek and search out by wisdom concerning all things that are done under heaven: this sore travail hath God given to the sons of man to be exercised therewith.
Ecclesiastes 1:13

This work could not have been achieved without the help, support, and encouragement of many people. My heartfelt thanks is owed to many people who made this journey possible. To Stan Zdonik, who started my whole graduate career, as he was the first to encourage me to even begin the journey. To Beau Freund, who at work wholeheartedly supported my desire to return to school and complete a master's degree. To Chad Jenkins, my advisor, who with his vision, was willing to take on a student with an interdisciplinary research topic and guide me in the right direction. To my machine learning study group, Jonas Schwertfeger and Anna Ritz, whose help got me through my first trial-by-fire exposure to graduate studies with the maxim "*Don't fear the Math.*" To Reed Hoyt, whom I have had the pleasure of working with for over 20 years, for his encouragement to go and get a doctorate and his willingness to suffer my absence from work during the whole process. And finally, to Lauren Clarke, who not only serves as the go-to person for all things process within the department but also serves as an unofficial counselor to many students in times of crisis.

For collaborating on the final human subjects experiment thanks goes to the research team at the Beltsville Human Nutrition Research Center (BHNRC). To William Rumpler who was willing to use his laboratory and team to help collect the data. To Andrei Gribok for all of his machine learning discussions and insights into data analysis. To Jayme Leger a final year Ph.D. student-compatriot, who helped keep the study running. And, to Michelle Stevens, who being thrown in at the deep-end, was not only able to swim, but pulled off a very well executed human research study.

A special thank you goes to Alex Welles, for his help in running the human research study; for reading, proofing, and providing criticism of this manuscript; and for rendering many of the graphics into a form that I could not hope to attain. As well, thanks go to Theresa Finch for all her encouragement and editing help.

Finally, this all would not have been possible without the love and support of my family: Joshua, Anna, Esther, Bethany, and my two graduate studies babies, Abigail and Benjamin, I love you all so very much. And most especially to my wife Mary, my very best of friends, who initially thought this was all a grand idea, as I only had "just one more class… ."

To Mary

Contents

List of Tables

List of Figures

Chapter 1

Introduction

1.1 Better Health State Estimation, Better Advice, Better Outcomes

Today, wearable physiological monitors are becoming common place. The daily use of these devices, along with smart phones, offers the possibility of determining and tracking health state. Automated human health-state monitoring aims to identify when an individual moves from a healthy to a compromised state. For example, changes in diet or physical activity can lead to life-threatening hypo or hyperglycemia in diabetics. Similarly, elderly individuals managing multiple chronic conditions may experience rapid changes in physical and cognitive health state that must be caught quickly for treatments to be most effective. Even in healthy individuals, heavy exertion in extreme climates can quickly lead to life-threatening situations.

The emergence of inexpensive and unobtrusive health sensors promises to shift the healthcare industry's focus from episodic care in acute settings to early detection and longitudinal care for chronic conditions in natural living environments. The same technologies can also be used to monitor healthy individuals in high-stress work situations. While these current sensing systems are able to provide a wealth of physiological information, these measurements are often quite different from those used by physicians. The medical community is accustomed to making decisions from high-quality clinical data from a limited set of sessions. Data from continuously-measuring sensors requires us to draw conclusions from large quantities of lower-quality data from sub-acute environments where these measures are often not specific to health states of interest and can reflect the output of multiple latent variables.

As the availability of body-worn data increases, we have an unprecedented opportunity to discover new and early predictors of clinically significant health states. Identifying these relevant health states will enable this information to be used to provide better and timelier interventions, leading to overall better health outcomes.

For this dissertation, we examine the problem in a more extreme setting, but we believe our approaches can be applied to the larger wearable-health state problem.

1.2 The Problem of Exertional Heat Illness

Heat illness is a risk to people in occupations where there are heavy workloads, hot environments, or where there is the use of protective clothing or equipment. Athletes must often compete with very high work rates in extremes of temperature. Miners and steelworkers can have very hot work environments. Firefighters, tactical law enforcement, first responders, and military must often wear personal protective equipment (PPE) to protect them from the threat of fire, chemical, biological, nuclear, or explosive agents or devices (e.g. see Figure 1.1).

Figure 1.1: National Guard Civil Support Team member during two training events wearing different levels of personal protective equipment.

While these PPE ensembles offer the individual protection, they limit one's ability to thermoregulate (Muza, Banderet and Cadarette 2001, Givoni and Goldman, 1972). With reduced vapor permeability, these PPE ensembles limit evaporative heat transfer from the body to the environment. In addition, the added insulative properties of these ensembles further decreases the rate heat can transfer to the environment by conductive and convective routes. Thus, even in temperate conditions, the rate of metabolic heat produced from physical work can often exceed the rate at which heat can be transferred to the environment. In these situations, first responders' core body temperatures will continue to rise while working. If this heat strain is not effectively managed, it can lead to heat exhaustion, collapse, or even death from heat stroke (Bouchama and Knochel 2002). These, heat strain risks can be accentuated in a team setting by the psychological pressure to continue working even if an individual is aware of feeling ill (Porter 2000).

The military often form an extreme example where they combine high work rates, wear protective clothing and equipment, and often have to work in extremes of climate. Steinman

(1987), in his historical review of the effects of heat on military operations, cites cases where heat illness played a significant degrading effect, including examples from the Roman army (Jarcho 1967), the European Crusaders in the middle-ages (Lindsay 1936), Napoleon (Dible 1970), the British Army in India in the 19th Century (Parkes 1864), and the First World War (Wilcox 1920). From 2008 to 2012, there were over 13,000 incidents of heat illness events in the U.S. Military (MSMR 2013), including 1,867 cases of heat stroke.

The National Fire Protection Agency has tracked firefighter fatalities in the U.S. for many years and finds that over the ten year period 2001-2010, heat stroke accounts for 5% of firefighter fatalities during training (Fahy 2012). Further, Karter and Molis (2014) identify that thermal stress accounts for 3% of 2013 firefighter injuries (over 2000 incidents). But this does not capture the full effect of thermal-work strain. The leading cause of firefighter deaths in the U.S. is myocardial infarction (~38%) (Fahy et al., 2006, 2013). In their analysis, Fahy et al. (2012) cite that the additional strain imposed by the high work demands of firefighting is likely a contributing factor to cardiac arrest. In these circumstances, the cardiovascular system is stressed from the competing needs of thermoregulation and metabolic requirements (Smith et al., 2001).

For other occupations, the U.S. Occupational Safety and Health Administration (OSHA) specifically records heat fatalities for their covered industries. Their map shows fatalities in most regions of the U.S.[1], and they document over 100 fatalities from 2008 to 2014[2].

Additionally, heat illness may be a contributing factor in other workplace accidents. While heat exhaustion can lead to dizziness and fainting (Bouchama and Knochel, 2002), there is some evidence that hyperthermia can degrade working memory (Stubblefield et al., 2006) and also decrease our ability to detect changes in the surrounding environment (Sun et al., 2011). These additional effects could easily be contributing factors for other physical workplace injuries.

Efforts to identify and control the incidence of heat illness or injury originally focused on identifying high-risk environments and providing guidance for acceptable work/rest schedules (Yaglow and Minard, 1956, 1957; OSHA 1985; NIOSH 1986). Risk of heat illness can be reduced by acclimation, appropriate work/rest schedules, and proper hydration (Minard, 1961). However, assessing risk of heat stress from environmental conditions alone fails to account for individual differences, such as acclimation status, fitness, body composition and morphology, and prior heat injury, which can play important roles in an individual's response to working in hot environments (Kark et al., 1996; Carter et al., 2005). A study of US military heat stroke training deaths during "World War II" found that most "fatalities associated with heavy exercise occur at

---

[1] OSHA Heat Fatalities Map https://www.osha.gov/SLTC/heatillness/map.html (accessed 2/1/2015)

[2] OSHA Heat Fatalities https://www.osha.gov/SLTC/heatillness/map_text (accessed 2/1/2015)

relatively low temperatures, when the total heat stress is commonly underestimated." (Schickele 1947). Similarly, recent work by Owen, Leon, and McKinnon (2013) found that ~35% of heat stroke cases in the U.S. military from 2000-2007 occurred in low risk individuals who were "practicing sound heat mitigation strategies." Abriat et al. (2014) have similar findings, where out of 182 cases of heat stroke, 19% occurred where the environmental temperature was less than 15°C. The major contributing factor over all the cases was individual motivation to complete the task. This is a common theme in team settings, where an individual may be feeling unwell but does not want to let down his/her other team members. Lui et al. (2014) detail two examples where very experienced wildland firefighters succumbed to heat stroke even though they maintained proper hydration.

It is not only the acute problem of heat illness that needs to be solved. Over the long run, thermal-work strain has a degrading effect upon performance (Cheuvront et al., 2010). Successive bouts of thermally-stressful work appear to have a cumulative effect on the thermal-work strain of the individual (Horn et al., 2013). The critical nature of effectively managing thermal-work strain over time is crystallized in the recent Ebola virus treatment centers. Here, Chertow et al. (2014) detail that physicians were only able to spend 45 to 60 minutes, two or three times per day, in direct contact with their patients because of the "substantial heat exposure and fluid losses". Roberts and Perner (2014) suggest more time-intensive care for Ebola virus patients was not available in part because of the limited time available to health workers when in personal protective gear.

Finally, while thermal-work strain may affect the performance or safety of the individual, the team perspective also needs to be considered. A team member not able to do his/her part means other team members must step in, which makes the whole team work harder. If an individual collapses from heat illness, this medical event is of concern to the whole team. Now one or more team members have to stop what they are doing and assist the individual with hyperthermia. This can be especially problematic for teams working in hazardous environments, where the team member has to be carefully extracted from a contaminated area.

1.3 Problem Statement

The challenge of excessive thermal-work strain has two research problems. 1) There is an acute component, where there is a risk of illness/injury or even death, and 2) a chronic component, where human performance is degraded over time. For first responders and emergency workers, both aspects can have life-impacting consequences. Although personal physiological monitoring has been suggested as a means to assess thermal-work strain and prevent injury (Bernard and

Kenny, 1994; Taylor and Amos, 1997; Hoyt et al., 1997), the needed physiological measures have proved elusive to obtain. Real-time ambulatory monitoring and management of an individual's thermal-work strain state is an open problem in physiology. The requisite measure of core body temperature needed for accurate thermal-work strain assessment is a challenge in an ambulatory setting. Specifically, this problem is one of state estimation of latent core body temperature from noisy and ambiguous observations produced by modern body sensors (such as heart rate and skin temperature). A lack of thermal-work strain state information has meant that management of heat injury and work scheduling is primarily conducted using environmentally-based work-rest tables. Without accounting for an individual's continuous thermal-work strain response to the environment and work goals, these schedules can increase heat injury risk and provide sub-optimal performance over the course of proscribed work.

To address these problems, we present an automated system that provides advice based upon physiological monitoring of an individual's thermal-work strain state and their overall task goals and safety constraints. The system is based upon a physiological feedback loop (see Figure 1.2), where given an individual's thermal-work strain state and their goals and objectives, the system will provide optimal pacing advice. Our two areas of work focus on the perception and decision-making portion of the physiological feedback loop.

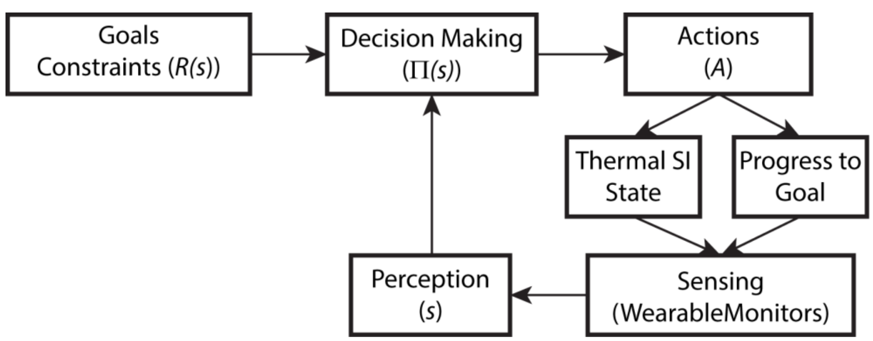

Figure 1.2: The physiological feedback loop. Where s = state (human thermal-work strain index, distance to goal and time), R is a reward function dependent on state, Π = a policy function dependent upon state, and A = actions (movement speed or pace).

Our first focus is to perceive an individual's current thermal-work strain state using data from commercially available physiological sensors. Here we wish to take the easily-measured, non-invasive variables and determine with a high degree of accuracy the latent thermal-work strain state. The perception algorithm will provide us with the most likely latent-thermal strain state given an input of readily measured physiological variables.

Once we can determine an individual's thermal-work strain health state(s), we wish to use this knowledge in the context of the goals and constraints of their current activity. Here we wish to estimate a policy that optimizes health and performance given a set of goals and constraints. Our estimated policy function Π(s) will provide an action (a) for a given health state (s) that is optimal in-terms of the current health state and the activity goals and constraints.

1.4 Contributions

In this dissertation, we present two main contributions to determine thermal-work strain state and improve human performance and health outcomes in extreme conditions. These contributions are:

- *A method for the state estimation of the latent human core body temperature from wearable physiological sensors that enables real-time thermal-work strain health state monitoring and heat injury prevention.*
- *Models for policy estimation to provide automated advice to improve thermal-work strain state and performance outcomes over a course of prescribed work.*

The outline of this dissertation is as follows. In Chapter 2, we present background material on exertional heat illness, thermal-work strain measurement, ambulatory physiological status monitoring, the problem and current approaches to measuring core body temperature, current approaches to managing thermal-work strain, current pacing strategies research in competitive sports, and how Markov decision processes can be used to model our physiological feedback loop. In Chapter 3, we describe our computational physiology approach to estimating core body temperature and thermal-work strain. We show our dynamic Bayesian network model of the human thermoregulatory system, and how we simplify this model to one input parameter readily measurable on commercially available sensing devices. We show the validation of this model across multiple studies, and how the technique was used in a real-time monitoring application during several field training exercises. In Chapter 4, we detail a Markov decision process method to capture activity goals and thermal-work strain constraints, and show through simulation how our method can lower overall thermal-work strain compared to human pacing strategies on the same task. In Chapter 5, we evaluate our combined work from Chapters 3 and 4 and its implementation as a real-time system for human participants in a laboratory study. We note that the work described in Chapters 3 and 4 has been published (see Buller et al., 2010, 2011, 2013a, 2013b, and 2015). Chapter 6 presents our conclusions and future areas of work.

Chapter 2

Background

2.1 Components of the Physiological Feedback Loop

The physiological feedback (see Figure 1.2) loop is intended to accomplish two goals. First, the thermal-work strain sensing component can prevent acute hyperthermia and the associated heat illness. Heat illness can lead to a marked reduction in work capacity and reduces the effectiveness of teams by taking time and effort of other team members to assist with treatment. Second, the feedback loop aims to take an individual's current thermal-work strain state and combine this information with progress towards a set goal or task, to the individual provide with an optimal set of actions that can safely get them to that goal. An overall work goal may be to travel a set distance, in a certain amount of time, given certain environmental conditions, and while wearing personal protective equipment. Another goal may be to assist in the extraction of casualties from a danger area. The actions may be a series of movements at different speeds interspersed with rest periods to accomplish the goal. These movement speeds will have different impacts on the thermal-work strain state of the individual, and progress to the ultimate goal. By perceiving the thermal-work strain state, our problem is to optimally control the pace of the individual to minimize immediate heat illness/stroke risk and to allow completion of the goal with the least thermal-work strain possible. The physiological feedback loop has two components that need solutions to make the system viable: 1) accurate thermal-work strain state estimation, and 2) estimation of a policy that for a given thermal-work strain state can provide a set of actions that optimize performance.

To provide an overview of the thermal-work strain state estimation problem, we first examine the basic physiology of exertional heat illness. We examine the physiological methods to assess thermal-work strain state that are present in the literature. Here, we identify, heart rate and core body temperatures as critical physiological measures needed for accurate assessment of thermal-work strain. A brief history of the development of physiological sensors and an overview of commercially available systems is presented. While many modern sensor systems track heart rate, there are few that can measure core body temperature. Of these systems, core body temperature is measured using an ingestible thermometer pill that, in many cases, is not appropriate for continuous monitoring purposes. The challenges of measuring and estimating core body temperature are detailed along with recent attempted solutions.

Current methods to manage the thermal-work strain risk of individuals and teams are also presented. We demonstrate that these methods lack individualization and act in a very conservative health protecting fashion. We review the literature on pacing strategies for elite athletes and identify several models that are presented to show how a pacing strategy is modified over time. The literature suggests that pacing is modified based upon subjective measures of perceived exertion which appears to be an integrator of afferent feedback signals and future effort required to complete the competitive event. These models suggest that the pacing strategy is a non-linear dynamical system control problem. We identify the Markov decision process (MDP) as a means to formulate this pacing control problem, and detail several methods that can be used to solve and MDP to provide an optimal policy. For performance optimization, individuals must complete the task safely (within thermal-work strain safety limits) and to complete the task in a cooler (according to core body temperature) and less fatigued (according to overall thermal-work strain) state. Finally, we identify the few examples in literature where an MDP has been used to help guide human actions.

2.2 Thermal-Work Strain State Estimation

2.2.1 The Physiology of Exertional Heat Illness

Across a range of thermal environments, human core body temperature (CT[3]) is usually maintained to such an extent (a few tenths of a degree Celsius) that deviation is suggestive of some medical condition (Romanovsky 2006). Regulation of CT occurs through the balance of heat production and heat transfer to the environment. If the rate of heat production exceeds the rate of heat loss to the environment, the body will store heat and CT will rise. Conversely CT will decrease, if the rate of heat loss exceeds the rate of heat production. Excessive storage or loss of heat can lead to illness or even death. Figure 2.1 shows a typical range of human CT temperatures.

[3] Throughout this document when CT is used both as an acronym and variable within equations. Italicized *CT* indicates a variable, and normal font CT indicates the acronym for core body temperature.

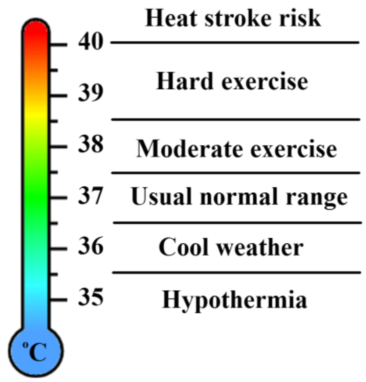

Figure 2.1: Core body temperature ranges (Hall 2011, Bouchama and Knochel 2002, Sawka and Young 2006, Dubois 1948)

Heat production is primarily a by-product of human metabolism. The overall metabolic rate includes a basal rate of all cells in the body, additional metabolism caused by the actions of hormones, the sympathetic stimulation of cells, demands of food digestion, and any additional metabolism caused by muscle activity.

Heat loss depends on how fast metabolic heat can be transferred from the body to the environment. Since most heat is generated deeper within the body, heat loss has two aspects: 1) how fast heat can be transferred to the surface of the body or skin and 2) how fast heat can be transferred to the environment. The primary mechanism for heat transfer to the skin is skin blood flow. Blood vessels near the surface of the skin can both constrict and dilate causing a respective decrease or increase in blood volume at the skin. Heat transfer to the environment can occur through a number of mechanisms: conduction (*K*), convection (*C*), radiation (*R*), and evaporation (*E*) (Sawka and Young 2006).

A change in CT can be explained by a heat balance equation (Equation 2.1).

$$S(\frac{dCT}{dt}) = H \pm K \pm C \pm R - E, \quad (2.1)$$

where the ± sign indicates heat can either lost or gained through this mechanism. Where S is the rate of heat storage: positive S means heat storage and an increase in CT; and negative S, heat loss, and a decrease in CT. H is the rate of heat production as a byproduct of the metabolic rate.

The rate of *K*, *C*, and *R* are dependent on the skin to environment temperature gradient, while the rate of E is additionally dependent on the amount of sweat and the evaporative potential of the environment. Thus, if the rate of H remains constant but the environmental temperature increases, heat transfer from the body becomes more and more dependent upon evaporative cooling. As environmental temperature increases, the skin temperature to environment temperature gradient decreases until it becomes negative. When this gradient is negative, heat is being added to the body from the environment through the K, C, and R mechanisms. Thus, heat loss in these conditions is dependent almost entirely on evaporative cooling alone.

Thermoregulation can be achieved by modification of behaviors that affect heat generation (H) or through physiological responses to affect heat loss to the environment. If heat loss is too great vasoconstriction can reduce blood flow to the skin and thus decrease the skin temperature's environmental temperature gradient. If heat loss is insufficient, vasodilation increases blood flow to the skin increasing the skin-to-environment temperature gradient. Similarly, sweat rate increases to increase heat loss from evaporation.

The classical control mechanism is a centralized feedforward controller that has a CT set point based upon biological rhythms, fever, heat acclimation and exercise training (Sawka and Young 2006). This set point is compared in the hypothalamus to an integrated core body temperature producing an error signal, which in conjunction with skin temperature, is integrated into thermal effector signals for combinations of behavioral change, vaso-constriction/dilation, and sweating (Sawka and Young 2006). Recently, the idea of a unified control mechanism has been challenged (Romanovsky 2007) from evidence of multiple distinct thermal effector pathways suggesting there are multiple control loops that activate at different temperatures. However, for the purpose of this dissertation, the practical result is the same: rise in CT increases skin blood flow and sweat rate increase in proportion.

The addition of protective clothing ensembles impact all the mechanisms of heat transfer. Once the skin is covered, heat has to be transferred through the garment to the external environment. The rate at which heat can be transferred is a combination of the garment's insulation and vapor permeability. The higher the insulation and the more attenuated the vapor permeability, the smaller the rate of heat loss by C, R, and E. Figure 2.2 shows an example of the effectiveness of these heat loss mechanisms while working with and without PPE in temperate and hot humid conditions and shows typical physiological responses.

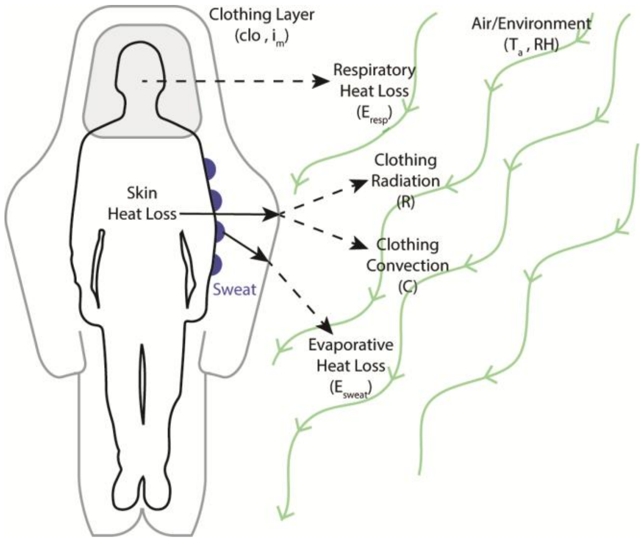

Figure 2.2: Components of heat transfer from clothed individual to surrounding environment.

Table 2.1: Effects of changes in environment and ensemble on convective (ΔC), radiative (ΔR), and evaporative (ΔE) heat loss where ΔE is evaporative heat loss from both sweat and respiration, and an increase in clo and decrease in i_m is indicative of greater encapsulation.

Δ Environment	**Δ Ensemble**	**ΔC**	**ΔR**	**ΔE**
↑Ta, ↑ RH	-	↓	↓	↓
-	↑clo, ↓i_m	↓	↓	↓
↑Ta, ↑ RH	↑clo, ↓i_m	↓↓	↓↓	↓↓

When the thermoregulatory system can compensate for the heat generated from exercise a steady state core body temperature will be reached. However, as the capacity of the thermoregulatory system for cooling is exceeded by heat generation from exercise core body temperature will continue to rise. The increased rise in CT and the demand for more cooling elicits further increases in skin-blood flow and sweat production (see Table 2.1 for examples).

Sweat loss can be as high as 2 liters/hour (Adams et al., 1975; Cheuvront and Haymes, 2001). If water and electrolytes are not replaced during exercise, more stress is placed on the thermoregulatory system. Dehydration can elevate core body temperature, reduce the tolerance to high core temperatures, and for a given core body temperature, reduce the amount of sweating and skin blood flow. Additionally, the skin blood flow and sweating effector responses are less sensitive and are triggered at higher core body temperatures. In terms of cardiovascular strain dehydration is additive to heat strain (Sawka and Young 2006).

The various strains of heat, exercise, dehydration and electrolyte loss can change compensable exercise into uncompensable exercise. As exercise continues and core body temperature rises, skin blood flow demands can be substantial approaching 8 liters/min (Rowell

1983, 1986). These skin blood flow demands compete with the finite resources of the heart to maintain the necessary cardiac output to service skeletal muscle and other organs of the body. Under these conditions, we find two physiological responses: 1) tachycardia, and 2) the convergence of skin temperature and core body temperature. Recent work by Cuddy et al. (2014) and Cheuvront et al. (2010) suggest that the skin temperature to core temperature gradient plays an important role in determining the level of aerobic performance. Sawka and Young (2006) also describe how the skin temperature to CT gradient is an indication of skin blood flow requirements. Indeed, Pandolf and Goldman (1978) suggested that the gradient of skin temperature to CT could be used as a means to assess time to fatigue.

2.2.2 Exertional Heat Illness

Exertional heat illness is comprised of a spectrum of heat exhaustion, heat illness and heat stroke. Heat exhaustion is defined by Sawka and Young (2006) as "a mild to moderate illness characterized by the inability to sustain cardiac output." Bouchama and Knochel (2002) also include elements of heat illness in their definition where illness can also be experienced from dehydration or lack of salts. Symptoms include: thirst, weakness, dizziness, headache, and fainting. More severe heat illness can lead to "organ (e.g. liver and renal) and tissue (e.g. gut and muscle)" injury (Sawka and Young, 2006). Heat stroke is a severe illness that if untreated can lead to permanent disability or death. Heat stroke is characterized by high core body temperatures (>40 °C), central nervous system abnormalities such as an abnormal gait or confusion, and dry skin. The exact nature of the transition from heat stress to heat stroke is not known. However, recent work suggests that other factors such as recent or current illness, use of pharmacological substances or alcohol use may play a role in reducing tolerance to heat stress. Bouchama and Knochel (2002) and Stacey et al. (2014) both develop pathophysiological models that suggest a mechanism where heat stroke is a combination of endotoxemia and a systematic inflammatory response and circulatory compromise. These causes can lead to the failure of thermoregulation, circulatory shock, and multiple organ dysfunction. Epstein et al. (2015) provide a review of clinical interventions beyond whole body cooling that may have a positive impact on heat stroke outcomes.

2.2.3 Heat Strain Measurement

Here, we wish to distinguish between methods that assess the potential heat stress that work, clothing, and environmental conditions impose on an individual and the assessment of the physiological strain experienced by a particular individual. Heat strain is often coupled in a very dependent way with the strain from work alone. It is the combination of the two that can lead to exertional heat illness. It is more practical to assess these two physiological strains together. The determination of thermal-work strain (TWS) has often involved measuring some combination of core body temperature, skin temperature, heart rate, and sweat rate or water loss (NIOSH 1986). None of these parameters alone can be used to accurately assess thermal-work strain. Core body temperatures can indicate thermal-work strain over a large range from 38.5 °C to more than 40.0 °C depending on the environment, clothing worn and fitness of the individual (Sawka and Young 2006; Ely et al., 2009). High heart rate can be due to exercise effort alone or include the strain of vaso-dilation and supporting increased blood flow. While a symptom of heat stroke is dry hot skin, skin temperature can vary quite dramatically depending on the environment, clothing, and thermoregulatory response. Sweat rate also varies greatly depending on the environment and clothing that is worn. In some instances, there may be equivalent sweat rates. In very humid environments or when clothing with vapor barriers is worn, the thermoregulatory effectiveness is lower and, thus, the overall TWS strain will be higher (Hatch 1963; Sawka and Young 2006; Cheuvront et al., 2007). It is a combination of these physiological measures that provides some indication of TWS.

Robinson et al. (1945) proposed an index that was an equally weighted combination of all four parameters. Their index of physiological effect is computed from Equations 2.2 to 2.6.

$$E_p = E_h + E_s + E_r + E_w \tag{2.2}$$

where E_p is the index of physiological effect, E_h is the heart rate component, E_s is the skin temperature component, E_r the core body temperature component, and E_w is the sweat rate. These component are specified as follows:

$$E_h = \frac{100}{168-H_{base}}(H_t - H_{base}) \,, \tag{2.3}$$

where H_{base} is an individual's baseline heart rate and H_t is the current heart rate.

$$E_s = \frac{100}{38.3-S_{base}}(S_t - S_{base}) \,, \tag{2.4}$$

where S_{base} is an individual's baseline skin temperature and S_t is the current skin temperature.

$$E_r = \frac{100}{40.4 - R_{base}} (R_t - R_{base}) \ , \tag{2.5}$$

where R_{base} is an individual's baseline core body temperature and R_t is the current core body temperature.

$$E_w = \frac{100}{1850 - W_{base}} (W_t - W_{base}) \ , \tag{2.6}$$

where W_{base} is an individual's baseline sweat rate and W_t is the current sweat rate.

This index was developed on a small number of volunteers and was not validated with new data.

Hall and Plote (1960) suggested an index that used heart rate, sweat rate, and core body temperature. The method however, while relatively simple, cannot be computed in real time and only provides an index of the physiological strain achieved after completing an exercise. The method is described below in Equation 2.7.

$$I_s = \left(\frac{HR}{100}\right) + \Delta T_r + \Delta W_n \ , \tag{2.7}$$

where I_s is the index of physiological strain, HR = heart rate, T_r is rise in rectal temperature (°C/ hr.), and W_n is total sweat production (nude wt. loss, kg / hr.).

A number of approaches have also been suggested using only two parameters. The convergence of skin temperature and CT has been used to predict time to exhaustion (Pandolf, and Goldman, 1978). While this method did not compute a thermal-work strain index explicitly, the time to exhaustion could be viewed as such an index. While the technique showed promise, it operated best in hot humid environments. The technique uses the rate of change in skin temperature to extrapolate a point where skin temperature and core body temperature converge.

Yokota et al. (2005) suggest a lookup table method for determining risk of heat strain using HR and skin temperature along with modification for body mass index. Building on this work Buller et al. (2008) suggested computing the likelihood of a person having high TWS using just HR and skin temperature. Figure 2.3 shows the results from a cubic logistic regression where the decision bounds can be tuned based upon the tradeoff of false negatives and false positives. The approach was further validated by Cuddy et al. (2013) using different exercise rates and environmental conditions.

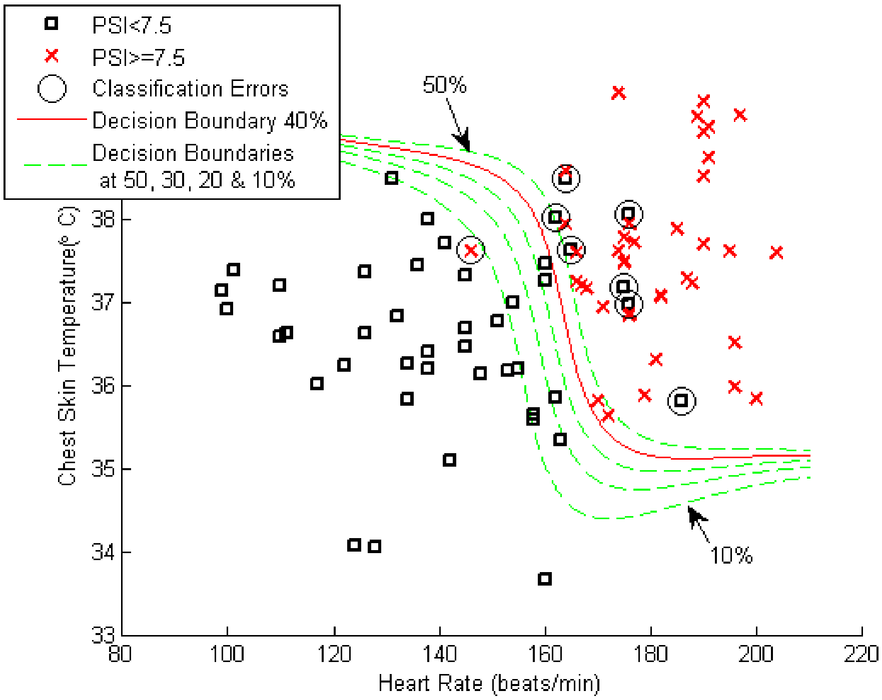

Figure 2.3: Cubic logistic regression to estimate likelihood of high TWSI (PSI) from TS and HR. Validation data classified using a 0.4 likelihood boundary (from Buller et al., 2008).

Heart Rate and CT were combined by Frank et al. (1996, 2001) for their cumulative heat strain index (CHSI). Equation 2.8 shows how to compute their index.

$$CHSI = \frac{[\sum_0^t hb - HR_0 t]}{10^{-3}} \left[\int_0^t T_r dt - T_{r_0} t\right] \tag{2.8}$$

where hb = heart beats, HR_0 is initial heart rate (beats/min), T_r is rectal temperature, T_{r0} is initial rectal temperature and t is time in minutes elapsed from the first measurement.

This index was validated on several large scale studies with over 50 participants and was designed to be used to evaluate heat-intolerant volunteers in the Israeli Defense Forces (IDF). However, while the index works for one bout of exercise, it continues to rise during rest even when both HR and CT decline. Identifying this drawback of the cumulative heat strain index, Moran et al. (1998) proposed an index that could be computed in real time from instant data, and that was able to reflect physiological strain from multiple bouts of work and during rest periods. It has the advantage of combining how hot an individual is getting (think of a temperature gauge) with how hard they are working (e.g. a tachometer). The physiological strain index (PSI) is a weighted combination of heart rate and core body temperature (see Equation 2.9) that ranges from 0 (no strain) to 10 (very high strain). A PSI of 10 is achieved at a HR of 180 beats/min. and an CT of 39.5 °C (103.1 °F) corresponding to a level of thermal-work strain associated with a 50% likelihood of becoming a heat casualty (Sawka and Young 2006).

$$PSI = 5(CT - CT_{rest})(39.5 - CT_{rest})^{-1} + 5(HR - HR_{rest})(180 - HR_{rest})^{-1} \quad (2.9)$$

Where PSI is the physiological strain index, CT is core body temperature, and HR is heart rate. The rest suffix denotes the HR or CT at rest prior to exercise. A high PSI indicates a person is hot and working very hard, therefore the strain is high. Conversely, a low PSI means the person is cool and is not working very hard. Table 2.2 shows the PSI scale from 0 to 10, the scale associated set of adjective anchors, and HR and CT values that can produce the associated PSI. Heart rate and CT values are based upon using CT_{rest} of 37.0 °C and HR_{rest} of 70 beats/min.

Table 2.2: The PSI scale and corresponding HR and CTs.

Strain	**PSI**	**HR (beats/min.)**	**CT (°C)**
	0	70	37.0
No/Little	1	81	37.25
	2	92	37.5
Low	3	103	37.75
	4	114	38.0
Moderate	5	125	38.25
	6	136	38.5
High	7	147	38.75
	8	158	39.0
Very High	9	169	39.25
	10	180	39.5

The PSI has demonstrated efficacy in identifying individuals with high heat strain in both hot-dry and hot-wet environments with or without PPE (Moran, 2000). This work also explored how the index can be used to assess the impact of different levels of hydration (Moran et al., 1998) and whether gender differences can be assessed utilizing the PSI (Moran 1999). Independently, Gotshall, Dahl and Marcus (2001) evaluated the index for exercise in a laboratory setting examining both hot-dry and hot-humid conditions. This work concluded that the PSI appropriately documented heat strain for both intermittent and continuous exercise. Yokota et al. (2002) examined the effectiveness of PSI in a field environment for vigorous military training activities and concluded that it is an appropriate index.

The physiological basis of this method, combined with the simplicity of the scale has made this scale attractive for summarizing thermal-work strain. Thus, this approach has often been adopted for use when measuring the thermal-work strain of workers outside of laboratory settings for example: wildland firefighters (Lui et. al . 2014), city firefighters (Gunga et al., 2008), construction workers (Chan et al., 2012), and the military (Buller et al., 2008). Finally, to avoid confusion Moran's acronym of PSI, the index will be called the thermal-work strain index (TWSI) in this document.

Subjective Measures of Thermal-Work Strain

Because the TWSI combines two physiological components into one scale, there is no readily available single subject scale equivalent. There are, however, two standard subjective scales that appear to capture both components of thermal-work strain. The rating of perceived exertion (RPE) (Borg 1970, 1982) is a scale from 6 meaning no exertion at all, to 20 meaning maximal exertion. Table 2.3 shows the scale and associated exertion adjectives. Because both HR and oxygen consumption increase linearly with work (see Fick equation Fick 1855), the scale was designed in a way to purposefully match HR from rest (60 beats/min.) to a maximum HR of 200 beats/min..

Table 2.3: Rating of Perceived Exertion (RPE) scale.

RPE Scale	Exertion Adjectives
6	No exertion at all
7	Extremely light
8	
9	Very light
10	
11	Light
12	
13	Somewhat hard
14	
15	Hard (heavy)
16	
17	Very hard
18	
19	Extremely hard
20	Maximal Exertion

Lamb et al. (1999) in their assessment of the test retest reliability of the RPE show how it has been used to assess exertion in: cycling, walking and running, stepping, swimming, and rowing. The RPE scale has also been adopted by the American College of Sports Medicine as a means to prescribe safe and effective training intensities (ACSM 2000). However, Lamb et al. (1999) caution practitioners that their 95% confidence intervals show ± 3 RPE units from one exercise to another.

For the thermal component, a number of different scales have been suggested in the literature (see Table 2.3 for examples). The American Society of Heating, Refrigerating and Air Conditioning Engineers (ASHRAE) (2001) recommend a 7 point hedonic scale developed by Fanger (1970). This scale has been found to be most sensitive to skin temperature and sweat evaporation (Fanger 1982). Young et al. (1987) examined thermal comfort using their own scale (see Table 2.4) when examining the perceived thermal sensation from the application of a range of cooling techniques. They find that skin temperature, more than core body temperature, plays a role in perceived thermal sensation. Finally, we present a modified scale that keeps the hot cold balance of Fanger's scale and extends the scale in a linear fashion. The modified scale is from -10 to +10, and has the addition of "extremely hot" and "extremely cold" anchors. The scale has been modified to avoid the apparent non-linearity of the jump from very hot to unbearably hot in Young et al.'s scale, and to allow the scale to be used in comparison to the thermal-work strain index.

Table 2.4: Thermal sensation scales.

Fanger (1970)		**Young et al. (1987)**		**Proposed**	
Scale	**Verbal Anchor**	**Scale**	**Verbal Anchor**	**Scale**	**Verbal Anchor**
				−10	Unbearably Cold
		0.0	Unbearably Cold	−8	Extremely Cold
−3	Cold	1.0	Very Cold	−6	Very Cold
−2	Cool	2.0	Cold	−4	Cold
−1	Slightly Cool	3.0	Cool	−2	Cool
0	Comfortable	4.0	Comfortable	0	Comfortable
+1	Slightly Warm	5.0	Warm	+2	Warm
+2	Warm	6.0	Hot	+4	Hot
+3	Hot	7.0	Very Hot	+6	Very Hot
		8.0	Unbearably Hot	+8	Extremely Hot
				+10	Unbearably Hot

Training individuals to utilize subjective rating scales may help to provide some self-awareness of increasing thermal-work strain. However, work by Soule et al. (1978) would suggest that self-perception of thermal-work strain is complex. In their work volunteers were trained to complete an 8km walk within 120 minutes, in hot (40 °C) conditions with a relative humidity of 50%. Volunteers were provided their speed of movement, distance to goal and core body temperature. They were instructed to complete the foot movement on time and to avoid heat exhaustion. When the task was replicated with high humidity (65%), subjects did not significantly adjust their pace and many succumbed to heat exhaustion before finishing the foot movement.

From this review of literature, it can be concluded that to assess thermal-work strain, measures of both heart rate and core body temperature are necessary. The thermal-work strain index, when coupled with a physiological monitoring system, would make a simple and effective means to avoid heat injury or illness.

2.2.4 Ambulatory Physiological Monitoring

The concept of directly monitoring the physiology of free living individuals draws from a long line of forward-looking research beginning in the early 20th century. Many of our modern wearable sensors have had a long history of development including respirometers, electro-cardiograms (ECG), and accelerometers. In 1906, Nathan Zuntz, a German physiologist, created a portable dry-gas measuring device capable of measuring expired gas volume to better aid his studies on the physiological effects of high altitude (McLean and Tobin, 1987) (see Figure 2.4).

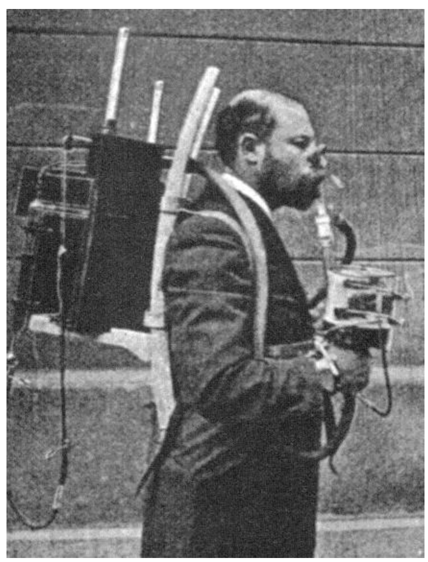

Figure 2.4: Nathan Zuntz wearing his portable dry gas volume measuring device. (Zuntz et al., 1906).

In 1902 Willem Einthoven, a Dutch physician, published the first accurate electrocardiogram data using a modified wire coil galvanometer (Moukabary, 2007), and in 1928 the first portable version (weighing 22.7 kg and powered by a 6-volt automobile battery) was created by the Sanborn Company (Zywietz, 2003). Accelerometers made their debut when McCollum and Peters developed a resistance-bridge accelerometer based on a Wheatstone half-bridge (McCullom et al., 1924) which was commercialized in 1923 for use in bridges, dynamometers, and aircraft (Walter, 2007). Initial models weighed around 450 grams and measured about 2 x 5 x 22 cm.

During the latter part of the 20th century, individual sensors were light and wearable enough to be incorporated into systems that monitored a number of physiological parameters. Pioneering work circa 1955 from the U.S. Army's Quartermasters Research and Development Center, Natick, MA produced a telemetry system to measure the physiological impact of clothing (see Figure 2.5).

Figure 2.5: Thermal physiological strain monitoring system, Quartermaster Research and Development Center, Natick MA (Circa 1955).

Later, prototype systems included: 1) Yale University and NASA's joint test of a physiological monitoring system capable of monitoring heart rate, accelerometry, skin and core body temperature during an ascent of Mt. Everest (Satava et al., 2000); 2) the monitoring of Boston Marathon runners by Massachusetts Institute of Technology (MIT) students during a project named Marathon Man (Redin, 1998); 3) the development of an ingestible core thermometer pill (sponsored by NASA and the U.S. Army) (O'Brien et al., 1998); and 4) the U.S. Army's field testing of an integrated sensor system that measured motion, heart rate, core body temperature, pedometry, and geo-location during military training events (Hoyt et al., 1997). Although nascent, these systems demonstrated the potential value of monitoring multiple physiological parameters. Figure 2.6 illustrates a real time monitoring system used to show the thermal-work strain index of a squad of warfighters using core body temperature pills and heart rate monitors (Hoyt et al., 2002).

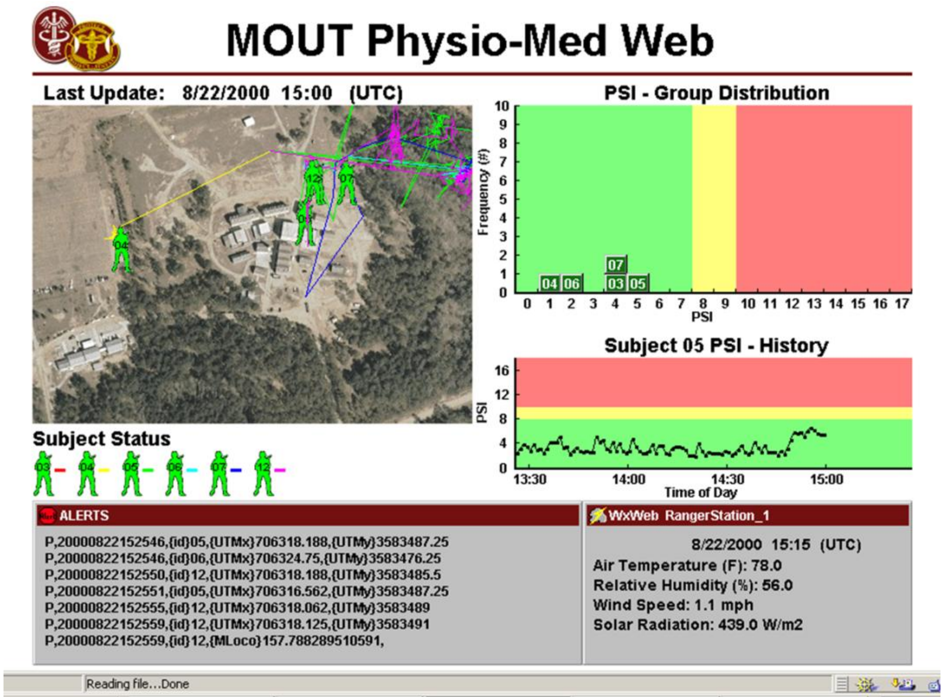

Figure 2.6: Physiological monitoring system that measured the thermal-work strain index in real time (2000).

Today, wearable physiological sensing devices have been demonstrated and are used in a wide variety of applications including home health care, elderly monitoring, physical training, industrial hygiene, and military uses. We refer the reader to the survey by Pantolopoulos and Bourbakis (2008). Fitness and training products include heart rate monitors, global positioning systems, physical activity monitors, and pedometers produced by a variety number of companies (See Appendix A, for a list of modern sensor devices). Generally, these devices are worn during exercise or everyday activity and integrate sensor data (e.g., HR, activity counts, distance traveled, time elapsed) with user input (e.g., gender, age, weight, stride length, resting HR, maximal HR) to estimate energy expenditure and or physical activity often using proprietary algorithms. Although small, unobtrusive, and non-invasive, fitness and athletic PSM devices do not often meet clinical standards and provide approximate measurements. Evaluations against standard measures of energy expenditure using either indirect calorimetry or double labeled water (Chen, 2003; Chen and Basset, 2005) have found that many pedometers and accelerometer-based physical activity monitors accurately detect physical activity, but often underestimate energy expenditure (Bassett and Strath, 2002; Welk 2002). Figure 2.7, depicts typical fitness devices that can be purchased today, such as the Actical (Philips Respironics, Bend OR), Actigraph GT3X

(Actigraph, LLC, Pensacola, FL), Direct Life (Philips Electronics, Andover, MA), and Fitbit Tracker (Fitbit, Inc., San Francisco, CA).

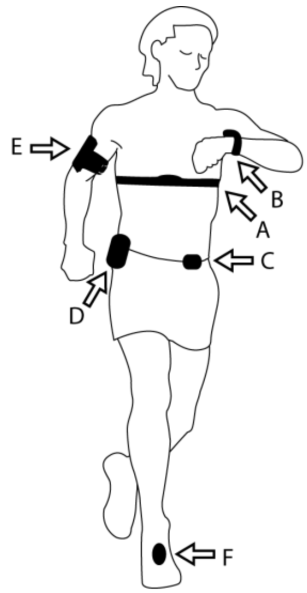

Figure 2.7: Various commercially available fitness physiological status monitoring devices commercially available for running and walking including: (A) heart rate monitor with (B) watch display; (C) waist and (F) foot mounted pedometers; (E) arm mounted triaxial accelerometer; and (D) smart phone/GPS unit.

While modern wearable sensors can provide a wealth of physiological information, they are quite different from what a physician might measure in a clinical setting where more controlled or invasive techniques are available. Often the measures from the non-invasive sensors are not specific to most health states of interest and can reflect the output of multiple latent variables. Consequently, the relationship of typical ambulatory monitoring data to standard health state metrics of interest is often tenuous. Additionally critical physiological functions may be strongly defended by compensatory biological mechanisms (e.g., symptoms of shock or dehydration may only be measurable at a point when an individual is already too injured for medical intervention to be effective) (Convertino et al., 2010; Committee on Metabolic Monitoring 2004). In our case, for example, internal body temperature is the key to understanding hyperthermia, but non-invasive measures such as heart rate and skin temperature are also driven by the environmental conditions, clothing characteristics, individual characteristics (e.g. % body fat), work rate, hydration state, and thermoregulatory factors, and have a complex relationship to internal temperature. It is only when thermoregulation begins to fail that heart rate and skin temperature correlate more directly with internal temperature.

Finally, several manufacturers have developed first responder style physiological status monitoring equipment that attempts both robust healthcare measures and the wearability of fitness devices. While these type of devices offer unique challenges the Equivital II (Hidalgo Ltd, Cambridge UK) and BioHarness (Zephyr Inc. Auckland, NZ) have received Food and Drug Administration (FDA) 510K certification as heart rate and respiration monitors. In addition the Equivital II has been shown to have good comfort and acceptability when worn for extended periods of time (Tharion et al., 2013).

Even though there has been great effort recently to produce wearable physiological monitors, the critical parameter of core body temperature is missing. While the Hidalgo Equivital system can receive transmissions from the core body ingestible thermometer pill, this has a number of drawbacks (discussed in the next section) making it impractical for daily monitoring. Aside from core body temperature, many of the most modern wearable physiological monitoring devices struggle to accurately measure core body temperature. Appendix A shows a survey of physiological status monitoring devices that are on the market today and the parameters they measure.

Finally, it can be concluded that to provide an accurate thermal-work strain assessment methods are needed to approximate or estimate core body temperature given our current state of physiological status monitoring technology.

2.2.5 Methods to Estimate Core Body Temperature

Medical grade CT measurement using pulmonary arterial blood temperature is only appropriate in a clinical setting. The traditionally accepted laboratory rectal and esophageal probe methods are impractical for ambulatory settings. Ingestible thermometer pills (e.g., Jonah Pill thermometer, Respironics, Bend, OR) have been used successfully in field settings (e.g. Lee et al., 2010), and have been within acceptable limits of agreement (± 0.4 °C) and bias (< 0.1 °C) when compared to esophageal temperatures (Byrne and Lim 2007). However, these thermometer pills have drawbacks: 1) they cannot be used by all people due to medical contraindications, and 2) can suffer from inaccuracy when hot or cold fluids are consumed (Wilkinson et al., 2008). The difficulty in directly measuring CT in ambulatory settings has led to the search for a practical alternative technique.

There have been a number of different efforts to measure or estimate core body temperature in a field setting, most of which fall into three main approaches: 1) temperature correlates, 2) multi-parameter approach, and 3) specialized heat flow sensors.

Temperature Correlates

The temperature correlate work has sought for different body sites where either surface temperature or sub-surface temperature can be used to approximate core body temperature. Skin surface temperature can vary quite differently from core body temperature based upon the environment, clothing, and whether a person is sweating or not. Blood flow to the skin in conjunction with sweating is a mechanism used to thermo-regulate. Thus, in many circumstances there is no clear correlation to core body temperature (Burton 1935, Nielson 1969). However, if the impact of the environment, clothing and sweating can be removed there is some evidence that an approximation to core temperature can be made (Barnes 1967). For example, axillary temperature is affected less by these factors, and can show a modest correlation to core temperature. A review by Taylor and Amos 1997 examined various approaches using skin temperature to approximate CT. They conclude that for field settings skin temperature alone without special modifications (specialized insulation or adoption of zero heat flow approach) does not track with core temperature.

Tympanic temperature measurement takes this idea one stage further, attempting to measure the temperature of the tympanic membrane in the ear. This approach to measurement has been used fairly widely both in clinical settings and in ambulatory environments. Close correlations can be found in fairly steady state exercises but during periods of intermittent work core body temperature and tympanic temperature diverge causing one author to suggest that firefighter authorities find other means of assessing core body temperature (Langridge et al., 2012). Even in clinical settings findings have been inconsistent. One clinical trial suggested that the method would fail to diagnose fever in 4 out of 10 children (Dodd et al., 2006). When conditions are ideal, it appears that the method works reasonably well, but the placement and particular individual differences in the ear canal can have significant impacts on the results (McCarthy and Heusch, 2006). Teunissen et al. (2011) suggested overcoming some of these problems by molding the sensor into a form fitting ear plug, but still concludes that this method may only be suitable in warm stable conditions. Overall Lim, Byrne and Lee (2008) report in their review article that using external measurements such as axillary or tympanic temperatures have proven unreliable.

Multi-Parameter Approach

Several recent approaches have examined using multiple non-invasive physiological measures to accurately estimate core body temperature. Kaufman and Coleman (2010), in their patent, show a 12 parameter regression model which is shown in Equation 2.9.

$$CT = 0.084198 + 0.230214HR - 0.25538MST - 0.09152TA + 0.045715(HT * WT) - 0.09063(HR * MST) - 0.06626(HR * TA) - 0.16768(HR * HT * WT) + 0.052633(VLF * MST) + 0.052633(VLF * TA) - 0.08471(VLF * HT * WT) + 0.211613(MST * TA) + 0.056554(HR * VLF) \quad (2.9)$$

Where *TA* is ambient temperature, *HT* is height, *WT* is weight, *MST* is mean skin temperature, and VLF is very low frequency spectral component of heart rate. While the regression is derived from 60 volunteers, no validation data are presented.

Niedermann et al. (2014) present a core body temperature estimation equation based on determining two independent factors derived from principal components analysis. The method relies on three skin temperature measurements, heart rate and two skin heat flux measurements Equations 2.10 to 2.12 show the estimation approach:

$$CT = 0.278(F1) + 0.275(F2) + 37.644\ , \quad (2.10)$$

where *CT* is core body temperature (°C) and *F1* and *F2* are the factor scores computed from equations:

$$F1 = 0.327\frac{(T_{u\,arm}-34.831)}{3.095} + 0.303\frac{(T_{l\,arm}-34.472)}{2.389} + 0.265\frac{(T_{thigh}-35.185)}{2.681} + 0.313\frac{(HR-108.23)}{29.891} + 0.084\frac{(HF_{front}-201.118)}{104.627} + 0.083\frac{(HF_{back}-328.077)}{122.751}\ , \quad (2.11)$$

where T_{uarm} is upper arm temperature, T_{larm} is lower arm temperature and T_{thigh} is skin temperature of the thigh all in °C, *HR* is heart rate (beats/min.), HF_{chest} is the heat flux on the chest (Wm^{-2}), and HF_{back} is heat flux on the back (Wm^{-2})

$$F2 = 0.033\frac{(T_{u\,arm}-34.831)}{3.095} - 0.038\frac{(T_{l\,arm}-34.472)}{2.389} - 0.084\frac{(T_{thigh}-35.185)}{2.681} + 0.252\frac{(HR-108.23)}{29.891} + 0.517\frac{(HF_{front}-201.118)}{104.627} + 0.514\frac{(HF_{back}-328.077)}{122.751}\ . \quad (2.12)$$

While the approach showed reasonable root means square errors from 0.24 to 0.34 °C, it has the limitation of needing measurements from multiple, at least five, sites around the body. It is also unclear whether the heat flux measurements would be affected by sweating. The problems of using heat flux sensors are addressed in the skin heat flux sensor section.

Thermoregulatory Model Approach

Human thermoregulatory heat transfer models (Kraning and Gonzalez, 1997; Fiala et al., 2001; Havenith, 2001) have been used successfully to estimate CT for groups. These models use an array of input variables that include metabolic rate, environmental parameters, individual characteristics, and clothing parameters. The SCENARIO model of Kraning and Gonzalez requires the following class of inputs: environmental conditions, clothing insulation and vapor permeability characteristics, individual characteristics (including height, weight, percent body fat and age), and work rate expressed in watts. In this model the human is represented as a series of concentric cylinders. The overall surface area of the cylinder is determined by an individual's body surface area (height and weight). These cylinders are shown in Figure 2.8.

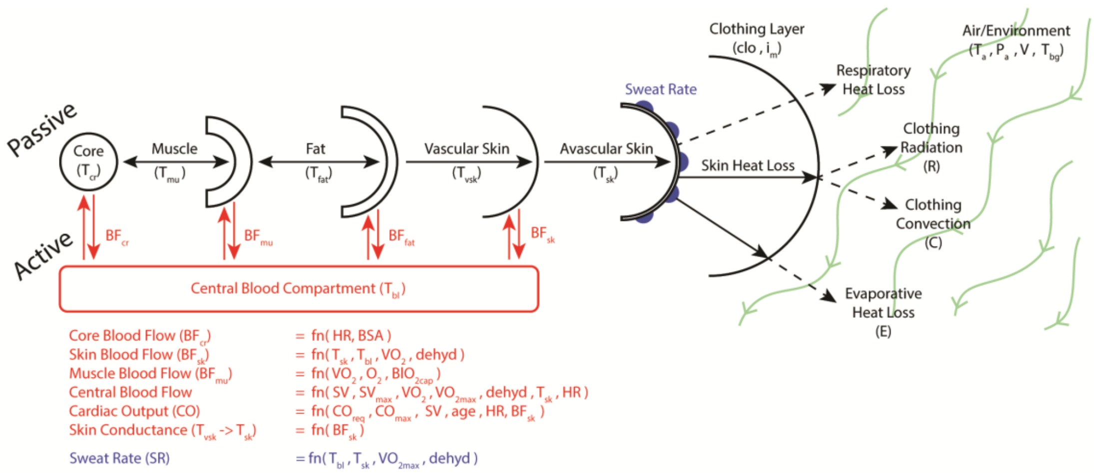

Figure 2.8: Physics based human thermoregulatory model SCENARIO (Kraning and Gonzalez 1997). Heat dynamics modeled as a series of differential equations.

In an ambulatory setting, these models suffer from the fact that not all inputs are available all of the time, and measuring or estimating metabolic rate in a field setting is difficult. From laboratory studies, where many of these model inputs are controlled, group mean core body temperature root mean square errors (RMSE) of 0.20 ± 0.05, 0.20 ± 0.11, and 0.19 ± 0.10 are reported for models proposed by Fiala et al. (2001), Havenith et al. (2001), and Kraning and Gonzalez (1997) respectively. The use of these models in an ambulatory environment requires measuring or estimating all of these input variables.

An integrated system developed by the US Army (Tatbul et al., 2004; Buller et al., 2005; and Tharion et al., 2007) attempted to use the SCENARIO thermoregulatory model and multiple sensor inputs including real time environmental information. The combination of models and sensors was a system level approach. A combination of physiological and environmental sensors, and physiological and physics based heat transfer models were used to attempt to estimate life sign and multiple health states (e.g., thermal, hydration, and cognitive). Figure 2.9 shows the dependencies of the health state algorithms. The system enabled relevant health states to be calculated in real time, but the accuracy of these health states were questionable given the indirect sensor readings and the number of measurements and assumptions required by the models.

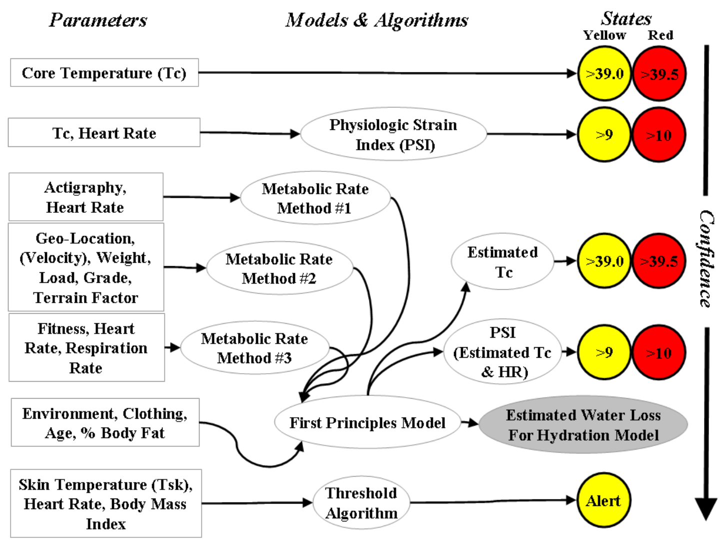

Figure 2.9: Thermal state estimation: input parameters, models, and state mappings. Metabolic rate method 1: Moran, Heled & Gonzalez (2004); method 2: Pandolf et al. (1997); method 3: Spurr, Prentice & Murgatroyd (1988).

One critical parameter to measure or estimate when using the thermoregulatory model approach is metabolic rate. In the US Army system, metabolic rate was estimated from GPS-measured movement rates (GPS device) using the Pandolf (1977) equation estimates metabolic rate from weight, load, speed of movement terrain type and grade (see Equation 2.13).

$$\dot{M} = 1.5W + 2.0(W + L)(L/W)^2 + \eta(W + L)(1.5V^2 + 0.35VG) \quad (2.13)$$

where $\dot{M}$ is metabolic rate (W), W is subject weight (kg), L is subject load (kg), η is terrain factor, V is movement rate (m/s) and G is terrain grade (%). Other similar methods have also been proposed (as surveyed by Potter et al., 2013).

The American College of Sports Medicine equation (ACSM 2000) has also gained quite a wide acceptance. However, accurate estimation across populations, terrain grades, and types still remains a significant problem in the practical use of the speed and body type estimators. Recent work from Weyand et al. (2013) extends this approach to include stature. The technique for moderate walking shows a marked improvement over previous approaches, with ongoing work to extend to different grades. Similarly, earlier work by Hoyt et al. (1994) based upon foot ground contact time and incorporated into an early Nike iPod accessory. This approach is accurate but has not been extended to different grades or loads.

One current area of research interest is to estimate metabolic rate or activity from body worn accelerometers. Today in the market place, there are many wearable accelerometer devices that provide proprietary estimates of metabolic rate and a very large body of work examining methods to classify activity and estimate metabolic rate. A survey from the IEEE Engineering in Medicine and Biology Conference 2012 found 33 papers using accelerometry to estimate activity or metabolic rate. At the 2013 Body Sensor Networks (BSN) conference there were 16 papers, and at the International Conference on Ambulatory Monitoring of Physical Activity and Movement there were 77 papers. Many of these papers examine new accelerometry sensor systems or proprietary algorithms. Dannecker (2013) provides a comprehensive validation of some of the more popular devices and they found that the Actical, Actigraph and Fitbit devices significantly underestimate energy expenditure by 26%, 27% and 29% respectively.

More sophisticated devices such as the SenseWear armband (Body Media Inc. Pittsburgh, PA) utilize accelerometers, and other sensor modalities such as galvanic skin response, and heat flux along with machine learning algorithms to estimate activity patterns. Different metabolic rate estimation techniques are then applied based upon the type of activity. The SenseWear armband performance compares well to other more complex laboratory/ambulatory approaches such as the IDEEA monitor (MiniSun LLC) (Welk et al., 2006). The IDEEA system consists of 5 integrated sensors that are taped to the soles of the feet, both thighs and the chest. The device applies a neural network to estimate postures and gaits from body segment angles and accelerations. Different metabolic rate estimators are used based upon posture and gait determination. However, while there is good agreement between these two devices when compared to indirect calorimetry methods the SenseWear arm-band can overestimate metabolic rate significantly (~70%) on level walking. (Machac, Prochazka, and Radvansky 2013).

Better estimates of metabolic rate can be obtained when heart rate is added as an additional modality Zakeri et al. (2008). Recent work has focused on combining thermoregulatory heat transfer models with metabolic rate estimators that use heart rate (HR) with ambient temperature modifiers to account for skin blood flow (Yokota et al., 2008). This real-time model provided accurate group-mean CT estimates in a number of different environmental and clothing conditions (Degroot et al., 2008). While this method shows promise, it still requires many input parameters that must be measured independently from an individual such as environmental conditions and clothing characteristics. We compare our findings to this approach in Chapter 3.

Skin Heat Flux Approach

One non-invasive approach that has received attention is the zero heat-flux (ZHF) method (Fox et al., 1973) where an insulated area of the skin is heated until there is no heat flow. The temperature of the skin is then assumed to be equivalent to deep body temperature. Most of the work on this approach has been in laboratory and clinical settings (Yamakage, Iwasaki and Namiki, 2002) with recent work focusing on improving measurement of dynamic temperature changes (Steck, Sparrow and Abraham, 2011), and decreasing the technique's response time (Teunissen et al., 2011). In clinical settings these devices have demonstrated good agreement with esophageal measures, while custom sensors developed for ambulatory environments have had varying degrees of success depending on environmental conditions. Work by Xu et al. (2013) shows the difficulty of the approach demonstrating how the relationship between core temperature and heat flux on the skin surface can be affected by the environment, sensor placement, clothing, and sweating. This approach was adapted for use in ambulatory environments with firefighters (Gunga et al., 2008, 2009). Specialized helmet sensors were produced that tried to minimize the effects of the environment on the ZHF method. In chapter 3 we examine the performance of this approach with our estimation algorithm.

Computational Physiology Approach

Much of the previous work in thermal-work strain state estimation has been focused on developing statistical associations for either core temperature directly or inputs to the thermoregulatory models from observed variables. However, these approaches neglect the complex relationships between the variables that impact core body temperature. The complexity of the human thermoregulatory models suggests that the responses of core body temperature and physiological measures are part of a dynamical system. Using current physiological monitoring techniques, certain variables (e.g. HR and skin temperature) can be readily observed; while others, core temperature in particular, can only be readily observed directly in a laboratory setting. Core body temperature among others is a latent variable that has an impact on our observed variables. Representing the dynamics and outputs of latent variables in some form should allow for better explanations of the observed variables. Exploiting knowledge of physiological relationships between variables has led to successful estimation of latent variables. Of note, Kashif et al. (2012) were able to estimate intracranial pressure from non-invasive sensors, by making use of the known physiological dynamics of blood flow through the brain represented in the form of an electric circuit. At their simplest, partially observable dynamical systems can be represented as Bayes filters with graphical model form below:

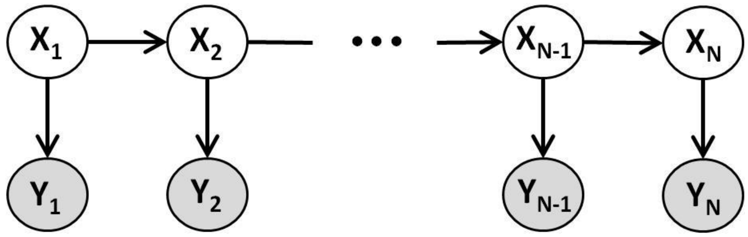

Figure 2.10: Graphical model showing how the typical health state estimation problem can be represented by a Bayes filter, where unobserved health states are represented by (X) and observed physiological measurements are represented by the vector (Y).

In this form we assume that the dynamics are Markovian, in that the current state is all that is needed to predict the future next state. The joint probability can be represented by three factors: a prior or initial starting value $P(X_t)$, a state-transition function $P(X_t|X_{t-1})$, and an observation function $P(Y_t|X_t)$ show in Equation 2.14:

$$P(X_{1-N}, Y_{1-N}) = P(X_1) \prod_{t=2}^{N} p(X_t|X_{t-1}) \prod_{t=1}^{N} p(Y_t|X_t) \quad (2.14)$$

At each time step (*t*), we wish to infer the most likely value of the latent variable given the last state and current observation ($P(X_t|X_{t-1}, Y_t)$). For either the discrete state Hidden Markov Model (HMM) (e.g. Rabiner 1989) or continuous Kalman Filter Model (KFM) (Kalman 1960) representation algorithms exist to iteratively compute the most likely latent variable value. These models have been used with some success in other human monitoring problems (e.g. Dadashi 2013, Sengul and Baysal 2012) but, to our knowledge, not for thermal-work strain state estimation.

Graphical models provide a natural way to further express the physiological variables and dependencies that form the basis of biological systems. By their nature, many physiological processes evolve naturally over time and can be represented as Dynamic Bayesian Network (DBN) (e.g., Murphy 2002). Dynamic Bayesian network (DBN) models allow more complex dependencies to be modeled but often require more complex algorithms for learning and inference. Previous work by Aleks et al. (2008) described the successful use of a Bayesian Network approach to improve intensive care unit patient monitoring by modeling both the physiology and measurement equipment. A similar, but minimally validated, approach was also described by Borsotto et al. (2004), where they describe a large Bayesian Network to estimate warfighter life sign status from non-invasive physiological status monitors. In Chapter 3 we develop a Bayesian network representation of the human thermoregulatory system as a starting point in the core body temperature estimation problem.

2.3 Policy Estimation for Managing Thermal-Work Strain

2.3.1 Work Rest Tables

Current techniques to manage the long term thermal safety and performance of individuals are based upon work-rest tables (OSHA 1985, TBMED 507, 2003). These tables prescribe alternating periods of work and rest, with the duration of each phase based upon the environmental conditions, proposed work rates, and protective equipment being worn. These tables were initially based on empirical data collected from large scale field studies (Yaglou and Minard, 1956, 1957; and Minard 1961). These studies also formed the basis of summarizing environmental conditions as a single index that tried to encompass air temperature, humidity, wind and the effect of direct sunlight. The wet-bulb globe temperature (WBGT) is shown in Equation 2.15 (see TBMED 507, appendix B).

$$WBGT = 0.7T_w + 0.2T_g + 0.1T_a \,, \tag{2.15}$$

where T_w is the wet-bulb temperature ("the wet-bulb temperature is the lowest temperature that can be reached under current ambient conditions by the evaporation of water only"[4]), T_g is the globe temperature which measures the temperature inside a standard size black globe (and is an indication of the added effect of solar radiation), and T_a is the air temperature. An example of a work rest guidance table is shown in Figure 2.11. This Figure shows the US Army's field guidance for work rest schedules for given work rates and environments as measured by the WBGT index. While the original tables were generated from empirical data modern versions are based on human thermoregulatory models such as SCENARIO (Kraning and Gonzalez 1997).

[4] Wikipedia: http://en.wikipedia.org/wiki/Wet-bulb_temperature, Accessed 1/19/2015.

Easy Work	Moderate Work	Hard Work
• Weapon Maintenance • Walking Hard Surface at 2.5 mph, < 30 lb Load • Marksmanship Training • Drill and Ceremony • Manual of Arms	• Walking Loose Sand at 2.5 mph, No Load • Walking Hard Surface at 3.5 mph, < 40 lb Load • Calisthenics • Patrolling • Individual Movement Techniques, i.e., Low Crawl or High Crawl • Defensive Position Construction	• Walking Hard Surface at 3.5 mph, ≥ 40 lb Load • Walking Loose Sand at 2.5 mph with Load • Field Assaults

Heat Category	WBGT Index, F°	Easy Work		Moderate Work		Hard Work	
		Work/Rest (min)	*Water Intake (qt/hr)*	*Work/Rest (min)*	*Water Intake (qt/hr)*	*Work/Rest (min)*	*Water Intake (qt/hr)*
1	78° - 81.9°	NL	½	NL	¾	40/20 min	¾
2 (GREEN)	82° - 84.9°	NL	½	50/10 min	¾	30/30 min	1
3 (YELLOW)	85° - 87.9°	NL	¾	40/20 min	¾	30/30 min	1
4 (RED)	88° - 89.9°	NL	¾	30/30 min	¾	20/40 min	1
5 (BLACK)	> 90°	50/10 min	1	20/40 min	1	10/50 min	1

Figure 2.11: U.S. Army work rest schedules based upon human thermoregulatory models.

While these tables address both the acute and chronic thermal-work strain concerns, they do not take into account the actual state of the human. Without accounting for an individual's continuous thermal-work strain response to the environment and work goals these schedules are by necessity conservative trying to ensure that 95% of the population do not experience heat injury. This conservatism almost certainly means that that they provide sub-optimal performance over the course of proscribed work.

Both the National Institute for Occupational Safety and Health (NIOSH) and the Occupational Safety and Health Administration (OSHA) suggest how the intermittent measurement of heart rate, core body temperature (oral thermometer) can help modify work-rest schedules for individuals. The guidance originally based on recovery time work by Brouha 1960, and Fuller and Smith (1980, 1981) shows how the work rest schedules can be modified. Table 2.5 shows how to modify work rest schedules by taking pulse or oral thermometer readings during rest periods.

Table 2.5: Modified work rest guidance based upon spot measure of heart rate or core body temperature.

	At beginning of rest period	Next work period adjustment (time multiplier)
Heart Rate (beats/min.)	>110	0.67
Core Temperature (°C)	>37.6	0.67

While these methods are useful in providing conservative bounds on preventing heat injury NIOSH (1986) admits that:

"…they do not permit a prediction of which individuals will become heat casualties. Because of the wide inter-individual tolerance to heat stress, predictions of when and under what circumstances an individual may reach unacceptable levels of physiologic and psychologic strain cannot be made with a high degree of accuracy. One solution to this dilemma might be and individual heat-load dosimeter."

Individual differences can be quite large. Figure 2.12 shows the individualized thermal-work strain responses from seven National Guard Weapons of Mass Destruction Civil Support Team (WMD-CST) members as they conduct a 45 minute movement while wearing fully encapsulating level "A" chemical/biological personal protective suits. Although the team members are doing exactly the same task, the thermal-work strain ranges from moderate (5) to very high (10). Almost half of the team have thermal-work strain index scores indicating a high risk of heat illness (see Tharion et al., 2013b).

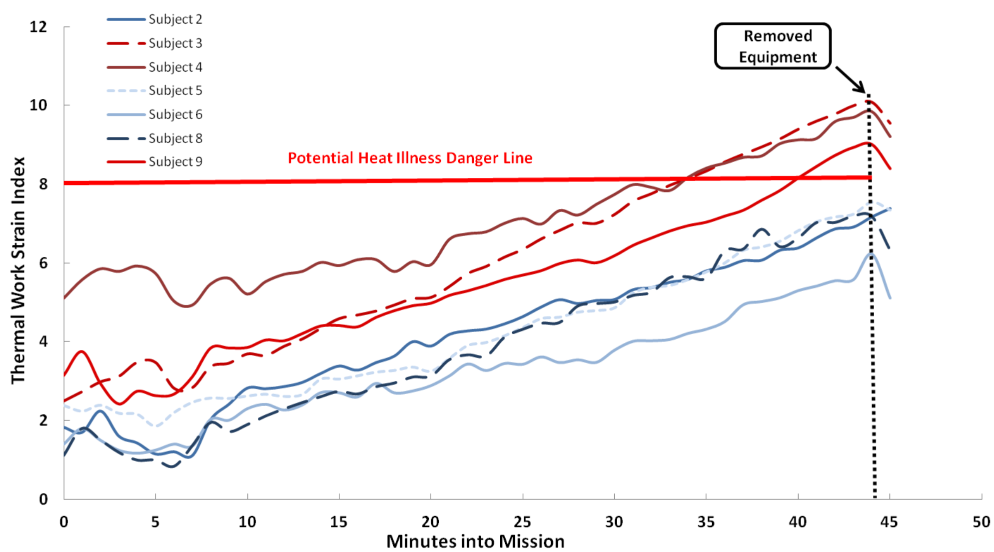

Figure 2.12: Individual differences in thermal-work strain index score for seven volunteers walking for 45 minutes in level A chemical/biological personal protective suits. Used by permission of the author (in Tharion et al., 2013b).

As human-thermoregulatory models have increased in sophistication adjustments can be made for individual characteristics such as age, height, weight and body fat allowing work rest schedules to be more tailored or to provide team managers with a range of risk. Figure 2.13 shows an example of a computer application that uses the Heat Strain Decision Aid (HSDA) human thermo-regulatory model to examine the impact of a timed U.S. Army road march across a range of individuals.

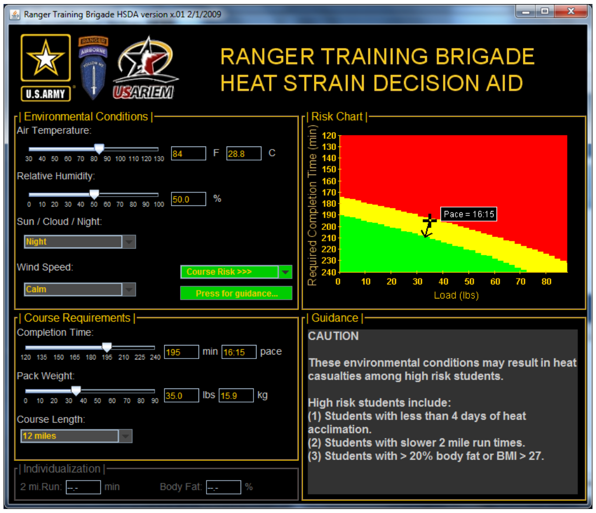

Figure 2.13: A tool that provides a range of risk based upon a spectrum of individuals and shows that risk by movement pace and load carried.

Timing of policy interventions is important. Buller et al. (2009) examined the physiological responses of three U.S. Marines at the end of a 90 minute foot patrol completed in hot dry conditions. While all the Marines rested, one removed their body armor, while the others did not. Previous analysis showed that removal of body armor when core temperatures were at resting levels had limited impact. However, removal of the body armor at the end of the foot patrol had a dramatic effect. For the Marine who removed body armor both skin temperature and core body temperature dropped by >2 ºC during a rest period (see Figure 2.14). A timely intervention of this sort also has long term consequences. Even though the other two Marines, who did not remove body armor rested they showed no skin temperature change and core body temperature declined by only a small amount 0.6 ºC in 30 minutes. Modeling work suggested that this Marine had more reserve capacity to accomplish missions with more demanding work rates. Thermoregulatory models showed that this Marine could work at a moderate intensity (patrolling or carrying out individual movement techniques, ~440W) for at least an additional 50 minutes. In contrast the other two Marines who only rested would reach critical thermal-work strain thresholds in less than 30 minutes.

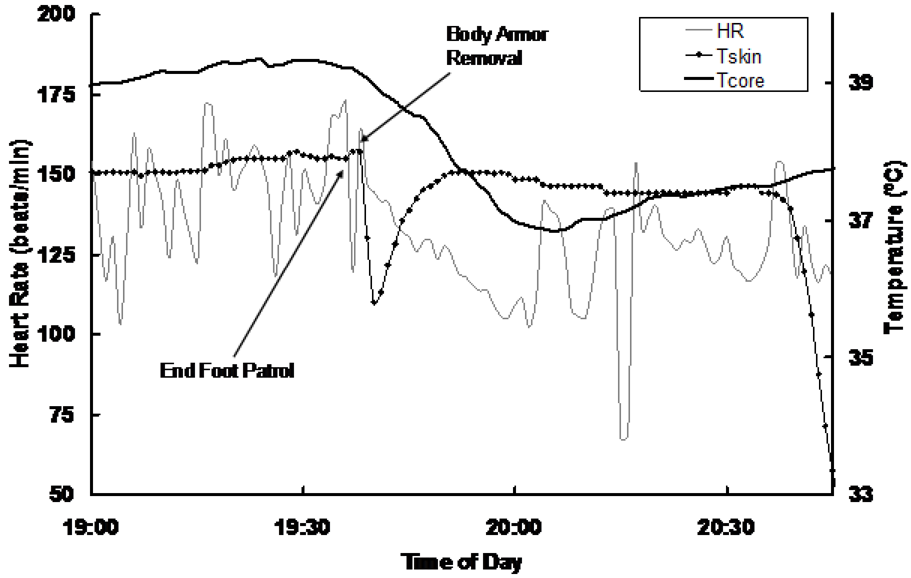

Figure 2.14: Individual physiology response to body armor removal at the end of a thermally stressful patrol.

In addition to knowledge of when and what to do, some evidence exists that there is a cumulative effect of thermal-work strain over time. Work by Horn et al. (2013) showed increasing thermal-work strain in firefighters over the course of a series of live fire training events. Horn's results indicated how physiological monitoring would be more important as the duration of an emergency response increases.

2.3.2 Pacing and Pacing Strategies in Competitive Sports

Pacing in competitive sports is an attempt to optimize an individual's energetic resources with the demands of the event and the environment. An athlete may approach an event with a pacing strategy based upon an understanding of the event demands and their own learned experience (Roelands et al., 2013). Their predefined pacing strategy may be modified during the event based upon the environmental conditions, the athlete's volition (Robsinson et al., 1958), and the onset of fatigue.

In their review article, Abbiss and Laursen (2008) identify six different pacing strategies found in competitive sports. "Negative" pacing, often found in "middle distance" events, is where both power and speed are increased at the end of the event from a slow start. The slower start is thought to minimize early carbohydrate depletion and limit early accumulation of fatigue inducing metabolites. "All-Out" pacing, as the name suggests, is best used in short distance events such as sprints. "Positive" pacing is where athletes start at a fast pace and then reduce their speed or power output throughout the race. This kind of profile can be seen in triathletes. However, as Abbis and Lausen (2008) admit, more work is necessary to determine if positive pacing is an optimal pacing strategy for these types of events. “Even” pacing is often found in sports where resistance of water or air plays an important role in the power output of the athlete. For example, in cycling races, where aerodynamic wind resistance is much higher compared to running, an optimal strategy may be to minimize the changes in acceleration through a medium that causes friction. “Parabolic” or “U” shaped pacing is where an athlete starts fast and then reduces speed in the middle of the race only to increase speed towards the end. In many instances, this speed increase can be thought of as the final sprint to the finish. Finally, “variable” pacing has been shown to provide improvements in cycling race times where athletes adjust their power output depending on the course. More power output during uphill sections, and less power output on downhill sections.

A pacing strategy is selected by an athlete depending on the anticipated exercise duration and their own prior experience (Roelands et al., 2013; Knechtle et al., 2014; Bertuzzi et al., 2014). However, different physiological responses to exercise are critical for determining performance over different time frames (de Konig, 2011). For short duration events <30 minutes, the changes in intra-muscle metabolism play an important role in determining muscle power output. Core body temperature plays an important role in determining fatigue for exercise durations from 30 minutes to 120 minutes (Nielsen et al., 2001; Gonzalez-Alonzo et al., 2008; and Laurensen, 2009). For events that are longer than 90 minutes, the availability of carbohydrates play an increasingly important role (Coyle et al., 1983; Karlsson and Saltin, 1971).

“Positive” pacing, where there is a fast start followed by a reduction in pace, is the typical pattern for prolonged exercise (>30 minutes) (Roelands et al., 2013). This pattern is also found in team sports such as soccer where Waldron and Highton (2014) found a “gradual decline in total running intensity”.

The addition of a hot environment poses an additional problem for pacing. Hot environments have been shown to impair both performance and time to exhaustion (Galloway and Maughan 1997). Several mechanisms have been suggested for this reduction in performance. Some have suggested that fatigue is induced, as a “critical core temperature” is approached (>39 °C), as a way for the body to guard against catastrophic collapse. Others have suggested that the body uses an anticipatory feed-forward control mechanism to regulate the rate of heat storage (see review by Cheung 2007). Ely et al. (2010) demonstrated that even with modest hyperthermia (CT <38.5 °C), performance in time trials was significantly reduced in the heat. Their work has also shown that the subjects started the hot time trial at a similar pace to the trial under temperate conditions. Recent work indicates that the onset of fatigue is driven by a complex integration of the state of the peripheral muscles/peripheral sensory system and the central nervous system

(Amann 2011). *"This complex regulatory system adapts the work rate in order to optimize performance and to prevent potentially harmful (e.g. catastrophic) changes to homeostasis"* (Roelands et al., 2013).

This control mechanism can be seen to great effect in the work by Adams et al. (1975) as they studied the thermoregulatory system of a marathon athlete across cold, moderate, and hot environments. In the cold (10 °C) and moderate (22 °C) conditions, heart rate, core body temperature and sweat rate were similar. For these two temperature conditions, the heart rate, sweat rate, and core body temperature were maintained throughout the run. For the hot condition (35.5 °C), the initial core body temperature was similar to the cold and moderate conditions for the first hour, as was sweat rate. However, heart rate increased in a linear fashion. At about 90 minutes, there was a marked increase in the rise of core body temperature and sweat rate until the athlete had to stop when CT >40.2 °C. It appeared that while the body was trying to regulate the heat gain from the run, at around 90 minutes, homeostasis was no longer possible leading to significant heat gain.

Ulmer (1996) proposed an optimization control mechanism of "teleoanticipation". Here they integrate the concept of the previous feedback control mechanisms with a central optimizer "programmer" that also controls metabolic rate in anticipation of the required work necessary to complete a bout of exercise. St. Clair-Gibson and Noakes (2004) extend this concept of a central programmer into, as they term "a complex non-linear dynamic system." Here they suggest that a "central integrator" can plan a pacing strategy based upon a known distance and required performance. As evidence, they cite the fact that humans can "faithfully reproduce almost identical pacing strategies" with little overt feedback. They also draw evidence from how ants can accurately determine distance over differing terrains, and how migratory birds can assess the metabolic requirements of their travels. Further, the "central integrator" continually adjusts the pacing strategy based upon the perception of the current physical state of exhaustion. While their paper suggests a theory of pacing control, they do not provide an actual model. Tucker (2009) proposes a conceptual model of how the state of "physical exhaustion" can be measured and modeled using the subjective Rating of Perceived Exertion (RPE) scale. Figure 2.15 shows his dynamical system model.

Of note is that this model is very similar to our physiological feedback loop. There is a known goal, a perception of the physiological state through the subjective RPE scale, and a "template" or policy that the brain uses to modulate pacing. There is also the concept of the distance remaining to the goal which in combination with RPE is important for adapting pace (Konig et al., 2011).

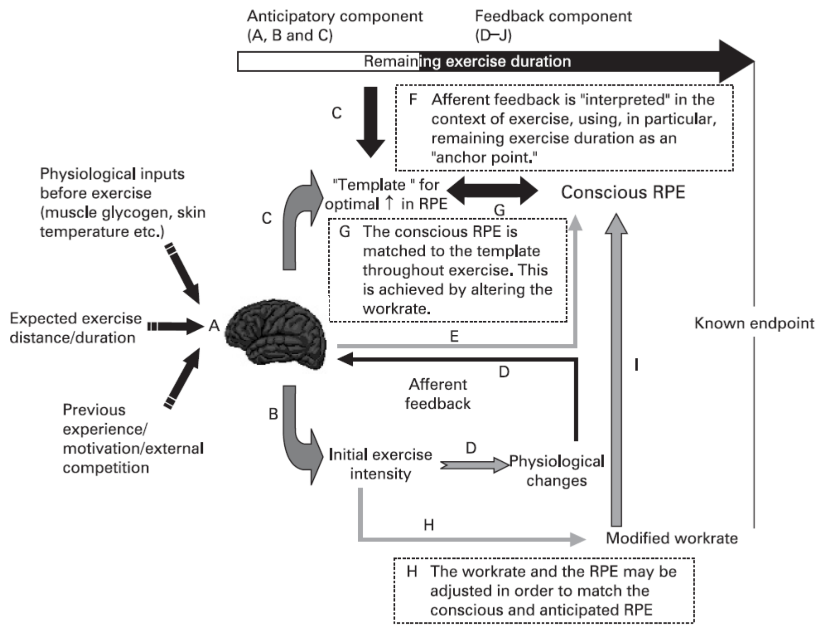

Figure 2.15: From Tucker (2009): "Schematic diagram showing the model for the anticipatory regulation of exercise performance during self-paced exercise. Black shading denotes input to the brain; grey shading denotes output or efferent processes. RPE, rating of perceived exertion."

Where our work differs is that we plan to learn this "hidden" policy offline from thermo-regulatory models and use it to provide optimal pacing strategies in real-time for a novel task. Additionally, instead of using the subjective rating of perceived exertion, we intend to monitor, physiology, directly to infer thermal-work strain state. It is unclear whether the "templates" used by the brain are innate or learned. For experienced athletes it appears they have a reasonable internal template. However, for new and novel tasks it is unclear how well their "templates" are optimized. An additional question is, that with the added stressor of heat, would the RPE still be as helpful in determining pace. Learned "templates" appear to still be used even when heat is added as an additional factor. In work by Soule et al. (1978) volunteers learned to complete a timed foot movement in a hot environment. The movement was self-paced and could be replicated. Volunteers were then placed in a thermally more stressful environment (relative humidity was increased), and told to complete the same self-paced task, but were also instructed to not get "too hot". Soule et al. (1978) found that the original learned "template" was followed and was not modified by the added environmental stressor which caused many volunteers to stop from heat exhaustion.

2.3.3 Markov Decision Process Models Applied to Humans

The physiological feedback loop presented in Figure 1.2 is analogous to a partially observable dynamical system control problem. For our purposes, an overall work goal may be to travel a set distance in a certain amount of time given certain environmental conditions and while wearing personal protective equipment. A policy (Π) may be set that prescribes a series of movements at different speeds to accomplish the goal. The policy will dictate a series of different actions (A) or movement speeds for the individual. These movement speeds will have different impacts on the thermal-work strain state of the individual and progress to the ultimate goal. By perceiving the thermal-work strain state, our problem is to optimally control the pace of the individual to minimize immediate thermal-work strain risk and to allow completion of the goal with the least thermal-work strain possible.

Bellman (1957b) developed a method to solve this kind of optimization problem by developing a discrete stochastic form of this type of dynamical system as a Markov decision process (MDP) and introducing the idea of an "optimal return function". In the MDP form, the optimized control problem of the dynamical system can be represented by a set of discrete system states (s), a set of possible actions (a), a reward function ($R(s)$) that assigns a value for being in a certain state, and a state transition probability model $P(s'|s,a)$. The MDP, can be optimized by finding the sequence of states that return the most value. The goals to be modeled by the MDP framework have a finite horizon and thus the utility of a sequence of states can be computed from the sum of rewards for being in each state over time. The Bellman equation (2.16) computes the utility (U) of being in any state and all subsequent states, assuming that all subsequent actions are optimal.

$$U(s) = \mathrm{R(s)} + \gamma \max_{a \in A(s)} \sum_{s'} P(s'|s,a) U(s'), \tag{2.16}$$

where $\gamma \in [0,1)$ is a discount factor that indicates the importance of future rewards.

For any starting state an optimal set of actions can be found using dynamic programming (Bellman 1957a). An overview of other methods to solve this kind of reinforcement learning problem can be found in Sutton and Barto (1998).

2.3.4 Human MDP Real-Time Applications

There are limited applications where MDPs have been used in real-time with humans. Atkinson et al. (2003) describe a desired application for cycling that would provide optimal pacing strategies for different race profiles, but provide no details on how such an application would be constructed. Physiological monitors that track activity and/or heart rate are being used with some virtual training applications (Chi-Wai et al., 2011). Applications can provide guidance to improve training based on exercise at the right heart rate intensity or activity profiles, that over time, will meet the Center for Disease Control (CDC) guidelines. A more advanced system proposed by Lopez-Matencio et al. (2010) uses a k-nearest neighbors approach to advise runners, in real-time, which training track to take. Track advice is based upon their current heart rate, desired training heart rate, track footing, and ambient temperature. However, these applications focus on open ended goals versus the time, safety and performance constraints placed upon emergency workers.

Hoey et al. (2007) developed a real-time system that models teeth brushing in terms of an MDP. This model is used to provide dementia patients guidance based upon real-time monitoring of their hand locations. Osais, Yu and St-Hilaire (2010) utilize an MDP model to provide optimal management of implanted rechargeable biosensors, controlling the sampling schedule and recharge schedule of the device. The paper examines constraints that the device cannot get too hot and must provide the longest period of sampling possible.

Using the MDP as a basic framework for our physiological feedback loop and using available modern physiological monitoring systems, there are two components that need solutions to make the system viable: thermal-work strain state estimation, specifically core body temperature estimation; and pacing policy estimation.

Chapter 3

Thermal-Work Strain State Estimation

From our review of the literature, thermal-work strain state can be estimated using the physiological strain index developed by Moran et al. (1998). This thermal-work strain index (TWSI) is a weighted combination of heart rate (HR) measurements and core body temperature measurements (CT). But as we showed measuring CT in an ambulatory setting using non-invasive sensors is an open problem. While are many physiological monitoring devices that measure HR, the ability to estimate thermal-work strain rests with the ability to estimate or measure CT. Thus, the goal of this work was to accurately estimate CT to allow the computation of the TWSI and thus assess an individual's latent thermal-work strain state.

This chapter details this work in three sections. In section 3.1 we show how a computational physiology approach proved successful in developing a CT estimation technique. In this work we examined the underlying physiological processes and developed a dynamic Bayesian network model to estimate CT. In section 3.2, we show how we simplify the parameters from the dynamic Bayesian network model and use only HR as a "noisy" observation of CT in a Kalman filter framework. This section details how we validated the model using data from 89 subjects in both laboratory and field settings comparing how well our estimation technique works across different work rates, clothing configurations, environmental conditions, heat acclimation states, and hydration states. Section 3.3 details how the CT estimation technique has been implemented in a commercial physiological monitoring system and used as part of a real-time monitoring system. Here we detail the performance of the algorithm in use in three training events with first responders encapsulated in chemical/biological personal protective equipment. Section 3.4 concludes by showing how our computational physiology approach was able to provide a technique to estimate CT from sequential observations of HR alone, and how this technique is being adopted by the National Guard as a requirement for a real-time telemetry monitoring system.

3.1 Dynamic Bayesian Network Model of the Human Thermoregulatory System

In this section we develop a model that aims to represent the underlying physiology and interdependencies of human thermo-regulation. The intent is to accurately estimate CT from non-invasive sensors and gain insight into the internal physiological processes that govern CT. Graphical models provide a natural way to express the physiological variables and dependencies that form the basis of biological systems. By their nature, many physiological processes evolve naturally over time and can be represented as Dynamic Bayesian Network (DBN) (e.g., Murphy 2002). Previous work by Aleks et al. (2008) described the successful use of a Bayesian network approach to improve intensive care unit patient monitoring by modeling both the physiology and measurement equipment. A similar but minimally validated approach was also described by Borsotto et al. (2004), where they describe a large Bayesian network to estimate warfighter life sign status from non-invasive physiological status monitors.

Figure 3.1 shows the key factors that affect human CT represented as a Bayesian network. Starting from the center of Figure 3.1, we observe that human core body temperature (CT) is dependent on both heat production (HP) and heat transfer (HT) to or from the body's core. In most exercise situations HT, results in heat loss from the core. HP is primarily dependent on the body's metabolism (M). Metabolism is dependent on a number of factors such as individual anthropometric differences, circadian rhythm (CR), pharmaceutical use (PH), and fever (FV) to name a few. Heat is also generated from food digestion (TEF) and during useful work (W). Heat is generated as a byproduct of metabolism. In the case of useful work by muscles, heat is generated due to inefficiencies in converting fuel (e.g. glycogen) and oxygen to muscle action. Much of the energy released from the chemical reaction is converted to heat (~80%) versus useful work (~20%). Aerobic metabolism is dependent on the transport of oxygen (O2) from the lungs to the muscles. On a simplified level, this supply of O2 to tissues is dependent on cardiac output which has a heart rate (HR) and stroke volume component (SV). HR is helpful in estimating metabolic rate because of the well-known relationship of oxygen consumption to cardiac output derived from the Fick principle (Fick 1855) where the rate of oxygen consumption is equal to the cardiac output (HR x SV) multiplied by the arterio-venous difference in blood oxygen concentration; thus: $\dot{V}O_2 = (HR \cdot SV) \cdot \left(C_{\bar{a}_{O_2}} - C_{\bar{v}_{O_2}}\right)$.

Heat transfer (HT) to or from the body core is influenced by a number of mechanisms. Heat is actively lost through water evaporation from the respiratory tract (RHL). Heat is transferred passively between the core and skin by conduction through body tissue (PHC).

Finally, heat is transferred between the core and skin by blood flow (SBF). Heat transfer to/from the skin is dependent on four heat transfer mechanisms: convection, radiation, conduction and evaporation. The effectiveness of these mechanisms is dependent on the environment and the insulation and water permeability of the clothing being worn. As human body temperature is regulated within narrow bounds (~35 - ~41 °C, Sawka and Young, 2006, p535) any change in CT results in a thermoregulatory response (TR). The primary mechanism for human thermoregulation is the control of the flow of blood to the skin (SBF) by vaso-constriction or dilation in conjunction with sweating. The rate of blood flow to the skin is dependent on the cardiac stroke volume (SV) and heart rate (HR).

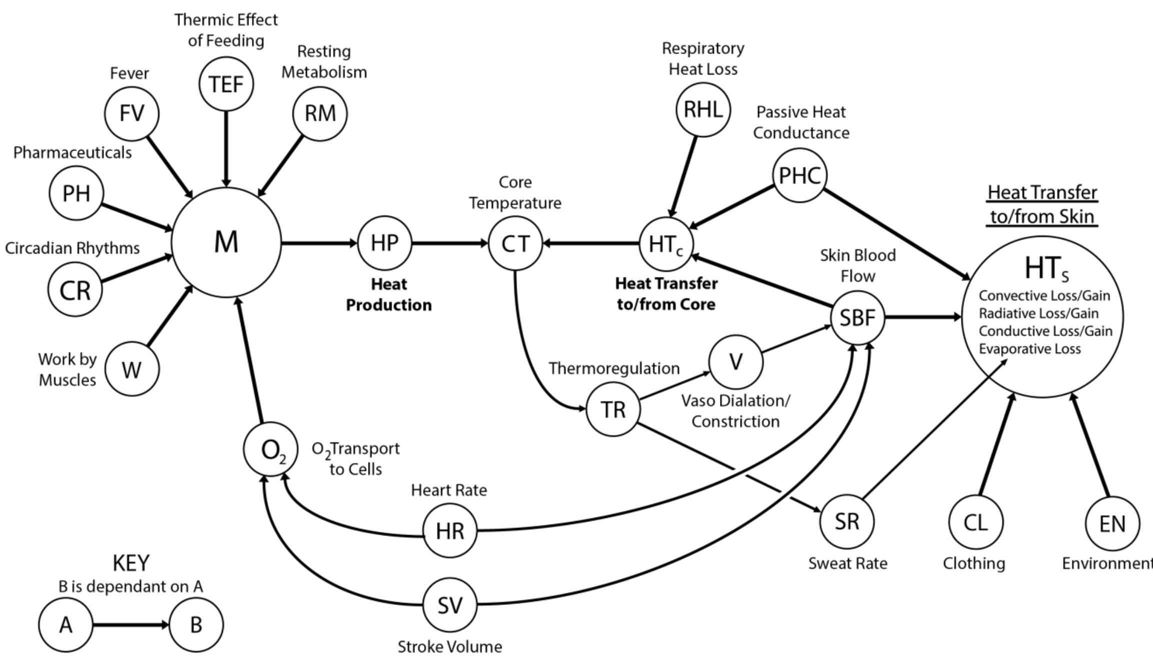

Figure 3.1: Factors affecting human core temperature (CT) represented as a Bayesian network. The figure shows CT at the center of the diagram with factors affecting heat production to the left and factors that provide heat transfer to or from the body core shown on the right. (See Sawka & Young, 2006; and Yokota et al., 2008).

3.1.1 Dynamic Bayesian Network Model

To simplify this complex Bayesian network, we constrain the problem to our specific area of interest, namely teams of young fit workers engaged in physical activity in warm environments. Under this constraint, we are not examining the case where fever (FV) or pharmaceuticals (PH) are affecting basal metabolic rates. In this area of interest, the change in CT from the other factors namely circadian rhythm (CR), thermic effect of food (TEF), and resting metabolic rate (RM), become negligible compared to the effect of physical activity (W). Thus, the heat production (left) side of our model can be simplified to one node to represent heat gain (HG) from exercise.

Similarly, the most effective means of heat transfer from the core to the environment is through the control of skin blood flow (SBF) and sweat rate (SR) which in exercise conditions overshadow the loss of heat through respiration (RHL) and the passive transfer of heat by conductance (PHC). As SBF and SR tend to work in tandem to effect cooling (Sawka and Young, 2006), the heat transfer portion (right) side of our model can be simplified to one node dependent on skin blood flow. For convenience, we label this heat loss (HL); acknowledging that heat can also be gained from the environment through this mechanism (i.e., negative heat loss). Figure 3.2 shows the graphical model representation of our DBN model.

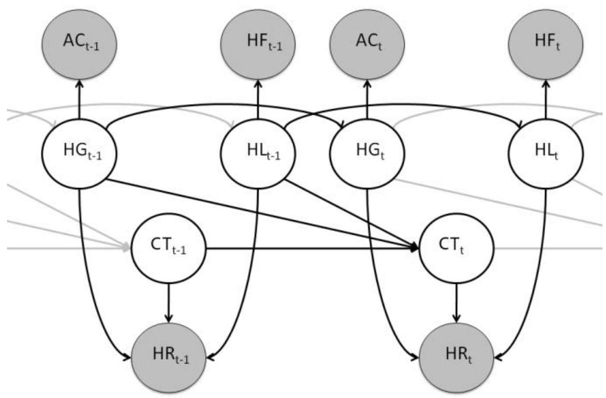

Figure 3.2: Physiology-based dynamic Bayesian network for thermoregulation. CT = core body temperature, HG = heat gain, HL = heat loss, HR = heart rate, AC = activity from accelerometry, and HF = heat flux. White nodes represent latent variables and gray nodes are observed variables.

Both HG and HL are dependent on cardiac output which has heart rate (HR) and stroke volume components. Stroke volume amongst individuals varies significantly, but for a given normal individual remains relatively constant, changing with levels of aerobic fitness and dehydration. Stroke volume is very difficult to measure in an ambulatory setting, and it would be convenient if we could remove this component from our model. Ideally, we would like to assume that given a matched population (age, gender and fitness), stroke volume will vary amongst individuals for a given relative work rate (i.e., percent of maximal aerobic capacity) such that HRs and CTs will respond similarly across the group. For our purposes, this assumption allows us to use HR instead of cardiac output. In a recent paper, we demonstrated that this assumption holds true as environmental conditions, heat acclimation, hydration level, and clothing encumbrances are varied (Buller et al., 2011).

Finally, in constructing the model we use measures from accelerometry (AC) to provide an independent observation of HG, and heat flux (HF) to provide an independent observation to HL. For HG, we assume that greater accelerations measured on the body mean more physical work and thus more HG. By measuring heat flux on the skin, we have a point measurement of heat transfer to the environment which we assume can be used as a "noisy" observation of HL.

As this is a directed acyclic graph, the joint distribution across all random variables can be factored by the chain rule for Bayesian networks as follows:

$$P(Y) = \prod_i P(Y_i | Y_{\Gamma(i)}) \tag{3.1}$$

Where *Y* is the set of random variables {AC, HF, HR, HG, HL, CT, CTt-1, HGt-1, HLt-1}, and Y_Γ refers to the joint distribution of the parents of node Xi. Thus:

$$P(Y) = P(AC|HG)P(HR|HG, HL, IT)P(HF|HL)\cdot$$
$$P(HG|HG_{t-1})P(HL|HL_{t-1})P(IT|HG_{t-1}, HL_{t-1}, IT_{t-1}) \tag{3.2}$$

Our model then can be defined by the conditional probability distributions (CPDs) of these factors. From our model and any series of observations of *X*={AC, HR, HF}, we wish to be able to infer the latent variables *Z*={HG, HL, CT} or the posterior distribution P(Z|X). By assuming that our CPD are Gaussian, we can make use of the Kalman filter (Kalman, 1960) algorithm to iteratively compute the latent variable probability density functions for a given series of observations.

3.1.2 Inference

The Kalman filter is a Gaussian filter where the posterior probability density of the latent variables is computed iteratively from "noisy" observations. The Kalman filter is defined by the following probability density functions:

Transition: $$p(\mathbf{z}_t | \mathbf{z}_{t-1}) = N(\mathbf{z}_t | \mathbf{A}\mathbf{z}_{t-1}, \boldsymbol{\Gamma}) \tag{3.3}$$

Observation: $$p(\mathbf{x}_t | \mathbf{z}_t) = N(\mathbf{x}_t | \mathbf{C}\mathbf{z}_t, \boldsymbol{\Sigma}) \tag{3.4}$$

Our DBN model can be defined in terms of the Kalman filter probability density functions, where our latent variable vector $\mathbf{z}_t$ = [hg_t, hl_t, it_t], and our observation vector $\mathbf{x}_t$ = [ac_t, hr_t, hf_t,]. The Kalman filter probability density functions are defined by the following matrices:

$$\mathbf{A} = \begin{pmatrix} \mathbf{a_1} & \mathbf{0} & \mathbf{0} \\ \mathbf{0} & \mathbf{a_2} & \mathbf{0} \\ \mathbf{a_3} & \mathbf{a_4} & \mathbf{a_5} \end{pmatrix} \boldsymbol{\Gamma} = \begin{pmatrix} \boldsymbol{\gamma_1} & \mathbf{0} & \mathbf{0} \\ \mathbf{0} & \boldsymbol{\gamma_2} & \mathbf{0} \\ \mathbf{0} & \mathbf{0} & \boldsymbol{\gamma_3} \end{pmatrix} \mathbf{C} = \begin{pmatrix} \mathbf{c_1} & \mathbf{0} & \mathbf{0} \\ \mathbf{c_2} & \mathbf{c_3} & \mathbf{c_4} \\ \mathbf{0} & \mathbf{c_5} & \mathbf{0} \end{pmatrix} \boldsymbol{\Sigma} = \begin{pmatrix} \boldsymbol{\sigma_1} & \mathbf{0} & \mathbf{0} \\ \mathbf{0} & \boldsymbol{\sigma_2} & \mathbf{0} \\ \mathbf{0} & \mathbf{0} & \boldsymbol{\sigma_3} \end{pmatrix}$$

For this model definition, variables have been normalized to have a zero mean and ± 1 standard deviation = ± 1 units. The transition matrix **A** defines how HG, HL, and CT map from one time step to the next. The covariance matrix **Γ** is the variances associated with this mapping function. Matrix **C** defines how the latent variables map to the observed variables. Similarly, matrix **Σ** holds the variances associated with these mapping functions.

The transition mean and covariance and the observation mean and covariance matrices must be learned. σ_{it}^2 was learned from our previous research. The initial state means (hg_0, hl_0, and it_0) can be set to normal human resting values and the starting covariance matrix V_0 has entries that are high as we are uncertain about our initial guess for the latent variables.

At each time step, the Kalman filter uses (1) a prediction step that estimates current latent variable estimates ($\widehat{\mathbf{z}_t}$) and their associated variances ($\widehat{\mathbf{V}_\mathbf{t}}$) based upon the previous time step, and (2) an update step where these estimates are updated based upon the current observations. The prediction and update steps follow the basic Kalman filter equations as outlined by Welch and Bishop (1995).

(1) Prediction step: $\widehat{\mathbf{z}_t} = \mathbf{A}\mathbf{z}_{t-1}$ (3.5)

$\widehat{\mathbf{V}_\mathbf{t}} = \mathbf{A}\mathbf{V}_{t-1}\mathbf{A}^T + \boldsymbol{\Gamma}$ (3.6)

(2) Update step: $\mathbf{z}_t = \widehat{\mathbf{z}_t} + \mathbf{K}_t(\mathbf{y}_t - \mathbf{C}\widehat{\mathbf{z}_t})$ (3.7)

$\mathbf{V}_t = (\mathbf{I} - \mathbf{K}_t\mathbf{C})\,\widehat{\mathbf{V}_\mathbf{t}}$ (3.8)

$\mathbf{K}_t = \widehat{\mathbf{V}_\mathbf{t}}\mathbf{C}^T(\mathbf{C}\widehat{\mathbf{V}_\mathbf{t}}\mathbf{C}^T + \boldsymbol{\Sigma})^{-\mathbf{1}}$ (3.9)

While the Kalman filter provides the basis for our inference, the model parameters $\boldsymbol{\theta}$ = {**A, Γ, C, Σ**} must be learned. Initial states for our latent variables (defined by $\mathbf{z}_0$ and $\mathbf{V}_0$) are assumed to take starting values typical of those found in a resting human.

3.1.3 Parameter Learning – Expectation Maximization

Expectation - Maximization (EM) (Dempster, Laird, and Rubin 1977) is an iterative algorithm that finds the maximum likelihood estimates of model parameters in cases where some of the variables are unobserved. The algorithm uses a two-step process. In the first step or E-step, the expected values of the latent variables (Z) are estimated using a current set of model parameters and observed data (X). In the second step, the M-Step, the model parameters are maximized according to the complete-data log likelihood P(Z,X|θ) with respect to the posterior distribution P(Z|X,θ). Ghahramani and Hinton (1996) and Bishop (2006) provide an overview of the EM approach for linear dynamical systems which is briefly reviewed here.

E-Step

The E-Step requires the computation of the posterior distribution of the latent variables P(Z|X, θ) to enable the computation of several expectations ($E[\mathbf{z}_t|\{\mathbf{x}\}]$, $E\left[\mathbf{z}_t\mathbf{z}_t^{\mathbf{T}}|\{\mathbf{x}\}\right]$ and $E\left[\mathbf{z}_t\mathbf{z}_t^{\mathbf{T}}|\{\mathbf{x}\}\right]$) that are necessary in the M-Step. These expectations require that the estimates of $\mathbf{z}_t$ are calculated using data from both the past and future. The Kalman filter alone only provides a posterior marginal of $\mathbf{z}_t$ based upon past and the current observations. The Kalman smoother equations (developed by Rauch et al., 1965; and presented in their current form by Jazwinski, 1970; and Shumway and Stoffer 1982) use values from the Kalman filter forward pass to compute the true marginals of $\mathbf{z}_t$ in a backward pass.

Kalman Smoother Equations

The Kalman smoother equations depend on a forward run of the Kalman filter to provide the values $\mathbf{z}_t$, $\mathbf{V}_t$, and $\widehat{\mathbf{V}}_t$ (computed in the prediction step) and take the following form:

$$\mathbf{z}_t' = \mathbf{z}_t + \mathbf{J}_t(\mathbf{z}_{t+1}' - \mathbf{A}\mathbf{z}_t) \tag{3.10}$$

$$\mathbf{V}_t' = \mathbf{V}_t + \mathbf{J}_t(\mathbf{V}_{t+1}' - \widehat{\mathbf{V}}_t)\mathbf{J}_t^T , \tag{3.11}$$

where: $\mathbf{J}_t = \mathbf{V}_n\mathbf{A}^T(\widehat{\mathbf{V}}_t)^{-1}$.

The expectations can now be defined for use in the M-step:

$$E[\mathbf{z}_t|\{\mathbf{x}\}] = \boldsymbol{z}_t'$$

$$E\left[\mathbf{z}_t\mathbf{z}_t^{\mathbf{T}}|\{\mathbf{x}\}\right] = \mathbf{V}_t' + \mathbf{z}_t'\mathbf{z}_t'^T$$

$$E\left[\mathbf{z}_t\mathbf{z}_{t-1}^{\mathbf{T}}|\{\mathbf{x}\}\right] = \mathbf{J}_{t-1}\mathbf{V}_t' + \mathbf{z}_t'\mathbf{z}_{t-1}'^T \tag{3.12}$$

M-Step

In the M-step, we wish to maximize the function $Q(\boldsymbol{\theta}, \boldsymbol{\theta}^{\text{old}})$ which is defined as the expectation of the data log likelihood with respect to the posterior distribution given by the model parameters θ:

$$Q(\boldsymbol{\theta}, \boldsymbol{\theta}^{old}) = E_{z|\theta^{old}}[\ln p(\mathbf{Z}, \mathbf{X}|\boldsymbol{\theta})], \tag{3.13}$$

where:

$$\ln P\,(\mathbf{Z}, \mathbf{X}|\boldsymbol{\theta}) = \ln p\,(\mathbf{z}_1|\mathbf{z}_0, \mathbf{V}_0\,) + \textstyle\sum_{t=2}^{T} \ln p\,(\mathbf{z}_t|\mathbf{z}_{t-1}, \mathbf{A}, \boldsymbol{\Gamma}) + \sum_{t=1}^{T} \ln p\,(\mathbf{x}_t|\mathbf{z}_t, \mathbf{C}, \boldsymbol{\Sigma}). \tag{3.14}$$

By substituting Gaussian probability density functions and taking the expectation:

$$E_{z|\theta^{old}}[\ln P\,(\mathbf{Z}, \mathbf{X}|\boldsymbol{\theta})] = -E_{z|\theta^{old}}\left[\tfrac{1}{2}(\mathbf{z}_1 - \mathbf{z}_0)^{\mathrm{T}}\mathbf{V}_{\mathbf{0}}^{-\mathbf{1}}(\mathbf{z}_1 - \mathbf{z}_0)\right] - \tfrac{1}{2}\ln|\mathbf{V}_0| \tag{3.15}$$

$$-E_{z|\theta^{old}}\left[\textstyle\sum_{t=2}^{T}\tfrac{1}{2}(\mathbf{z}_t - \mathbf{A}\mathbf{z}_{t-1})^{\mathrm{T}}\boldsymbol{\Gamma}^{-1}(\mathbf{z}_t - \mathbf{A}\mathbf{z}_{t-1})\right] - \tfrac{\mathrm{T}-1}{2}\ln|\boldsymbol{\Gamma}| \tag{3.16}$$

$$-E_{z|\theta^{old}}\left[\textstyle\sum_{t=1}^{T}\tfrac{1}{2}(\mathbf{x}_t - \mathbf{C}\mathbf{z}_t)^{\mathrm{T}}\boldsymbol{\Sigma}^{-\mathbf{1}}(\mathbf{x}_t - \mathbf{C}\mathbf{z}_t)\right] - \tfrac{\mathrm{T}}{2}\ln|\boldsymbol{\Sigma}| + \;const \tag{3.17}$$

Equations (3.15 – 3.17) can maximized with respect to each of the Kalman filter PDFs individually. To maximize the observation PDFs only element (3.17) is dependent on **C** and **Σ**, and thus elements (3.15) and (3.6) become part of the constant term. To optimize the time dynamics which are dependent on the parameter **A** and **Γ** elements (3.15) and (3.17) become part of the constant term giving:

$$Q(\boldsymbol{\theta}, \boldsymbol{\theta}^{old}) = -E_{z|\theta^{old}}\left[\textstyle\sum_{t=2}^{T}\tfrac{1}{2}(\mathbf{z}_t - \mathbf{A}\mathbf{z}_{t-1})^{\mathrm{T}}\boldsymbol{\Gamma}^{-1}(\mathbf{z}_t - \mathbf{A}\mathbf{z}_{t-1})\right] - \tfrac{\mathrm{T}-1}{2}\ln|\boldsymbol{\Gamma}| + const \tag{3.18}$$

Similarly, for the observation parameters **C** and **Σ** Equation elements (3.15) and (3.16) become part of the constant term giving:

$$Q(\boldsymbol{\theta}, \boldsymbol{\theta}^{old}) = -E_{z|\theta^{old}}\left[\textstyle\sum_{t=1}^{T}\tfrac{1}{2}(\mathbf{x}_t - \mathbf{C}\mathbf{z}_t)^{\mathrm{T}}\boldsymbol{\Sigma}^{-\mathbf{1}}(\mathbf{x}_t - \mathbf{C}\mathbf{z}_t)\right] - \tfrac{\mathrm{T}}{2}\ln|\boldsymbol{\Sigma}| + \;const \tag{3.19}$$

Equations (3.18) and (3.19) can be maximized by taking the partial derivative with respect to each of the Kalman filter model parameters $\boldsymbol{\theta}$ = {**A, Γ, C, Σ**} to provide the following general M-step equations:

$$\mathbf{A}^{new} = (\sum_{t=2}^{T} E[\mathbf{z}_t \mathbf{z}_{t-1}^T])(\sum_{t=2}^{T} E[\mathbf{z}_{t-1} \mathbf{z}_{t-1}^T])^{-1} \quad (3.20)$$

$$\mathbf{\Gamma}^{new} = \frac{1}{T-1} \sum_{t=2}^{T} \left\{ E[\mathbf{z}_t \mathbf{z}_t^T] - \mathbf{A}^{new} E[\mathbf{z}_{t-1} \mathbf{z}_t^T] - E[\mathbf{z}_t \mathbf{z}_{t-1}^T] \mathbf{A}^{new^T} + \mathbf{A}^{new} E[\mathbf{z}_t \mathbf{z}_t^T] \mathbf{A}^{new^T} \right\} \quad (3.21)$$

$$\mathbf{C}^{new} = (\sum_{t=1}^{T} \mathbf{y}_t E[\mathbf{z}_t^T])(\sum_{t=2}^{T} E[\mathbf{z}_t \mathbf{z}_t^T])^{-1} \quad (3.22)$$

$$\mathbf{\Sigma}^{new} = \frac{1}{T} \sum_{t=1}^{T} \left\{ \mathbf{x}_t \mathbf{x}_t^T - \mathbf{C}^{new} E[\mathbf{z}_t] \mathbf{x}_t^T - \mathbf{x}_t E[\mathbf{z}_t^T] \mathbf{C}^{new^T} + \mathbf{C}^{new} E[\mathbf{z}_t \mathbf{z}_t^T] \mathbf{C}^{new^T} \right\} \quad (3.23)$$

However, to maintain the sparse model structure, the individual elements of the model matrices are made explicit in Equations (3.4) and (3.5) and each individual parameter is optimized (i.e. a_1, a_2, a_3 ... $\boldsymbol{\sigma}_1$, $\boldsymbol{\sigma}_2$, $\boldsymbol{\sigma}_3$).

3.1.4 Experiments

Five distinct data sets were used for our experiments with a total of 23 volunteers. In all data sets, both observable model parameters (AC, HR, and HF) and the latent variable CT were collected. Table 1 presents the details of each of these studies.

Table 3.1: Model training and test data sets.

Data Sets	Description	Environment: Temp. (°C), RH (%)	n	Age (yr.), Ht. (m), & Wt. (Kg) (mean±SD)
Train: USA	Continuous 48 hr. military training exercise	21-23.5°C, 77-86% RH	7	26.8±2.1, 1.78±0.08, 85.7±6.2
A. Australia 1	5km march in encapsulating protective equipment	18°C, 72% RH,	8†	27.7±6.0, 1.95±0.09, 85.7±14.2
B. Australia 2	5 Hour high intensity military training exercise	15 – 20°C, 85 – 65% RH	8†	27.7±6.0, 1.95±0.09, 85.7±14.2
C. Afghan 1	4 hr. military patrol	13-22°C, 13-51% RH	4	21.0±1.7, 1.86±0.01, 92.5±15.3
D. Afghan 2	5 hr. military patrol	23-27°C, 13-18% RH	4	21.2±1.9, 1.77±0.04, 79.1±3.7

†Same Subjects, RH=Relative Humidity, SD=standard deviation.

CT data were collected using an ingestible thermometer pill (Jonah™ Core Temp. Pill, Mini Mitter, Bend, OR), while the non-invasive measures of AC, HR, and HF were collected using a chest worn physiological monitor (Equivital I, Hidalgo Ltd., Cambridge UK). Data set A was used for parameter and model learning. The DBN model CPD's were learned using Maximum Likelihood (ML), or EM. These CPD's were then used in the Kalman filter detailed in section 3.1.2 to infer CT given a sequence of AC, HR, and HF observations. Differences between the Kalman filter CT estimate and the observed CT were examined using summary statistics of root mean square error (RMSE), and non-parametric Bland-Altman percentage (BAP) (Bland and Altman 1999). The BAP calculates the percentage of estimated CT points falling within an a priori zone of the actual CT (± 0.5 ºC was used in this analysis). Differences between summary statistics are examined by paired Student's t-test or Analysis of Variance (ANOVA).

Individual model parameters were learned in the following way: Parameters a_1 and a_2 (HG and HL temporal mapping function), γ_1 and γ_2 (HG and HL temporal mapping function variances), c_1 - c_3 and c_5 (HG and HL observation mapping functions), and γ_1 and γ_2 (HG and HL observation mapping function variances) were learned using the EM algorithm. Parameters a_3 and a_4 (HG and HL to ΔCT mapping function) along with this function's variance was learned using Maximum Likelihood (ML). Parameters c_4 and σ_3 (CT to HR observation mapping function and variance) were learned using ML but modified according to Buller et al. (2010) to better account for steady state HR and CT values. Parameter a_5 and γ_3 used the values from our previous research (Buller et al., 2010), where γ_3 was modified with the variance from the HG and HL to ΔCT mapping function.

Model Implementation

Two methods of implementing the DBN model were examined. Method 1 implemented the model outlined in section 3 as a single DBN. Method 2 implemented the model using a Kalman filter for estimating ΔCT from HG and HL, which in turn was used to provide a temporal update in a second Kalman filter that estimates CT from HR. Figure 3.3 shows the two DBN models used for this method. The performance of each implementation was examined using RMSE and BAP statistics comparing inferred CT to observed CT for the seven subjects from the training data. We also used the model generated in our previous work (Buller et al., 2011), which used just HR to estimate CT, as a comparison baseline.

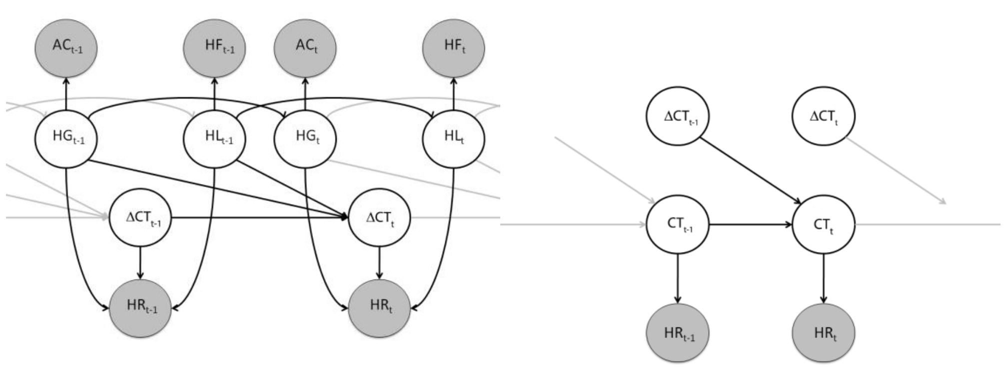

(A) (B)

Figure 3.3: Two Physiology-based dynamic Bayesian network models used for estimation of core body temperature (CT) from observations of heart rate (HR), activity from accelerometry (AC), and heat flux (HF). Panel (A) DBN model to estimate ΔCT. Panel (B): DBN model to estimate CT.

Heat Gain Estimation

As part of the "training" data total daily energy expenditure (TDEE) values were obtained for five of the seven subjects using the Doubly Labeled Water (DLW) method (Montoye et al., 1996). This method relies on differing rates of expulsion of isotopic water from the volunteers to measure TDEE. Assuming a fairly consistent efficiency factor (~20) from converting energy stores and oxygen to mechanical work, our model's HG parameter should be proportional to a minute-to-minute estimate of energy expenditure. To examine this relationship and our model's ability to accurately estimate HG, we summed our minute-to-minute estimates of HG and perform least squares regression with the measured TDEE values.

Model Validation

To test the generalizability of our model, we examined the RMSE and BAP using four new test conditions with different volunteers.

3.1.5 Results

Model Implementation

Table 3.2 shows the RMSE and BAP statistics for both methods of implementing the DBN. The two phase model performed significantly better than the single phase model for both the RMSE and BAP statistics $P<0.01$.

Table 3.2: RMSE and BAP statistics for the two model implementations.

DBN Implementation	RMSE (Mean ± SD °C)	BAP (Mean ± SD %)
Method 1: One Step Model	0.38 ± 0.09†	72.4 ± 11.4‡
Method 2: Two Step Model	0.27 ± 0.06†	86.6 ± 7.8‡

† ‡ Denotes significant difference $p<0.01$.

Figure 3.4, shows the typical results for observed CT and CT estimated from each of the two DBM implementations for one volunteer. Estimated CT from Method 1 is more attenuated than estimated CT from method 2.

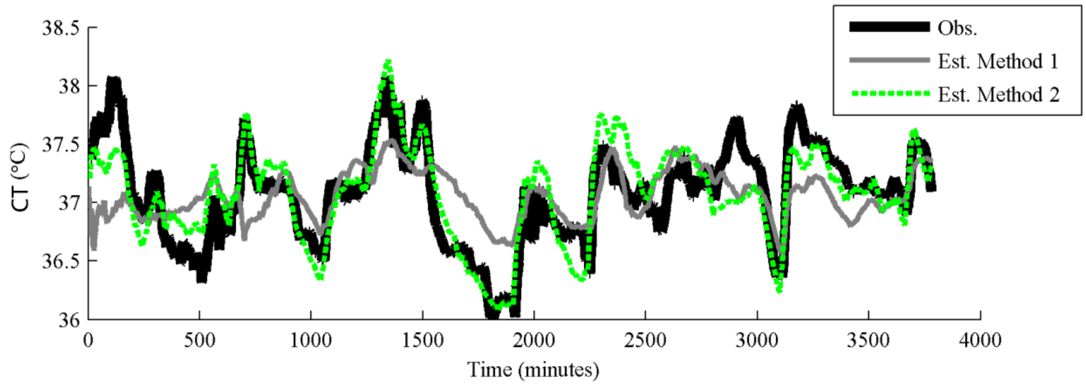

Figure 3.4: Typical CT estimation performance for each method for one volunteer.

The learned parameters for method 2 are as follows:

For kalman filter 1 to estimate HG and HL:

$$\mathrm{A} = \begin{pmatrix} 0.9569 & 0 \\ 0 & 0.9517 \end{pmatrix}, \mathrm{G} = \begin{pmatrix} 0.2799 & 0 \\ 0 & 0.2056 \end{pmatrix}, \mathrm{C} = \begin{pmatrix} 0.3869 & 0 \\ 0.5840 & 0.04323 \\ 0 & 0.6240 \end{pmatrix},$$

$$\mathrm{S} = \begin{pmatrix} 0.5053 & 0 & 0 \\ 0 & 0.0622 & 0 \\ 0 & 0 & 0.0290 \end{pmatrix}, \ \boldsymbol{z}_{\mathbf{hghl}} = \begin{pmatrix} hg \\ hl \end{pmatrix}, and\ \mathrm{x} = \begin{pmatrix} \boldsymbol{ac} \\ \boldsymbol{hr} \\ \boldsymbol{hf} \end{pmatrix}.$$

For kalman filter 2 to estimate CT: A = (1), G = (0.000784), C = (0.9197), S = (1.6876), D = (0.0057 -0.0005), z = (it), and x = (hr). The equation for the prediction step is:

$$\hat{z_t} = \mathbf{A}z_{t-1} + \mathrm{D}z_{\mathbf{hghl_{t-1}}} \tag{3.24}$$

Heat Gain Estimation

Figure 3.5 (Panel A and C), shows observed and estimated CT along with HG and HL estimations for the 2 step DBN model for one volunteer. Figure 3.5 (Panel B) shows a scatter plot of ΣHG versus TDEE values for the five subjects with TDEE data. One volunteer's TDEE value appeared excessively high, and TDEE data from an earlier time period are also presented.

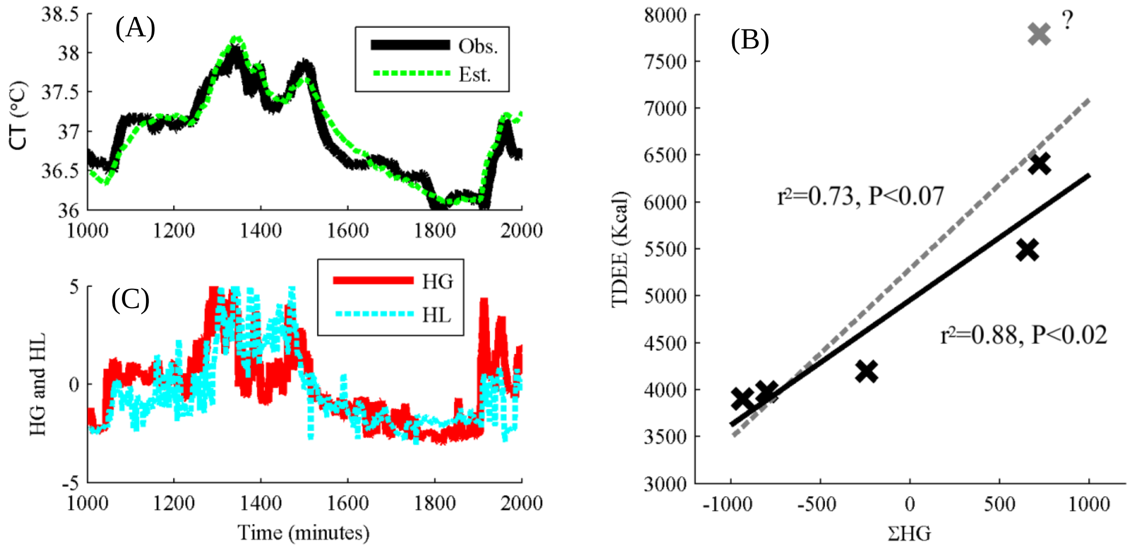

*Figure 3.5: Selected period of observed and estimated CT (**A**) to illustrate estimated HG and HL (**C**). (**B**) Correlation of ΣHG and TDEE. Gray dashed line in the least squares regression using an unusually high TDEE for one subject (marked '?'). Black solid line represents the regression equation using a prior estimate of TDEE.*

Model Validation

Overall, the DBN model has a bias of -0.01 °C and variance of 0.12 with a RMSE of 0.27±0.14 °C, and correctly estimates CT within ± 0.5°C 85.2% for all 7324 data points. Table 3.3 shows the RMSE and BAP performance of the DBN model for each data set, along with the performance of our previous baseline model. No significant differences were found between the DBN model and our previous work model for both RMSE and BAP comparisons (P=0.92 and 0.87 respectively).

Table 3.3: DBN 2 Step model performance compared to previous work on four test data sets.

	RMSE (Mean ± SD °C)		BAP (Mean ± SD %)	
Data Set	DBN Model	Previous Work	DBN Model	Previous Work
A. Australia 1 (n=8)	0.28±0.13	0.39±0.11	84.7±14.9	70.0±11.6
B. Australia 2 (n=8)	0.26±0.17	0.22±0.07	81.2±23.8	90.3±8.1
C. Afghanistan 1 (n=4)	0.32±0.20	0.24±0.19	83.4±25.6	88.0±24.1
D. Afghanistan 2 (n=4)	0.22±0.02	0.19±0.09	95.8±5.3	98.9±2.2
Overall (n=24)	**0.27±0.14**	**0.28±0.14**	**85.2±18.9**	**84.6±16.1**

Figure 3.6 shows the observed, DBN, and previous work estimated CT group mean responses for each of the four datasets.

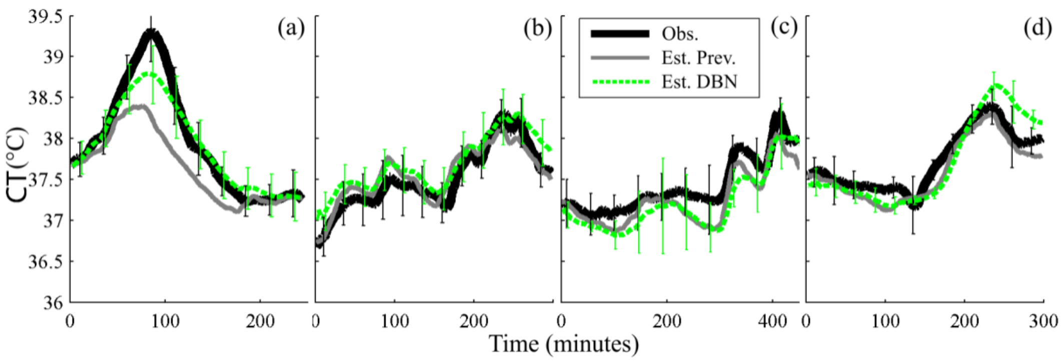

Figure 3.6: Mean observed, DBN model estimation and previous work estimation of CT for: (a) Australia 1, (b) Australia 2, (c) Afghanistan 1, and (d) Afghanistan 2 data sets. For observed and DBN estimated CT error bars represent ±1 SD.

3.1.6 Discussion

Our data show that we were able to learn a DBN model of the human thermo-regulation system using the EM algorithm and a comprehensive field data set. The DBN model when applied to new data, was able to provide internal temperature estimates that were statistically no different to our well validated previous model. By providing the model with additional information from accelerometry and heat flux, we demonstrated that it was possible to model heat gain and heat loss. Using this additional information, we were also able to identify when the thermoregulatory system allowed CT to rise while limiting skin blood flow and adjust our CT estimates accordingly.

The better performance of the two step DBN model over the one step model is likely explained by the fact that HG and HL actually provide an estimate of change in CT rather than a steady state observation of CT. The one step DBN model convolves the HR observation of steady state CT and the ΔCT observations from HG and HL. A similar ΔCT can occur at any CT and thus it appears this convolution leads to an underestimate of CT with the HG and HL moderating or smoothing the expected HR from CT.

The close correlation of ΣHG and total daily energy expenditure (r^2=0.88 or r^2=0.73,) provides confidence that the HG estimates are within the realms of reality.

The DBN model when applied to new data, was able to provide internal temperature estimates that were statistically no different to our well validated previous model with an overall RMSE 0.27 ± 0.14 °C and estimating over 85% of the data points within ± 0.5 °C. The DBN model showed a small negative bias of −0.01 °C and moderate variance of 0.12 °C. For context, comparisons between "gold standard" methods of measuring CT (thermometer pill, rectal and esophageal probes) have RMSE reported differences of 0.22 ± 0.13 ºC (Kolka et al., 1993) and 0.23 ± 0.07 ºC (O'Brien et al., 1998).

Since both HG and ΔCT are accurately estimated, it follows that HL must also be well estimated. The HL component of the thermoregulatory system can provide insight into aerobic performance. Recent work has demonstrated that high skin blood flow requirements can lead to a reduction in aerobic performance (Kenefick et al., 2010). The HL component of our model should provide insight some insight into the cardiovascular strain, even when CT is not particularly high. By utilizing the DBN model's HG and HL information, we were able to detect and adjust our model output when the thermoregulatory system allowed CT to rise while limiting skin blood flow. Test data set A contains a specific example of this thermoregulation, and over the group of test subjects, our modified model is able to more accurately estimate the peak in core temperature (See Figure 3.6, panel a) than when we use just HR alone. The modification had minimal impact in the estimation of CT for the other test data sets, except in data set D, where CT was slightly overestimated at the CT peak. For a system that is designed to prevent thermal injury, such an overestimation may be a trade that can be made for safety.

3.1.7 Conclusion

By translating physiological knowledge into a graphical model we have been able to represent human thermo-regulation in terms of a dynamic Bayesian network. We were able to learn the conditional probability distributions of our DBN from real data using the expectation maximization algorithm. Using these learned conditional probability distributions in a Kalman filter, we were able to infer estimates of human heat production heat transfer to the environment and internal temperature given observations of activity from accelerometers, heart rate, and heat flow from the chest. The DBN model performed statistically the same as our previous well validated HR CT estimation model. Importantly, with the additional model information the DBN is able to correctly model high peaks in CT in cases where estimates from HR alone cannot. Representing thermo-regulation as a DBN allows for a more comprehensive understanding of the internal thermal state variables and shows promise to enable real time heat strain state monitoring applications. This *computational physiology* approach has demonstrated how formalizing an open physiology research problem into a graphical model can produce estimation results that improve upon current techniques and that also provides additional insight into important, otherwise unseen, internal states and their dependencies.

3.2 Estimation of Human Core Body Temperature from Sequential Heart Rate Observations

In the previous section, we demonstrated how core body temperature (CT) can be estimated from observations of heart rate (HR), accelerometry (AC), and heat flux (HF). While the results showed promise, sensor systems that combine all three of these parameters do not exist in the commercial market place.

Concentrating on estimating CT in warm to hot conditions during exercise, we simplified the DBN method further to use time series observations of HR only to track CT over time. Our method relies on a Kalman filter (Kalman 1960) which has been used extensively in engineering tracking problems. Here, an item or variable of interest must be tracked from a series of "noisy" observations and knowledge of the temporal dynamics. The Kalman filter (KF) requires two models defined by linear Gaussian probability density functions. One model relates how the variable to be tracked changes over time, while the other model relates current observations to the variable of interest. We hypothesized that HR could be used as a "noisy" observation of CT. Thus, by understanding how CT changes over time and the most likely CT for a given HR, a KF model to estimate a series of CT values could be learned. HR is a convenient observation of the expected CT at steady state or a leading indicator of CT as it contains information about both heat production (through the Fick (1855) equation and VO_2) and heat transfer since HR is related to skin profusion. In our previous work (Buller et al., 2010), we demonstrated the feasibility of the KF method for estimating CT, but the model artificially limited CT estimation to values below 39.5 °C and lacked systematic validation using data from a variety conditions known to impact CT. This paper extends our previous KF CT estimation model in the following ways: (1) we use an extended KF (see Welch and Bishop, 1995) to allow estimation of CT up to 41 °C, (2) the model's CT time update and CT to HR mapping functions are derived from a single study with 17 volunteers where CT ranges from 36 °C to over 40 °C, and (3) the model is validated against original data sets from laboratory and field experiments where work rates and environment, hydration, clothing, and acclimation states are varied. Our goal was to provide a method of estimating CT in warm-hot environments that is simple to use, works with equipment that is readily available and provides a valid estimate of time-varying CT.

3.2.1 Test Volunteers

Data from ten laboratory and field studies with a total of 100 test volunteers were used in the development (N=17) and validation (N=83) of the KF model. Original data from the studies were used in consultation with the principal investigators. These studies are described in detail in their original cited publications. All research was conducted under the oversight of Institutional Review Boards. In some instances, the number of volunteers used for our analyses was less than those reported in the cited studies. These instances occur where either the HR and/or CT data were not available for these participants from the original research data or where volunteers failed to complete the whole experiment. Table 3.4 contains a summary of study volunteers, work rates, and environmental conditions.

Model Development Data (T)

HR (Equivital EQ02, Hidalgo Cambridge UK) and CT (ingested - Jonah Thermometer Pill, Respironics, Bend OR) data were collected from 17 male U.S. Army volunteers (age = 23 ± 4 yrs, height = 1.79 ± 0.08 m, weight = 81.3 ± 10.8 Kg, body fat = 18 ± 3% mean ± standard deviation (SD)) on one of two days of a field training exercise during July 2011 (air temperature 24 - 36 °C, 42 - 97% relative humidity (RH), wind speeds from 0 to 4 ms^{-1} with activities during the day conducted under full sun) at Fort Bragg, North Carolina. The field exercise included periods of sleep, rest, foot movement and periods of vigorous upper body work, providing a very wide range of work rates. These data were chosen to develop the model as they included the largest range (36 – 40 °C) and most dynamic CT responses of our analyzed data.

Model Validation

Data from nine studies were used to examine the performance of the model in a number of different conditions. Four laboratory studies were used for controlled comparisons of the effects of different environments, hydration states, clothing ensembles, and acclimation state; and five field physiological monitoring experiments were used to examine the performance under different climates and different levels of protective clothing.

*Laboratory Study (**A**) Environmental Conditions (Cheuvront et al., 2007):* 18 volunteers (1 female) (22 ± 4 yrs, 1.77 ± 0.04 m, 80.9 ± 15.3 kg) participated in six eight-hour bouts of intermittent treadmill exercises while wearing U.S. Army battledress uniform (BDU). Volunteers were euhydrated and heat acclimated. CT was measured using a thermometer pill suppository. The six test conditions were: (**A.1**) 20 °C, 50% RH and a total energy expenditure (TEE) rate of ~460W; (**A.2**) 27 °C, 40% RH and a TEE rate of ~350W; (**A.3**) 27 °C, 40% RH, and a TEE rate of ~470W; (**A.4**) 35 °C, 30% RH and an TEE rate of ~350W; (**A.5**) 35 °C, 30% RH and a TEE rate of ~470W; and (**A.6**) 40 °C, 40% RH and a TEE rate of ~360W.

*Laboratory Study (**B**) Hydration State* (*Montain & Coyle 1992):* 8 heat acclimated male volunteers (23 ± 3 yrs, 71.9 ± 11.6 kg) completed 2 hours of cycle ergometer exercise at a TEE rate of ~1000W while wearing shorts and a t-shirt in environmental conditions of 33°C, 50% RH. CT was measured with a rectal probe. Conditions were: (**B.1**) Hydrated with 80% fluid replacement; and (**B.2**) Dehydrated with no fluid replacement.

*Laboratory Study (**C**) Clothing* (*Latzka et al., 1997; 1998):* 8 heat acclimated euhydrated male volunteers (23 ± 6 yrs, 1.76 ± 0.06 m, 76.0 ± 15.1 kg, 18 ± 6 % body fat) participated in treadmill exercise at TEE rates of ~675W in an environment of 35°C and 55% RH. CT was measured with a rectal probe. Conditions were: (**C.1**) shorts and a t-shirt (n=6) for 111 minutes of exercise; and (**C.2**) totally encapsulating chemical protective clothing (n=8) for 28 minutes of exercise.

*Laboratory Study (**D**) Acclimation State (Kenefick et al., 2011):* 7 male euhydrated volunteers (24 ± 7 yrs, 1.78 ± 0.08 m, 80.2 ± 21.3 kg , 16 ± 11 % body fat) participated in a treadmill exercise at a TEE rate of ~550 W while wearing shorts and a t-shirt in environmental conditions of 45°C, 20% RH. CT was measured using a thermometer pill used as a suppository. Conditions were: (**D.1**) unacclimated for 59 minutes of exercise; and (**D.2**) acclimated (10 previous days of exercise in the heat) for 100 minutes of exercise.

*Field Study (**E**) U.S. Army Ranger Training Brigade (RTB) (Unpublished):* 11 male acclimated euhydrated RTB students (27 ± 6 yrs, 1.77 ± 0.05 m, 81.7 ± 5.3 kg, 14 ± 3 % body fat) participated in an eight mile timed road march (140 minutes) while carrying ~ 35kg at night. Volunteers wore the Army combat uniform and had TEE rates of ~675W in 25°C, 85% RH environmental conditions with wind speeds ranging from 0 to 3 ms^{-1}. CT was measured by ingested thermometer pill.

*Field Study (**F**) U.S. Special Forces (Buller et al., 2011b):* 7 male heat acclimated euhydrated Special Forces military students (27 ± 2 yrs, 1.78 ± 0.08 m, 85.7 ± 6.2 kg) who were participating in multi-day selection course were studied. Volunteers were studied over a 24 hour period which included various training activities and sleep. Volunteers wore the Army combat uniform and had average TEE rates ~200W. Environmental conditions ranged from 9 to 13 °C and 83 to 95 % RH with wind speeds of 0.4 to 3.0 ms^{-1} with some sun during outdoor activities. CT was measured by ingested thermometer pill.

*Field Study (**G**) Iraq (Buller et al., 2008):* 8 male heat acclimated euhydrated U.S. Marines (21 ± 1 yrs, 1.80 ± 0.07 m, 85.1 ± 9.0 kg, 15 ± 3 % body fat) who conducted one of two foot patrols

(209 and 250 min.) in Iraq were studied. Volunteers wore the standard Marine Corps combat shirts and body armor (~37 kg load) and had an average TEE rate of ~200W. Environmental conditions were 42 to 47 °C and 9 to 11% RH; and 39 to 44 °C, and 9 to 13% RH with wind speeds <2.0 ms^{-1}. Both patrols were conducted in full sun. CT was measured by ingested thermometer pill.

*Field Study (**H**) Afghanistan (Buller et al., 2011a):* 8 male heat acclimated U.S. Marines (21 ± 2 yrs, 1.84 ± 0.04 m, 85.7 ± 6.2 kg, 16 ± 3 % body fat) who conducted one of two foot patrols during a full mission day in Afghanistan were studied (683 and 488 min.). Volunteers wore the standard Marine Corps combat shirts and body armor (~32 kg load). Patrols were conducted with average TEE rates ~400W. Environmental conditions were 20 ± 3 °C and 20 ± 11 % RH with wind speeds of 2.4 ± 0.8 ms^{-1}; and 20 ± 5.3 °C, 26 ± 13 % RH with wind speeds of 2.0 ± 1.1 ms^{-1}. Both monitoring periods were under full sun. CT was measured by ingested thermometer pill.

*Field Study (**I**) Australian Army Soldiers (Unpublished):* 8 male heat acclimated euhydrated Australian Army Soldiers (28 ± 6 yrs, 1.95 ± 0.09 m, 85.7 ± 14.2 kg, 13 ± 4 % body fat) participated in two training activities. Conditions were: (**I.1**) A simulated patrol and ambush (15 – 20°C, 65 – 85% RH, wind speed <1.5 ms^{-1}, limited sun) which included periods of strenuous activity (297 min.). Volunteers wore chemical biological protective gear in an open configuration (Military Operational Protective Posture (MOPP) II). (**I.2**) A 5 km road march conducted in fully encapsulating chemical biological protective equipment worn in the MOPP IV configuration (18°C, 72% RH, wind speed <1 ms^{-1}, dusk) with an average TEE rate of ~685W (244min.). CT was measured by ingested thermometer pill.

Table 3.4: Volunteer characteristics, TEE rate and environment summary by study.

Study	Time (min.)	n	Age (yrs)	Height (m)	Wt. (kg)	Body Fat (%)	TEE Rate (W)†	Air Temp. (°C)	RH (%)
T	~840	17	23±4	1.79±0.08	81±11	18±3	Various	24–36	42–97
A	~480 x 6	18*	22±4	1.77±0.04	81±15	N/C	350/470	20–40	30–50
B	121/121	8	23±3	N/C	72±12	N/C	1000	33	50
C	111/28	6/8	23±6	1.76±0.06	76±15	18±6	675	35	55
D	59/100	7	24±7	1.78±0.08	80±21	16±11	550	45	20
E	140	11	27±6	1.77±0.05	82±5	14±3	675	25	85
F	1441	7	27±2	1.78±0.08	86±6	N/C	200	9–13	83–95
G	209+250	8	21±1	1.80±0.07	85±9	15±3	200	39–47	9–13
H	683+488	8	21±2	1.84±0.04	86±6	16±3	400	20	20–26
I	297/244	8	28±6	1.95±0.09	86±14	13±4	Var./685	15–20	65–85

TEE = Total energy expenditure rates. †Values reported are approximate. T=Training/Development Data. *Includes 1 female. N/C = Not Collected. Var. = Various. Means ± SD.

3.2.2 Kalman Filter Model Development

A KF model is comprised of two relationships: a *time update model* and an *observation model*. In the estimation of CT, the *time update model* relates how CT changes from time step to time step along with the uncertainty/noise of this change. The *observation model* relates an observation of HR to a CT value along with the uncertainty of this mapping. The *time update* and *observation* models are shown in Equations 3.25 and 3.26 as regression models with the uncertainty/noise represented as zero mean Gaussian distributions with variances of γ^2 and σ^2. If the model parameters (a_0, a_1, γ, b_0, b_1, b_2, and σ) can be found, a standard set of KF equations can be used to iteratively compute the most likely CT given a series of HR observations (see Equations 3.27 through 3.32 in the results section). The equations in the results section are shown using the model parameters from Equations 3.25 and 3.26, and where the learned model parameters have been substituted. Thus, given any series of one minute HR observations, these equations can be used to iteratively compute a series of minute-by-minute CT estimates. Welch and Bishop (1995) provide an extensive tutorial on the KF and the extended KF which is used in this paper. However, at each time step, the KF equations can be thought of as operating in the following way: (1) Compute an estimate of the current CT using the time update model (see Equation 3.27). (2) Compute the uncertainty of the current CT estimate using the time update model uncertainty (see Equation 3.28). (3) Adjust the current CT estimate using the current observation of HR and the observation model weighted by the uncertainty of the observation versus the uncertainty of the current CT estimate (see Equation 3.31). (4) Adjust the CT estimate uncertainty based upon the uncertainty of the observation (see Equation 3.32). The KF model parameters were learned in the following way:

The time update model: was defined as a linear regression equation as follows:

$$CT_t = a_1 CT_{t-1} + a_0 + f \quad \text{Where: } f \sim N(0, \gamma) \qquad (3.25)$$

Where CT = core temperature, subscript t = time point, a_1 = time update model coefficient, a_0 = time update model intercept, f = noise drawn from a Gaussian distribution (N) with mean 0 and SD γ. Parameters a_1 and a_0 were found by least squares regression of CT_t by CT_{t-1}. The parameter γ was derived from the SD of the discrete probability distribution of ΔCT points from the development data.

The observation model: was defined as a quadratic regression model as follows:

$$HR_t = b_2 CT_t^2 + b_1 CT_t + b_0 + g \text{ Where: } g \sim N(0,\sigma) \tag{3.26}$$

Where b_2 = observation model quadratic coefficient, b_1 = observation model coefficient, b_0 = observation model intercept, g = noise drawn from a Gaussian distribution with mean 0 and SD σ. Equation 3.26 shows a quadratic regression model as this was found to better fit the development data necessitating the use of the extended KF. Parameters b_0, b_1, and b_2 were found by quadratic least squares regression fit to eight pairs of CT - HR points found by searching for the optimal CT estimation performance of our previous KF model (Buller et al., 2010). The parameter σ was found by computing the mean and SD of HR values binned by CT at 0.1°C intervals and taking the mean of the SD values for each bin.

Our original KF model (Buller et al., 2010) was used to search for the optimal CT - HR points using our developmental data. The original KF linear observation model was split into 7 line segments at eight CT values of 36.5, 37.0, 37.5, 38.0, 38.5, 39.0, 39.5, and 40.0 °C. Our original KF model was modified to be run in a piecewise fashion using these seven line segments. For each CT (listed above) starting with the lowest, we systematically varied the HR value (±50 beats/minute in 1 beat intervals) to redefine the KF observation model at this point. For each HR, we used the redefined KF model to provide estimates of CT given our development data. The HR that provided CT estimates with the minimum root mean square error (RMSE) compared to the observed development data was selected. The next highest CT line segment point was then selected and the process repeated. In this way, the eight CT-HR pairs were modified by our developmental data from our earlier observation model to a new model that better defined the relationship between CT and HR. A quadratic least-squares regression was fit to these points to become our optimized observation model.

3.2.3 Statistical Analysis

The limits of agreement (LoA) method (Bland and Altman, 1986) was selected as the most appropriate means for assessing agreement between the observed CT and KF model estimate. This method plots the average of observed and estimated values against the difference (estimate – observation). Bias is computed as the mean of the differences. Limits of Agreement are computed as bias ± 1.96 × standard deviation (SD) of the differences. The LoA provide a range of error within which 95% of all estimates using the KF approach should fall assuming a normal distribution. The initial observed CT values for each study were used as starting values for the KF model and the initial variance was set to zero indicating high confidence in these values. The Kalman Filter model was developed using data with one minute intervals. Where data had sampling rates more frequent than the one minute intervals, the mean of all values occurring in that minute was used. Where the sampling rate was greater than one minute, values were linearly interpolated.

The Bland and Altman method specifies no *a priori* limits on what forms an acceptable bias or range of LoA; instead they suggest these values depend on the measure and its intended use. For this analysis, we compared our model's performance to how the accepted laboratory measures of rectal and esophageal temperatures compare. Bias limits were set to the individual biological variation of ±0.25°C found by Consolazio, Johnson and Pecora (1963). To set LoA we examined the literature for comparisons of rectal to esophageal temperatures. Table 3.5 shows results of bias ± SD and LoA for five studies. Taking a weighted mean of all studies suggests that 95% of comparisons of rectal versus esophageal CTs fall within ± 0.58 °C. This LoA appears to reflect the difficulty in obtaining tight agreement in different methods of CT measurement. This difficulty is highlighted when both esophageal and rectal temperature methods are compared to pulmonary arterial blood temperature where LoAs are ±0.59 and ±0.78 °C respectively (Lefrant et al., 2003).

Table 3.5: Bias and LoA for studies comparing rectal and esophageal measure of CT.

Citation	Bias ± SD	LoA (1.96 * SD)	N
Kolka*	-0.21±0.17	± 0.33	4
Lee*	-0.35±0.20	± 0.40	7
Teunissen et al., 2011	0.01±0.32	± 0.63	10
Brauer et al., 1997	-0.03±0.42	± 0.82	60
Al-Mukhaizeem et al., 2004	0.05±0.22†	± 0.43†	80
	Weighted Mean	± 0.58	161

*In Byrne and Lim (2007). †Weighted mean of 3 periods in Table 1, Al-Mukhaizeem et al. (2004).

We also computed the root mean square error (RMSE) for each individual volunteer and computed the mean RMSE ± SD for each condition. A single factor (study condition) analysis of variance (ANOVA) was used to test for differences in KF model performance (RMSE, bias, and LoA) across conditions in study A and across field studies E through I. To readily identify what factors were causing main effect differences we used the least significant difference (LSD) post-hoc test. T-tests were used to examine differences in performance between laboratory baseline measures and dehydration, acclimation and clothing configurations studies B, C and D respectively. An overall RMSE was computed, weighted by each individual and study duration. Overall bias and LoA were computed from all data points. Grubbs (1969) outlier detection test was used to identify RMSE and bias measures that differed significantly from each study's group responses.

3.2.4 Results - Model Development

Figure 3.2.1 (A) shows the discrete probability distribution of ΔCT used for the time update model and (B) a scatter plot of all CT by HR points showing the mean HR ± SD for CT binned by 0.1 °C intervals. The discrete probability distribution mean was found to be 0.001 ± 0.022 °C/min. The regression of previous CT with current was found to be $CT_t = 0.9984 \cdot CT_{t-1} + 0.0622$ with an r^2=0.99. With the mean of the discrete probability distribution close to zero, and the regression coefficient close to one, and because we expect it to be equally likely that CT will either increase or decrease we set our time update model to $a_1 = 1$, $a_0 = 0$ and $\gamma = 0.022$.

The optimal piecewise line segment points that provided the best RMSE (0.27 ± 0.10 °C) and largest number of points within ± 0.58 °C (96.1 ± 6.7%) are shown in Figure 1(B). A quadratic fit to these points defines the observation mapping function as $b_0 = -7887.1$, $b_1 = 384.4286$, and $b_2 = -4.5714$. The mean SD for the binned HR = 18.88 ± 3.78 beats/min. so σ is set to 18.88. To keep the KF model simple the positively (low CT) and negatively (high CT) skewed HR distributions at the extremes of CT are ignored. Keeping the assumption that HR is normally distributed across all CT has the effect of slightly under and over estimating the rate of rise of CT for low and high CTs respectively.

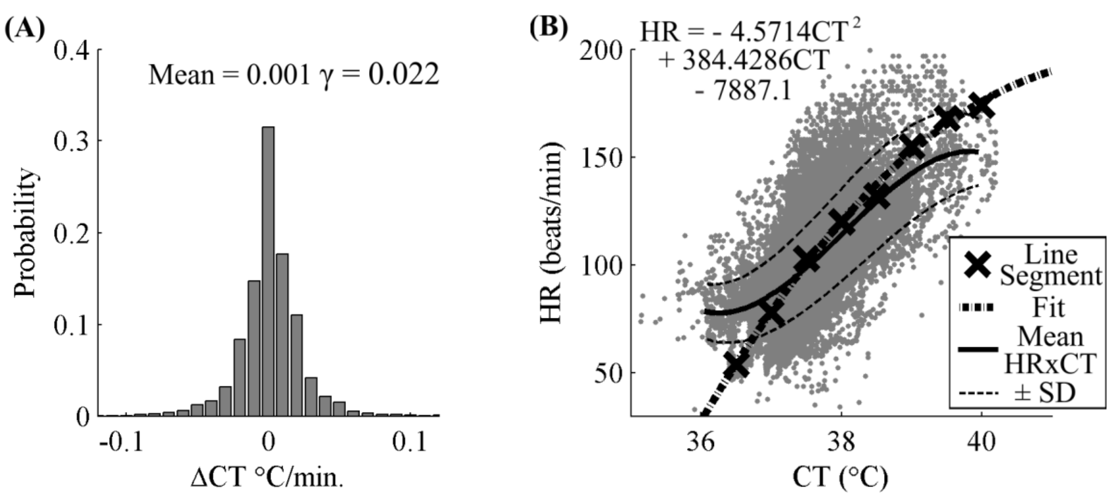

*Figure 3.7: **(A)** Time update model represented as a discrete probability distribution found from the development data. **(B)** Observation model. Scatter plot of development data points showing mean HR by CT ± SD the optimal CT-HR line segment points (Line Segment) and the CT to HR mapping function (Fit).*

The extended Kalman filter model is described in Equations 3.27 through 3.32 (below) and provided as a Matlab script in below.

```
function CT=KFModel(HR,CTstart)
%Inputs:
  %HR = A vector of minute to minute HR values.
  %CTstart = Core Body Temperature at time 0.
%Outputs:
  %CT = A vector of minute to minute CT estimates
%Extended Kalman Filter Parameters
  a=1; gamma=0.022^2;
  b_0=-7887.1; b_1=384.4286; b_2=-4.5714; sigma=18.88^2;
%Initialize Kalman filter
  x=CTstart; v=0; %v=0 assumes confidence with start value.
%Iterate through HR time sequence
  for time=1:length(HR)
  %Time Update Phase
    x_prd=a*x;                                          %Equation 3.27
    v_prd=(a^2)*v+gamma;                                %Equation 3.28
   %Observation Update Phase
    z=HR(time);
    c_vc=2.*b_2.*x_prd+b_1;                             %Equation 3.29
    k=(v_prd.*c_vc)./((c_vc.^2).*v_prd+sigma);          %Equation 3.30
    x=x_prd+k.*(z-(b_2.*(x_prd.^2)+b_1.*x_prd+b_0));    %Equation 3.31
    v=(1-k.*c_vc).*v_prd;                               %Equation 3.32
    CT(time)=x;
  end
```

The model is based on the linear algebra equations from Welch and Bishop (1995) which we have simplified for use with scalar variables. For our analysis we selected a starting CT_0 value from the data and set the initial variance (v_0) = 0. At each new one minute time point (t) the six equations were applied iteratively to provide a new estimate of CT_t and its associated variance (v_t) given a current observation of HR_t, the previous CT_{t-1} estimate, and previous variance (v_{t-1}), thus:

1) Compute a CT preliminary estimate ($\hat{C}T_t$) based upon the previous CT estimate (CT_{t-1}) and the time-update mapping function (a_1 and a_0).

$$\hat{C}T_t = a_1 \bullet CT_{t-1} + a_0 = 1 \bullet CT_{t-1} + 0$$

$$\hat{C}T_t = CT_{t-1} \tag{3.27}$$

2) Compute a preliminary estimate of the variance of the CT estimate ($\hat{v}_t$) based upon the previous CT variance (v_{t-1}) the time-update mapping function (a_1) and variance (γ^2).

$$\hat{v}_t = a_1^2 \bullet v_{t-1} + \gamma^2 = 1 \bullet v_{t-1} + 0.022^2$$
$$\hat{v}_t = v_{t-1} + 0.000484 \tag{3.28}$$

3) Compute the extended Kalman filter mapping function variance coefficient.

$$c_t = 2 \bullet b_2 \hat{C}T_t + b_1 = 2 \bullet \text{-}4.5714 \bullet \hat{C}T_t + 384.4286$$
$$c_t = -9.1428 \bullet \hat{C}T_t + 384.4286 \tag{3.29}$$

4) Compute the Kalman gain (k_t) weighting factor based on the preliminary estimate of variance and using the extended KF variance coefficient.

$$k_t = \frac{\hat{v}_t c_t}{c_t^2 \hat{v}_t + \sigma^2} = \frac{\hat{v}_t c_t}{c_t^2 \hat{v}_t + 18.88^2}$$
$$k_t = \frac{\hat{v}_t c_t}{c_t^2 \hat{v}_t + 356.4544} \tag{3.30}$$

5) Compute the final estimate of CT_t using the preliminary time-update estimate, the error between the HR_t observation and the expected HR given the preliminary estimate of CT:

$$CT_t = \hat{C}T_t + k_t(HR_t - (b_2 \bullet \hat{C}T_t^2 + b_1 \bullet \hat{C}T_t + b_0))$$
$$CT_t = \hat{C}T_t + k_t(HR_t - (-4.5714 \bullet \hat{C}T_t^2 + 384.4286 \bullet \hat{C}T_t - 7887.1)) \tag{3.31}$$

6) Compute the variance of the final CT estimate (v_t):

$$v_t = (1 - k_t c_t)\hat{v}_t \tag{3.32}$$

Table 3.6 shows the iterative application of these equations to a series of HR observations given a starting CT_0 = 37.94 °C and a starting variance of v_0 = 0.

Table 3.6: Use of the extended KF equations on a portion of the observed HR data.

HR	*t*	$\hat{CT}_t$ (eq. 3)	$\hat{v}_t$ (eq. 4)	c_t (eq. 5)	k_t (eq. 6)	CT_t (eq. 7)	v_t (eq. 8)
	0					**37.94**	**0**
124	1	37.94000	0.00048	37.55077	0.00005	37.94031	0.00048
111	2	37.94031	0.00097	37.54791	0.00010	37.93962	0.00096
119	3	37.93962	0.00145	37.55427	0.00015	37.93979	0.00144
145	4	37.93979	0.00192	37.55266	0.00020	37.94525	0.00191

Bold font = observed or initialization data. Eqs. 3 to 8 are applied iteratively to compute CT_t and v_t.

Figure 3.8 illustrates the performance of our learned model on the development data. Panel (A) shows a scatter plot of estimated CT by observed CT, the line of identity and a least squares linear regression fit to the development data. Panel (B) shows a Bland Altman Plot of mean of observed and estimated CT versus estimated – observed CT. The bias = -0.04 ± 0.28 °C with the LoA = ± 0.55°C. Panel (C) shows a normalized histogram of the model error.

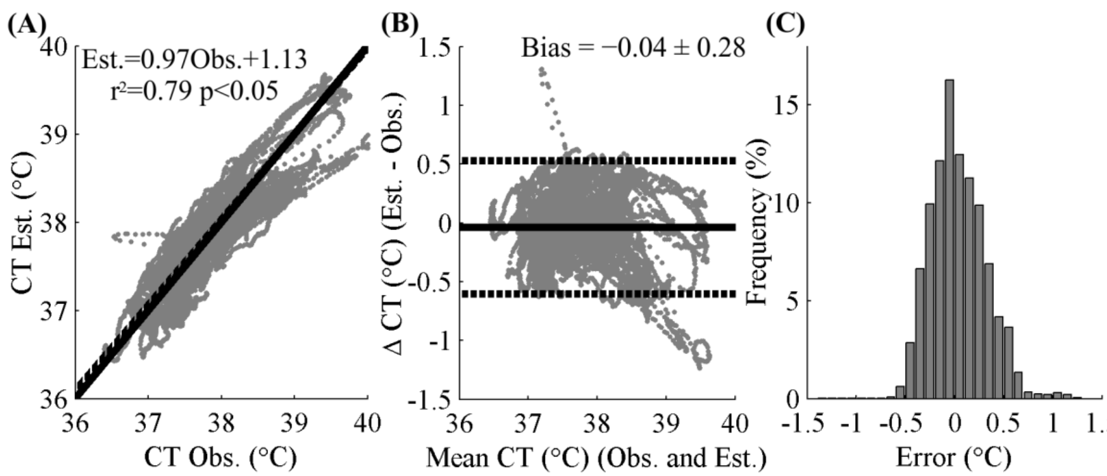

*Figure 3.8: **(A)** Scatter plot of observed (Obs.) CT versus estimated (Est.) CT for the development data, showing the line of identity (solid) and least squares regression line (dashed). **(B)** Bland Altman plot showing bias (solid) and ± 1.96SD (dashed) for the development data. **(C)** Normalized histogram of model error for all training data.*

3.2.5 Results - Model Validation

The KF model was validated against 150 individual test sessions with 83 different volunteers (>52,000 CT observations) and had an overall bias of − 0.03 ± 0.32 ºC with the LoA = ± 0.63 ºC. The overall weighted mean RMSE was 0.30 ± 0.13 ºC. Figure 3.9 (A) shows a scatter plot of estimated CT by observed CT, the line of identity and a least squares linear regression fit to the validation data. Figure 3.9 (B) shows a Bland Altman Plot of mean of observed and estimated CT versus estimated – observed CT of the validation data. Figure 3.9 (C) shows a normalized histogram of the model error for all the validation data.

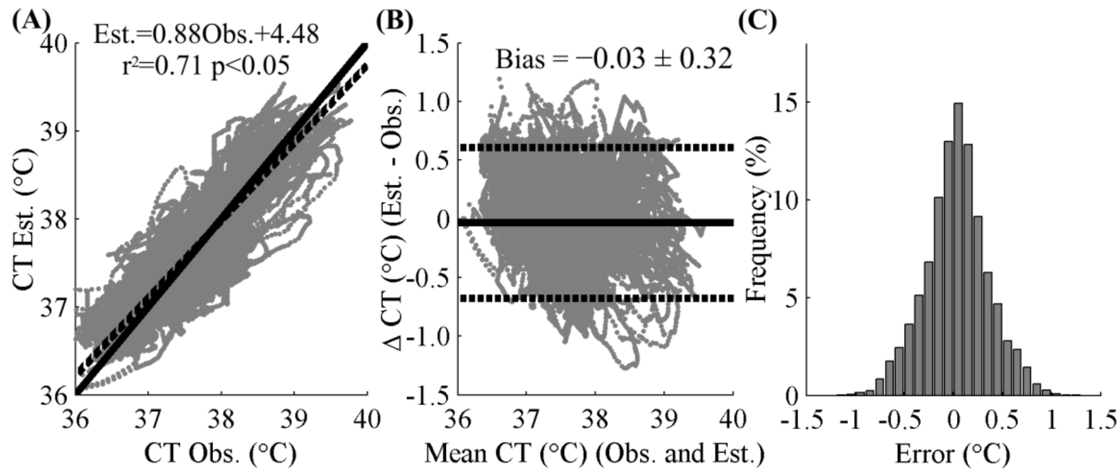

*Figure 3.9: **(A)** Scatter plot of observed (Obs.) CT versus estimated (Est.) CT for the validation data, showing the line of identity (solid) and least squares regression line (dashed). **(B)** Bland Altman plot showing bias (solid) and ± 1.96SD (dashed) for validation data. **(C)** Normalized histogram of model error for all validation data.*

Table 3.7 presents the mean RMSE, bias, and limits of agreement (LoA) for estimated versus observed CT for the laboratory and field validation studies. Individual Bland-Altman (Figure 3.10) and mean observed and estimated CT (Figure 3.11) plots for all the studies provide a more detailed overview of the model performance.

Table 3.7: Mean RMSE, bias, and limits of agreement (LoA) for validation data.

Study	Condition	# min.	n	RMSE	Bias	LoA
A.1. Environment	20ºC, 50%RH, 460W	507	9	0.32 ± 0.16	-0.12 ± 0.33	**±0.65**
A.2	27ºC, 40%RH, 350W	461	11	0.25 ± 0.14	-0.09 ± 0.27	±0.53
A.3	27ºC, 40%RH, 470W	461	10	0.32 ± 0.13	0.07 ± 0.33	**±0.65**
A.4	35ºC, 30%RH, 350W	461	12	0.33 ± 0.18	**-0.25 ± 0.28†**	±0.54
A.5	35ºC, 30%RH, 470W	461	7	0.25 ± 0.12	0.07 ± 0.26	±0.52
A.6	40ºC, 40%RH, 360W	461	7	0.29 ± 0.09	0.00 ± 0.30	**±0.60**
B.1. Hydration	Hydrated	121	8	0.44 ± 0.19†	**0.31 ± 0.36**	**±0.71†**
B.2 (33°C, 50%)	Hypohydrated	121	8	0.26 ± 0.11	0.14 ± 0.24	±0.48
C.1. Clothing	Shorts & T Shirt	111	6	0.21 ± 0.11	0.05 ± 0.23	±0.45
C.2 (35°C, 55%)	Chem. Bio. PPE	28	8	0.19 ± 0.16	-0.12 ± 0.21	±0.40
D.1. Acclimation	Heat Acclimated	59	7	0.28 ± 0.11	-0.13 ± 0.27	±0.52
D.2 (45°C, 20%)	Unacclimated	100	7	0.26 ± 0.19	-0.01 ± 0.31	**±0.60**
E. U.S. Army Rangers (24°C, 85%)		140	11	0.29 ± 0.09	-0.06 ± 0.30	±0.58
F. U.S. Special Forces (SF) (11°C, 91%)		1441	7	0.29 ± 0.07	0.06 ± 0.29	±0.56
G. USMC Iraq (42 °C, 11%)		225	8	0.23 ± 0.08	-0.05 ± 0.24	±0.48
H. USMC Afghanistan (20 °C, 20%)		586	8	0.32 ± 0.14	-0.07 ± 0.34	**±0.66**
I.1. Austral. Sol. (MOPP II) (18°C, 75%)		297	8	0.26 ± 0.07	0.03 ± 0.27	±0.53
I.2. Austral. Sol. (MOPP IV) (18°C, 72%)		244	8	0.42 ± 0.14†	**-0.28 ± 0.34†**	**±0.67†**
Overall*				0.30 ± 0.13	-0.03 ± 0.32	**± 0.63**

Values are mean ± SD. † Significant difference at $p<0.05$. PPE = Personal Protective Equipment. Bolded results indicate Bias and LoA thresholds have been exceeded. USMC = U.S. Marine Corps. *Overall RMSE weighted by study duration & n. Overall bias and LoA computed from all data points.

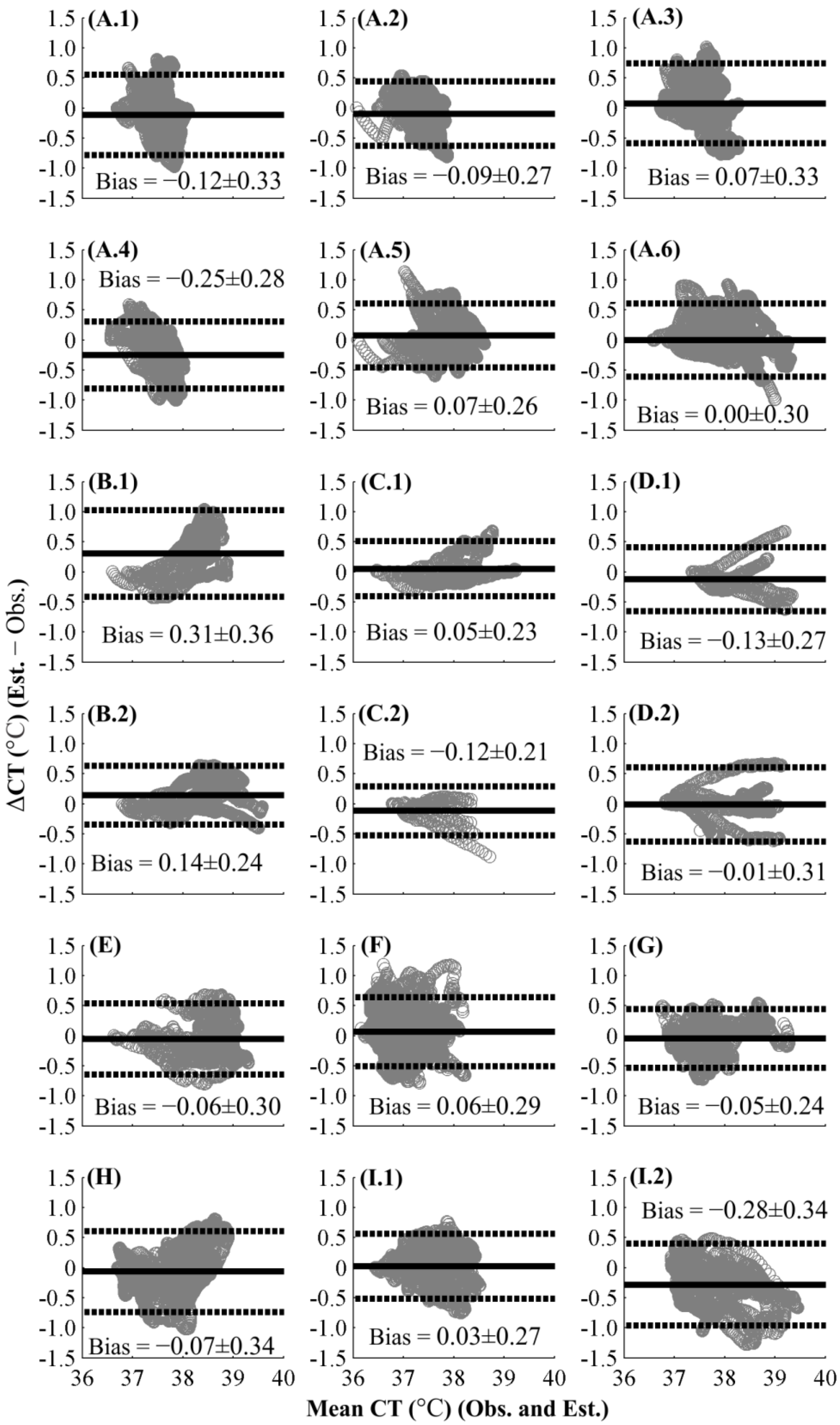

Figure 3.10: Bland Altman plots for individual studies with bias (solid) and ± 1.96SD (dashed)

.

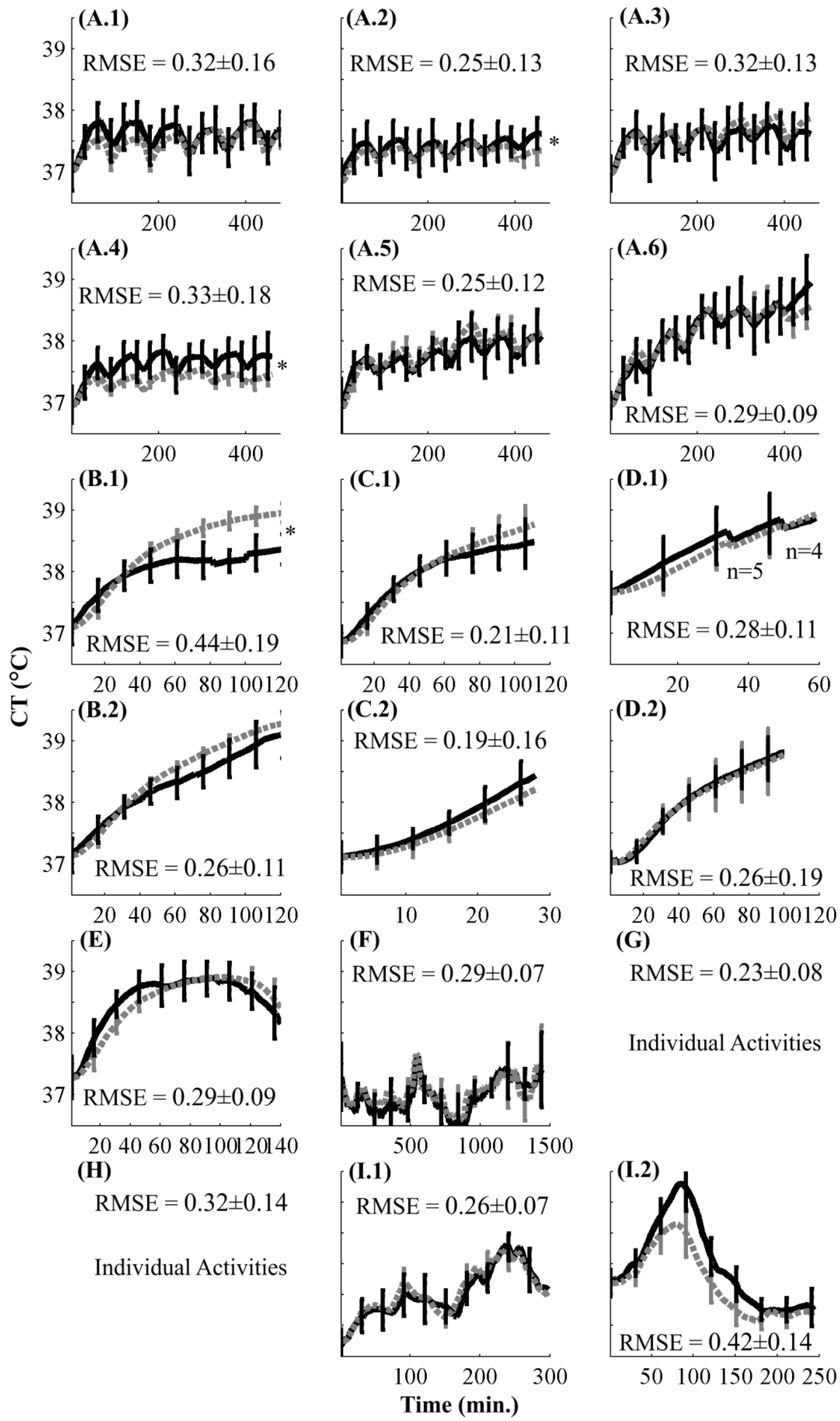

*Figure 3.11: Mean observed CT (solid - black) and mean estimated CT (dashed - gray) for individuals studies with ± 1 SD. Means for studies G and H are not shown as they are a combination of several activities over the study period. * = end points significantly different p<0.05.*

At environmental conditions 35ºC, 30%RH, and an EE rate of 350W (Study A.4) the bias exceeded our acceptability threshold and is significantly more negative than the study conditions A.3, A.5, and A.6 ($F=2.77$, $P<0.03$). The hydrated baseline condition (B.1) exceeded both the bias and LoA criteria, and is significantly different from the dehydrated condition (B.2) on the measures of RMSE and LoA ($t=2.21$, $P<0.05$; and $t=3.05$, $P<0.01$ respectively). For the field studies mild conditions (18°C) with high EE rate (~685W) and encapsulation in PPE (I.2) has significantly greater RMSE, and negative bias ($F=4.24$, $P<0.004$, $F=3.78$ $P<0.007$ respectively) than the other filed studies (E, F, G, H, and I.1); and significantly greater LoA than studies G and I.1 ($F=2.68$ $P<0.03$, respectively).

Table 3.8 presents four individuals identified as outliers using the Grubbs criterion test from 7 of the studies. No individual characteristic stands out as a factor in determining the outliers.

Table 3.8: Individuals with RMSE and/or bias identified as outliers from 2-tailed Grubbs test.

Individual (age, ht., wt., %fat)	Study	Outlying RMSE (°C)	Outlying Bias (°C)
23, 1.70 m , 69 kg	A.2, A.3, A.4	0.60†, 0.58 , 0.74‡	−0.59†, −0.55†, −0.72
*, 1.73 m, 72 kg, 9%	C.2	0.48‡	−0.39
38, 1.86 m, 98 kg, 28%	D.1, D.2	0.38, 0.54	0.29†, 0.50‡
22, 1.85 m, 88 kg, 15%	H	0.60‡	−0.55†

*Individual age not available. †$p<0.05$, ‡Approaching significance.

Table 3.9, summarizes the performance of the KF model across a range of temperatures and TEE rates with clothing configurations from shorts and t-shirts to partial encapsulation.

Table 3.9: KF model performance for a variety of temperatures and energy expenditure rates with acclimated, hydrated volunteers, not encapsulated in personal protective equipment.

		Environmental Temperature (°C)				
		9 to 13	18 to 20	24 to 27	33 to 35	40 to 45
Energy Expenditure Rate	Low (<=375W)	O	O$^{\uparrow}$	O	−	O$^{\uparrow}$
	Moderate (376 - 525 W)		O$^{\uparrow}$	O$^{\uparrow}$	O	
	High (526 – 675 W)		O	O	O	O
	Very High (>675 W)				+↑	

O = bias is < ± 0.13, $^{\uparrow}$ LoA exceeds ± 0.58 by less than 0.1 °C, ↑ LoA exceeds ± 0.58 by more than 0.1 °C, − underestimation of CT, + overestimation of CT, grey area = no data.

3.2.6 Discussion

The Kalman filter model has an overall bias of only −0.03 ± 0.32 °C and limits of agreement of ± 0.63 °C, indicating that 95% of all KF model estimates fell within this range of the observed CT. The KF model has a similar LoA to those found when comparing rectal and esophageal measurements of CT (± 0.58 °C see Table 2) and is within the LoA for rectal and esophageal measures found by Teunissen et al. (2011) and Brauer et al. (1997) of ± 0.63 and 0.82 °C respectively.

Using the aggregated results of the various studies, with clothing configurations from shorts and t-shirts to partial chemical biological encapsulation; it is possible to examine the performance of the KF model across a large temperature range for several different rates of energy expenditure. Table 6, summarizes the performance of the KF model in terms of our comparison criteria. For most temperatures and work rates the KF model provides CT estimates with a bias and LoA that are similar to those found in comparisons of rectal versus esophageal temperatures. However, at temperatures of 33 to 35 °C there are two exceptions. First, at low work rates the KF model significantly underestimates CT, and second at very high work rates the model significantly overestimates CT. These errors can be tolerated in the context of using the KF model for maintaining the safety of individuals. At low work rates the underestimation poses limited risk for missing individuals under thermal strain. In fact, the CT observations for this 8 hour series of work rest cycles (study A.4) never exceeded 38.5 °C. Conversely, at very high work rates the KF model tends to err on the side of false positives rather than missing thermally stressed individuals.

Analysis of the laboratory studies also demonstrates that the model provides CT estimates with small bias and LoAs within or close to our comparison threshold when volunteers are dehydrated, encapsulated in chemical biological PPE, or in an unacclimated state.

Only one set of conditions proved difficult for using the model in a safety assessment context. The KF model performs significantly less-well estimating CT of individuals engaged in very strenuous activity, in cooler temperatures while encapsulated in chemical biological PPE (MOPP IV) (study I.2). This particular study examined volunteers on a 5 Km road march conducted at a 15 min/mile pace in full chemical biological protective garments. Here the model clearly does not account for the full rise in CT seen during the road march (see Figure A2, panel I.2 in appendix A) and hence has a large negative CT bias. Although the work rate and clothing vapor occlusiveness are similar to that in the clothing laboratory study (study C), the ambient temperature was cooler (18 °C versus 35 °C). Under these conditions it appears that the thermoregulatory response of the volunteers was to widen the CT-to-skin temperature gradient, by allowing CT to rise, rather than increase skin blood flow (see Sawka and Young 2006). Thus, the observed rise in CT was greater than the rise our model would estimate from HR. Under the warmer conditions of the clothing laboratory study (study C) our model performed adequately.

When compared to the other recent approaches at providing non-invasive estimates of CT the KF model performs well. The KF model estimates of CT have a similar bias when compared to the heat flux sensor proposed by Gunga et al. (2008). However, LoAs for the heat flux sensor in environmental conditions of 25 °C and 40 °C were much higher (± 0.71 °C and ± 0.74 °C respectively) than all our conditions except study B.1. Similarly, when the KF model is directly compared to a real time implementation of a physics based thermo-regulatory model (Yokota et al., 2008) across study conditions A.1-A.5 (bias ± LoA: −0.24 ± 0.67; −0.25 ± 0.66; −0.08 ± 0.77; −0.23 ± 0.65; 0.10 ± 1.09 °C, respectively) (DeGroot et al., 2008, personal communication.) the KF model performs better with a bias closer to zero in four out of the five conditions and has LoAs less than those provided by the thermoregulatory model.

As with any method there is a distribution in performance (see Figure 3) where the model will more accurately estimate CT in some individuals than others. The overall and individual study Bland Altman charts in combination with the outlier analysis show that the KF model predicts CT very well except for a small number of individuals. The outlier analysis (see Table 5) identified 4 individuals where the model did not perform as well as the group. This same number is predicted by the LoA methodology (5% of 83) where 5% of the population would be expected to fall outside of the ± 0.63 °C LoA bounds. For the outlier from study A.2, A.3, and A.4 the error is systematically negative. Similarly, the individual identified as an outlier in D.1 and D.2 has a systematic positive bias in CT estimations. With these outliers performance of the KF model appears to be individual specific rather than condition specific, and so systematic biases for individuals appear to be correctable. The model parameters do allow for individualization by both age and fitness and future research will examine how individualizing the model for these parameters can improve CT estimation. As most volunteers in our data were drawn from relatively young and fit male military populations, further work will also be necessary to expand the model's generalizability to females, and older and less fit populations.

Other factors can affect HR, and thus our CT estimation, such as diet, caffeine, sleep, and psychological stress. The effects of diet and caffeine on HR will likely be outweighed by activity and thermoregulation. There were no controls for these factors in the field studies. Since it is likely that many volunteers were taking caffeinated products, the performance of the model includes the potential influence of caffeine. During sleep HR is reduced to low levels, but the KF model's estimation of CT appears appropriate in these situations given the sleep data at the mid-point of Study F. However, the impact of elevated HR from sustained psychological stress on the KF model's performance is unknown. While, studies G and H contain active military patrols, further research is necessary to examine the effects of sustained stress on the model's performance.

Although in some conditions the KF model provides LoAs that exceed our comparison threshold, it is important to highlight both the simplicity of the present KF model and that the LoA calculations include all data with HR transients from the start and end of exercise. These transient periods are included to demonstrate that the model can track CT during dynamic real-world periods of work and rest. Teunissen et al. (2011) examined the LoA between rectal and esophageal CT across periods of rest, exercise and recovery and found a similar LoA of ±0.63°C. Our KF model is simple using only one variable, HR, to estimate CT, with no adjustment for height, weight, body composition, fitness, or age.

Finally, while the model is not a replacement for the direct measurement of CT the findings suggest the KF model is accurate, precise and practical enough to provide an indication of thermal-work strain for use in the work place. Using an estimate of CT in conjunction with HR to obtain a thermal-work strain index (TWSI) value would provide a simple mechanism for alerting workers to possible excessive thermal-work strain.

3.2.7 Conclusion

Core body temperature can be estimated by a Kalman filter model using a single parameter, heart rate, to within similar bias and limits of agreement seen when comparing rectal and esophageal measurements of core temperature. The model was validated against a series of laboratory and field studies with 83 volunteers and 150 experimental runs across a range of environmental temperatures from 18.0 °C to 45 °C and work rates. We demonstrate that the model performs similarly in different environments, in the presence of dehydration, with limited or complete clothing occlusion, and whether volunteers are heat acclimated or not. While this technique is not a replacement for direct core temperature measurement, it offers a simple and promising new method for estimating individual core temperature and is accurate and practical enough to provide a means of real-time heat illness risk assessment.

3.3 Real-Time Thermal-Work Strain Application

In developing a practical real-time thermal-work strain risk assessment system there are a number of practical questions. For example: Who will be monitored and for how long? Who should be presented with thermal-work strain state information? Should this information go to individual team members, medical oversight professionals or team leaders? How should the thermal-work strain state index information be acted upon? Is the information absolute or used as part of an integrated approach to heat illness management? How will the information be telemetered from the individual to commanders and medical personnel?

The National Guard Weapons of Mass Destruction Civil Support Teams (WMD-CST) are usually comprised of approximately 22 full time personnel specially trained in chemical/biological weapon response. Each U.S. state has at least one specially trained unit that will often attend large scale high profile public events and are often the first to respond to unknown hazardous material events. The WMD-CST missions offer a fairly constrained scenario. A few team members will be fitted with chemical/biological personal protective equipment and will often walk into a "hot zone" to conduct surveys of sites, sampling of unknown substances, and casualty extractions. They have a dedicated medical officer to oversee the health and safety of team members, and also set up their own communications infrastructure. Since 2006 the WMD-CST at a national level have called for a real-time medical telemetry system, that includes measurement of both heart rate and core body temperature (National Guard 2006) in an effort to monitor thermal-work strain in national guardsmen as they conduct their chemical biological hazard missions (e.g. see Figure 1.1). Their document and standard operating procedures answer many of the questions necessary to build a real time monitoring system.

In 2007 the U.S. Army's Warfighter Physiological Status Monitoring-Initial Capability (WPSM-IC) was adapted to demonstrate real-time physiological status of WMD-CST team members engaged in a two training events (Buller et al., 2007). The system was viewed well but was only able to provide heart rate, activity, respiration rate and skin temperature. While these parameters were useful the system could not provide core body temperature nor a simple index of thermal-work strain.

The development of the Kalman filter method detailed in the previous section was part of an ongoing U.S. Army Research Institute of Environmental Medicine (USARIEM) research effort into real-time thermal-work strain monitoring. The validation was successful enough that USARIEM submitted a patent on the approach (Buller 2013) and asked the WPSM-IC vendor to implement the algorithm in their physiological monitoring system (Equivital EQ-02, Hidalgo Ltd., Cambridge UK). In addition, USARIEM in collaboration with Massachusetts Institute of Technology-Lincoln Laboratory (MIT-LL) and Hidalgo Ltd. developed a complete system to meet the needs of the WMD-CST real-time medical telemetry system. Tharion et al. (2013) details the complete system, how well it functioned, and concluded that that real-time monitoring was useful to the WMD-CST.

The work in this section examines how well the core body temperature estimation algorithm performed in a real-time setting. Generally we found that using HR data alone the Kalman filter approach estimated CT with a bias of −0.03 ± 0.32 °C with 95% of all CT estimates falling within ± 0.63°C. However, the validity of the CT estimates where participants were in encapsulating PPE was unclear. In a laboratory treadmill exercise conducted in CBRNE PPE the CT estimates were valid with slight negative bias (−0.12°C), and where 95% of CT estimates within −0.52 to +0.28°C. But for a field exercise conducted in CBRNE PPE the bias was larger (−0.28°C) and 95% of estimates fell within −0.91 to +0.35°C. Buller et al. (2013) suggest that, under this study's particular conditions, high metabolic work rate > 680 W, and temperate ambient conditions (Tair = 18 °C); it appeared that the thermoregulatory response of the volunteers was to widen the core-to-skin temperature gradient (with increasing CT and static Tsk), rather than increase skin blood flow (see Sawka and Young 2006). Under these circumstances the HR to CT mapping learned for the algorithm was inadequate to fully model the increased rise in CT.

The purpose of the present study was to examine the performance of the CT estimation algorithm in first responders wearing fully encapsulating PPE across three different field exercises with different environmental conditions and training scenarios. Specifically, answering the question does the work under fully encapsulating PPE; and whether the algorithm could be used in real-time using both a measured and "good guess" CT as the algorithm starting point.

3.3.1 Methods

Volunteers

A grand total of 25 male and 2 female volunteers (Age: 30 ± 6 yr, ± SD) from the U.S. Army and U.S. Army National Guard took part in three different CBRNE training events. These studies were approved by the institute's Institutional Review Board (IRB). Volunteers were briefed on the purpose, risks, and benefits of the study and each gave their written informed consent prior to participation. All had previous CBRNE training, had worn CBRNE-PPE previously, and had been training with their units a minimum of two years. Table 3.9 presents the volunteer characteristics at each of the training events (Event 1: Edgewood MD, Event 2: Hayward, CA, Event 3: Hanscom Air Force Base (AFB), MA).

Table 3.10: *Descriptive statistics for the study volunteers shown as mean ± standard deviation.*

Training Event #	n	Age (yr.)	Height (cm)	Weight (kg)	Body Fat (%)
1: Men	10	27.7 ± 4.5	176.8 ± 5.7	77.3 ± 11.8	13.8 ± 3.7
1: Women	2	30.0 ± 2.8	165.4 ± 5.8	74.4 ± 1.0	35.5 ± 0.7
2: Men	8	28.1 ± 4.6	178.5 ± 9.7	85.5 ± 16.9	16.9 ± 5.8
3: Men	7	35.1 ± 8.7	177.6 ± 7.5	88.9 ± 12.4	22.1 ± 5.1
Overall	27	29.9 ± 6.4	176.7 ± 7.9	82.5 ± 13.3	18.5 ± 7.4

Real-time Physiological Monitoring System

The real-time physiological monitoring system was based upon the Hidalgo Equivital EQ-02 (Hidalgo Ltd., Cambridge UK) chest belt sensor (see Figure 3.12 panel A). The Hidalgo Equivital™ EQ-02 is an FDA 510(k) certified system (K113054). The sensor electronic module weighs 38 gm, is IP67 certified and has a Class 1 Bluetooth interface. The EQ-02 system can record CT by receiving transmissions from the MiniMitter (Bend OR) Jonah thermometer pill. The thermometer pill is a food grade polycarbonate capsule that conforms to U.S. Food and Drug, Cosmetic Act and Food Additive Regulations 21 CFR 177.1580.

The EQ-02 sensor connects via Bluetooth to an Android smartphone (Figure 3.12 panel B) and one of two radio systems (Figure 3.12 panel C). The Android smartphone was used as a "Buddy" display. The intent was for team members who worked in pairs to be aware of the current thermal-work strain state of their partner.

Figure 3.12: Real-time physiological monitoring system. Panel A: Hidalgo Equivital EQ-02 chest belt sensor. Panel B: Android smart phone displaying thermal-work strain index taped to the outside of level A personal protective equipment. Panel C: Radio worn inside personal protective equipment to telemeter physiology back to the medical command post.

The android phone displayed the thermal-work strain index monitored in real-time from the EQ-02 sensor using both observed HR and observed CT from the ingested thermometer pill.

The display was color coded green for TWSI values below 8, yellow for TWSI values above 8 and below 10 and red for values above 10. The Android phone was also programmed to vibrate to provide a haptic alert when thermal the TWSI was at 10 or more. A TWSI of 10 relates to the USARIEM human use limits of CT (39.5 °C) and HR of 180 beats/min.. Figure 3.13 shows the Android smart phone display in each of these colored states.

Figure 3.13: Android smart phone real-time thermal-work strain index display.

The radio worn under the suit telemetered the real-time physiology back to an integrated display at the medical officer's work station. This display was a modified screen from Hidalgo's Black Ghost® real-time monitoring system and shows a history of the observed or estimated TWSI, along with a projection of the TWSI assuming HR remains the same for the next 15 minutes. Figure 3.14 shows one version of the display used in the real time system.

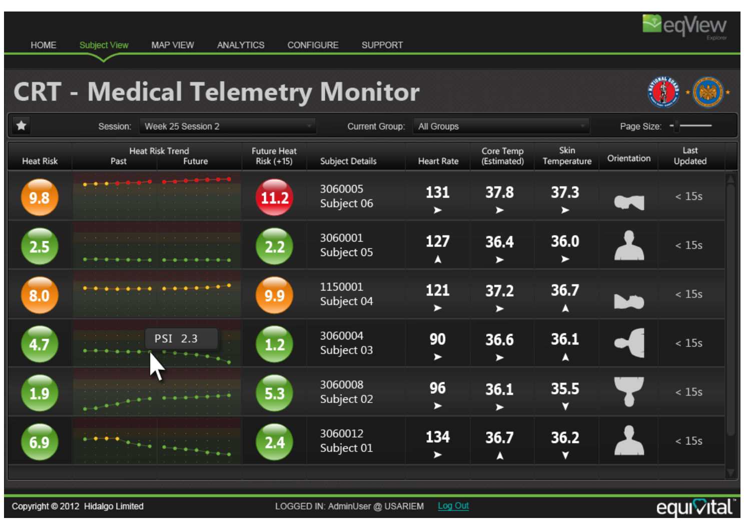

Figure 3.14: WMD-CST Medical Telemetry Monitor showing the estimated thermal-work strain index value on the left and the 15 minute predict ahead TWSI value for each team member along with heart rate, estimated core body temperature, skin temperature, and body orientation.

Training Events

All data were collected during regularly scheduled training where the programs of instruction were developed by the units prior to the study. A description of the training was obtained from the unit prior to the study. In addition, data collectors recorded the activities during the training to verify the descriptions provided by the units. A general description of the training is provided below for each training event. Figure 3.15 illustrates the CBRNE-PPE used by volunteers during their training.

Event 1 Event 2 Event 3

Figure 3.15: Personal protective equipment worn by Soldiers from three training events.

Event 1 (Edgewood, MD)

The training exercise had a total of 12 U.S. Army Soldiers participate. On the first day of training all were outfitted with the data collection system, while on the second day only seven individuals wore the data collection system. The total duration of each day's training exercise was approximately 75 minutes; individuals were fully encapsulated in their PPE for about 45 minutes and partially encapsulated for the remainder of the time. The PPE consisted of the Joint Service Lightweight Integrated Suit Technology (JSLIST) uniform, rubber boots, protective mask (M40, M50, or M52) in the Mission Orientated Protective Posture IV (suit, mask, boots, and gloves worn). Three individuals from the day 1 group of 12 were part of an Explosive Ordinance Disposal (EOD) team. In addition to the ensemble worn by the other participants they wore the Improved Outer Tactical Vest (IOTV) with body armor and a Kevlar Helmet.

The exercise took place indoors in a large warehouse with no-air conditioning (Day 1: Air Temperature (Tair) = 28.7°C, Relative Humidity (RH) = 67.2%; Day 2: Tair = 28.1°C, RH = 68.9%). On both days the training took place in the morning.

The exercise began with EOD personnel conducting an initial entry after walking approximately 10 meters in their PPE. Personnel searched and disarmed simulated explosive devices. The Chemical Response Team (CRT) individuals (n=4) wore the same equipment and then followed the EOD personnel to the site. That is, after any simulated explosives were disarmed, the EOD personnel left and the CRT sampling teams arrived to secure any chemical, biological, radiological, or nuclear (CBRN) samples of material. After the EOD and CRT sampling teams left the site they traveled approximately 10m and went through a decontamination procedure, which included washing the PPE down and suit removal. There were four Soldiers that worked the Decontamination Station. One soldier was the supervisor and was not part of the EOD, CRT sampling or CRT decontamination teams. Because the training was staggered each of these three groups worked including planning, waiting, and including their physical work for approximately 45 minutes (time encapsulated in PPE) of the entire 75 min exercise. Training was similar on both test days.

Event 2 (Hayward, CA)

Approach March (Day 1): Army National Guard Soldiers (n=7) in Level A CBRNE-PPE with self-contained breathing apparatus (SCBA) walked self-paced for approximately 45 minutes covering just less than 2 kilometers. This simulated an approach to a CBRNE contamination site (Tair = 21.9°C, RH = 36.2%). The training took place in the morning under direct sunlight with no cloud cover.

Sampling (Day 2): Soldiers (n=6) walked approximately 400 meters into a designated contaminated area which simulated an illicit drug laboratory. Soldiers were required to search and secure the room. They also secured a sample of the simulated chemical materials present, properly packaged and documented the sample, then returned the sample to the decontamination line for processing prior to transferring the sample to the CST mobile Analytical Laboratory System (ALS) for analysis. All volunteers were encapsulated in Level A for approximately 45 min while doing their assigned jobs (Tair = 14.6°C, RH = 79.3%). Most of the time was spent in a non-air conditioned room with the doors and windows open to the outside. The training took place in the morning with partly cloudy skies.

Search and Rescue (Day 3): Soldiers (n=6) completed a search and rescue operation in a four-story fire tower. They searched the area, cleared rooms, and rescued a downed person (~85 kg manikin). All volunteers were encapsulated in Level A for approximately 45 min while doing their assigned jobs (Tair = 16.0°C, RH = 48.5%). Most of the time was spent in a non-air conditioned fire tower with the doors and windows partially opened to the outside. The training took place in the morning, with cloudy skies.

Event 3 (Hanscom Air Force Base, MA)

All volunteers (n=7) wore Level A CBRNE-PPE during two days of training exercises. Five volunteers used SCBA while two volunteers used Powered, Air-Purifying Respirator systems. The training exercises were less than 60 min in duration and were repeated on the second day. For day 1 the training took place in the morning in direct sunlight with no cloud cover (Tair = 18.1°C, RH = 42.9%). For day 2 the training took place in the morning under an overcast sky of dark clouds (Tair = 17.7°C RH = 84.7%).

Two soldiers constructed a subway track berm. Activities included carrying a heavy container (~23 kg) and assembling materials according to a standard operating procedure to create this berm. The constructed berm would collect runoff of decontaminated liquids used to clean the contaminated subway tracks. The WMD-CST personnel wore CBRNE-PPE while constructing this berm. Five other soldiers participated in a search and rescue operation in an abandoned building simulating a chemical laboratory. They were required to secure and move a flexible stretcher with a simulated human casualty (~85 kg manikin), inventory chemical glassware, and reassemble the chemical glassware equipment in the way they found it (cognitive and fine motor tasks). Throughout this exercise, they moved up and down stairwells of a three-story building.

Physiological Measures

For all three training events, HR and CT were recorded every 15s using a chest belt physiological monitoring system (Equivital™ EQ-02, Hidalgo Ltd., Cambridge UK) with an associated ingestible thermometer pill (Jonah Core Temperature Pill, MiniMitter, Respironics, Philips, Bend OR). Participants ingested one thermometer pill at least 12 hours prior to the training event and a second pill on the morning of the training event. On subsequent days additional thermometer pills were administered if participants passed one of the earlier pills. This method allowed for at least one thermometer pill to be far enough along in the intestinal tract to avoid errors from ingested fluids. Prior to the training events, participants donned the physiological monitoring system according to the manufacturers' instructions. Each participant's real time data were checked for accurate reporting of HR and CT prior to the training event. In some circumstances, thermometer pills could not be given prior to the start of the training event. Core temperature data were not used if there were obvious signs of drink signatures (rapid decrease in CT below 35 ºC and slow recovery to normal body temperature).

Core Temperature Estimation

Core body temperatures were estimated using measures of HR and the Kalman filter algorithm Buller et al. (2013). Heart rate and CT were reduced to one minute intervals by taking the median of the four 15s samples for each one minute epoch. The CT algorithm was seeded with the actual starting core body temperature as measured by the ingestible thermometer pill; with the assumption that initial CT during these real-life events could be estimated or measured prior to mission start.

Thermal-Work Strain Index (TWSI)

Observed HR and CT were used to compute the Thermal-Work Strain Index (TWSI) according to Moran et al. (1998) see Equation 3.33.

$$TWSI \; = 5(CT - CT_{rest})(39.5 - CT_{rest})^{-1} + 5(HR - HR_{rest})(180 - HR_{rest})^{-1} \quad (3.33)$$

Where TWSI is the thermal-work strain index, CT is core body temperature, and HR is HR. The *rest* suffix denotes the HR or CT at rest prior to exercise. For this analysis CT_{rest} was set at 37.1 °C and HR_{rest} at 71 beats/min.. An Estimated TWSI was computed using HR and the CT estimate.

Statistical Analysis

Work rates of participants varied greatly within events, with some getting hot and others remaining cool. For each event the grand mean HR and mean maximum CT were computed for the hottest four runs (“hot”) (those runs where participants had the highest CT), coolest four runs (“cool”) (those runs where the participants had the coolest CT) and for the remainder of the runs (“moderate”). The mean maximum TWSI was computed according to Moran et al. (1998) for each of the three temperature groups.

To examine the performance of the CT_est algorithm the limits of agreement (LoA) method (Bland and Altman 1986) and root mean square error (RMSE) ($RMSE = \sqrt{\sum_{t=1}^{N}(Tc_t - Tc\_est_t)^2/N}$) were selected as the most appropriate means for assessing agreement between the observed CT and CT_est. The LoA method utilizes a Bland-Altman chart to plot the average of observed and estimated values against the difference (estimate –

observation). The method also computes bias as the mean of the differences between CT and CT_est LoA are computed as bias ± 1.96 × SD of the differences. The LoA provide a range of error within which 95% of all CT_est should fall assuming a normal distribution. Bias and LoA from all data were computed for each training event. Root mean square errors were computed for each individual volunteer for each training session and an overall mean RMSE was computed for each training event. At each training event there were either two or three training scenarios on different days that were grouped together for this analysis. This grouping meant that individual participants had data from one to three training sessions included in the overall event analysis. Overall RMSE for each training event was weighted by participant and training session duration. A single factor (training event) analysis of variance (ANOVA) was used to test for differences in CT estimation performance (RMSE, bias, and LoA) across study events. For the ANOVA analysis RMSE, bias, and LoA were calculated for each participant for each training session.

To examine whether there was a difference in the algorithm's performance between those participants who were hotter and cooler based on CT and to identify whether performance changed over time a mixed model two factor [time (within participant) x temperature group (between participant)] ANOVA was conducted for RMSE and bias. The temperature group was composed of "hot", "cool", and "moderate" groups. The "hot" group was composed of the four runs with the highest CT from each event. The "cool" group was composed of the four runs with the lowest CT's from each event; with the "moderate" group composed of the remaining runs. RMSE and bias were computed for each individual run at 10, 20, 30, and 40 minutes from data ± 5 minutes around these time intervals. Pairwise comparisons were not adjusted for multiple comparisons to lean towards making Type I errors and identify a possible area where the algorithm is performing differently. To examine the limitation of knowing or measuring a starting CT the algorithm was re-run using an assumed resting CT of 37.1 °C and an initial model variance of v_0=0.01. The mixed model two factor ANOVA was repeated using the RMSE and bias from the algorithm using the fixed start CT.

An overall RMSE was computed, weighted by each individual and duration of the training event. Overall bias and LoA were computed from all data points. Finally thermal-work strain index values were computed from HR and both the observed and estimated CT. Overall bias, RMSE and LoA were computed for the observed versus estimated TWSI. The alpha significance level was set at 0.05. Mean values are reported with ± SD.

3.3.2 Results

Table 3.11 presents the weighted mean RMSE, bias and limits of agreement (LoA) for each training event showing the length of each individual training session and the number of participants who completed each training session. RMSE was weighted by length of training session and number of participants. Bias and LoA were computed from all data points for each training event and overall.

Table 3.11: Mean root mean square error (RMSE), bias, and limits of agreement (LoA) for each of the three training events and overall.

Event #	No. of min.	n	RMSE (ºC)	Bias (ºC)	LoA (ºC)
1	~95 each	12	0.20 ± 0.11	0.01 ± 0.26	± 0.50
2	~45 each	8	0.24 ± 0.11	0.04 ± 0.26	± 0.51
3	~45 each	7	0.17 ± 0.09	0.03 ± 0.19	± 0.37
Overall	†	†	0.21 ± 0.11	0.02 ± 0.25	± 0.48

†Overall RMSE, Bias and LoA weighted by participant and exercise duration.

Figures 3.16, 3.17, and 3.18 show two panels mean HR (A), and mean CT (B) for the "hot", "moderate", and "cool" groups from each event. Panel B also shows mean estimate CT (dashed line) for these same temperature groups. Error bars show the SD for the "hot" and "cool" groups. Table 3.12 shows the grand mean HR and mean maximum CT and TWSI for each event for the "hot", "moderate", and "cool" groups.

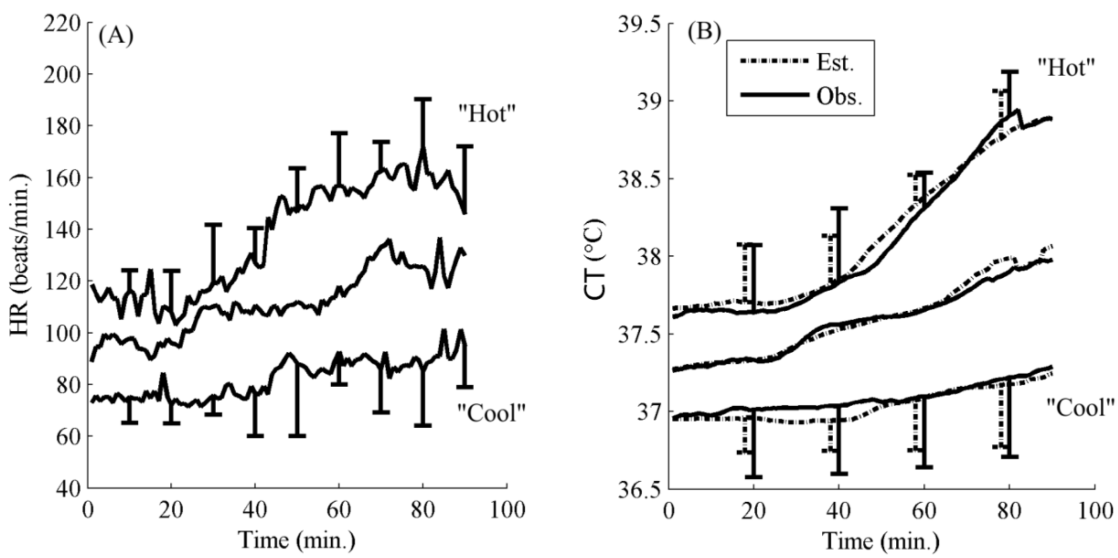

Figure 3.16: Event 1. Panel (A) Mean HR for "hot", "moderate", and "cool" training sessions showing SD error bars for "hot" and "cold" sessions. Panel (B) Mean CT (Obs.) and mean estimated CT (Est.) for "hot", "moderate", and "cool" training sessions showing SD error bars for "hot" and "cold" sessions.

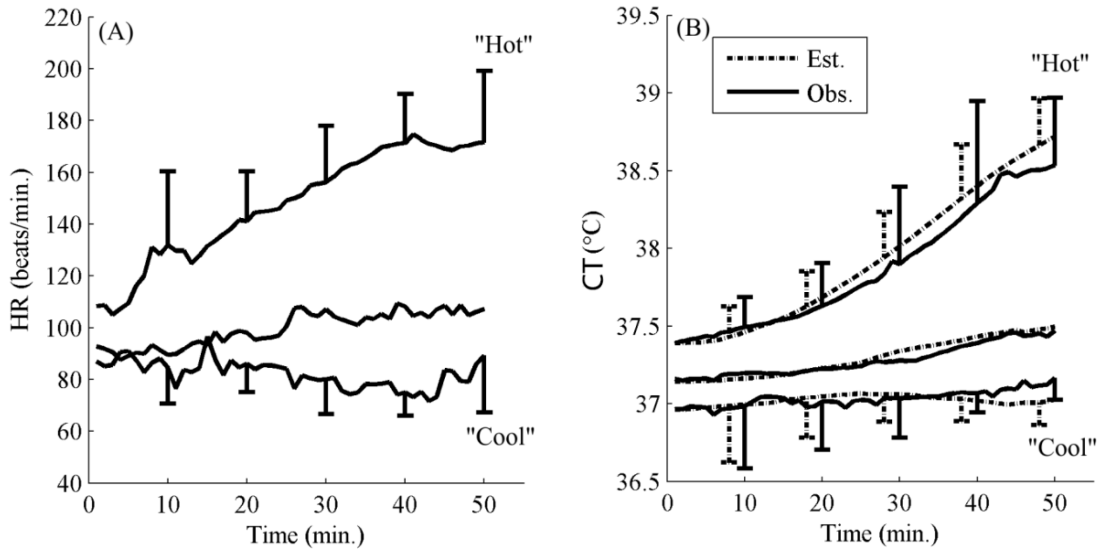

Figure 3.17: Event 2. Panel (A) Mean HR for "hot", "moderate", and "cool" training sessions showing SD error bars for "hot" and "cold" sessions. Panel (B) Mean CT (Obs.) and mean estimated CT (Est.) for "hot", "moderate", and "cool" training sessions showing SD error bars for "hot" and "cold" sessions.

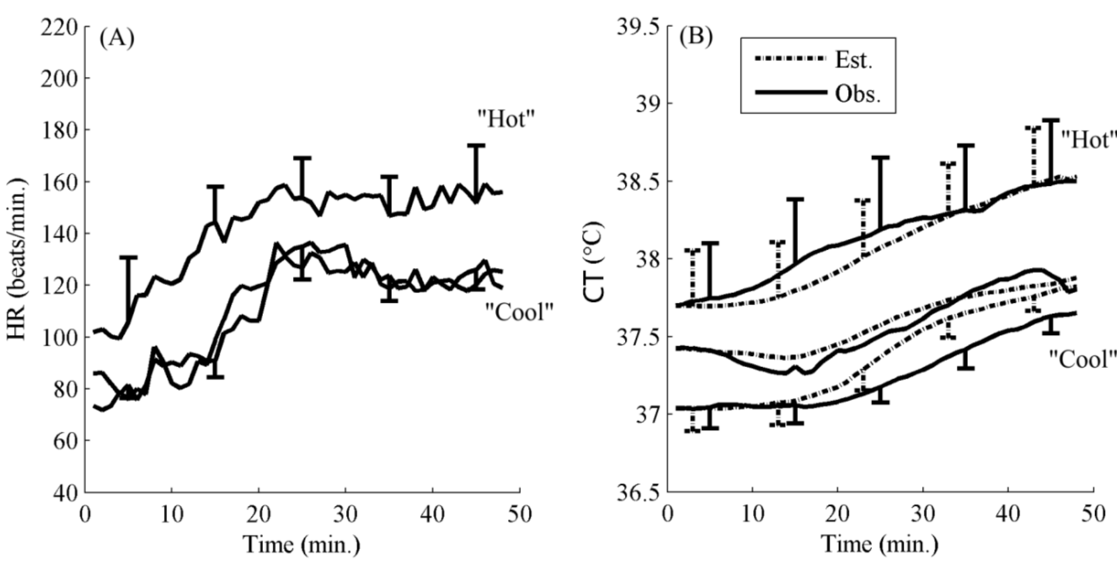

Figure 3.18: Event 3. Panel (A) Mean HR for "hot", "moderate", and "cool" training sessions showing SD error bars for "hot" and "cold" sessions. Panel (B) Mean CT (Obs.) and mean estimated CT (Est.) for "hot", "moderate", and "cool" training sessions showing SD error bars for "hot" and "cold" sessions.

Table 3.12: Mean heart rate (HR), and mean maximum core body temperature (CT) for each of the three training events for the most hottest ("Hot"), coolest ("Cool"), and other subjects ("Moderate").

	"Hot"			"Moderate"			"Cool"		
Event	Mean HR (bpm)	Max CT (°C)	Max TWSI	Mean HR (bpm)	Max CT (°C)	Max TWSI	Mean HR (bpm)	Max CT (°C)	Max TWSI
1	135±8	38.9±0.3	8.1±1.2	110±10	38.1±0.2	5.2±1.2	82±15	37.3±0.6	2.2±1.8
2	148±16	38.9±0.6	8.8±1.1	103±14	37.7±0.2	4.4±1.5	91±13	37.4±0.1	3.2±0.3
3	144±21	38.6±0.4	7.8±1.6	112±10	38.1±0.2	5.2±1.2	112±4	37.7±0.1	4.3±0.2

No significant differences were found for the estimation algorithm performance measures of RMSE, bias and LoA between testing events ($F(2,49)$ = 1.15, p = 0.32; $F(2,49)$ = 0.16, p = 0.85; $F(2,49)$ = 0.96, p = 0.39 for event 1, 2 and 3 respectively). Figure 3.19 shows a scatter plot, Bland-Altman plot and histogram for the data combined from all three training events. The combined data show good agreement between CT and CT_est across a range of CT (36 to 39.5 ºC) with minimal bias with 95% of errors within ± 0.48 °C.

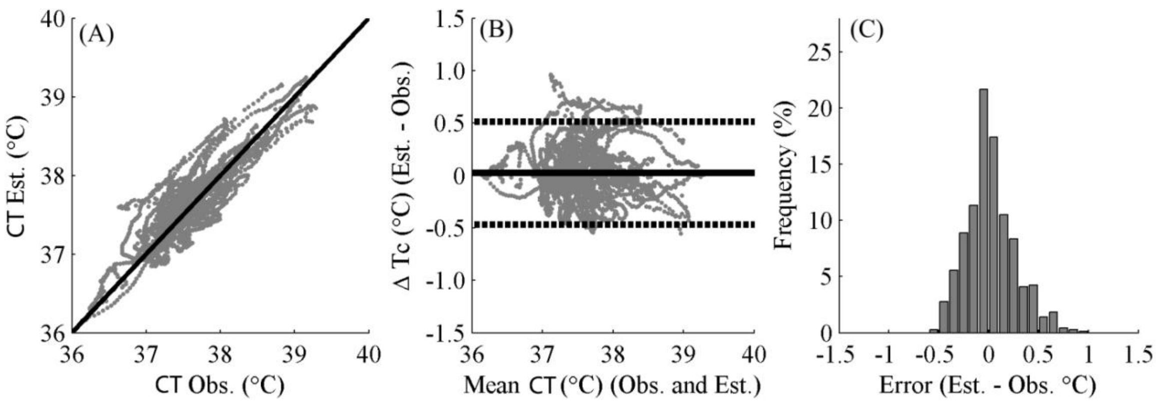

Figure 3.19: Overall results. Panel (A) scatter plot of observed (Obs.) CT versus estimated (Est.) CT showing the line of identity (solid). Panel (B) Bland Altman plot showing bias (solid) and ± 1.96 SD (dashed). Panel (C) normalized histogram of algorithm error.

No significant differences were found in bias for the main effect of temperature group ($F (2,49)$ = 0.002, p = 0.99); time point ($F(3,147)$ = 0.217, p = 0.88); and the interaction of temperature group and time point ($F(6, 147)$ = 0.939, p = 0.47). RMSE did not vary significantly ($F(2,49)$ = 0.62, p = 0.54) between temperature groups. The interaction between temperature group and time point was not significant ($F(6,147)$ = 0.48, p = 0.83). However, RMSE did vary significantly between time points (F (3,147) = 17.33, p < 0.001). Table 3.13 shows the marginal means for the temperature and time point groups.

Table 3.13: Marginal means and SD for algorithm runs with CT start set by the initial observed CT, and fixed at 37.1 °C by time period and temperature group.

		Time Period				Temperature Group		
		10 min.	20 min.	30 min.	40 min.	Low	Mod.	Hot
CT Start = Obs.	RMSE (°C)	0.09 [a] ± 0.06	0.15 [b] ± 0.10	0.20 ± 0.15	0.23 ± 0.17	0.17 ± 0.08	0.18 ± 0.12	0.14 ± 0.08
	Bias (°C)	0.00 ± 0.12	0.01 ± 0.20	0.01 ± 0.25	−0.02 ± 0.28	0.02 ± 0.18	0.01 ± 0.20	0.01 ± 0.17
CT Start = Fixed (37.1 °C)	RMSE (°C)	0.25 ± 0.21	0.24 ± 0.17	0.26 ± 0.19	0.26 ± 0.20	0.26 ± 0.12	0.26 ± 0.17	0.25 ± 0.15
	Bias (°C)	−0.09 [a] ± 0.31	−0.02 ± 0.29	0.04 ± 0.31	0.01 ± 0.33	0.08 ± 0.28	−0.03 ± 0.29	−0.07 ± 0.28

[a] Significantly different from time points 20, 30, and 40 minutes (p<0.05).
[b] Significantly different from time points 30 and 40 minutes (p<0.05).

Figure 3.20 (panel B) shows the marginal RMSE means for each of the time points of 10, 20, 30, and 40 minutes. RMSE increases significantly from 10 to 20 minutes (p <0.001) and 20 to 30 minutes (p = 0.02). However, RMSE is not significantly different between 30 and 40 minutes (p = 0.99).

When the algorithm was run with a fixed starting CT of 37.1 °C weighted mean RMSE was 0.29 ± 0.14, bias = −0.002 ± 0.32, and LoA = 0.63. No significant differences in RMSE were found between time points ($F(3,147)$ = 0.23, p = 0.87); temperature group ($F(2,49)$ = 0.02, p = 0.98); and the interaction term (F(6,147) =1.16, p = 0.33). Figure 3.20 (panel B) shows the marginal mean RMSE for each of the four time points.

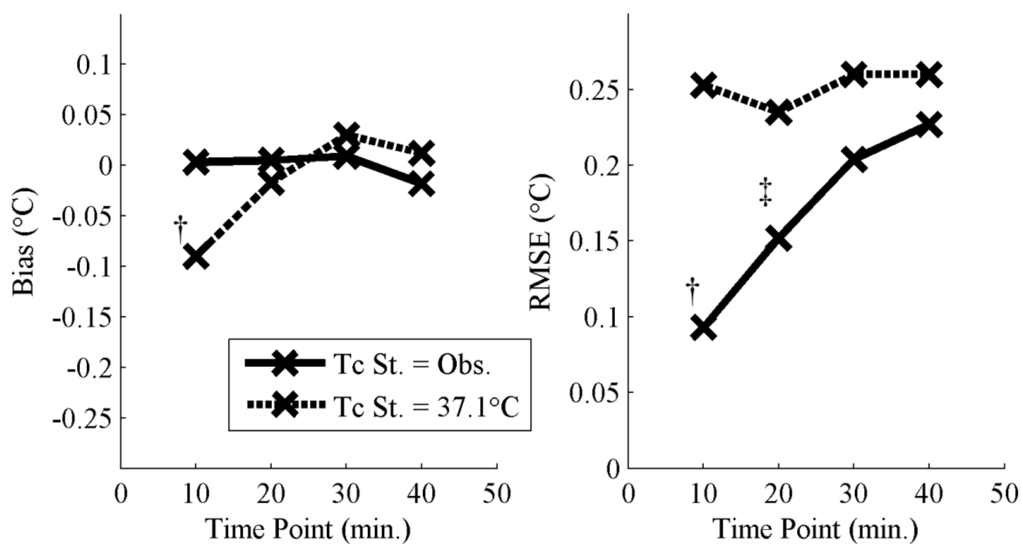

Figure 3.20: Marginal mean bias (Panel A) and marginal mean RMSE (Panel B) for algorithm runs using observed (Obs.) start (St.) CT (solid line) and fixed start CT = 37.1 °C (dashed line) for time points 10, 20, 30 and 40 minutes into runs. † Time point 10 is significantly different from time points 20, 30, and 40 (p <0.05). ‡ Time point 20 is significantly different from time points 30 and 40 (p <0.05).

Bias was not significantly different by group (*F(2,49)* = 0.98, *p* = 0.38). However, bias was significantly different by both time period (*F(3,147)* =19.87, $p < 0.001$); and the time period by group interaction (*F(6,147)* = 4.06; *p* = 0.001). Figure 3.20 (panel A) shows the marginal mean bias for each of the time points. Table 3.13 shows the marginal means for the temperature and time point groups. Bias at time point 10 is significantly different from the bias at the other time points ($p < 0.03$). Bias is initially negative for the "hot" and "moderate" groups and positive for the cool group converging to around zero at time points 30 and 40.

Thermal-Work Strain Index Comparison

Overall the TWSI RMSE was 0.39±0.34 units, with a bias of 0.04±0.51 TWSI units. Of all the data points 95% fell within ±1.00 TWSI unit. Figure 3.21 shows the Bland-Altman plot (bias – solid; limits of agreement ±1.96•SD – dashed) which indicates there is good agreement between observed and estimated TWSI across the 0 to 10 range.

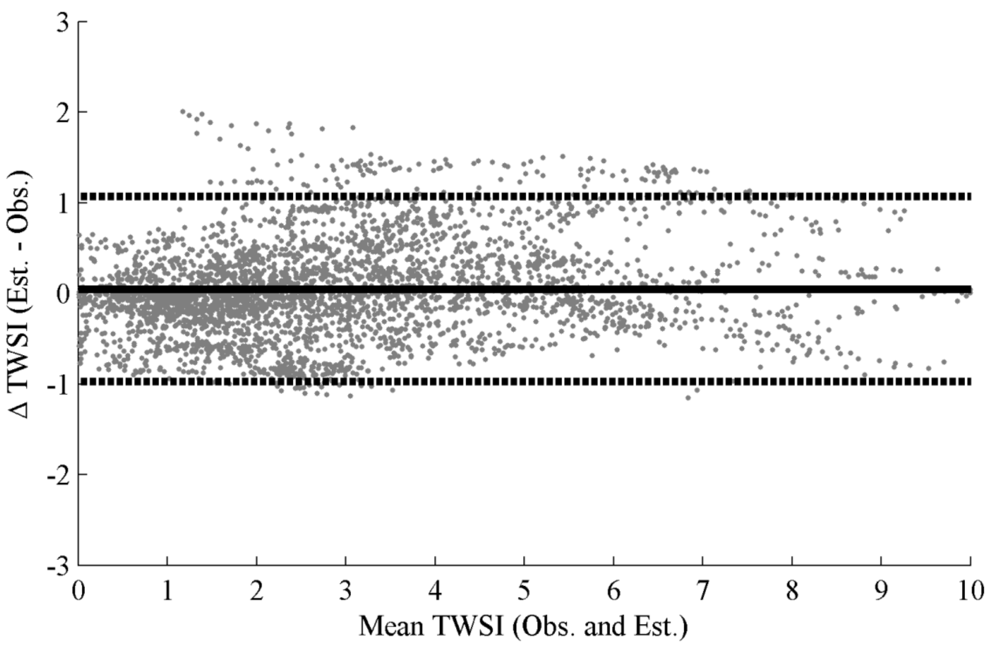

*Figure 3.21: Bland Altman plot of observed versus estimated thermal-work strain index for data from all three training events. Bias is the solid line, ±1.96*SD are shown as dashed lines.*

3.3.3 Discussion

The CT_est algorithm was validated against three groups of Soldiers conducting different field training exercises. The algorithm overall performed similarly to the original paper CBRNE laboratory study, suggesting that it is a valid estimate of CT under different field CBRNE conditions. Using only measures of HR, the CT_est algorithm estimated CT with a small overall bias of 0.02 ºC, well within the individual biological variation of ± 0.25 °C found by Consolazio, Johnson and Pecora (1963), and less than the more conservative bias threshold of ± 0.1 ºC suggested by Byrne and Lim (2007). The overall mean RMSE of 0.21 °C ± 0.11 ºC is similar to the result for the laboratory study of encapsulated test volunteers (RMSE = 0.19 ± 0.16) reported in the original article (Buller et al., 2013). The overall RMSE is also less than that found in other comparisons of different measures of core temperature (rectal vs. esophageal; rectal vs. ingested pill; and esophageal vs. ingested pill) with exercise under warm (RMSE = 0.30 ± 0.03, 0.22 ± 0.06, 0.26 ± 0.03 ºC, respectively) and cold (RMSE = 0.35 ± 0.06, 0.36 ± 0.08, 0.24 ± 0.02 ºC, respectively) conditions reported by O'Brien et al. (1998). While the overall LoA of ± 0.48 ºC exceeded Byrne and Lim's (2007) suggested acceptance threshold of ± 0.4 ºC, it is within the weighted average ± 0.58 ºC of five other studies (Kolka et al., 1993; Lee et al., 2000, Teunissen et al., 2011; Brauer et al., 1997; Al-Mukhaizeem et al., 2004) that examined how rectal and esophageal methods of measuring CT compare (see Buller et al., 2013, Table 2 for more details). In addition, when temperature measurement techniques are compared during transitions from rest-to-exercise, and from exercise-to-rest these laboratory probe comparison LoAs increase further, e.g., a LoA of ± 0.63 ºC (Teunissen et al., 2011). Data from this study include these types of transition periods. Most errors beyond ± 0.5 ºC were overestimates. While this may lead to several false positives for high thermal-work strain, from a safety point of view it is better to produce false positives rather than problematic false negatives.

For this series of CBRNE studies the CT_est algorithm showed similar performance across different training activities with different environmental conditions (Tair range: 14 to 29 ºC). The CT_est algorithm results from these CBRNE field studies had RMSE's and LoAs less than when compared the performance from non-CBRNE conditions (Overall RMSE = 0.30 ± 0.13 ºC, bias = −0.03 ± 0.32 °C, and LoA of ± 0.63 from Buller et al., 2013). The microclimate within the encapsulating PPE worn by the test volunteers in this study may serve to limit variability in CT estimation as the effects of air movement and clothing parameters are minimized. Importantly the CT estimation algorithm worked similarly between the participants who reached high core temperatures approaching 39 °C and those who remained cooler during the exercises.

As one would expect starting the algorithm with an observed CT leads to initial RMSE's that are small and get larger as time passes. However, at 30 minutes the RMSE begins to asymptote (no significant difference in RMSE at 30 and 40 minutes). A similar pattern can be seen in the increase in the standard deviation of the bias (see Table 4). Conversely providing the model with a best guess for the starting CT (e.g. a resting CT of 37.1 °C) leads to estimates where the RMSE remains constant across time points, but where bias at time point 10 (bias = −0.09 °C) is significantly different from the bias at time point 20 (bias = −0.02 °C). When the algorithm is started with an with a best guess CT and the initial variance is appropriately set (a non-zero value) to indicate lack of confidence in the initial value, the algorithm will quickly seek an appropriate CT based upon the observed HR. This effect can be seen in the convergence of the bias values to zero as time progresses (Figure 3.20, panel A).

These results suggest that measuring and using an initial CT provides an early accuracy benefit. However this benefit is lost by about minute 30 when the RMSE asymptotes. Similarly when using a best guess for the initial CT the algorithm bias will initially be poor since a first "guess" may under or overestimate the true CT. However, the model's ability to seek the most appropriate CT appears to remove this early bias by minute 20.

This effect of the algorithm to seek the most appropriate CT based upon HR is important to account for the increase in CT due to heat storage over successive work rest periods. Horn et al. (2013) demonstrated that in addition to increases in peak CT, there was a correlated rise in peak HR for successive work rest training exercise bouts. While our data do not contain successive bouts of work the correlated rise in HR along with rises in CT found by Horn et al. (2013) are suggestive that the algorithm would respond appropriately. In the previous work Buller et al. (2013) presented a series of validation studies consisting of laboratory studies in the heat with six work rest periods over the space of eight hours. In these studies there does not appear to be any significant increase in absolute bias (group mean estimated values track observed values), or LoA (SD of estimated values do not appear to increase during latter parts of the study) for successive work bouts.

Limitations

There are several limitations in generalizing this work. The efficacy of the algorithm in detecting thermal-work strain needs to be tested in a larger population where the specificity and sensitivity can better be determined. The participants in this study also represent a fairly homogenous group in terms of age and fitness level (all had to pass the yearly U.S. Army physical fitness test) and the algorithm would need to be adjusted for populations that differed in these respects. For older volunteers the HR to CT observation function will likely need to be adjusted for maximal heart rate reductions with increased age. Similarly, the temporal response of the model will likely need to be adjusted for individuals with substantially different fitness levels. For example, an increase in aerobic fitness leads to an increase in stroke volume (Cox, Bennett and Dudley 1986) and thus a greater cardiac output per heartbeat, greater oxygen uptake and subsequently more rapid heat production / blood flow to the skin.

While there were only two women subjects in this analysis the algorithm should have applicability beyond just the majority population of men used in this analysis and the previous validation paper. Gagnon and Kenny (2012) indicate that sex differences in metabolic heat production and cooling can be normalized by body weight and surface area, and Cramer and Jay (2014) and the accompanying editorial by Cheuvront (2014) provides further evidence that sex plays a limited role in thermoregulation.

Finally, the algorithm works best when started with a known CT. However there may be times when this is not possible. In these cases providing an initial estimate of CT can suffice, but overall RMSE and LoA will increase. In the case of these events when we assumed a starting CT of 37.1 °C the CT_est values had a weighted mean RMSE of 0.29 ± 0.14, a bias −0.002 ± 0.32, and LoA = 0.63 which as argued above are still reasonable estimates.

Thermal-Work Strain Estimation

Finally, when estimated CT is used to calculate the TWSI, 95% of all estimates fall within ±1 TWSI unit. This appears to hold true whether the individual is at a low or high thermal-work strain. Most errors beyond ±1 TWSI occur when the individuals are at lower thermal-work strains and are almost always over estimates. When the TWSI scale is examined the difference between anchor words is always 2 units. This would suggest that in 95% of cases if an individual is truly at a TWSI of 9 (“Very High”) then the estimate derived from estimated CT would fall between a TWSI of 8 and 10. This at the very least this would be interpreted at the high end of “High” thermal-work strain.

3.3.4 Conclusion

Individualized thermal-work strain monitoring is important given that thermal strain responses differ for individuals conducting the same task (Tharion et al., 2013b). The core temperature estimation algorithm evaluated in this first-responder chemical-biological context was able to provide valid estimates of core temperature in different ambient environments. Thus, when this algorithm is used in conjunction with a physiological monitoring system individualized thermal-work strain can be estimated in real-time and used to help prevent heat illness or injury and better manage work schedules.

3.4 Overall Conclusions

Our *computational physiology* approach has demonstrated how formalizing an open physiology research problem into a graphical model can produce estimation results that improve upon current techniques and that also provides additional insight into important, otherwise unseen, internal states and dependencies in the human thermoregulatory system. Using these insights we were able to simplify the model and provide a general core body temperature estimation algorithm based only upon sequential observations of heart rate. Using previously collected data we were able to show that the model had a performed almost as well as laboratory methods for measuring core body temperature. We were able to demonstrate that the estimation technique performed similarly for different work rates, across a wide range of environments, when subjects wore just shorts and t-shirts to when they were fully encapsulated in chemical/biological personal protective equipment. Finally we show the estimation technique in use as part of a wearable thermal-work strain physiological monitoring system during real-time training missions for two National Guard Weapons of Mass Destruction - Civil Support Teams. When the core body temperature is estimated in real-time and is used in conjunction with heart rate to estimate the thermal-work strain index (TWSI) 95% of all estimates fall within ± 1 TWSI unit. In fact focus groups identified that all subjects felt that the TWSI provided in real time was an accurate reflection of how they were feeling (Tharion et al., 2013b). Thus we conclude that this algorithm when used in conjunction with a physiological monitoring system that individualized thermal-work strain can be estimated in real-time and used to help prevent heat illness/injury and to better manage work schedules and practices.

As detailed in the previous sections, the core body temperature estimation technique does have some limitations. The technique was validated and tested in real-time on a fairly homogenous set of subjects. The participants were generally young (early 20s), fairly fit - most having to have passed the Army physical fitness test. For older volunteers the heart rate to CT observation function will likely need to be adjusted for maximal heart rate reductions with increased age. Similarly, the temporal response of the model will likely need to be adjusted for individuals with substantially different fitness levels. Our future work will focus on adapting the model for age and fitness and testing the model in a larger population where the specificity and sensitivity can better be determined.

This section has demonstrated how we have taken an open problem in the literature and developed a simple one parameter solution using a computational physiology approach. We have shown how our solution works across a wide range of settings in both laboratory and field experiments with better performance compared to previous work all the while using only one input parameter. We have demonstrated how our solution was implemented into a real-time commercial physiological monitoring system and used during several first responder training events. The approach has been patented by the U.S. Army Research Institute of Environmental Medicine (Buller 2013), and has been licensed to two commercial vendors (Hidalgo Ltd, Cambridge UK; Zephyr Inc, Annapolis MD). Finally, the approach is being adopted by the National Guard as a requirement for physiological monitoring systems to be bought for the 57 Weapons of Mass Destruction – Civil Support Teams. Our approach appears to be not only valid in an academic sense but shows real potential as practical solution to thermal-work strain monitoring. It can be readily adopted by any device that accurately measures heart rate and when used in conjunction with the TWSI can accurately estimate thermal-work strain state.

Chapter 4

Policy Estimation using Markov Decision Processes

The second component of the physiological feedback loop is to provide optimal advice to in completing a defined goal, based upon an individual's thermal-work strain health state. We focused on two questions: 1) is it possible to adequately express the tasks, risks and goals surrounding thermal-work strain management in terms of a simple MDP that would provide a realistic policy, and 2) would any derived policy perform better than the solution provided by the human agents themselves, responding to their own self-perceived physiology? To answer these questions we developed an MDP to model the U.S. Army Ranger Training Brigade course selection road march, and compared our optimal policy and its effect on TWSI to real world data. The road march had several attractive features that relate to our overall systems goals. First Ranger school has a series of arduous tasks that must be completed for students to graduate. Thus finishing the road march with as low an TWSI as possible is an advantage, conserving physiological reserves needed for subsequent events. Second as the Ranger students are very fit, motivated, and experienced in extreme conditions, finding a policy that improves upon their performance is non-trivial. Finally, the TWSI safety constraints we wish to place upon our policy are needed in this training environment, as one student from our data collection was medically withdrawn from the road march due to hyperthermia with an TWSI of 10.

4.1 Modeling Experiment

The U.S. Army Ranger students needed to complete an eight-mile road march while carrying 32 kg (70 lbs.) within 130 min or be dropped from the Ranger School. The road march was one of a series of demanding tasks scheduled for the week. The road march was conducted at night in temperatures of ~25 °C and 85 % relative humidity. The required march pace was such that students often needed to run parts of the course. Students applied different strategies to completing the march. Some started quickly and then reduced speed, while others started slowly then increased speed to complete on time, yet others kept a consistent pace. Our experimental goal was to demonstrate: 1) we can learn a policy that allows students to complete the course on-time and avoid hyperthermia; and 2) that the policy also allows students to complete the course with lower final TWSI scores than without using our policy.

4.2 Subjects and Measures

Fourteen male U.S. Army Ranger students who averaged 26 ± 4 years of age; 1.77 ± 0.04 m in height; weighed 78.3 ± 7.3 kg; who carried loads of 31.5 ± 1.1 kg and had 14.4 ± 3.8% percent body fat (mean ± standard deviation (SD)) were used for this analysis.

Direct measures of HR (Equivital I heart rate monitor, Hidalgo Inc. Cambridge UK), and CT (Jonah Ingestible Thermometer Pill, Respironics, Bend OR) were collected in 1 minute intervals. Times to complete each mile of the course were derived from location data collected from GPS units worn by each student (Foretrex 101, Garmin, Olathe, KS). TWSI scores were computed according to Equation (2.9) using observed IT and HR and resting values of 71 beats/min and 37.1 °C (Moran et al., 1998). Tri-axial accelerometry data were collected at the chest at 25.6 Hz.

4.3 Markov Decision Process

An MDP describes an environment by a set of states (e.g. S:={SI, distance to goal, time}) an agent can assume, and a set of possible actions (A:={movement speeds}) that can be taken from those states. An in-depth description of an MDP can be found in Russell and Norvig (2010). In our environment the goals and health constraints are described by assigning rewards (R) and penalties (negative rewards) for being in various states at certain times. Our Ranger training road march has a finite horizon. Thus the utility (U) of a sequence of states can be computed from the sum of rewards (R) for being in each state over time (Equation 4.1):

$$U(s_0, s_1, s_2, \dots, s_{n-1}, s_n) = \sum_{t=0}^{n} R(s_t) \quad (4.1)$$

The transition from one state to another is determined by the current state, the chosen action and the transition probabilities to the new state (P(S'|S, A)). A policy (π) is a mapping from states to actions that prescribes an action to be taken in each state. For any policy we can compute a utility function over states for that policy starting in state s as the sum of expected rewards over time (Equation 4.2).

$$U^{\pi}(s) = E[\sum_{t=0}^{n} R\,(S_t)] \tag{4.2}$$

At each time point there will be an optimal policy that for each state will determine the optimal action to be taken which provides the most utility from that point on until the end goal is reached:

$$\pi^{*}(s) = \text{argmax}_{\pi} U^{\pi}\,(s) \tag{4.3}$$

With a constrained state space, known transition probabilities, and finite horizon this optimal policy can be computed using dynamic programming.

4.3.1 Ranger Road March MDP Definition

The goals of the actual road march were simple. Complete the 8 mile road march in 130 min or less or be dropped from the course. Given that thermal state (CT) changes relatively slowly, a time interval of 5 min was selected enabling a more thorough search of the transition probabilities state-action space.

State Definition

For states we use TWSI, in integer units; distance (D), completed in units of 0.0417 miles or the fraction of a mile that can be completed at 0.5 miles per hour (mph) within 5 minutes; and time. Thus: St:={{TWSI},{D}} Where: TWSI:={1,…,14}, D:={0, 0.0417, … , 8.9583, 9}.

Action Definition

Actions were constrained to just movement speeds from 0 to 7 mph in 0.5 mph increments, thus A:={0, 0.5, 1,…, 6.5, 7.0}. Figure 4.1 shows the resulting directed acyclic graph that represents our state-action space.

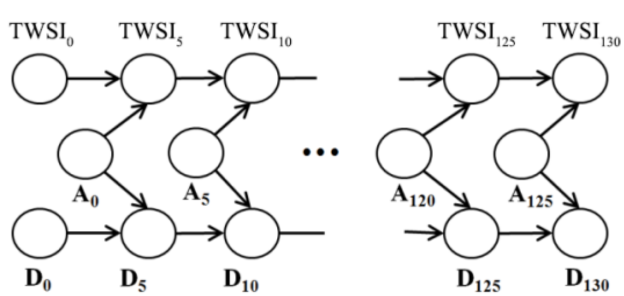

Figure 4.1: Graph representation of state-action space.

Reward Definition

Two types of rewards were used in the definition of our MDP, (a) immediate rewards for TWSI at each time point to model safety limits; and (b) end state rewards for D and TWSI to model the course completion requirement, and the goal to finish with as low an TWSI as possible. The end state reward (t=130) for D was represented by a reward of 0 for completing the course on time (D≥8 miles), and a penalty of −1000 (D<8 miles) for not. Immediate and goal reward functions for TWSI are presented in Table 4.1.

Table 4.1: Immediate and end-state reward functions for TWSI.

SI	1 to 8	9	10	11	≥12
$R_{t<130}$	0	−100	−500	−2000	−5000
$R_{t=130}$	100−10(SI−1)		−100	−2000	−5000

The end-state TWSI rewards are designed to allow the students to complete the course with the lowest possible TWSI. R(TWSI)t=130 shows that finishing with a lower TWSI is better than finishing with a higher SI. However, finishing with TWSI's > 9 is not good. The −100 reward for an TWSI of 10 indicates that it is acceptable to push to complete the course on time. However, an TWSI > 10 is an unacceptable end state, hence the large negative penalties. The immediate reward function R(TWSI)t<130 shows that it is equally fine for students to have an TWSI between 0 and 8 during the race but above 8 penalties will accrue. The negative rewards for both TWSI's of 9 and 10 allow for one or several steps to be taken at these high SI's and still receive higher utility than not completing the race on time. However, the very large negative rewards of TWSI's > 10 are designed to indicate that stopping the race for health is better than completing.

Transition Probabilities

For distance traveled we placed a small amount of uncertainty (N(0,1)) around the distance traveled in 5 minutes for a given movement speed. The transition probabilities are shown in Table 4.2 where d=D+A(5/60).

Table 4.2: P(D'|D,A), where d= D+A(5/60).

D'	−.126	−.084	−.042	d	+.042	+.084	+.126
P	.01	.05	.24	.4	.24	.05	.01

In general, the TWSI transition probabilities are complex, and are dependent on a large number of factors such as work rate, personal characteristics (body surface area, fat mass, fitness, acclimation), environmental conditions (ambient temperature, relative humidity, wind speed, solar load), and clothing characteristics (insulation properties and vapor permeability). While these dynamics are complex they have been captured to a high fidelity in physics- and physiology- based thermoregulatory models. The TWSI transition probabilities were learned by Monte Carlo approximation using the SCENARIO (Kraning and Gonzalez, 1997) thermoregulatory model to simulate the responses of humans under similar conditions to the Ranger training road march. For the model runs the mean personal characteristics of our students were used. Mean environmental conditions obtained from a nearby airport weather station were air temperature = 24.4 °C, relative humidity = 85.3%, black globe temperature = 24.4 °C, and wind speed 2.75 m/s. Clothing insulation and vapor permeability parameters for the modeling were measured from copper manikin tests of the uniform used by the students (clothing insulation factor = 1.3 CLO, and vapor permeability (im) = 0.42). Metabolic rate was computed from movement speed, height, weight and load (assuming an average course grade of 0 and movement over hard top for a terrain factor of 1) using the equation developed by Pandolf, Givoni and Goldman (1977) with the Givoni and Goldman (1971) running correction factor. With starting SI's ranging from 1 to 9 all combinations of actions in our action set were run over six 5 minute intervals. Each conditional transition probability space had at least 10^4 samples.

4.3.2 MDP Learning

We wish to learn a policy function that for any state (Time=t, SI=si and D=d) provides us with an action that maximizes the expected utility until our goal is reached. An optimal policy for any time point on our road march course can be defined as follows:

$$\pi_t^*(s) = \text{argmax}_{a\in A(s)}\, \mathrm{R(s)} + \textstyle\sum_{s'} P(s'|s,a)U_{t+5}(s') \tag{4.4}$$

A set of optimal policies can be solved iteratively using dynamic programming. Starting at the end of the race the policy at time point 125 ($\pi_{125}^*(s)$) is easily computed, as the utility function (U_{130}(s)) is defined by the goal rewards. Next $\pi_{120}^*(s)$ can then be computed using the previously computed U_{125}(s) function and so on, where the current U is computed as:

$$U_t(s) = \max_{a\in A(s)}\, \mathrm{R(s)} + \textstyle\sum_{s'} P(s'|s,a)U_{t+5}(s') \tag{4.5}$$

4.4 Analysis

For this analysis, since we were unable to provide real-time guidance to Ranger students during the road march, we utilized the SCENARIO model to both simulate the individual TWSI responses of the students using their self-paced movement ($\text{TWSI}_{\text{model}}$), and simulate the TWSI responses when conforming to the learned policy ($TWSI_{policy}$). Observed TWSI ($TWSI_{obs}$) was compared to $TWSI_{model}$ by examining the mean root mean square error (RMSE) and bias to verify that the model provided an accurate simulation of the Ranger student's responses. We then compared $TWSI_{model}$ and $TWSI_{policy}$ values at the end of the road march using a paired t-test. We examined the relationship between the degree of impact ($TWSI_{model}$–$TWSI_{policy}$, at t=130) of the learned policy to the maximal $TWSI_{model}$ and $TWSI_{obs}$ reached during the march by Pearson correlation. Finally, we examined the actual movement profile (presented as stride frequency spectrograms for the road march) of four students; two where the policy had the least impact and two where the policy had the most. Stride frequencies (proportional to movement speed) were found by applying fast Fourier transforms (FFTs) to the vertical axis accelerometry data. The alpha level for all hypothesis testing was set at 0.05.

4.5 Results

4.5.1 TWSI Transition Probabilities

Figure 4.2 shows three sets of TWSI transition probabilities in a gray scale map where black = 0 and white = 1. The learned policy can be found in Appendix B.

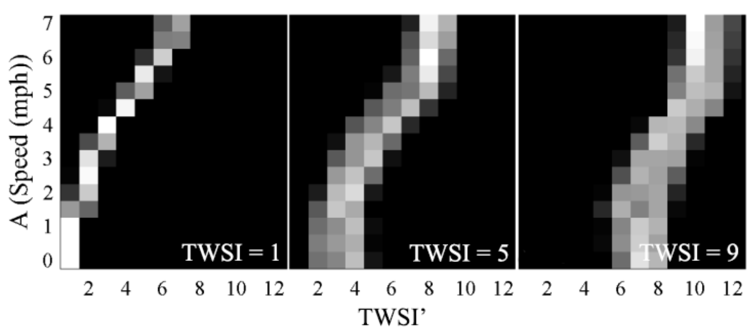

Figure 4.2: Transition probabilities for TWSI of {1, 5, 9}. Grid shade=P(TWSI'|TWSI,A) where white =1 and black=0.

4.5.2 Policy Efficacy

Figure 4.3 shows the mean group responses for the $TWSI_{obs}$ (gray), $TWSI_{modeled}$ (black), and $TWSI_{policy}$ (dashed). $TWSI_{modeled}$ differs from $TWSI_{obs}$ with a bias of −0.26 and RMSE of 1.34 ± 0.45 TWSI units.

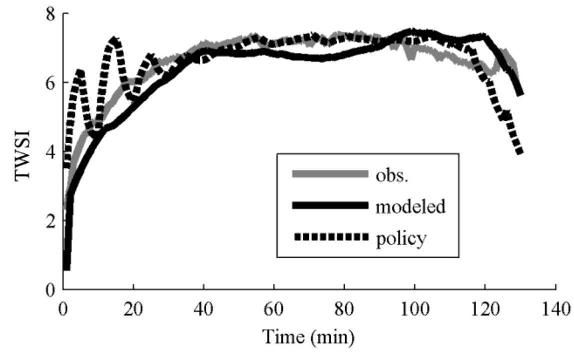

Figure 4.3: Mean group responses for the $TWSI_{obs}$ (gray), $TWSI_{modeled}$ (black), and $TWSI_{policy}$ (dashed).

The $TWSI_{policy}$ responses have a significantly lower end point at 130 minutes than $TWSI_{model}$ with a mean of 3.94 ± 0.88 versus 5.62±1.20 ($t=2.16$, $P<0.001$). Thus the policy had an overall mean impact of 1.67 TWSI units, and allowed the students to end with a "Low" thermal strain compared to a "Moderate" thermal strain (Moran et al., 1998). For all students the end-point $TWSI_{policy}$ was lower than the end-point $TWSI_{modeled}$ and the maximum $TWSI_{policy}$ score reached by any student was < 8.6.

The mean of each student's movement speeds when following our policy are shown in Figure 4.4.

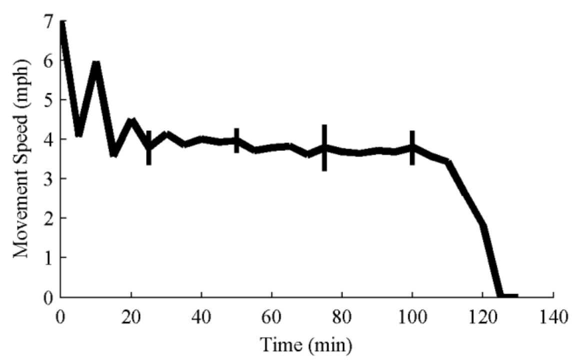

Figure 4.4: Mean of speeds taken for each student according to our optimal policy ± SD. Running is at speeds > 4.5 mph.

Figure 4.5 shows the stride frequency spectrograms for the whole road march course for four students. Panel A and B show the movement profiles where the policy had the least impact with differences in end point TWSI of 0.63 and 0.75 units. Panel C and D show the movement profiles where the policy had the most impact with end point differences in TWSI scores of 3.14 and 2.18 units. The movement rates of the students can be seen as highlights around ~2 Hz (walking) and ~3 Hz (running). These charts show that where our policy had least effect these students were already following our optimal policy (start fast, end slow). For the two students where the policy had the most affect it can be seen that one continually transitioned between walk and run (C), while the other starts and ends with walk run transitions (D).

The correlation between the policy impact and maximum $TWSI_{modeled}$ is 0.635 ($P < 0.05$); and maximum $TWSI_{observed}$ is 0.352 (not significant, N=14) but 0.622 ($P<0.05$, N=13).

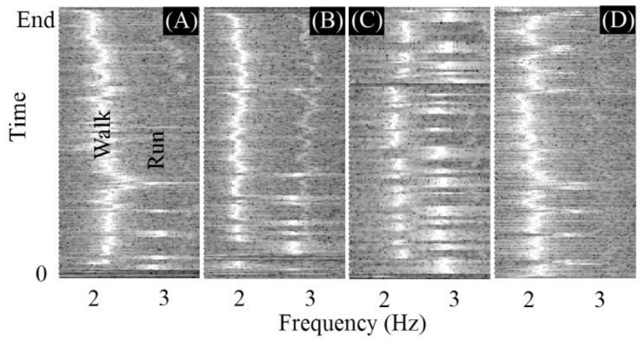

Figure 4.5: Stride Frequency Spectrograms of Students where the Policy had the Least (Panel A and B) and Most (Panel C and D) Impact. Light shades indicate more energy. Stride frequency is proportional to movement speed. Walking speeds are around 2Hz, and running speeds around 3Hz. Movement patterns for the whole road march run from the bottom of the chart to the top.

4.6 Discussion and Conclusions

The SCENARIO human thermo-regulatory model was able to accurately estimate the TWSI responses of the Ranger students with a small bias and RMSE close to one. Thus, SCENARIO provided a means to generate valid estimates of the student's thermoregulatory responses to our policy. Using this modeling approach, we found that the learned policy allowed all students to complete the course on time, with a lower SI, and without hyperthermia. Even though our learned policy is conservative with respect to avoiding high SI's, the policy allowed the students to finish in a significantly less thermally stressed state. Thus we conclude that this road march task can be modeled as a simple MDP which can generate a policy that is likely to improve the performance of these experienced students. This suggests that other MDP policies could be developed for other physically-demanding Ranger School events which could help students finish tests with the least amount of work and thermal stress possible.

While the modeling suggests that our learned policy is effective at reducing the end state TWSI score is it a reasonable policy that could be followed by people? The initial fast run and walk transitions appear, at first glance, peculiar. However, when we examine the actual movement rates of students (see Figure 6) many adopt this same movement pattern. This reflects the fact that the needed early steady state pace would force an unnatural, and energy inefficient gait that is between a walk and a run (Paroczai and Kocsis, 2006). To avoid this awkward gait the policy we learned instead alternates between an energy-efficient walk and an energy-efficient run. The fact that this pattern is learned by the model where only thermal-work strain is a factor is notable. When we examined the movement profiles of students where the policy had minimal impact we found that their actual movement profiles were similar to the learned policy (start fast, end slow). Conversely where the policy had a large impact the student's movement profiles were quite different. Additionally, we found a positive relationship between the degree of impact and the maximal TWSI obtained during the road march. This relationship held for TWSI from both modeled mile times and the observed data (albeit a student with highest TWSI had to be removed for the relationship to hold for N=13), suggesting that our learned policy was realistic and achievable and likely to result in an overall less thermally stressful road march.

Deploying this as a real system for the Ranger students would be fairly simple. Our thermal-work strain state estimator is already implemented in an Android tablet that receives data from a wearable physiological status monitor (see Figure 1). The tablet is GPS enabled and thus distance could be calculated. A policy would need to be generated for the environmental conditions of each prospective road march. Then, given the real time estimates of TWSI the tablet would be able to prompt the student with the optimum pace for each 5 minute segment.

These results also suggest that this technique shows promise for other areas such as marathon races where an athlete may desire to finish with the best time possible but avoid hyperthermia. Similarly, in cycling a safe and effective pacing strategy is desired. Atkinson et al. (2003) suggest "More research, using models and direct power measurement, is needed to elucidate fully how … pacing strategy might save time in a real race and how much variable power output can tolerated by a rider."

In conclusion this study has shown that it is possible to adequately express the tasks, risks and goals of an arduous physical activity in terms of a simple MDP. Solving the MDP for an optimal policy provided a realistic policy that allowed humans to perform their task according to pre-set goals and finish in a state of less thermal strain than would occur if they were left to follow their own training and instincts. These results suggest that live physiological state estimation, when coupled with MDP models of constrained real-world tasks, can optimize work rate policies to improve safety and reduce overall thermal-work strain burdens.

Chapter 5

Human Performance Optimization

Up to this point in this dissertation, we have developed an accurate thermal-work strain state estimator and showed that simple work goals and safety constraints could be modeled successfully as an MDP. This chapter examines the convergence of these two techniques working in real-time on human participants.

5.1 Laboratory Experiment Hypotheses

Based upon our previous work, we wanted to test the following hypotheses:

- Real-time automated pace guidance will allow participants to complete a timed treadmill exercise with lower thermal-work strain (e.g. lower TWSI, core body temperature, skin temperature, and/or heart rate) compared to completing the same goal using their own self-paced approach.
- Real-time automated pace guidance will allow participants to complete a timed treadmill exercise with less time exceeding thermal-work-strain-prescribed “safety limits” compared to completing the same goal using their own self-paced approach.
- Real-time automated pace guidance will allow participants to complete a timed treadmill exercise with lower perceived levels of exertion compared to completing the same goal using their own self-paced approach.
- Participants will show no difference in subjective thermal sensation scores between automated pacing and self-pacing.
- Real-time automated pace guidance will allow participants to complete a timed treadmill exercise with overall lower energy expenditure levels compared to participants who are self-paced (60 minute exercise session).

Additionally, we were interested in how the thermoregulatory-model-derived-transition probabilities compared to actual thermal-work strain state transitions and to how well the core-body-temperature-estimation algorithm performed on a young and fit population.

5.2 Laboratory Experiment Definition

The subject's goal of the laboratory exercise was to complete 5 miles of movement within one hour. This distance and time were chosen to balance several factors. First, we wanted a middle distance task that could be open to a variety of fit individuals. We wanted enough time to be able to manipulate the environmental, clothing, and load conditions to cause core body temperatures to rise to moderately high levels (around 39.0 °C), and we wanted a distance and time that would set an average pace that was somewhere between a comfortable run and a comfortable walk.

The 5 mph movement speed was chosen as one of the speeds that would typically fall between a comfortable walk and a comfortable run. Speed and selected gait has an impact on the metabolic cost of movement. Paroczai and Kocsis (2006), show equations for estimating metabolic cost of movement at different movement speeds for walking and running (See Figure 5.1).

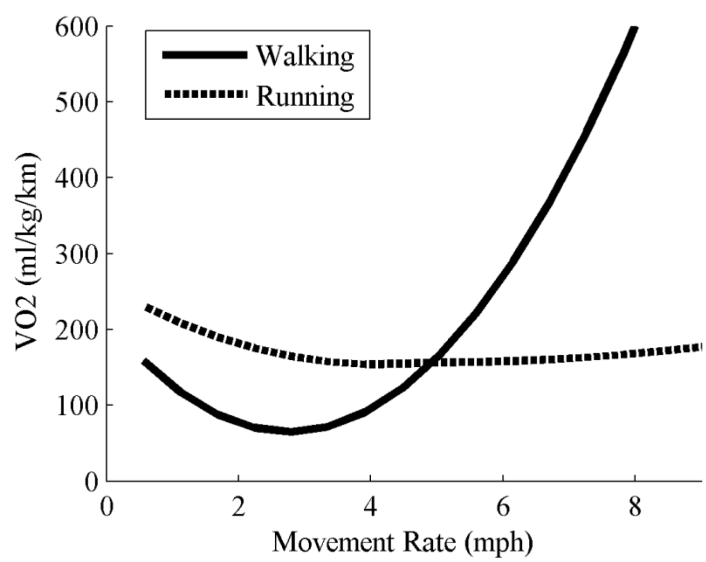

Figure 5.1: The volume of oxygen (VO2) consumed per kg per km for different walking and running speeds. Lower VO2 indicates more efficient movement.

Figure 5.1 shows that at around 5 mph there is a transition point. At speeds lower than 5 mph, walking is more efficient. At speeds above 5 mph, running is more efficient. The average movement speed of 5 mph for this study falls right at this transition point. Long and Srinivasan (2013) have shown that under time-constrained trials for these transition speeds, pace is alternated between a comfortable walk and a comfortable run. One hypothesis for the success of our earlier policy estimation work was that the computed policy makes better use of these metabolic efficiencies than the volunteers when left to pace themselves.

Room environmental conditions were selected to approximate an office environment with a temperature of 22 °C and relative humidity of 50%. Our rationale was to avoid specialized environmental chambers. Instead, we planned to manipulate thermal-work strain by: 1) providing clothing that had high insulation and low vapor permeability; 2) increasing work load by adding a load to be carried; and 3) by including an uphill grade.

Load and grade conditions were derived from experiments using the SCENARIO model (Kraning and Gonzalez 1997). The details of using the SCENARIO model and the specific model settings are outlined in the MDP transition probability modeling section. Here, we show the results of our early modeling work to explain our final selection of experimental conditions.

Figure 5.2 shows modeled CT, heart rate, and thermal-work strain index from early model runs, where speed is 5 mph, grade is 1%, and load carried is 7.5% of body weight. This profile was thought ideal, as moving at the metabolically inefficient speed of 5 mph, subjects would end the exercise with a relatively high state of thermal stress TWSI > 8, but below protocol safety limits. Under these conditions, applying even a simple policy of alternating between a fast walk (4 mph) and a slow run (6 mph) lead to an end CT 38.5 °C and an end TWSI of 7.5 (see Figure 5.2).

However, after several practice sessions, these experimental conditions appeared to be too difficult. The main reason for the difficulty was that, to ensure completion of the task, participants had to move faster, on average, than the 5 mph modeled. Figure 5.3 shows model responses for experimental conditions of 22 °C, 50 % relative humidity, 0 % grade, and no load, for speeds of 5.2 and 5.4 mph. These speeds would allow subjects to finish in 58 or 56 minutes respectively.

When the modeled speed is increased slightly to 5.4 mph, there is a significant rise in thermal stress. With no load and 0% grade, the thermal response to 5.4 mph is similar to the 5 mph speed with a load of 7.5% of body weight and a 1% grade. In response to our modeling of initial conditions and the results of our practice runs, we removed the load and grade components from the experimental design. The final experimental conditions were set at an air temperature of 22 °C, 50 % relative humidity, no load, and 0 % grade.

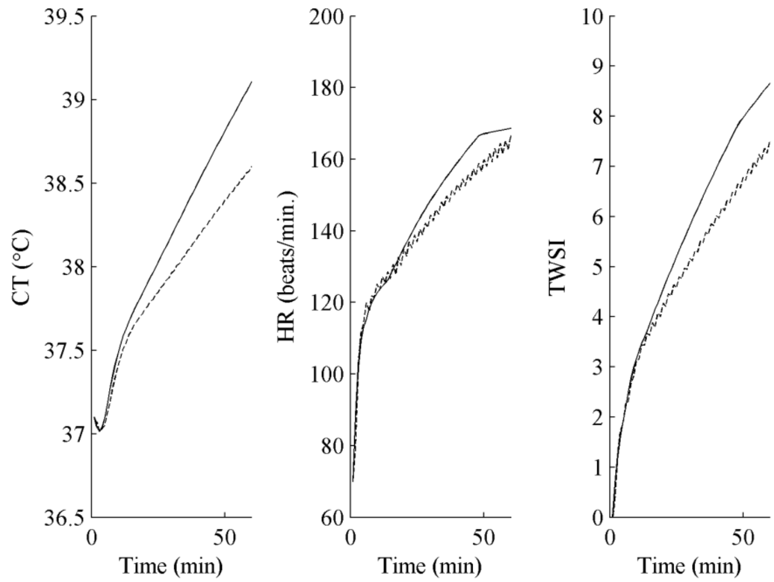

Figure 5.2: SCENARIO modeling of core body temperature (CT), heart rate (HR), and thermal-work strain index for experimental conditions of 7.5% of body weight load, 1% grade, 5 mph pace, 22 °C air temperature, and 50% relative humidity.

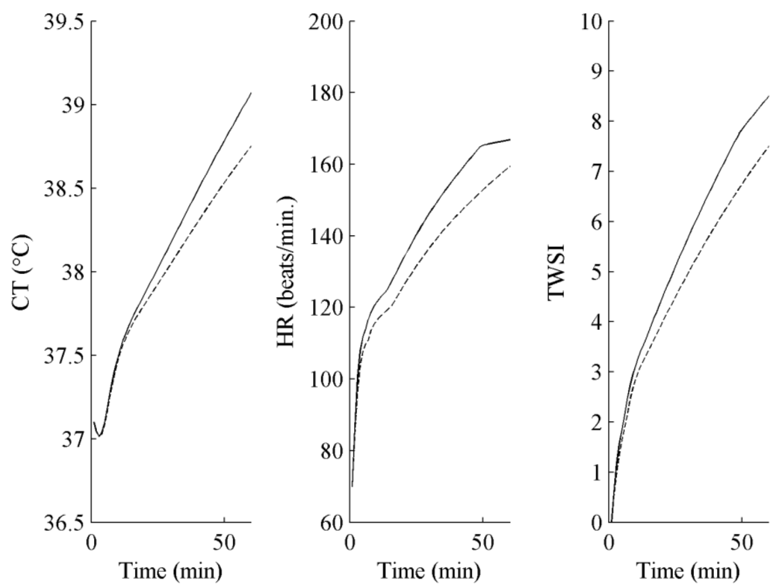

Figure 5.3: SCENARIO modeling of core body temperature (CT), heart rate (HR), and thermal-work strain index for experimental conditions of no load, 0% grade, 22 °C air temperature, 50% relative humidity, and movement speeds of 5.2 (dashed) and 5.4 mph (solid).

These experimental conditions formed the basis of our experiment and optimization problem. Modeling showed that by selecting an alternating pace, under these conditions that the TWSI could be kept to below 7.5. This was a TWSI threshold originally chosen as a conservative safety line to prevent individuals from transitioning to “Very High” thermal-work strain (Buller et al., 2008). Our final goals for the optimization problem were for the individual to finish the 5 miles in one hour, for TWSI to remain below a safety value of 7.5, and for an individual to finish as “cool” as possible in terms of having the lowest possible TWSI.

5.3 Experimental Design

The experiment was a within-subjects design examining the impact of the timed foot movement on physiological measures and self-report scales. Volunteers participated in both a GUIDED and UNGUIDED condition. In the UNGUIDED condition, participants completed the 5 miles using their own pacing strategy. In the GUIDED condition, the MDP-derived policy guided the pace of the participants based upon their thermal-work strain state, distance completed, and the time remaining. The UNGUIDED session was presented first, followed by the GUIDED session. An ordered presentation of conditions was adopted, rather than a counter-balanced design. Presenting the UNGUIDED session first avoided a training effect from presenting some subjects with our GUIDED session first. In the GUIDED session, we are dictating the movement strategy to the participant, and their previous UNGUIDED session will have a very minimal training effect. At a minimum, participants waited at least one week before completing their second session to allow adequate recovery time. Participants exercised wearing their own shorts and t-shirts under the US Army Physical Training (PT) long-sleeved shirts and pants.

5.4 Markov Decision Process Definition

As detailed in Chapter 4, a Markov decision process (MDP) is defined by a set of states (S), a set of actions (A), a state transition matrix (T) containing the transition probability mass function (PMF), and a reward function R(S). For this laboratory study, the set of states and actions were well defined. The state transition PMF was estimated from a physics/physiology based human-thermo-regulatory model. The reward function was more subjective in its definition, as it balanced the competing goals of completing the task and finishing safely. Each of these elements of the MDP are defined in the following sections.

5.4.1 State Space Definition

In an MDP, the state space defines all the components necessary to model the relevant state of the world. For our laboratory experiment, the following three parameters were used to specify the state of the task: 1) time completed (t), 2) the thermal-work strain of the subject (TWSI), and 3) distance completed (D).

It was necessary to discretize time completed into two minute increments, where t:={0, 2, …, 58, 60}. Changes in TWSI for time resolutions < 2 minute intervals for most actions were very small (< 0.25 TWSI units). Without decreasing the discrete steps of the TWSI beyond 0.25 units, there would often be no transitions from one state to the next. It was also too impractical to guide participants more often than every two minutes.

The thermal-work strain index was discretized into 0.25 TWSI units starting at 0.5 and ending at 10, where TWSI:={0.5, 0.75,…,9.75,10}. Distance (D) completed was discretized into units of 0.0067 miles, or the fraction of a mile that can be completed at 0.2 miles per hour (mph) within 2 minutes, where D:={0, 0.0067, … , 5.9933, 6}.

Our final state action space was comprised of 30 x 39 x 900 (t x TWSI x D) discrete states with 27 actions permissible from each of these states. Figure 5.4 shows the resulting directed acyclic graph that represented our state-action space.

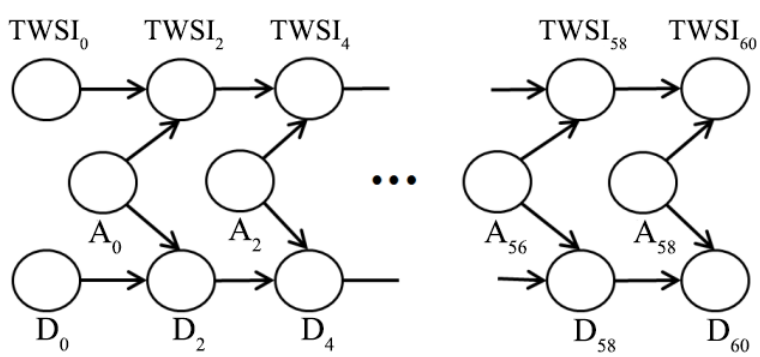

Figure 5.4: Graph representation of the problem state-action space. TWSI is the thermal-work strain index, D is distance, and A is action.

5.4.2 Action Space Definition

Actions define what an agent or subject can do in a particular state. For our experiment, actions were constrained to movement speeds from 0 to 7 mph in 0.2 mph increments. Except for no movement (0 mph) speeds < 2 mph were excluded, as they are not typical movement speeds and would be more awkward than helpful to a pacing strategy. Thus, A:={0, 2.0, 2.2, …, 6.8, 7.0}. These actions were the same for every state.

5.4.3 Transition Probabilities

A critical element to using dynamic programming in solving MDPs is that the transition probabilities (*P(S'|S, A)*) are known or can be approximated. In this MDP, there were two transition probability mass functions that had to be found. For any action undertaken, there will be a certain amount of distance completed and a change in the TWSI state.

Distance Completed Transition Probabilities

Modeling distance completed on a treadmill is a relatively simple process. The treadmill will be set at a certain speed and there will be limited possibilities for a change in distance, unless a subject cannot keep the requested pace. For the distance probability mass function we placed a small amount of uncertainty $N(0,0.2)$ around the distance traveled in 2 minutes. The transition probability mass function is shown in Table 5.1.

Table 5.1: Transition probabilities for distance completed.

D'	−0.0201	−0.0134	−0.0067	d	+0.0067	+0.0134	+0.0201
P	0.01	0.05	0.24	0.40	0.24	0.05	0.01

d=D+A(2/60).

Thermal-Work Strain State Transition Probability Estimation

In contrast to distance completed, the TWSI transition probabilities can be complex and are dependent on a large number of factors such: as work rate, personal characteristics (body surface area, fat mass, fitness, and acclimation), environmental conditions (ambient temperature, relative humidity, wind speed, and solar load), and clothing characteristics (insulation properties and vapor permeability). As detailed in Chapter 2, TWSI is a weighted combination of CT and heart rate. While the dynamics of CT seem relatively simple if heart rate is known (Chapter 3), the heart rate response to different conditions is more complex. Thus, understanding how both heart rate and CT change given a large number of factors is critical.

While the dynamics of HR and CT are complex, they have been captured to a high fidelity in physics- and physiology- based thermoregulatory models (e.g. Kraning and Gonzalez, 1997; Fialah et al., 2001; and Havineth, 2001). The inner workings of these models will not be covered here to any great extent. However, given a current physiological state and an action, these models will provide the correct dynamic change in physiology (CT and HR) for a given time step (see Figure 2.8). The TWSI transition probabilities were learned by Monte Carlo approximation using the SCENARIO (Kraning and Gonzalez, 1997) thermoregulatory model to simulate the responses of humans under our laboratory conditions. This model requires the following class of inputs: environmental conditions; clothing insulation and vapor permeability characteristics; individual characteristics (including height, weight, and age); and work rate expressed in watts. Obtaining accurate TWSI transition probabilities is dependent on accurately modeling the experimental conditions. We will examine each of the four input areas to show how we defined and successfully modeled our laboratory conditions in SCENARIO.

Environmental Conditions

The SCENARIO model requires the basic environmental information of air temperature, black globe temperature (T_g, see Equation 2.15), relative humidity, and wind speed. The model air temperature parameter was set according to our research protocol to 22 °C. New air handlers specifically installed for this work maintained the temperature to within ±2 °C. The study was conducted within one of three identical, indirect calorimetry chambers (as shown in Figure 5.5). As the exercise took place indoors, and since there was negligible radiative sources of heat within the indirect calorimetry chambers, T_g was also set to 22 °C. As the chamber air temperature was controlled by an individual air handler, we estimated that relative humidity was similar to an office environment and set at 50%. Wind speed can have a large impact on model outcomes affecting the clothing vapor permeability and insulation factor, as well as aiding in convective heat loss. The chambers where we conducted our study had a constant air flow into the room from an outside air source and out through the O_2 and CO_2 gas analyzers. Additionally, a ceiling fan in the room was used to mix the air.

Figure 5.5: The indirect calorimetry chamber.

To determine air flow in the chambers, we used a hot-wire anemometer (CIH20DL, General Tools and Instruments, New York, NY) placed at waist height on the hand rail of the treadmill while a person was walking and running on the treadmill. On average, wind speeds were low at 0.35 ± 0.2 ms^{-1}.

Clothing Characteristics

Clothing characteristics of vapor permeability and thermal insulation were measured on a sweating "copper" thermal manikin using ASTM standards (ASTM F1291-10 for thermal insulation and ASTM F2370-10 for evaporative resistance) (see Potter et al., 2014). Figure 5.6 shows the sweating copper thermal manikin with our study exercise clothing.

Figure 5.6: Sweating "copper" manikin with study exercise clothing.

Vapor permeability (i_m) is measured on a range from 0 (vapor impermeable) to 1 (no barrier). The SCENARIO model utilizes an insulation factor measured in CLO is closely correlated with the R-values used for home insulation[5]. Depending on the environment, the impact that a clothing ensemble can have on heat stress is a factor of both the insulation factor and vapor permeability. This combination is often expressed as a ratio i_m/CLO. Table 5.2 shows some typical values CLO and vapor permeability for different clothing ensembles.

Table 5.2: Insulation and vapor permeability values for different clothing at wind speeds of 1ms^{-1}.

	Insulation (CLO)	Vapor Permeability (I_m)	i_m/CLO
Shorts and t-shirt	0.51	0.78	1.41
Long pants long sleeved shirt	1.08	0.51	0.47
U.S. Army combat shirt and body armor	1.52	0.44	0.29
Chem. bio. full encapsulation	1.92	0.11	0.06
U.S. Army P.T. gear (study clothing)	1.22	0.41	0.34

[5] Clothing Insulation – WikiPedia http://www.wikipedia.org accessed 2/17/2015

As these insulation and vapor permeability values for different clothing ensembles have non-linear relationships with wind speed, they are often approximated by a power curve. The SCENARIO model takes inputs of the CLO and i_m/CLO at 1ms^{-1} and the exponent of a power fit curve to these parameters across the three wind speeds. The clothing insulation and vapor permeability measures were taken in a chamber set to a temperature of 23 °C and RH of 50% at wind speeds of 0.4, 1.2 and 2.0 ms^{-1}. Figure 5.7 shows the i_m and CLO values for the 3 wind speeds for our PT clothing along with the power curve fits. Equations 5.1 and 5.2 show the power curve equations for the CLO and i_m to wind speed relationships, respectively.

$$CLO = 1.2158ws^{-0.216} \tag{5.1}$$

$$i_m = 0.4121ws^{0.0817} \tag{5.2}$$

Where ws=wind speed.

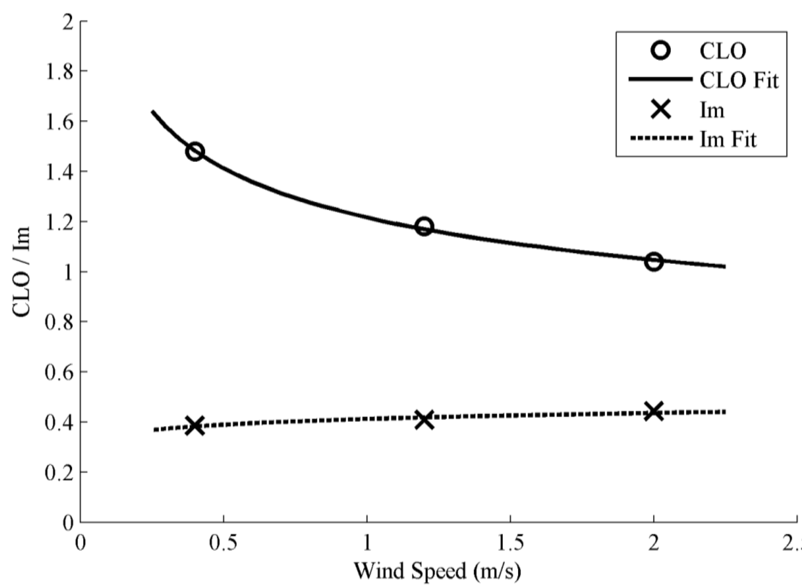

Figure 5.7: CLO and i_m at varying wind speeds and power fit curve.

What is important to note is that at the wind speeds associated with our chamber, the PT clothing has a low vapor permeability (i_m=0.38) and high insulation factor (1.53 CLO).

In the SCENARIO model, a combination of movement speed and air speed are used to adapt dry conductance (Kc), i_m, and CLO. The effect of air movement on dry conductance is specifically modeled for a number of conditions, including free walking, walking on a treadmill, no movement, or for cycling on an ergometer (Equations (5.3), (5.4), (5.5) and (5.6) respectively).

Free Walking: $$K_c = 8.6V_{move}^{0.53} + K_1 \tag{5.3}$$

Treadmill Walking: $$K_c = 6.5V_{move}^{0.39} + K_1 \tag{5.4}$$

Stationary: $$K_c = 11.6\sqrt{V_{air}} \tag{5.5}$$

Ergometer: $$K_c = 5.5 + K_1 \tag{5.6}$$

Where:

$$K_1 = 1.96V_{air}^{0.86} \tag{5.7}$$

Where V_{move} = movement velocity ms^{-1} and V_{air} = air movement velocity ms^{-1}.

CLO and i_m are adjusted for effective air movement (V_{eff}) (Equation 5.8) according to the power curves shown in Equations 5.1 and 5.2. The effective air movement attempts to quantify the reduction in insulation and increase in vapor permeability that comes from body movements. The reduction in insulation can come from the "pendulum effect" of moving limbs (Clark et al., 1974); the disruption of the boundary layer of air on the skin surface; and heat loss due to the "pumping effect" of air and vapor expelled from the clothing due to movement. These effects are simply expressed as a combination of air speed and movement rate. Equation 5.8 shows the SCENARIO model calculation of V_{eff},

$$V_{eff} = V_{air} + V_{move} \tag{5.8}$$

where V_{air} is the wind speed or air movement speed (ms^{-1}) and V_{move} is the rate of movement (ms^{-1}).

This approach at first appears to be overly optimistic for our low air movement treadmill exercise conditions, especially as some studies have shown cooling effects when forward movement is simulated using fans (Shaffrath and Adams, 1984). These studies demonstrated that under conditions of high workload and limited air movement, performance was worse compared to a condition when forward air flow is simulated by use of a fan.

However, rather than movement speed, some argue that effective air flow should be adjusted for whole body metabolic rate according to Equation 5.9 (Santee and Matthew (2012),

$$V_{eff} = V_{air} + 0.004(\dot{M} - 105)\,, \tag{5.9}$$

where $\dot{M}$ is metabolic rate in watts.

For our conditions, this is comparable to $V_{eff} = V_{air} + 0.95V_{move}$. Further, the movement effects appear to differ based upon garments. Holmer et al. (1992) found that body movement reduced CLO to a greater extent on ensembles with lower insulative properties. More recently Qian and Fan (2006) used an articulated manikin to develop regression equations to estimate the effect of body movement at different walking speeds for different garments. They concluded that for high air flow environments, V_{eff} could be calculated as a sum of air speed and a multiple of movement speed (see Equation 5.10). However, their articulated "walking" manikin only provided data on relatively slow movements of up to 0.7 ms^{-1} or 1.6 mph.

$$V_{eff} = V_{air} + 1.8V_{move} \tag{5.10}$$

As our experimental conditions consisted of low airflow around a clothing ensemble with a fairly high CLO and low vapor permeability, we directly measured the CLO of the PT uniform using our articulated or "walking" manikin. The manikin was able to replicate the movement of walking speeds between 2 and 3 miles per hour. Figure 5.8 shows the effect of the manikin movement on the CLO of the PT uniform measured with an air movement of 0.4 ms^{-1}. The figure also shows the Veff adjustments using the standard SCENARIO equation, that proposed by Qian and Fan (2006), and our own Veff adjustment based upon the manikin data.

Both the SCENARIO equation and the Veff equation proposed by Qian and Fan (2006) appear to underestimate the effect of movement on the PT uniform CLO. We used our lab measurements to adjust the Veff according to Equation 5.11.

$$V_{eff} = V_{air} + 2.3V_{move} \tag{5.11}$$

Our lab measurements and adjusted Veff equation allowed us to fix problems originally seen in our TWSI transition probabilities. Our original modeling did not account enough for the effects of body movements in reducing the CLO and i_m values for the ensemble. Consequently we had transition probabilities that gave greater positive changes to TWSI and limited negative changes to the TWSI.

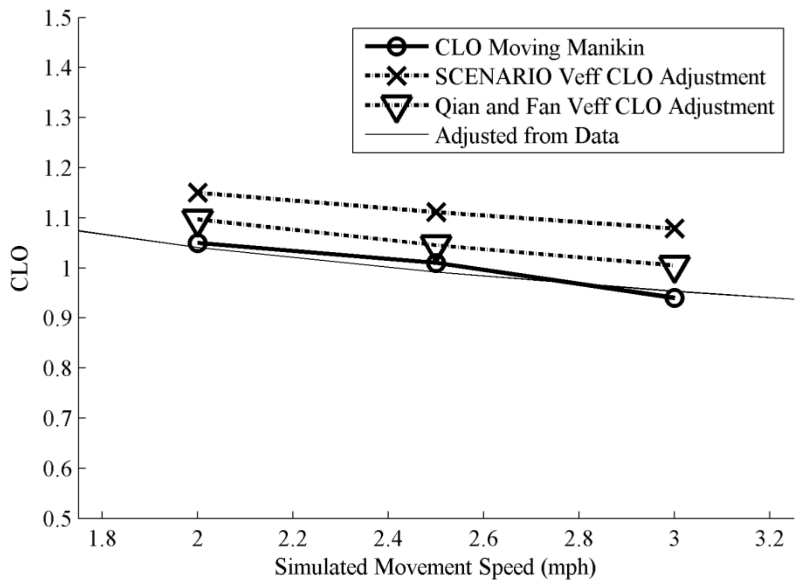

Figure 5.8: CLO of PT uniform measured on a moving manikin at simulated walking speeds of 2, 2.5 and 3 miles per hour, with adjustment for CLO and Movement speed using Equation 5.9, 5.10, and a custom fit Equation 5.11.

Metabolic Rate

The SCENARIO model estimates metabolic rate using the Pandolf equation (Pandolf, 1977):

$$\dot{M} = 1.5W + 2.0(W + L)(L/W)^2 + \eta(W + L)(1.5V^2 + 0.35VG), \tag{5.12}$$

where $\dot{M}$ = Metabolic rate (W), W=subject weight (kg), L=subject load (kg), η=terrain factor, V= movement rate (ms^{-1}) and G=terrain grade (%).

For free-moving individuals, this equation is convenient as metabolic rate estimates for combinations of movement speed, load, grade and terrain can be computed. For our study, a terrain factor of 1 was chosen, as participants are running on a hard surface. Our experimental conditions had no load and no grade. In addition to the Pandolf equation, we included a running correction proposed by Givoni and Goldman (1971) (see Equation 5.13). This addition corrects for the over-estimates in metabolic rate for running. Figure 5.9 shows the Pandolf estimated volume of oxygen (VO2) per kg per km compared to the equations for walking and running generated by Paroczai and Kocsis (2006) with and without the running correction factor.

$$\dot{M}_{running} = \left[\dot{M}_{walking} + 0.47\left(900 - \dot{M}_{walking}\right)\right]\left(1 + \frac{G}{100}\right) \tag{5.13}$$

where $\dot{M}$=metabolic rate (W), and G=grade (%).

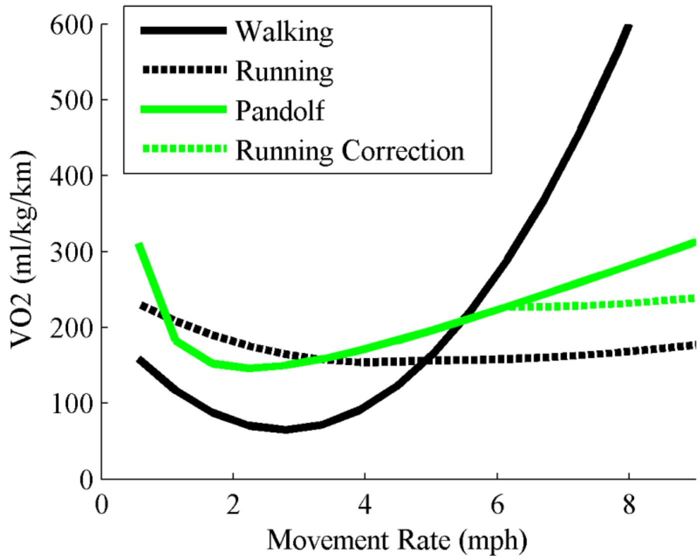

Figure 5.9: Volume of oxygen (VO2) consumed per kg per km for different walking and running speeds from Paroczai and Kocsis (2006), along with modeled estimates from the Pandolf Equation (5.12)(Pandolf 1977) without and with the Givoni and Goldman (1971) running correction factor (5.13).

Individual Differences

The SCENARIO model takes the following four input parameters to characterize individuals: age, height, weight, and percent body fat. Height and weight are used to compute body surface area using the Du Bois (1916) method (Equation 5.14).

$$SA = 0.202BW^{0.425}\left(\frac{HT}{100}\right)^{0.725} \tag{5.14}$$

where *SA* is body surface are in m^2, *BW* is body weight in kg, and *HT* is height in m.

Body surface area in conjunction with body weight and percent body fat sets the volume of each of the modeled heat exchange compartments and total blood volume. These settings are used during the computation of the heart's stroke volume and as one aspect in determining sweat rate. Age is used to compute maximum HR with the American College of Sports Medicine's formula as given in Equation (5.15).

$$HR_{max} = 220 - age \tag{5.15}$$

where *HR* is heart rate in beats/min. and age is measured in years.

A significant modeling concern was whether different transition probabilities and, therefore, different policies would be needed for people of different ages, statures, weights, and percents body fat. Recent empirical work has shown that changes in core body temperature are similar for different sized individuals, when the work rate is normalized by body mass (Cramer and Jay 2014, and Cheuvront 2014). According to the Pandolf equation (Pandolf et al., 1977) (Equation 5.12), the absolute metabolic rate increases for heavier individuals, but it is the same when normalized by body weight. Table 5.3 shows a range of body types and the estimated metabolic rates.

Table 5.3: Metabolic rate for exercise at five miles per hour for a range of body sizes expressed in absolute and body mass relative terms.

Weight (Kg)	Height (m)	Age	Body Fat (%)	Metabolic Rate (W)†	Metabolic Rate (W/Kg)
50	1.55	25	15	450	9
60	1.60	25	15	540	9
70	1.70	25	15	630	9
80	1.75	25	15	720	9
90	1.80	25	15	810	9
100	1.85	25	15	900	9
110	1.90	25	15	990	9

†Metabolic rate estimated using the Pandolf equation (Equation 5.12).

Since the exercises' weight-adjusted metabolic rate is similar across body types, we set the weight and height inputs to 70 Kg and 1.7m, respectively. These values represent the defaults used in the original SCENARIO model. With these two inputs set, we examined the effect of changing both age and body fat proportion on thermal-work strain modeled over the course of the hour-long exercise. Figure 5.10 shows CT, heart rate, and the TWSI modeled for a movement speed of 5.4 mph for body fat percentages from 10 to 25 with age fixed at 25 years.

The results showed little effect for different body compositions of fat. This parameter would likely have a greater impact for cold exposure.

Figure 5.11 shows CT, heart rate, and the TWSI modeled for a movement speed of 5.4 mph for ages from 18 to 29 with body fat percentage fixed at 15%.

Similarly, across our narrow range of age there is limited impact on CT, HR, or TWSI. Thus, the final individual model parameters were set to age = 25 years, weight = 70 kg, height 1.7m, and 15 % body fat.

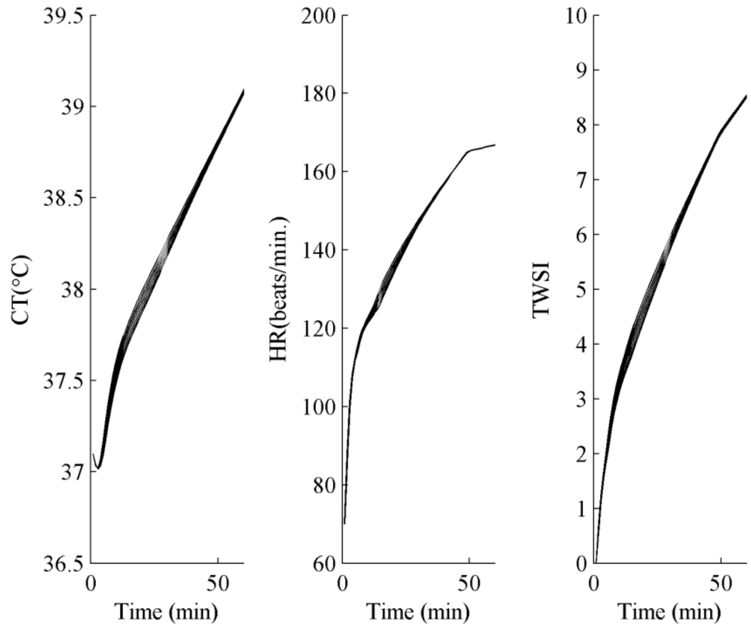

Figure 5.10: Modeled core body temperature (CT), heart rate (HR), and thermal-work strain index for different levels of body fat (10% to 25%).

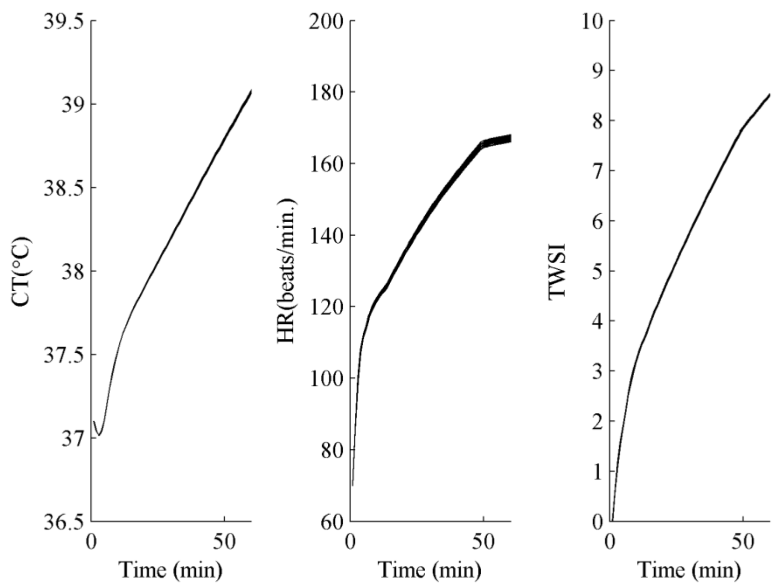

Figure 5.11: Modeled core body temperature (CT), heart rate (HR), and thermal-work strain index for different ages (18 to 29 years).

After defining the input parameters for the SCENARIO model, we could simulate the laboratory experiment to estimate the TWSI transition probabilities. For our simulations, the model was started with TWSIs from 0 to 10 and simulated 30 random actions from our action state space (A) over the course of 1 hour. For each model run, the air temperature was randomly set within the range of 20 to 24 °C, to simulate the room AC control envelope. Transitions from one TWSI to another for a given action were recorded as a count for each of our discrete TWSIs. Modeling runs were repeated to ensure that cells of our transition probability matrix (T) had at least 10^5 samples for a given action. A discrete probability mass function was generated by dividing the counts for a recorded transition by the total number of all transitions for each action.

Thermal-Work Strain State Transition Probability Results

Initial model runs generated PMFs for every 2 minutes within the laboratory experiment simulation. Since we found negligible difference between the PMF's at different time points, we collapsed the PMFs across time. Figure 5.12 shows the transition PMF plots for TWSIs 1 to 9.

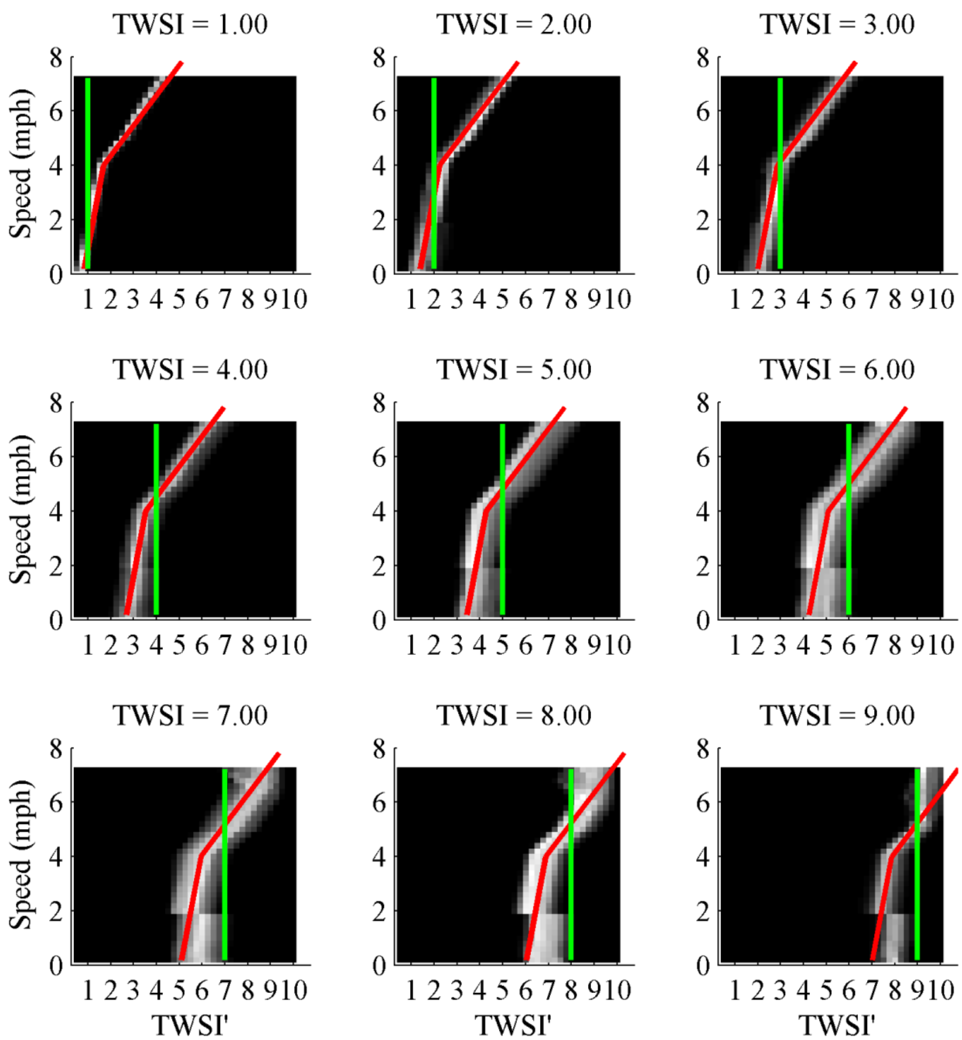

Figure 5.12: Learned discrete transition probability distributions. Current TWSI state is indicated by a green vertical line. The learned discrete probability distribution is shown as a grey scale heat map. White shows the highest density. Black = 0. Overlaid are learned linear regression equations for computing the expected TWSI' (Equations 5.16 and 5.17).

From Figure 5.12, two distinct relationships can be seen that reflect transitions due to walking and running speeds. We found that these transition relationships were remarkably similar, with only their intercept differing by the current TWSI state. We decided to take advantage of this property, and developed two regression equations, to compute the mean TWSI' from current TWSI, and the action to be taken. One equation was for walking speeds ≤ 4.0 mph (Equation 5.16) and one for running speeds > 4.0 mph (Equation 5.17). These regression lines are overlaid on the PMF in Figure 5.12. The walking and running regression equations remain the same for each starting TWSI, just with an offset which is dependent on the current TWSI.

$$TWSI'_{walk} = 0.2221A + (0.0312TWSI^2 + 0.4625TWSI) + 0.3365 \tag{5.16}$$

where A=movement speed in mph.

$$TWSI'_{run} = 0.9012A + (0.0312TWSI^2 + 0.4625TWSI) - 2.2443 \tag{5.17}$$

The increased sheering of the transition probability mass function at low walking speeds as the TWSI increased was thought to be an effect of the slower movement speeds on the effective air velocity calculation. Since we were excluding these movement speeds from our MDP, we did not model this effect. We were also not certain why the model provided such a low variance for the lower TWSIs. One explanation may be that this is a function of how the model returns to resting conditions, where the active physiological components may respond in a very deterministic way. We hypothesized that the actual transition variance would in fact appear similar to the higher TWSIs PMFs.

We used Equations 5.16 and 5.17 as linear Gaussian probability density functions (PDF) with a fixed standard deviation of 0.4 TWSI units. These PDFs allowed us to generate a smooth transition PMF. To avoid having some probability of physiologically improbably transitions, we set the probability to zero, if transition probabilities were < 0.00001 and re-normalized.

5.4.4 Reward Function Definition

The reward function R(S) of an MDP provides a measure, score, or value for being in any particular state. The utility (U) of any sequence of states can be computed simply from the sum of rewards (Equation 5.18):

$$U(s_0, s_1, s_2, \ldots, s_{n-1}, s_n) = \sum_{t=0}^{n} R(s_t), \tag{5.18}$$

where *U* is utility, *s* is state, *R(s)* is the reward function, and *t* is time.

A policy function (Π(S)) provides an action for any given state. In our MDP definition, actions are not deterministic, but have a stochastic element. This stochastic element is defined by the transition probability mass function *P(S'|S,A)*. The utility of a policy starting in state S can be computed as the expected sum of rewards by following the policy until the end state (Equation 5.19).

$$U^{\pi}(s) = E[\sum_{t=0}^{n} R\,(S_t)] = \sum_{t=0}^{n} P(S_{t+1}|S_t, A_t)R(S_{t+1}) \tag{5.19}$$

A single objective MDP can be solved using dynamic programming (Bellman 1957a) by making use of the Bellman equation (Bellman 1957b) (Equation 5.20). Here, the utility of being in any state can be computed as the sum of the immediate reward for being in the current state and the maximum of the discounted (γ) expected utility of the action taken to reach each next state.

$$U(s) = \mathrm{R(s)} + \gamma \max_{a\in A(s)} \sum_{s'} P(s'|s,a)U(s') \tag{5.21}$$

Where γ is the discount factor.

Since for our experiment we have a finite time horizon $\gamma = 1$, an optimal policy for being in any state in our lab study can then be defined as follows:

$$\pi_t^*(s) = \mathrm{argmax}_{a\in A(s)}\, \mathrm{R(s)} + \sum_{s'} P(s'|s,a)U_{t+2}(s') \tag{5.22}$$

Similarly, the utility for taking the optimal action is computed from Equation 5.23.

$$U_t(s) = \max_{a\in A(s)} \mathrm{R(s)} + \sum_{s'} P(s'|s,a)U_{t+2}(s') \tag{5.23}$$

A set of optimal policies can then be solved iteratively using dynamic programming. Starting at the end of 5 mile movement, both the optimal policy and utilities for all states at time point 58 can readily be computed from Equations 5.22 and 5.23 respectively, as the final utilities for all states at minute 60 are known. The policy and utilities for all states at earlier time points can then be computed working backwards from time point to time point until the start of the exercise.

This approach depends on the fact that the utilities used to compute a policy impose an ordering on the policies such that $U^{\Pi}(s) > U^{\Pi'}(s)$. However, the reward function (R) for the laboratory study MDP is complex as it combines three distinct objectives:

1) Complete the 5 miles of foot movement within an hour.
2) Remain under a "safety" TWSI of 7.5.
3) Complete the foot movement with as low a TWSI as possible.

These three objectives are not necessarily compatible, as maximizing one objective may mean minimizing another. For example, to maximize objective three, objective number two may have to be ignored. In this case, the policy ordering that is used to determine an optimal policy does not hold with our multiple objectives. Instead of a scalar utility being returned in Equation 5.23, there will be a vector of three utility values, one for each of the laboratory study's goals. In this case, for any given state, there may not be one policy that optimizes all three goals. It may be the case that $U_2^{\Pi}(s) > U_2^{\Pi'}(s)$, but it is very possible that $U_3^{\Pi}(s) < U_3^{\Pi'}(s)$. In this situation, what forms an optimal policy? Depending on the nature of a multiple objective MDP, there can be a number of different definitions of optimal. Roijers et al. (2013) propose a multiple objective MDP taxonomy to help classify the different problems and help identify the nature of the optimal solution. They examine how objectives can be "scalarized," or how the individual objectives can be combined, to provide one measure of utility. In a general form, they define a scalarization function that combines the individual objective utilities using weights (see Equation 5.24):

$$U_w^{\Pi}(s) = f(\mathbf{U}^{\Pi}(s), \mathbf{w}) \tag{5.24}$$

where **w** is a vector of weights.

Depending on how the scalarization function combines the weights, and whether the weights are known, determines the kind of optimal solution. For this study, we chose to stick to a very simple scalarization function where:

$$f(\mathbf{U}^{\Pi}(s), \mathbf{w}) = w_1 U_1^{\Pi}(s) + w_2 U_2^{\Pi}(s) + w_3 U_3^{\Pi}(s) \tag{5.25}$$

Additionally, instead of tuning each of the weights, we set $w_1=w_2=w_3=1$ and adjusted the rewards of each objective in relation to all the objectives. Under this type of scalarization function there will be a single optimal solution to the MDP. However, in our application, there will be a range of valid weights that balance our “safety” objective and “end TWSI” objective. Some of these weights may favor increasing, or being more generous, in terms of exceeding the TWSI “safety” threshold to finish cooler. Others weight combinations may favor avoiding any high thermal-work strain but finish warmer. The literature is unclear on which of these is more beneficial for keeping individuals less thermally strained over the long run. Thus, our optimal solution will live within a family of optimal solutions, where the weights of our competing goals are adjusted differently.

To define reward functions for our MDP, we started with our end goal of “complete 5 miles in 1 hour”. This was a fairly simple goal that could be defined and around which the other rewards and penalties could be calibrated. We provided a large penalty for not completing 5 miles in one hour:

$$R_1(s) \coloneqq \begin{Bmatrix} t < 60: 0 \\ t = 60 \; \& \; d \geq 5: 0 \\ t = 60 \; \& \; d < 5: -1000 \end{Bmatrix},$$

where t is time (min.) and d is distance completed (miles).

With the end point set, the other goals could be defined in relation to this penalty. The “safety” goal could have been modeled in a couple of ways. A large penalty can be set for reaching a high TWSI. Alternatively, as risk of heat illness increases with increasing thermal-work strain, an increasing penalty can be set for exceeding the safety threshold of 7.5. The rewards for the “end TWSI” goal are implied in the goal definition, that a lower TWSI is better than a higher TWSI. To examine how to balance the “safety” goal and “end TWSI” goal, we adjusted the weights for these two rewards from 0 to 1, where the “safety” weight was initially set to 0 and the “end TWSI” weight set to 1. Tables 5.4 and 5.5 show the reward functions for these two goals. Policies were computed for the differently weighted reward functions and used with the SCENARIO thermoregulatory model to predict the physiology responses of humans acting under these different policies.

Table 5.4: Prototype rewards for “safety” goal, $R_2(s)$.

TWSI	<7.5	7.5	7.75	8	8.25	8.5	8.75	9	9.25	9.5	9.75	10
R_2	0	−4	−9	−13	−17	−21	−25	−29	−33	−37	−41	−45

Table 5.5: Prototype end state rewards for “end TWSI” goal, $R_3(s)$ for t=60.

TWSI	≤ 7.5	>7.5
R_3	500 – (4·TWSI−2)	0

Figure 5.13 shows the SCENARIO model runs for weights of (0,1) (.1,.9) (.2,.8) (.5,.5) (.7,.3) (1,0) for “safety” and “end TWSI” goals, respectively.

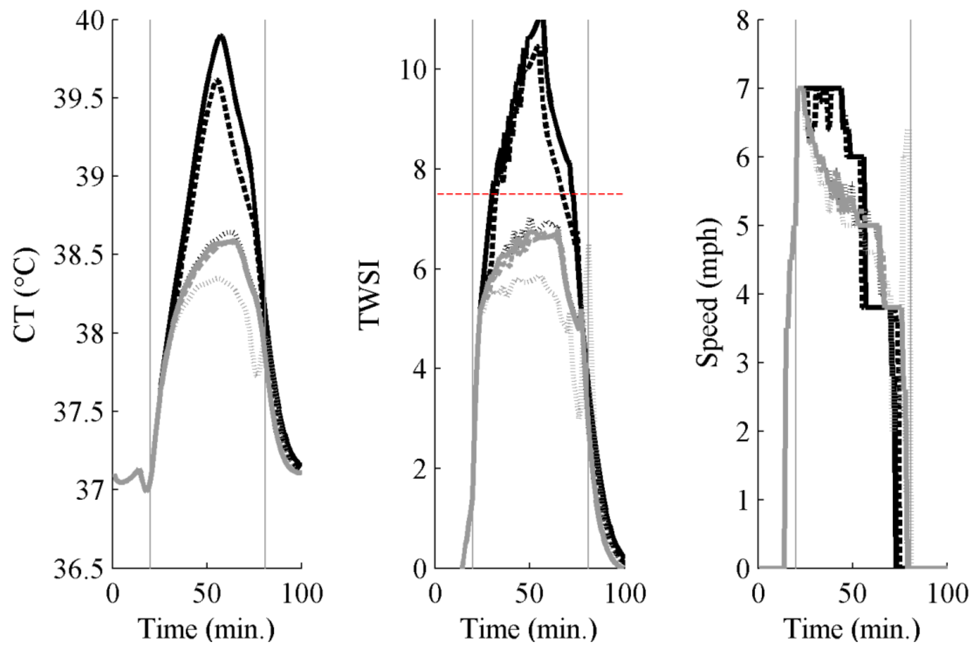

Figure 5.13: SCENARIO model runs for policies with reward weights of (0,1)[solid black], (.1,.9)[dashed black], (.2,.8), (.5,.5)[solid grey], (.7,.3), (1,0)[dotted grey] for “safety”, “end TWSI” respectively. Red dashed line indicates the TWSI “safety” threshold. Grey vertical lines indicate the 60 minute exercise period.

Initially, when there are limited penalties for exceeding the TWSI “safety” threshold (black solid and black dashed line), the policy starts the agent with a high speed of movement. This drives TWSI to very high, and potentially physiologically dangerous, levels. However, these early speeds allow the agent to slow and finish early, allowing TWSI to cool by the end of the 60 minutes. Weights of 0.3 and above for the “safety” objective appear to temper the “finish early” policy, as all these runs keep TWSI below the 7.5 threshold.

These runs, however, do not tell the whole story. Figure 5.14 shows a sample (time points 0, 18, 38, and 58 minutes) of the policy generated for a weighting of (0.5, 0.5). From this figure, it is important to note that when the agent is at a high TWSI but falling behind in the distance necessary to finish, the policy accelerates the pace (circled in red). Although this makes sense, given the large penalty associated with failing to complete the necessary distance, it ultimately pushes the human agent to dangerously high thermal-work strain levels.

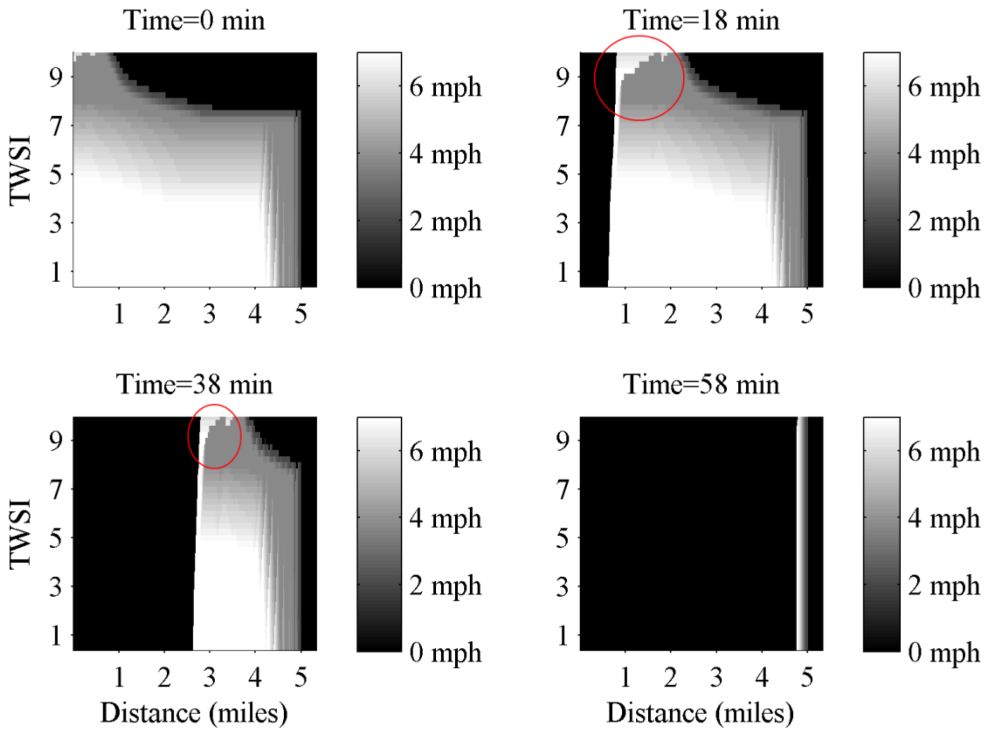

Figure 5.14: Policy for minute 0, 18, 38, and 58 with equally weighted (0.5, 0.5) "safety" and "end TWSI" reward functions from Tables 5.4 and 5.5. Red circles indicate where the policy will direct an agent with very high thermal-work strain and lagging in distance to increase speed regardless of the increase in TWSI.

To avoid this policy behavior, we added a very large penalty to both the "safety" and "end TWSI" reward functions of −2000 for TWSI = 10. The rationale was that there is more utility to not completing the five miles of movement versus completing the five miles and reaching a TWSI of 10. Figure 5.15 shows the same sample (time points 0, 18, 38, and 58 minutes) of the policy generated for the same weighting (0.5, 0.5) of the reward functions, but where the penalty of −2000 has been added for TWSI of 10.

To examine the extremes for "safety" and "end TWSI" reward, we also ran the SCENARIO model on policies derived from reward functions that contained only a large negative penalty at the TWSI of 10. Figure 5.16 shows the SCENARIO predicted CT, TWSI, and policy speeds for weightings of (0,1) (.1,.9) (.2,.8) (.5,.5) (.8,.2) (1,0) for "safety" and "end TWSI" reward functions, respectively. Even when the weight for the "safety" reward function was 0, the agent almost completes the policy run without exceeding the "safety" threshold. Once there is some weight to the "safety" penalty, the agent behavior appears to converge. While these policies meet the idea of not exceeding the safety threshold, they do not attempt to end with a low TWSI.

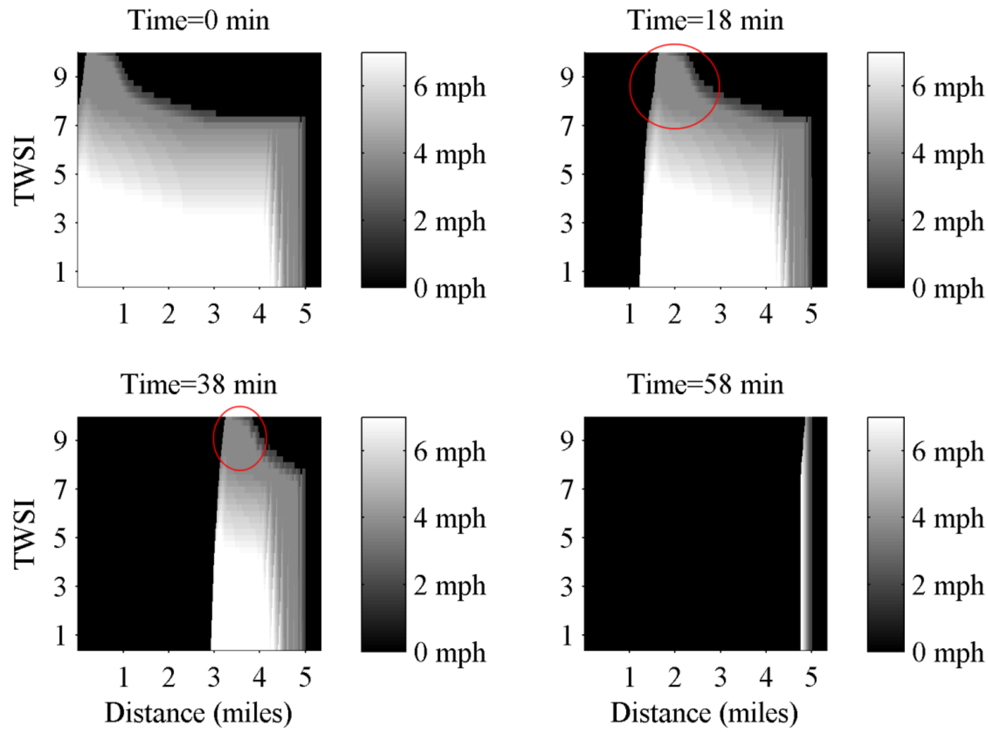

Figure 5.15: Policy for minute 0, 18, 38, and 58 with equally weighted (0.5, 0.5) "safety" and "end TWSI" reward functions from Tables 5.4 and 5.5 with an added −2000 penalty for TWSI = 10 . Red circles indicate where the policy no longer directs an agent with very high thermal-work strain and lagging in distance to increase speed.

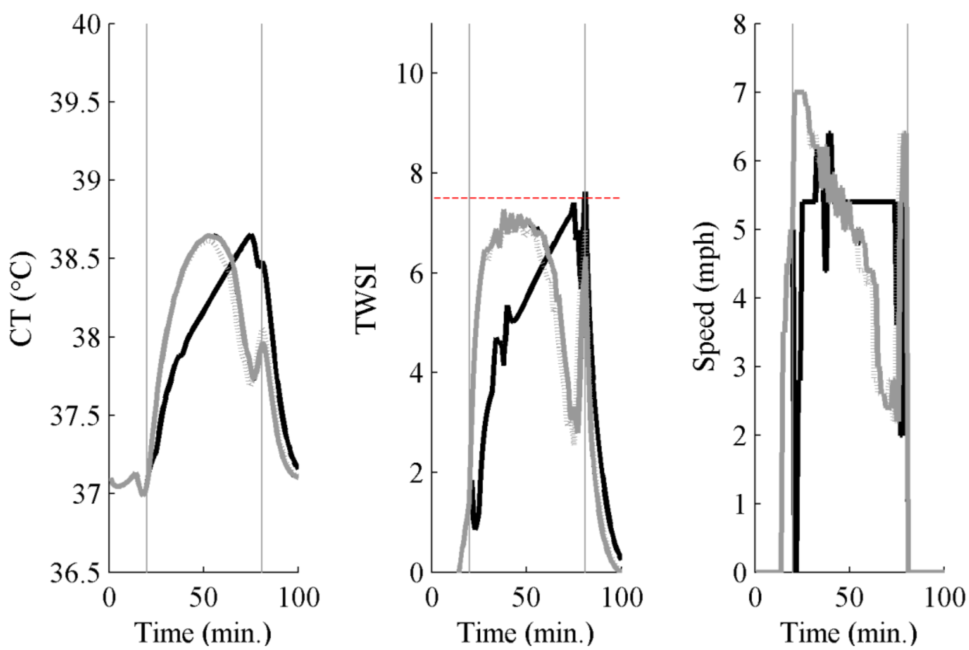

Figure 5.16: SCENARIO model runs for weights of (0,1)[solid black], (.1,.9)[dashed black], (.2,.8), (.5,.5)[solid grey], (.7,.3), (1,0)[dotted grey] for "safety", "end TWSI" with only a high penalty of -2000 for reaching TWSI of 10. Red dashed line indicates the TWSI "safety" threshold. Grey vertical lines indicate the 60 minute exercise period.

In the end, we chose to model the problem using a fairly balanced weighting between the "safety" and "end TWSI" penalties. The rewards and penalties are designed to reflect the ideas that "ending with a low TWSI is better" and "a greater violation of the safety threshold" is worse. The "safety" limit penalties for exceeding the TWSI threshold of 7.5 are shown in Table 5.6, and the rewards and penalties for the "end TWSI" reward function are shown in Table 5.7.

Table 5.6: Final rewards for $R_2(s)$ for t<60.

TWSI	<7.5	7.5	7.75	8	8.25	8.5	8.75	9	9.25	9.5	9.75	10
R_2	0	−2	−4	−8	−16	−32	−64	−128	−256	−512	−1024	−2000

Table 5.7: Final end state rewards for $R_3(s)$ for t=60.

TWSI	≤ 8	8.25	8.5	8.75	9	9.25	9.5	9.75	10
R_3	$100 - (4 \cdot \text{TWSI} - 2)$	−4.3	−7.6	−10.9	−50	−100	−300	−700	−2000

The end-state TWSI rewards are designed to promote completion of the run with the lowest possible TWSI. Table 5.7 shows that finishing with a lower TWSI is better than finishing with a higher TWSI. However, finishing with TWSIs > 8 is not beneficial, and is increasingly penalized. The increasing penalties for higher and higher TWSIs reflect the increasing risk of thermal-injury. The very large penalty of −2000 for a TWSI of 10 indicates that ending here is unacceptable. It is more appropriate to stop the exercise than to push to complete. In fact, a TWSI of 10 reflects our human use institutional review board limits set for a maximum core body temperature of 39.5 °C with an accompanying heart rate of 180 beats per minute. The lower penalties below an end state TWSI of 10 indicate that it is acceptable to push, by varying degrees, to complete the course on time.

The reward function R_2(TWSI) t<60 shows that it is equally fine for students to have TWSI between 0 and 7.25 during the race, but at or above 7.5, penalties will accrue. The negative rewards for TWSIs above 7.5 allow for several steps to be taken at these higher TWSI's and still receive higher utility than not completing the race on time. However, the exponentially increasing penalties are designed to discourage straying too far into higher and higher TWSIs. These very large negative rewards at high TWSIs ≥ 9.5 are designed to indicate that stopping the exercise for health is better than completing. Figure 5.17 shows a sample (time points 0, 18, 38, and 58 minutes) of the final policy used for the laboratory study (see Appendix C for the full policy).

Figure 5.18 shows the SCENARIO-modeled physiological response of an agent following this policy. Of note is that even though the transition probabilities have been smoothed in the simulation, the agent is either running at or above 5 mph or walking below 4 mph, avoiding a range of awkward movement speeds.

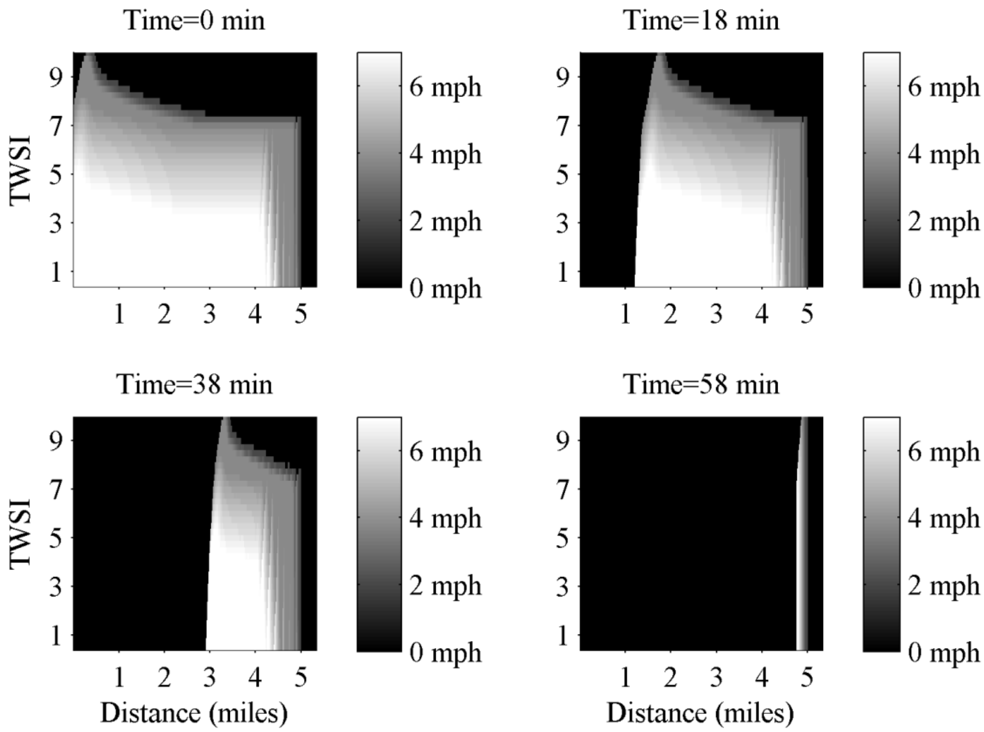

Figure 5.17: Final policy (minutes 0, 18, 38, and 58) used for the laboratory study using the reward functions from Tables 5.6 and 5.7. The full policy is shown in Appendix C.

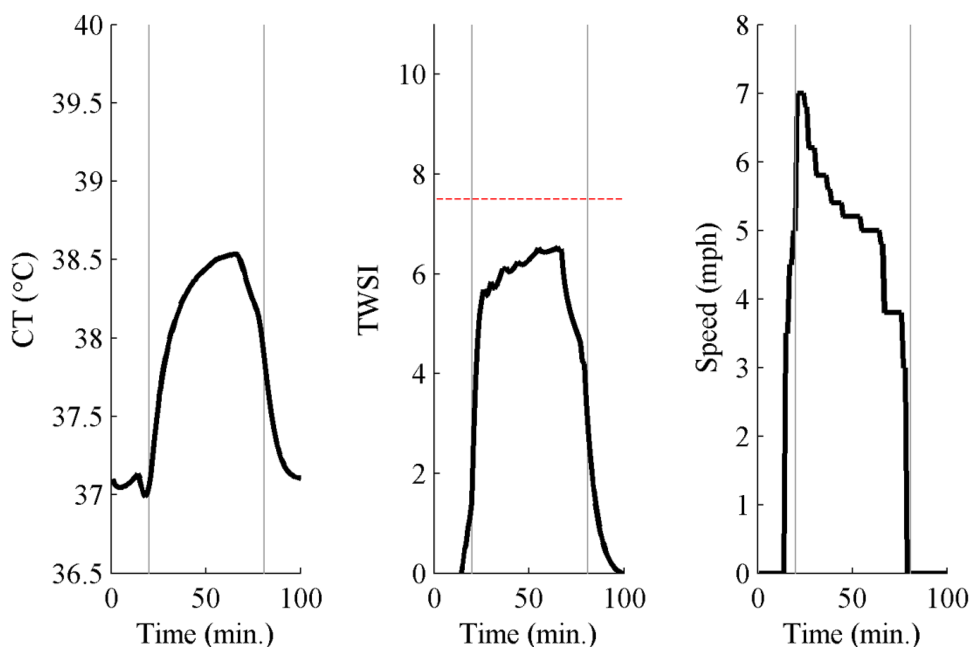

Figure 5.18: SCENARIO model runs for final policy. Red dashed line indicates the TWSI "safety" threshold. Grey vertical lines indicate the 60 minute exercise period.

5.5 Methods

5.5.1 Participants

Sixteen volunteers (11 males and 5 females) participated in the laboratory study. Table 5.8 shows their individual characteristics.

Table 5.8: Participant characteristics.

	Gender	Age (yrs.)	Ht. (m)	Wt. (kg)	%Body Fat	SA (m^2)†
	M	23	1.62	62.4	13	1.66
	F	21	1.69	55.3	19	1.63
	M	22	1.80	65.5	13	1.83
	M	21	1.79	70.2	11	1.88
	M	21	1.74	83.9	15	1.98
	M	22	1.71	67.4	9	1.78
	F	29	1.68	61.6	26	1.70
	M	19	1.79	72.2	14	1.90
	M	24	1.70	65.7	15	1.76
	M	29	1.81	74.4	12	1.94
	M	22	1.86	87.7	14	2.12
	M	21	1.64	63.2	11	1.67
	M	26	1.69	57.5	5	1.66
	F	28	1.62	66.5	31	1.71
	F	22	1.68	63.5	26	1.72
	F	21	1.64	56.7	22	1.61
Male	n=11	22.7 ± 2.8	1.74 ± 0.07	70.0 ± 9.1	11.9 ± 2.8	1.83 ± 0.14
Female	n=5	24.2 ± 4.0	1.66 ± 0.03	60.7 ± 4.7	24.8 ± 4.5	1.67 ± 0.05
Overall	N=16	23.2 ± 3.1	1.71 ± 0.07	67.1 ± 9.0	15.9 ± 7.0	1.78 ± 0.14

Ht. = Height, Wt. = Weight. SA = Surface Area. Values are Mean ± Standard Deviation.
†Computed using the Du Bois method (1916).

5.5.2 Measures

Individual Characteristics

Measurements of height were made with a stadiometer and clothed weight was measured using a scale. Percent body fat was calculated using the U.S. Army circumference technique with procedures outlined in AR 600-9 (Department of the Army, 2006). Circumference measurements were made using a fiberglass anthropometric tape at the neck, just below the larynx; at the abdomen coinciding with the navel; and for women, at the hip. Measurements were made three times by the same individual. Age and gender were self-reported. Body surface area was calculated using height and weight and the Du Bois (1917) formula.

Movement Progress

Speed of movement was recorded from a reflective light tachometer (Omegaette HHT-1501, Omega Inc., Stamford CT) on an Android tablet. Treadmills were individually calibrated. Time was recorded on the Android tablet. Distance was computed from time and speed of movement.

Physiology

Measurements of heart rate, skin temperature, and core body temperature (CT) were recorded by a Hidalgo (Cambridge UK) Equivital™ EQ-02 physiological status monitor (see Figure 5.19). The Hidalgo Equivital™ EQ-02 is an FDA 510(k) certified (K113054) device. The system recorded CT by receiving transmissions from the MiniMitter (Bend, OR) Jonah thermometer pill. The core temperature thermometer pill was ingested orally at least 12 hours preceding physical exercise. This would ensure that the thermometer pill temperature reading was not compromised by ingested water. The pill is constructed from food-grade polycarbonate and conforms to U.S. Food and Drug, Cosmetic Act and Food Additive Regulations 21 CFR 177.1580. Thermometer pill data were used to verify the previously-defined core body temperature estimation algorithm and to monitor for safety during the exercise session.

Figure 5.19: Equivital™ EQ-02 sensor electronics module (left) and the EQ-02 belt (right).

Additionally, we used a modified version of the Equivital system to measure heat flux. Two high resolution thermistors and a comparator circuit were used to measure the temperature difference between the front and the rear of the sensor electronics module. The heat flux devices have been compared to calibrated ceramic heat flow discs (Concept Engineering, Old Saybrook, CT) and shown to have a proportional relationship.

Thermal-Work Strain Index (TWSI)

The TWSI is an index that combines scaled heart rate and scaled core body temperatures with equal weights into an index from 0 to 10+. TWSI was calculated according to Moran et al. (1998) from measures of heart rate and core body temperature (see Equation 2.9). Additionally, an estimated TWSI was calculated using an estimated CT calculated according to Chapter 3 (see Buller et al., 2013a) from measurements of HR.

Metabolic

Metabolic readings were taken using indirect whole room calorimetry (USDA, Beltsville MD). As the whole room calorimeter needs approximately 10 hours to stabilize, volunteers were monitored for approximately 24 hours. Volunteers slept overnight in the chamber and were then fed a standardized breakfast before completing the prescribed exercise bout. O_2 and CO_2 concentrations were sampled every 1.3 minutes using a Mass Spectrometer (model MGA-1200, Perkin-Elmer Industrial Instruments, Pomona, CA). The following parameters were derived from these measures: oxygen consumption rate in L/min; carbon dioxide production rate in L/min; respiratory exchange ratio (unit less); and energy expenditure in kcal/min.

Self-Perception Scales

Self-perception scales were used to measure subjective ratings of perceived exertion, thermal sensation, and affective feelings. Volunteers completed the self-perception scales prior to exercise (baseline), immediately following exercise, and every 10 minutes during exercise. Scales were fixed above the treadmill and study staff recorded the rating scales on an Android tablet.

Thermal Sensation Scale

A thermal sensation scale (Young et al., 1987) was modified to align with the TWSI. Table 2.4 shows the modified scale with the original anchor words, along with the addition of "extremely hot" and "extremely cold" anchors. The scale was been modified to try and fix the apparent non-linearity of the jump from very hot to unbearably hot and to allow the scale to be used in comparison to the thermal-work strain index.

Perceived Exertion Scale

The Borg (1970) rating of perceived exertion (RPE) is a scale from 6 to 20, from no exertion at all (rest) to maximal exertion see Table 2.3.

Feeling Scale

The feeling scale is an affective valence measure. Volunteers were asked to rate how they felt on an 11-point good/bad scale (+5 very good, +3 good, +1 fairly good, 0 neutral, -1 fairly bad, -3 bad, -5 very bad) (Rejeski et al., 1987; Ekkekakis, 2003) pre-and-post exercise and every 10 minutes during exercise.

5.5.3 Procedures

On the day prior to exercise, participants reported to eat a standard breakfast and collect a packed lunch. At 5:00 pm, they returned to start a calorimeter chamber stay. Height, weight, and circumferences were measured at this time. The participant was fit with the ambulatory monitoring device and instructed regarding the calorimeter procedures, including operation of the air lock, entertainment equipment (computer, TV, DVD player, radio), treadmill, air conditioning, telephone system, bathroom, and sleeping facilities. At this time, participants ingested a core body temperature thermometer pill. The study procedures are outlined in Figure 5.20.

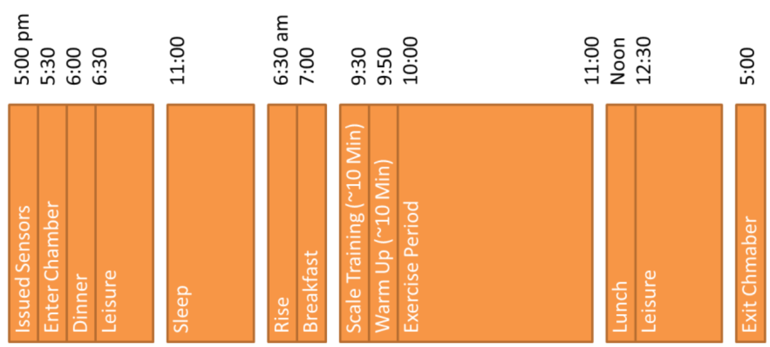

Figure 5.20: Study timeline.

At 5:30 pm, the calorimeter door was closed (not locked), and participants resided in the calorimeter for the next 23.5 hours. During the stay, participants could drink as much water as they liked, but could only consume the provided standardized meals. Dinner was provided at 6:00 pm, and participants were expected to completely consume all food within 30 minutes. The remainder of the evening was spent by the participant in leisure activities with no exercise periods. Calorimeter lights were extinguished at 11 pm, and participants were instructed to lie quietly in bed until awoken in the morning.

After approximately 13.5 hours in the calorimeter, participants were woken at 6:30 am. At about 7:00 am, a standardized breakfast of waffles and syrup (486 kcal, 91g CHO, 11g fat, 8g protein) was provided, and participants were expected to consume this meal within 30 minutes. Following breakfast, volunteers performed sedentary tasks until about 9:30 am, when they begin preparation for the exercise session. At around 10:00 am, participants began either the GUIDED or UNGUIDED exercise protocol under the supervision of study staff. At approximately 5:00 pm, subjects left the calorimetry chambers .

Treadmill Exercise Session

Prior to starting the treadmill exercise, written instructions for either the GUIDED or UNGUIDED condition were given to the volunteers to read.

GUIDED Instructions

This is a treadmill exercise where we want you to complete 5 miles within 60 minutes. We will use measurements of your heart rate to determine how fast you should go. Every 2 minutes, we will tell you how fast you should go based upon your heart rate measurements and the distance you have completed already. To successfully complete this study, you should adjust your pace to match the speed suggested by the investigator as closely as possible.

UNGUIDED Instructions

This is a treadmill exercise where we want you to complete 5 miles within 60 minutes. We want you to pace yourself so that at the end of 60 minutes, you have completed the 5 miles AND are as cool as possible AND have not gotten too hot during the exercise. To complete these goals, there are a number of strategies that may be useful: e.g. starting quickly and ending slowly; starting more slowly and ending quickly; or maintaining a constant pace. Some of these strategies are better than others and you are free to try your own strategy. You will be given feedback about how far you have gone and how much time is remaining. But it is VERY important that you complete the 5 miles within 60 minutes. For your safety, we will be monitoring how hot you get. If your core body temperature is beginning to get too hot, we will suggest you slow your pace. If your core body temperature reaches 102.5 °F, we will tell you to slow your pace to 3 miles per hour until your core body temperature is 102 °F. If your core body temperature reaches 103.1 °F, we will tell you to stop, sit on a chair, and remove your jacket. In this case, once your core body temperature is about 102 °F and the on-site registered nurse says you are fit to continue, you may elect to put on your jacket and continue the exercise session to complete the five miles within the hour.

Once dressed in their exercise clothing, subjects completed a baseline set of self-perception scales. At approximately 10:00 am, subjects began a standard warm-up sequence of walking at 3.5 mph, walking or running at 4.5 mph, and running at 5.00 mph each for 2 minutes. Once the warm-up period was completed, the subject either started a GUIDED or UNGUIDED exercise session.

The exercise session was conducted on a standard powered treadmill (e.g. Smooth Fitness 7.11.HR). Control of the speed was via the "+" and "−" buttons. Participants were able to see the display of the treadmill speed, time elapsed, and the distance they had moved on the treadmill. However, participants were warned that the treadmill display was not entirely correct and that the correct distance and time would be provided by the study staff. Ideally, the five miles would be completed as close as possible to the 60 minutes; however, if completed before 60 minutes, volunteers were asked to stand next to the treadmill until the full 60 minutes had elapsed.

5.5.4 Statistical Analysis

For most statistical hypothesis testing in this study, we utilized either a within-subject paired t-test or t-test assuming equal variances. Since we had a fairly large number of statistical comparisons, we conservatively set the level of significance at $\alpha = 0.01$. This was to avoid making a type I errors, where we would declare a statistical difference when one did not really exist. Unless otherwise stated, the results are presented as mean ± one standard deviation (SD).

SCENARIO Model

To examine how well the choice of SCENARIO model inputs represented the live experimental conditions, all human subject chamber-runs were simulated. The SCENARIO model inputs used to develop the TWSI transition probability mass function were used in addition to the observed movement speeds to simulate CT, heart rate, and TWSI response. The agreement of the model estimated CT, heart rate, and TWSI with observed values was examined using the limits of agreement (LoA) method (Bland and Altman 1986) and by computing the root mean square error (RMSE) $= \sqrt{\sum_{t=1}^{N}(OBS_t - MOD_t)^2/N}$. The LoA method utilizes a Bland-Altman chart to plot the average of observed and estimated values against the difference (estimate – observation). The method computes bias as the mean of the differences between the observed and estimated values. LoA are computed as bias ± 1.96 × SD of the differences. The LoA provides a range of error within which 95% of all estimates fall, assuming a normal distribution. Paired t-tests were used to examine the differences in RMSE and Bias for the three CT, heart rate, and TWSI between the two experimental conditions. Overall, RMSE, bias, and limits of agreement LoA were computed for all SCENARIO model compared to the observed data for CT, heart rate, and TWSI.

Transition Probability Mass Function Check

With only 480 observed TWSI transitions from the 60 minute exercise, it is difficult to directly assess the validity of the TWSI probability matrix. Instead, we used visual inspection to assess where our learned TWSI transition probabilities were appropriate and where discrepancies arose.

Core Temperature Estimation Algorithm Performance

To examine how well the core body temperature estimates agreed with the observed core body temperatures, we computed the bias and LoA from all data for each experimental condition. Root mean square errors and bias were computed for each individual volunteer for both the GUIDED and UNGUIDED conditions. Paired t-tests were used to compare the mean RMSE and mean Bias computed from the individual subject runs. This same approach was used to compare TWSI computed from estimated CT to the TWSI computed from observed core body temperature.

Effect of GUIDANCE on Physiology

To examine whether the automated guidance allowed subjects to complete the five miles of movement with lower physiological strain, we directly compared a number of physiological measures using a within-subjects t-test. Parameters were compared at the end of the 60 minutes, at the maximum value reached, and by the mean across the one hour of movement. The following measures were compared: CT, TWSI, heart rate, skin temperature, and heat flux. Only subjects who completed the five miles of movement in both conditions were compared. The total energy expenditure for each session was also compared using a within-subjects t-test.

The utility of the runs were compared for the “safety” objective and the “end TWSI” objective, using a within-subjects t-test. To examine whether speed of completion played a role in end times, we correlated time to complete the five miles with the utility scores for the “safety” objective and the “end TWSI” objective.

The subjective mean, max, and endpoint RPE, Thermal and Feeling indices were compared between the GUIDED and UNGUIDED conditions using a within-subjects t-test. Correlations between the RPE, Thermal, and Feeling indices were computed against CT, TWSI, heart rate, and skin temperature.

Guidance to Stop

Part of the balancing of the rewards and penalties for the MDP was to try and model when someone should stop versus trying to complete the goal. Individual differences for age, height, weight, percent body fat, and body surface area were examined by comparing the group means of those guided to stop and those guided to complete using a t-test. Similarly, differences in mean, maximum, and end point CT, TWSI, and HR were examined by comparing the group means (guided to stop/complete) for both the UN/GUIDED conditions using a t-test.

For those subjects who were given guidance to stop versus completing the 5 miles, we examined whether the stopping guidance was accurate based upon their estimated TWSI state. We also examined whether the estimated TWSI state was accurate compared to the observed TWSI state. As the only estimated portion of the TWSI was core body temperature, we classified the estimated TWSI state as accurate if the core temperature component fell within ± 0.32 °C of the observed CT. This represented the standard deviation found in the data from the original validation of the CT estimation algorithm from Chapter 3 (see Table 3.7).

To examine whether there was any systematic difference between the CT estimation algorithm performance between those guided to stop and those guided to complete, the RMSE and bias of the estimated CT were compared using a t-test for both the UNGUIDED and GUIDED conditions.

5.6 Results

5.6.1 SCENARIO Model Performance

No significant differences were found between RMSE and bias in the SCENARIO model estimations of CT, heart rate, and TWSI, between the GUIDED and UNGUIDED sessions. Table 5.9 shows the RMSE and bias for the model estimates of CT, heart rate, and TWSI by experimental condition.

Table 5.9: RMSE and bias for the SCENARIO modeled CT, heart rate, and TWSI compared to the observed values for both the GUIDED and UNGUIDED conditions.

	CT (°C)		Heart Rate (beats/min.)		TWSI	
	RMSE	Bias	RMSE	Bias	RMSE	Bias
UNGUIDED	0.44 ± 0.21	0.13 ± 0.32	21.3 ± 7.6	−8.9 ± 13.4	1.5 ± 0.4	−0.1 ± 1.1
GUIDED	0.40 ± 0.15	0.00 ± 0.29	23.3 ± 10.9	−16.1 ± 16.1	1.5 ± 0.7	−0.7 ± 1.2

Figure 5.21, shows the mean observed and modeled CT, heart rate, and TWSI for all subjects from both the GUIDED and UNGUIDED runs combined. While a positive bias of the modeled CT can be seen in the left figure, and a negative bias of the modeled HR in the middle plot, these two effects appear to cancel out in the plot of the mean modeled TWSI (right). However, there is a large variability in the modeled responses versus the observed data. Figure 5.22 shows the level of agreement according to a Bland Altman plot for the modeled TWSI. The modeled TWSI has a RMSE of 1.53 ± 0.58, a bias of −0.44 and limits of agreement where 95%

of all modeled TWSIs fall within ± 3.09 units of the mean, indicating a large degree of variance. For CT, the overall RMSE is 0.44 ± 0.21 °C with a bias of 0.07 °C and limits of agreement of ± 0.88 °C. Heart rate has an RMSE of 22.3 ± 9.6 beats/min. with a bias of −12.5 beats/min. and limits of agreement of ± 40.7 beats/min..

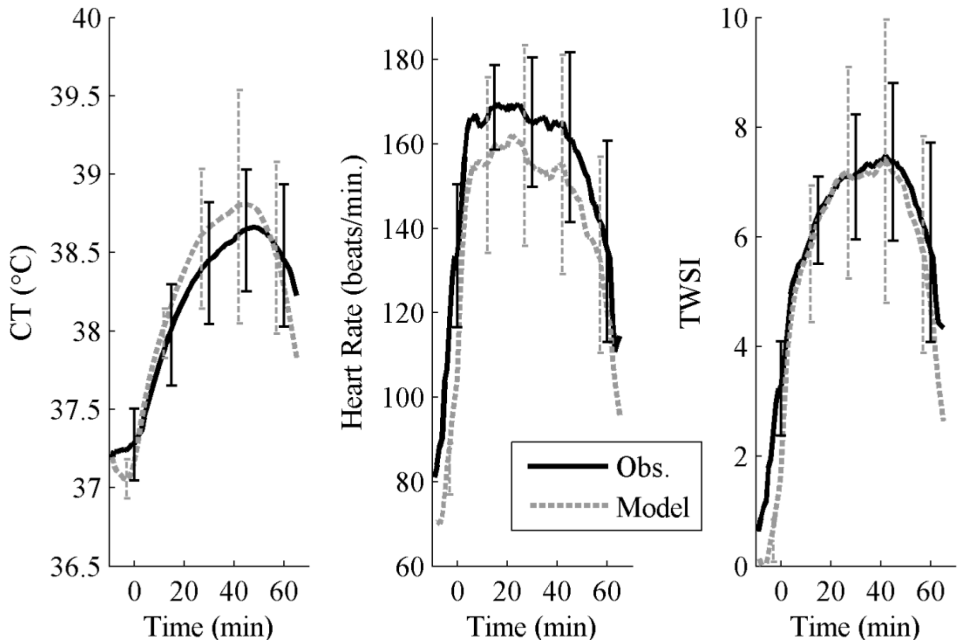

Figure 5.21: Mean observed (Obs.) and mean modeled CT (left), heart rate (middle), and TWSI (right). Error bars are ± 1 SD.

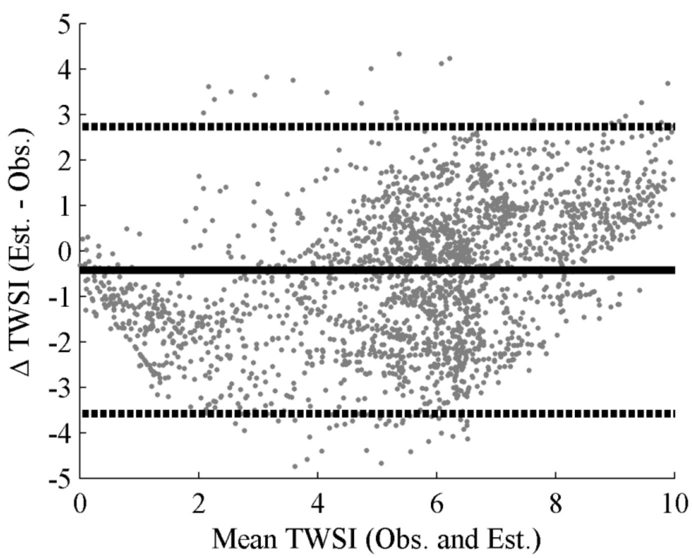

Figure 5.22: Bland Altman plot of SCENARIO modeled TWSI versus observed. Bias = solid line, dashed line is ± 1.96 SD.

5.6.2 Observed TWSI Transitions

Figure 5.23 shows a heat map of the transition probability distributions learned from the SCENARIO thermo-regulatory model overlaid with the observed transitions for TWSIs from 1 to 10 inclusive.

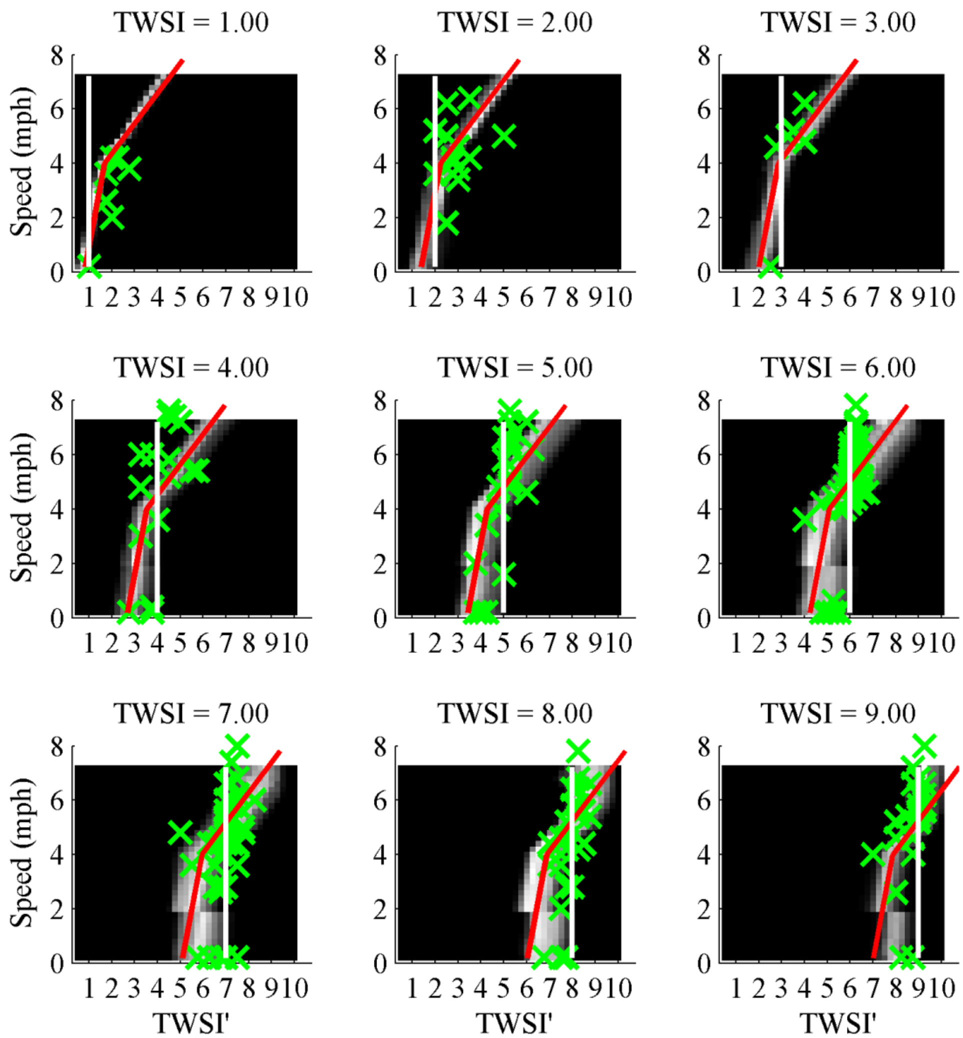

Figure 5.23: Observed TWSI transitions (green 'X') overlaid on the learned discrete transition probability distributions. Current TWSI state is indicated by a white vertical line. The learned discrete probability distributions are shown as a grey scale heat maps, white shows the highest density black =0.Red lines indicate the expected TWSI' computed from the regression functions used to smooth the transition probability mass function.

5.6.3 Pacing Styles

Figure 5.24 shows the different pacing strategies used by each subject to complete the 5 miles within one hour.

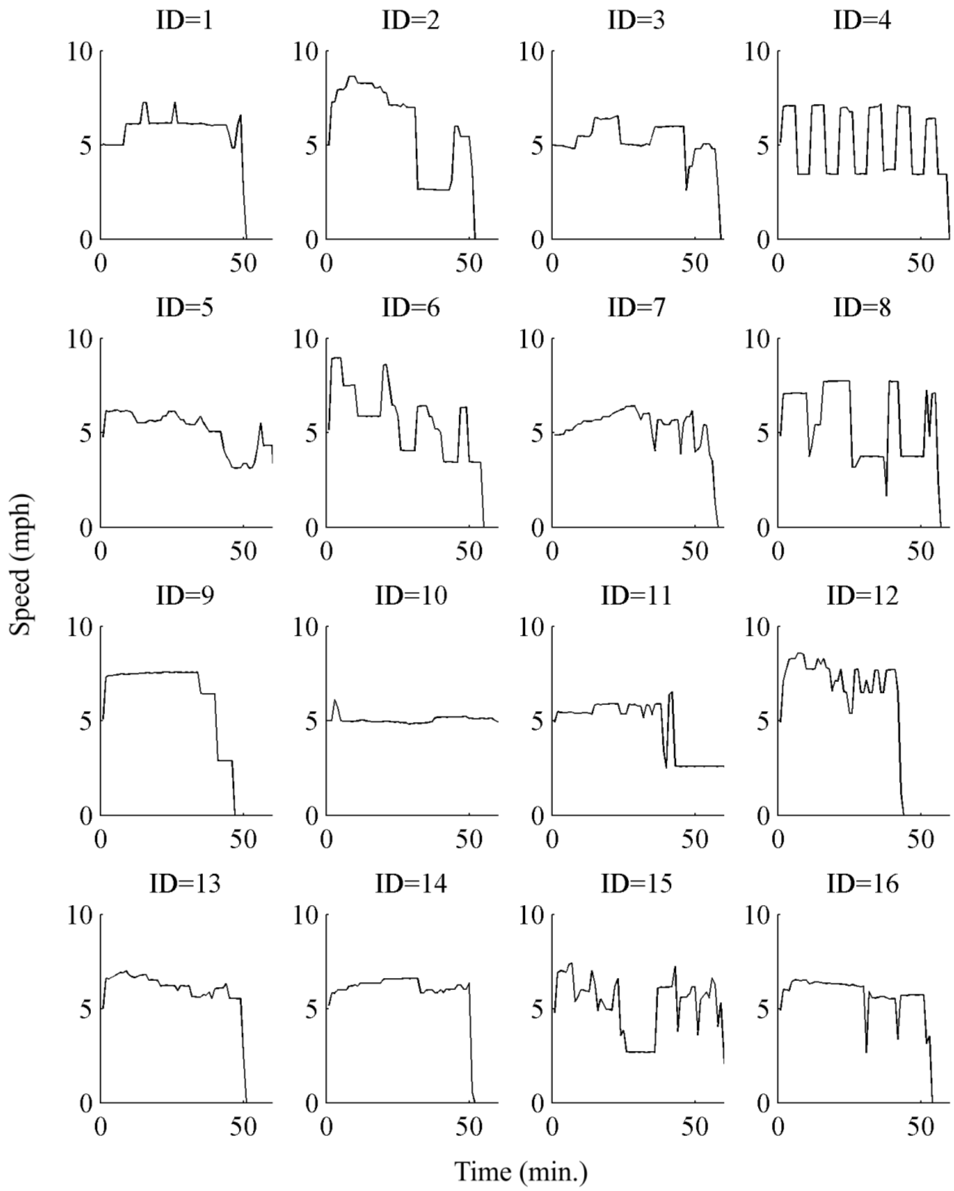

Figure 5.24: Self-pacing profiles for the 16 subjects. Subject ID 11 did not complete the 5 miles within the hour. This subject was forced to finish walking as their core body temperature exceeded the safety limits set by the protocol.

Figure 5.25 show a correlation matrix for the sixteen pacing profiles. Using this and the speed profiles in Figure 5.24, it's possible to group the strategies into three broad categories: finished early (EARLY), steady pace (STEADY), and alternating or variable speed (ALTER). Where EARLY:={1,9,11,12,13,15}, STEADY:={3,5,7,10}, and ALTER.:={4,6,8,14}. Subject ID 2 is unusual in that he/she would have been a very early completer except he/she was forced by the protocol to walk at ~3.0 mph for a time as his/her core body temperature had exceeded the IRB approved safety limit for the self-guided period.

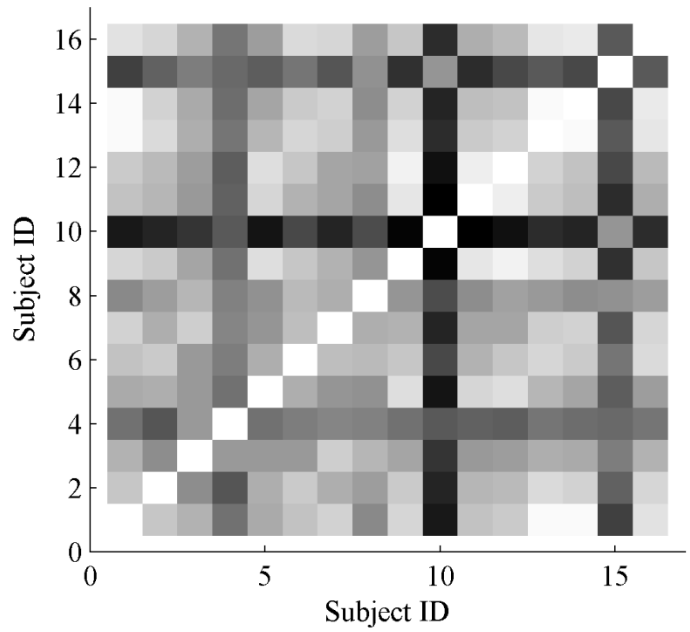

Figure 5.25: Correlation matrix for the different speed profiles of each subject. White is a correlation close to 1 and black is a correlation close to -1.

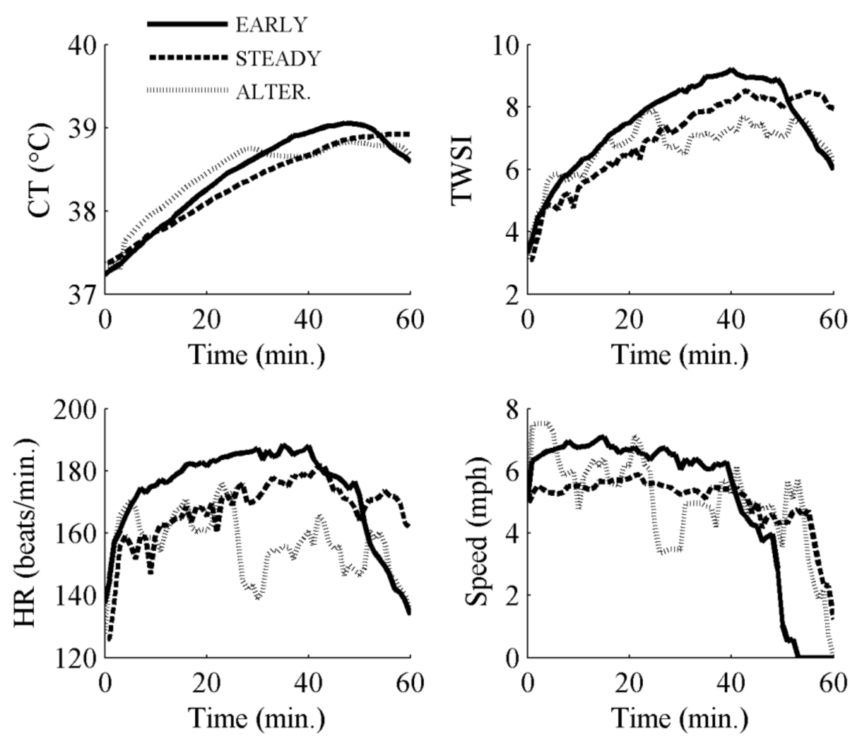

Figure 5.26: Mean core body temperature (top left), mean TWSI (top right), mean heart rate (bottom left), and mean speed (bottom right) for each of the three movement groups.

Figure 5.26 shows the movement profiles for each of the three groups, along with CT, TWSI, and heart rate. On average, the group that alternated between speeds almost kept their TWSI below the 7.5 "safety" threshold. The other two groups, however, exceed this threshold either during the mid-point or towards the end of the exercise session.

5.6.4 GUIDED versus UNGUIDED

Of the 16 subjects, 15 completed the 5 miles in one hour for the UNGUIDED session. For the GUIDED session, 9 subjects completed the 5 miles in one hour while 7 subjects were guided to stop. Figure 5.27 shows the maximum and end thermal-work strain for all subjects for both the GUIDED and UNGUIDED sessions. Subjects 1 and 2 completed the GUIDED session with an earlier version of the policy based on incorrect transition probabilities. These two subjects were dropped from the comparison analysis.

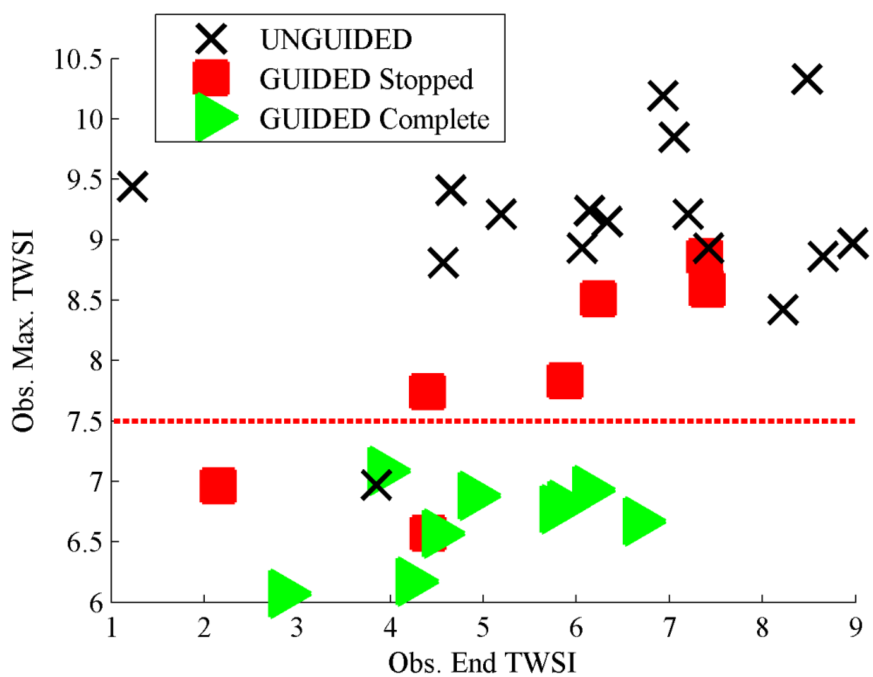

Figure 5.27: End and maximum TWSI for all subjects for both the GUIDED and UNGUIDED sessions, indicating those guided to completion and those guided to stop.

The "Stopped" group was comprised of three "EARLY" finishers (IDs=13, 14, 16), one "STEADY" pacer (ID=5), one subject who adopted an alternating strategy (ALTER) (ID=15), and one subject who did not complete the 5 miles in the UNGUIDED session.

5.6.5 Core Temperature Estimation Algorithm Performance

Figure 5.28 shows the mean-observed and mean-estimated core body temperature and TWSI for both the GUIDED and UNGUIDED sessions for all subjects.

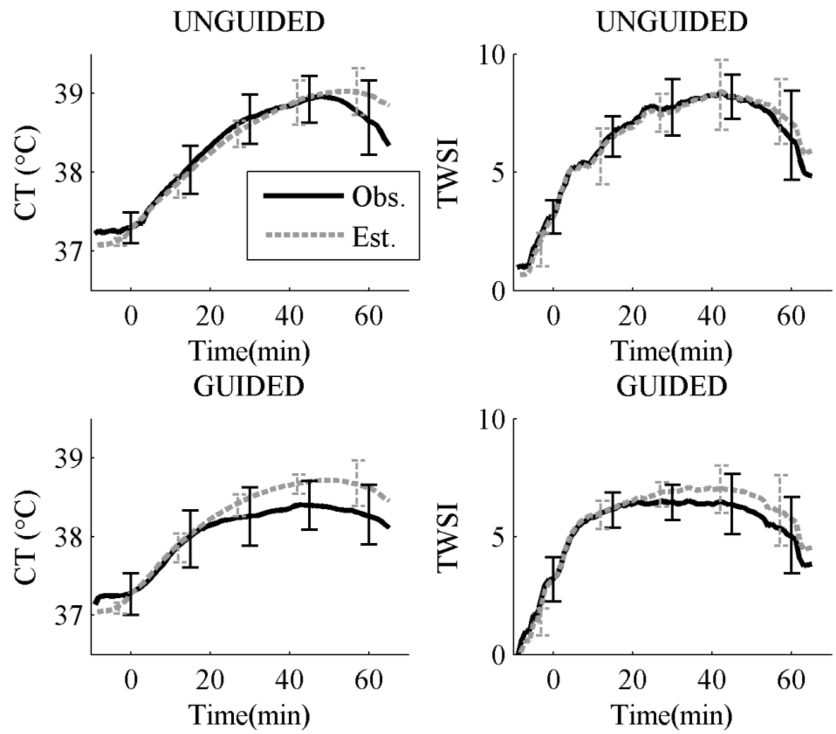

Figure 5.28: The mean observed and mean estimated CT and TWSI for both the GUIDED and UNGUIDED sessions. Error bars are ± SD.

Table 5.10 shows the mean RMSE, mean bias, and LoA for both the GUIDED and UNGUIDED conditions. Bias for both CT and TWSI is around zero for the UNGUIDED session. However, for the GUIDED session there is a significant positive bias for both CT and TWSI. The LoA indicate that 95% of all estimates fall within the same range around the mean bias for both the GUIDED and UNGUIDED groups.

Table 5.10: Mean bias, mean RMSE, and overall LoA between obs. and estimated CT and TWSI.

	CT (°C)		TWSI	
	UNGUIDED	GUIDED	UNGUIDED	GUIDED
Mean RMSE	0.28 ± 0.15	0.32 ± 0.16	0.59 ± 0.32	0.68 ± 0.33
Mean Bias	0.01 ± 0.19*	0.17 ± 0.21*	0.02 ± 0.39*	0.35 ± 0.44*
LoA	± 0.62	± 0.63	± 1.30	± 1.30

* Significant difference between GUIDED and UNGUIDED *p<0.008.*

Figure 5.29 shows the Bland-Altman plots between the observed and estimated CT and TWSI for the GUIDED and UNGUIDED conditions.

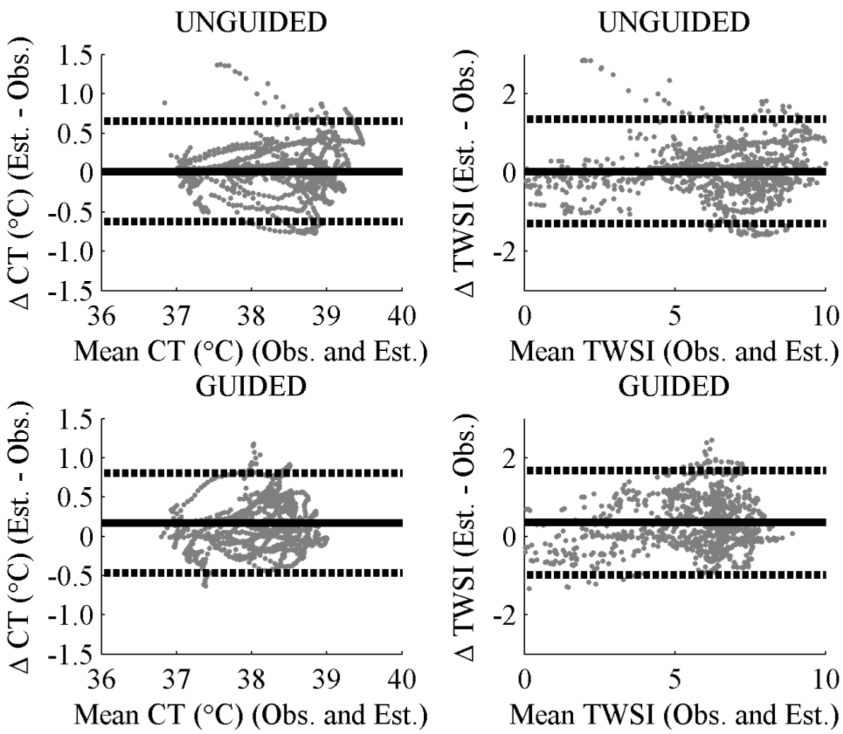

Figure 5.29: Bland-Altman plots showing the level of agreement between estimated and observed CT and TWSI for the UNGUIDED and GUIDED sessions. Bias is a solid black line and ± 1.96 SD is shown as a dashed line.

5.6.6 Physiological Differences between GUIDED and UNGUIDED Sessions

Results in this section are from the 8 subjects who were guided to complete the 5 miles within an hour. Figure 5.30 show the mean responses for CT, TWSI, heart rate, skin temperature, and the heat flux correlate for both the GUIDED and UNGUIDED sessions. Additionally, the figure shows the mean movement speeds for the GUIDED and UNGUIDED sessions. The movement speeds from the UNGUIDED session have a large variability while the movement speeds from the GUIDED session show small variability, indicating that most subjects followed the speeds indicated by the mean fairly closely.

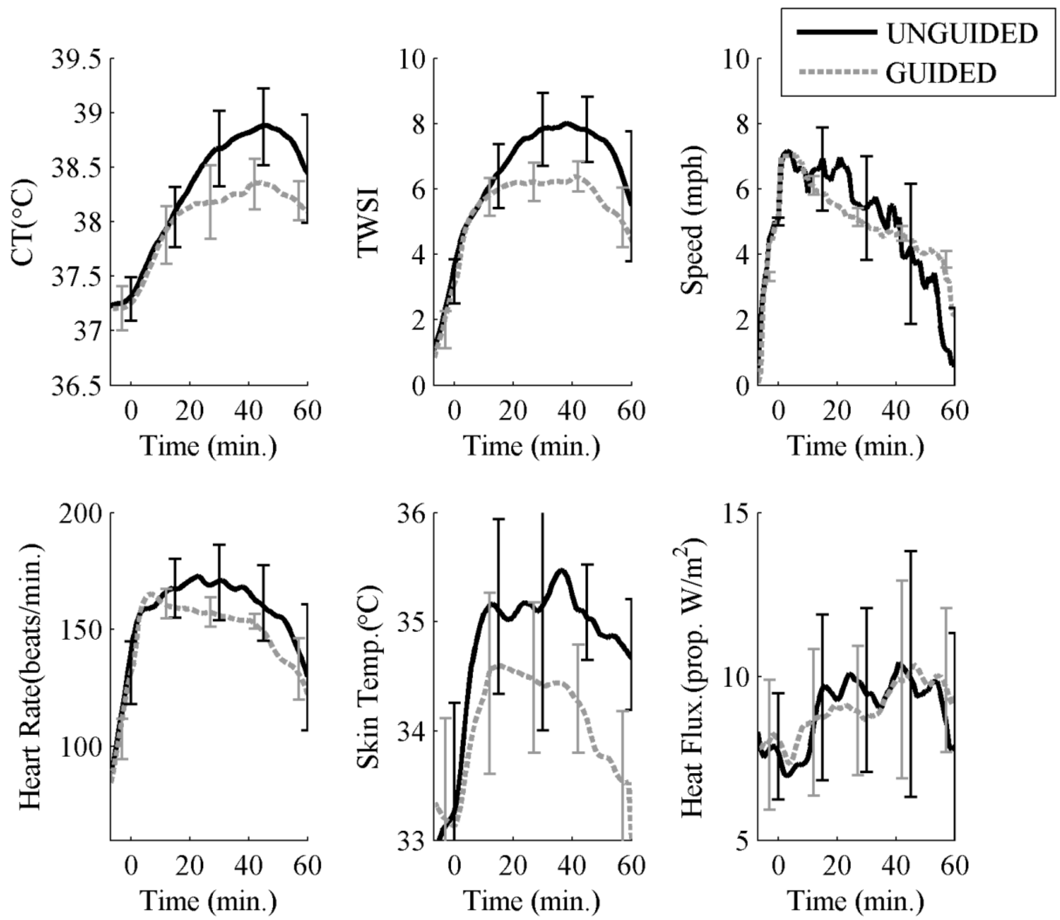

Figure 5.30: Mean CT, TWSI, movement speed, heart rate, skin temperature, and a heat flux correlate for both GUIDED and UNGUIDED sessions. Error bars are ± 1 SD.

Table 5.11 shows the differences in CT, TWSI, heart rate, skin temperature, heat flux, and metabolic rate between the GUIDED and UNGUIDED conditions, for the exercise average, maximum, and end point. Mean CT and mean TWSI across the 60 minute exercise time are significantly lower in the GUIDED session.

Table 5.11: Comparison of physiology between UNGUIDED and GUIDED conditions.

	UNGUIDED			GUIDED		
	Average	Maximum	End Point	Average	Maximum	End Point
CT (°C)	38.4 ± 0.2*	39.0 ± 0.3*	38.5 ± 0.6	38.1 ± 0.2*	38.4 ± 0.2*	38.1 ± 0.2
TWSI	6.8 ± 0.8*	9.0 ± 0.9*	5.7 ± 2.4	5.7 ± 0.4*	6.7 ± 0.4*	4.8 ± 1.1
HR (bpm)	160 ± 12†	186 ± 9*	134 ± 30	151 ± 7†	167 ± 6*	129 ± 17
ST (°C)	34.7± 0.5†	35.7 ± 0.5†	34.7 ± 0.5†	34.0 ± 0.5†	34.9 ± 0.6†	33.0 ± 1.6†
HF	8.9 ± 2.3	12.7 ± 3.0	7.9 ± 3.5	9.0 ± 1.6	11.9 ± 2.5	9.4 ± 2.7
EE (Kcal)‡		599 ± 84			617± 104	

**Difference between GUIDED and UNGUIDED p<0.003. † p<0.05 . ‡Total energy expended (EE) during the exercise period. HR = heart rate, ST = skin temperature, and HF = heat flux.*

Maximum CT, maximum TWSI, and maximum heart rate reached in the GUIDED session are significantly lower than in the UNGUIDED session. Skin temperature appears to be trending lower across the mean, maximum, and end values in the GUIDED session.

Figure 5.31 shows the utility for the two goals of finish as cool as possible (“end TWSI”) and do not get too hot (“Safety”). In addition, the figure shows the maximum TWSI compared to the end state TWSI. These are the two factors that we would like the MDP to minimize while still completing the five miles of movement.

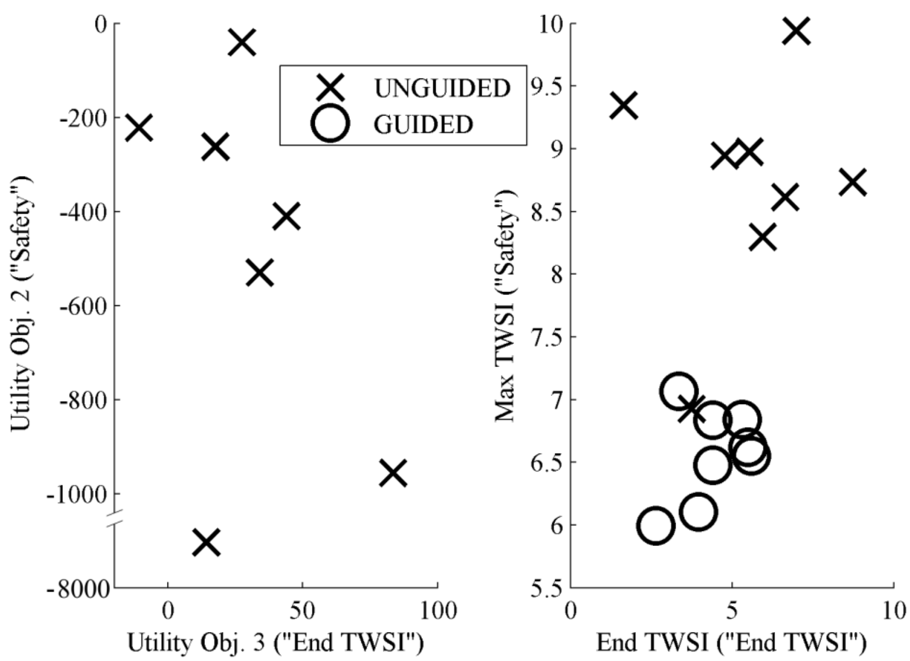

Figure 5.31: Utility of “End TWSI” and the “Safety” objectives (Left) and the maximum TWSI versus the end state TWSI (Right) for the UNGUIDED (Cross) and GUIDED (Circle) Conditions.

There was no significant difference between the “end TWSI” objective where utility was 33.3 ± 28.8 and 48.4 ± 13.5 for the UNGUIDED and GUIDED conditions respectively. The utility of the “safety” goal was significantly greater for the GUIDED (0 ± 0) condition compared to (−428 ± 382) for the UNGUIDED session at $p<0.02$ level. The one unguided subject whose “end TWSI” utility was zero was a very fit tri-athlete who planned an alternating pace based both on his/her experience and scientific articles showing the inefficiencies of the 5 mph pace. There was a significant correlation between the time to complete the 5 miles and the utility score for the “safety” goal (r=0.73, p=0.03), indicating that the quicker a subject finished, the lower the utility score. Table 5.12 shows the number of minutes subjects had TWSIs at or above our safety threshold of 7.5 TWSI units.

Table 5.12: Minutes subjects were at TWSIs ≥ 7.5.

UNGUIDED (min.)	GUIDED (min.)
25	0
0	0
33	0
27	0
12	0
26	0
23	0
44	0

Table 5.13 shows the correlation coefficients for the subjective scales (RPE, thermal, and feeling) against the physiological parameters of CT, TWSI, heart rate, and skin temperature.

Table 5.13: Subjective scale correlations with physiological variables.

	RPE	Thermal	Feeling	RPE+Thermal
CT	0.30*	0.51*	0.26*	0.42*
TWSI	0.55*	0.61*	0.13	0.63*
HR	0.67*	0.57*	0.00	0.68*
ST	0.35*	0.41*	0.08	0.41*

CT = core body temperature, TWSI = thermal-work strain index, HR = heart rate, ST = skin temperature.
** p<0.05.*

The RPE scale was most highly correlated with HR, the thermal scale was most highly correlated with the TWSI, and the feeling scale does not have any strong correlations with the physiological variables. The combined RPE and thermal scale has slightly better correlations than the individual scales to both TWSI and HR.

The mean average, maximum, and end-point subjective ratings for both the UNGUIDED and GUIDED conditions are shown in Table 5.14.

Table 5.14: Mean average, maximum, and end-point subjective ratings for both the UNGUIDED and GUIDED conditions.

	UNGUIDED			GUIDED		
	Average	Maximum	End Point	Average	Maximum	End Point
RPE	9.5 ± 0.8	12.6 ± 1.3	6.5 ± 1.1	8.7 ± 1.5	11.3 ± 2.4	6.5 ± 0.8
Thermal	2.5 ± 0.7*	5.1 ± 0.8*	2.1 ± 1.9	1.3 ± 0.9*	3.0 ± 1.1*	1.5 ± 1.8
Feeling	2.5 ± 1.2	3.8 ± 1.3	3.25 ± 1.3	2.9 ± 1.4	3.8 ± 1.4	3.5 ± 1.3

** Significant differences between GUIDED and UNGUIDED conditions (p<0.01).*

The RPE and Feeling scale had no significant differences between the GUIDED and UNGUIDED sessions. However, the mean maximum Thermal rating for the GUIDED condition was significantly lower (3.0 ± 1.1 between "Warm" and "Hot") than the mean maximum thermal rating for the UNGUIDED condition (5.1 ± 0.8 between "Hot" and "Very Hot"). Similarly, the mean average thermal rating for the GUIDED condition was significantly lower (1.3 ± 0.9 between "comfortable" and "warm") than the UNGUIDED condition (2.5 ± 0.7 between "warm" and "hot").

5.6.7 Guidance to Stop

Six subjects were stopped by the algorithm prior to completing the five miles. No significant differences were found between those subjects who were guided to completion and those guided to stop for age, height, weight, percent body fat, or body surface area. Table 5.15 presents the means and standard deviations for these two groups.

Table 5.15: Subject characteristics for those guided to completion and those guided to stop.

	N	Age (yrs.)	Ht. (m)	Wt. (Kg)	%Body Fat	SA (m^2)†
Completed	n=8 (2F)	23.3 ± 3.8	1.73 ± 0.06	66.3 ± 6.2	14.9 ± 3.9	1.78 ± 0.11
Stopped	n=6 (3F)	23.3 ± 2.9	1.71 ± 0.09	69.3 ± 13.4	18.8 ± 9.4	1.80 ± 0.21

Ht. = height, Wt. = weight. SA = surface area. Values are mean ± SD. There are no significant differences between the groups. †Computed using the Du Bois method (1916).

Similarly, no significant differences were found in the performance of the CT estimation algorithm between the stopped group and those who were guided to stop for both the GUIDED and UNGUIDED conditions. Table 5.16 presents the mean RMSE and Bias for the CT estimation algorithm for each condition and those guided to stop and those guided to completion.

Table 5.16: Mean RMSE and Bias for the CT estimation algorithm for those who were stopped and those guided to completion.

	UNGUIDED		GUIDED	
	Stopped (n=6)	Completed (n=8)	Stopped (n=6)	Completed (n=8)
RMSE (°C)	0.26 ± 0.14	0.30 ± 0.17	0.32 ± 0.22	0.32 ± 0.10
Bias (°C)	0.02 ± 0.26	−0.01 ± 0.14	0.17 ± 0.28	0.17 ± 0.17

Values are mean ± SD.

Table 5.17 shows the group means for the mean, maximum, and end point CT, TWSI, and HR for those who were stopped by the algorithm and those who completed for both the GUIDED and UNGUIDED sessions. Mean maximum TWSI and maximum HR were significantly higher for those who were stopped in the GUIDED session versus those who completed in the guided session. However, there was no significant difference in the measured physiological parameters between those who were guided to complete and those who were guided to stop when looking at the UNGUIDED condition.

Table 5.17: Group mean of the average, maximum, and end point CT, TWSI, and HR for those stopped by the algorithm and those who completed the 5 miles for both the GUIDED and UNGUIDED conditions.

		UNGUIDED		GUIDED	
		Stopped (n=6)	Completed (n=8)	Stopped (n=6)	Completed (n=8)
CT (°C)	Ave.	38.5 ± 0.18	38.39 ± 0.21	38.18 ± 0.38	38.06 ± 0.19
	Max.	39.17 ± 0.14	39.04 ± 0.28	38.60 ± 0.43	38.43 ± 0.20
	End	38.88 ± 0.28	38.47 ± 0.59	38.45 ± 0.50	38.11 ± 0.19
HR (beats/min.)	Ave.	167 ± 12	160 ± 12	157 ± 10	151 ± 7
	Max.	185 ± 10	186 ± 9	178 ± 7*	167 ± 6*
	End	147 ± 25	143 ± 30	125 ± 26	128 ± 17
TWSI	Ave.	6.65 ± 0.51	6.11 ± 0.81	5.66 ± 0.84	5.09 ± 0.5
	Max.	9.25 ± 0.71	8.97 ± 0.91	7.76 ± 0.89*	6.66 ± 0.36*
	End	7.19 ± 1.60	5.74 ± 2.37	5.27 ± 2.03	4.78 1.12

** Significant difference between those stopped versus not stopped for the GUIDED session $p<0.01$. Values are mean ± SD.*

Table 5.18 shows, for each subject who was stopped, the time they were stopped, their estimated and observed CT, their estimated and observed TWSI, the distance they had to complete, the speed needed to complete on time, and the projected end TWSI.

Table 5.18: Ending conditions for subjects stopped by the policy before completing the 5 miles.

Stop Time (Min.)	Distance Completed (miles)	Speed needed for completion (mph)	CT (°C)	Estimated CT (°C)	TWSI	Estimated TWSI	Project Estimated End TWSI
58	4.68	9.6	39.01	38.99	7.88	7.83	>10
50	4.15	5.1	38.79	38.95	7.97	8.32	9.5 †
54	4.33	6.7	38.05	38.96*	5.82	8.07	>10
52	4.17	6.2	38.69	39.01	7.28	7.96	>10
58	4.73	8.1	38.52	38.99*	6.56	7.62	>10
30	2.25	5.5	37.89	38.75*	5.88	7.48	>10

** Estimated CT > 0.32 °C above observed CT.*

† This subject did not finish the five miles for the UNIGUIDED condition. During the GUIDED condition, at minute 50, the physiological monitor was giving erroneously low heart rate readings. This provided a low TWSI state, and at minute 54, the subject was instructed to run at 6.7mph to try and complete the difference. At minute 56, the subject complained that he/she was feeling dizzy. The run was stopped at this point, and it is unknown whether the subject would have been able to complete.

Of the six subjects who were stopped by the policy, one was stopped early according to the protocol safety procedures, when they complained of feeling dizzy. For this subject, the physiological monitor at minute 50 was providing erroneously low heart rate readings which provided a low TWSI state. At minute 54, the policy instructed the subject to run at 6.7 mph to try and make up lost distance. At minute 56, the subject complained that they were feeling dizzy. The run was stopped at this point, and it is unknown whether the subject would have been able to complete. This subject was included in this analysis as he/she was also unable to complete the UNGUIDED condition by himself/herself.

Using the speed necessary to complete the final distance in the remaining time, all five of the subjects were projected to have had an end TWSI of >10 at minute 60. In the MDP, this would impose a penalty of −2000. The utility calculation at this point is simple. An end penalty of −1000 for not making the distance is better than the end penalty of −2000 for a high end state TWSI. Thus, according to the MDP reward structure, it is better to stop the subject and have them cool a little versus have them complete an end too hot. However, for three of these subjects the estimated CTs exceed the observed CTs by more than 0.32°C.

5.7 Discussion

The goal of this experiment was to examine how the combination of our thermal-work strain state estimation and policy estimation techniques performed with human subjects. We found that with these two techniques, we were able to accurately pace 11 out of 14 subjects, while the remaining three were guided to stop prematurely. Of those who completed the five miles in both the GUIDED and UNGUIDED sessions (n=8), the automated pacing allowed them to complete with overall less thermal-work strain. The pacing guidance allowed participants to complete with significantly lower average CTs (38.1 ± 0.2 °C versus 38.4 ± 0.2 °C) and lower average TWSIs (5.7 ± 0.4 versus 6.8 ± 0.8) over the course of the 60 minutes of exercise. The guidance prevented participants from reaching high core temperatures and very high levels of thermal-work strain with significantly lower maximum CTs (38.4 ± 0.2 °C versus 39.0 ± 0.3 °C) and significantly lower maximum TWSIs (6.7 ± 0.4 “High Strain”, versus 9 ± 0.9 “Very High Strain”). Additionally, the pacing guidance kept the completing participants below the TWSI “safety” threshold of 7.5, whereas all but one participant exceeded this threshold when self-paced, spending at least 12 minutes above the threshold.

Contrary to our hypotheses for the subjective scales, participants reported no difference in their perceived level of exertion, but rated the GUIDED session significantly cooler both on average (1.3 ± 0.9 “Comfortable to Warm” versus 2.5 ± 0.7 “Warm”) and by their maximum thermal sensation level (3.0 ± “below Hot” versus 5.1± “above Hot”). Additionally, the expected metabolic pacing efficiency in the GUIDED session was not observed, as no difference was found in the overall metabolic energy expenditures between conditions.

5.7.1 Guided to Stop versus Guided to Complete

Our experiment had two conditions of UNGUIDED and GUIDED and was designed to examine whether the MDP could 1) prevent acute thermal-work strain and 2) improve thermal-work strain outcomes over the course of a simple exercise session. Our MDP policy guided 9 volunteers to complete the 5 miles in 60 minutes, while for the remaining 7 subjects, the policy guided them to stop the exercise. For those guided to stop, the policy provided the correct guidance given the MDP structure. All stopped subjects had estimated TWSIs > 7.5, and if they were guided at the speed necessary to complete the 5 miles, the transition probabilities indicated they would end with an estimated TWSI > 10.

The thermal responses of the volunteers from their UNGUIDED session indicated that the treadmill task was thermally stressful with all but one subject reaching TWSIs above 8 ("Very High") thermal-work strain. Similarly, these same subjects spent at least 12 minutes above our MDP TWSI "safety" threshold of 7.5. A combination of our low "safety" threshold and the task's high level of thermal stress likely contributed to so many subjects being stopped by the MDP. While for some subjects core temperature was over-estimated, the results indicate that the policy was able to prevent acute hyperthermia. However, in the design of our experiment, we did not anticipate so many subjects not completing the task.

In the analysis of whether the MDP was able to guide subjects with overall lower TWSI levels, the stopped subjects are a confounding element. Subjects who were guided to stop completed less distance within the 60 minutes invalidating a direct comparison of their physiology between UNGUIDED and GUIDED sessions. While the policy successfully showed a reduced thermal-work strain impact for those subjects guided to complete, the experimental design was not readily able to examine this effect in those subjects that were stopped. The only difference between the stopped subjects was a significantly higher maximal heart rate than those guided to complete. This higher maximal heart rate indicates that the task was physiologically more stressful under policy guidance for those guided to stop compared to those guided to complete. There are several reasons that the MDP-derived policy may be more effective on some subject's than others. First, given our thermally stressful environment and MDP definition, these results may reflect normal individual differences split in a binary fashion between stopped and completed. These results may also indicate that the thermal-work strain efficiencies identified by the policy may be muted on the subjects that were stopped. Finally, these results may also indicate that the pacing policy determined from the MDP and transition probabilities may not be optimal for all people. For example, the pacing profile of the one subject who matched the MDP during their UNGUIDED session is completely different from the MDP policy (see Figure 5.24, ID=4). Further experimentation is necessary to identify the reasons behind the differences in those guided to stop and those guided to completion. While the stopped subjects pose a confounding element for our simple experimental design, requiring future experimentation, the thermo-regulatory effects discovered in those guided to completion are nonetheless still significant and germane.

5.7.2 Thermoregulatory Efficiencies

We had anticipated that the overall thermal-work strain benefit would be derived by the policy avoiding the metabolically inefficient paces between a comfortable walk and a comfortable run (~4.25 mph to ~5.25 mph). These metabolic efficiencies could be achieved by providing alternating pacing above and below these values. In fact, the one subject who did not exceed the TWSI "safety" threshold during their self-paced exercise employed this strategy, switching off between 3.5 mph and 7.0 mph runs about every 4 minutes. This pacing strategy matched the MDP policy in terms of overall utility. However, the MDP-derived policy started fast with a gradual reduction in speed over the course of the sixty minutes, with minimal switching between walks and runs. In practice, the policy often paced subjects at these awkward speeds, and we found that, overall, there was no significant difference in total energy expenditure between the GUIDED and UNGUIDED sessions.

So, where did the thermal efficiencies come from? The difference in maximum core body temperature between the two runs of 0.5 °C is a meaningful difference, as it represents about 20% of the usual operating range of CT. Re-examining our thermoregulatory dependencies from Chapter 3 is helpful (see section 3.1). Figure 5.32 is a simplified version of Figure 3.1 and shows the variables that effect core body temperature (CT). In our experiment, core body temperature increase is primarily due to heat production (HP) from metabolism (M) to sustain the exercise work. Heat is transferred away from the core (HTc) and to the skin both by skin blood flow (SBF) and passive heat conductance (PHC). Heat transfer to the environment (HTe) is through several mechanisms that include conductance, convection, and evaporation. For each session, HR, O_2, M, and CT were measured directly. Heat transfer to the environment (HTe) and skin temperature were measured at a single point. In the GUIDED session, average CT decreased, while O_2, M, and thus heat production (HP) remained the same. For CT to decrease with the same heat production, the average rate of heat transfer away from the core (HTc) must increase, along with the average rate of heat transfer to the environment (HTe). While our point measure of heat flow to the environment was the same between conditions, this was likely due to its enclosed location under the arm. Here, the sensor was not able to reflect an overall increase in heat loss across the whole body surface area. Our data show some indications for improved evaporative effectiveness through a trend in lower skin temperatures ($p \leq 0.05$) for the GUIDED session, as one possible route of increased cooling.

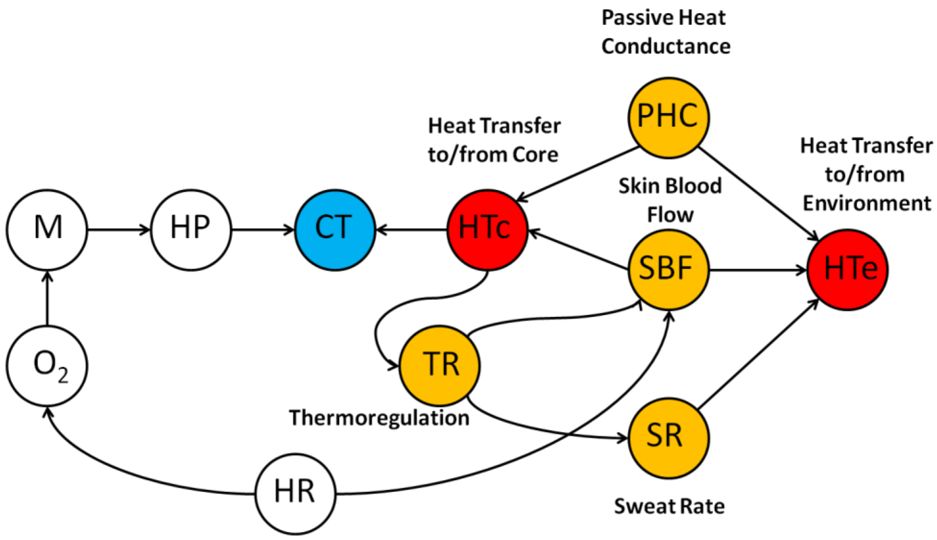

Figure 5.32: Factors affecting core body temperature. Where CT = core temperature, M = metabolic rate, HP = heat production, HTc = heat transfer from the core, SBF = skin blood flow, HTe = heat transfer to the environment, and HR = heart rate. Arrows indicate dependencies. White indicates variables that stay the same between GUIDED and UNGUIDED sessions. Blue indicates variables that decrease in the GUIDED session. RED indicates variables inferred as increasing in the GUIDED session. ORANGE indicates possible mechanism for efficiencies.

Our heart rate-based core body temperature estimator provides some evidence of an increase in the proportion of cardiac output directed to skin blood flow. Heart Rate is determined by the stroke volume and the cardiac output required for bodily functions (e.g. blood flow to muscles for work, skin blood flow (SBF) necessary for heat transfer, and brain and organ function). The core body temperature estimation algorithm successfully takes advantage of a fairly consistent ratio of cardiac output for work and cardiac output for skin blood flow. However, in the GUIDED session, we found a significant positive bias in the estimation of core body temperature. If the portion of cardiac output for work remains the same between the GUIDED and UNGUIDED session, this then suggests that there is a larger portion of the cardiac output directed for skin blood flow.

In the current study, we lack the additional skin temperature sites necessary for a mean weighted skin temperature, as well as measures of local and whole-body sweat rate to identify which mechanisms are in play. However, our data provide evidence that the lower CTs and TWSIs over the course of the event were realized through efficiencies in the thermo-regulatory system instead of metabolic efficiencies.

5.7.3 Self Perception

The rating of perceived exertion (RPE) scale has been linked with modern pacing models as a feedback mechanism for adjusting pace based upon a predefined template stored in the brain (Tucker 2009). In our experiment, we found no difference in RPE ratings between the GUIDED and UNGUIDED conditions. Not surprisingly (Borg 1970 and 1982), the RPE was most highly correlated with HR (r=0.67) and least correlated with CT (r=0.30). The similar RPE ratings for the GUIDED and UNGUIDED conditions match the findings from the average HR responses.

We had anticipated that with limited change in skin temperature, the thermal sensation scale would not be useful in alerting participants to their thermal-work strain state. Early thermal sensation work (Gagge et al., 1969) suggests that a 2.0 °C difference in skin temperature is needed to perceive changes from "warm" to "hot". However, we found that the average and maximal thermal perceptions were significantly lower in the GUIDED condition versus the UNGUIDED. Contrary to the literature (Gagge et al., 1969; Fanger, 1982; and Young et al., 1987) the scale was least correlated with skin temperature (r = 0.41), and was most highly correlated with TWSI (r = 0.61). As with TWSI, the average and maximal values of the thermal sensation scale were significantly lower for the GUIDED session than the UNGUIDED session.

It appears that using RPE as a feedback mechanism for optimizing pace when thermal-work strain is a factor may not be appropriate. Whether the RPE is rating metabolic rate or heart rate there is no indication in this scale of the reduction in thermal-strain. Participants were, however, able to perceive a lower thermal sensation in the GUIDED session versus the UNGUIDED. The mean maximal thermal sensation scale rating was 3.0 ("Warm/Hot") in the GUIDED session versus 5.3 ("Hot/Very Hot") in the UNGUIDED. These mean ratings indicate that the thermal sensation scale could have been used by subjects in the UNGUIDED session to follow the instructions "do not get too hot".

5.7.4 MDP Policy

The underlying model parameters that were used to estimate the MDPs transition probabilities appear to be acceptable, on average, for our group of subjects. When the subjects' actual speeds are used in the SCENARIO model, the TWSI appears to be modeled appropriately with a small bias (-0.44 ± 1.57) with a RMSE of ~1.5 TWSI units.

With so few observed total transitions (480), it is difficult to conduct a direct comparison with our learned transition probability estimates. However, there appear to be two important features that our smoothed transition probability distributions miss. 1) For no movement, the rate of reduction in TWSI is less, and closer to the original Monte-Carlo values, than our smoothed transition probabilities suggest. 2) At high thermal-work strain states (e.g. TWSI > 7), and for high speed actions (speed > 6 mph) thermal-work strain increases more gradually than modeled by our smoothed transition probability distributions. This effect is observed in Figure 5.23 for TWSI 8, where an observed movement speed of 8 mph transitions to an observed TWSI of about 8.5 versus the transition to an expected TWSI of 10 indicated by our smoothed probability mass function. These slower increases for the higher speeds can be seen in the original Monte-Carlo transition probability distributions (see Figure 5.12: TWSI index 8 and 9). The change in shape of the expected mean of the distribution is likely due to an individual reaching their heart rate maximum. At this point, only a change in CT will increase the TWSI, leading to a much smaller increment in TWSI even at high speeds. Not accounting for this different structure in our smoothed transition probability distribution likely led to at least three of our subjects being stopped before completing the 5 miles.

Overall, the policy was effective at reducing thermal-work strain for those who were guided to completion. Additionally, the policy was able to enforce the hyperthermia "safety" requirement by stopping subjects when their projected end TWSI would be > 10. The MDP was able to balance both the "end TWSI" and "Safety" goals, whereas all but one subject in the UNGUIDED session appeared to sacrifice the "Safety" goal. Individuals in the UNGUIDED session appeared to be following a strategy where the TWSI profiles were similar to those found through our simulations where we set no penalties for exceeding a TWSI threshold of 7.5.

The policy of starting fast and then slowing is similar to that of athletes exercising longer than 30 minutes (Roelands et al., 2013). The one subject who matched the MDP in terms of utility 57.1 (UNGUIDED) compared to 53.8 (GUIDED) was a trained athlete. But, this athlete adopted a pacing strategy avoiding the metabolically inefficient speeds between ~4.25 and ~5.25 mph, by walking and running at 3.5 mph and 7.0 mph, respectively. This subject had specifically read research articles showing these metabolic efficiencies. It is possible, that by smoothing the transition probability mass function, that information regarding these metabolic efficiencies were removed. However, even with unsmoothed transition probabilities, it is not certain that the metabolic efficiencies could be easily found with our choice of metabolic estimator. The Pandolf equation (Figure 5.9) appears to overestimate the metabolic rate of walking, and provides little benefit for alternating paces versus moving at "awkward" movement speeds. The curves from Paroczai and Kocsis (2006), however, show much more potential for identifying these efficiencies.

An improved metabolic rate estimator could provide additional metabolic efficiency benefits missing in our current policy. However, these benefits for finding an alternating pace appear to only come into play in certain constrained tasks where an "awkward" overall speed is required. The thermoregulatory efficiencies found by our MDP appear to offer a more general pacing solution.

5.7.5 Core Temperature Estimation Algorithm Performance

In the UNGUIDED session, the core body temperature estimation algorithm had an overall RMSE of 0.28 ± 0.15 °C with a small bias of 0.01 ± 0.19 °C and with 95% of all estimates falling within ± 0.62 °C of the observed values. These results replicate the findings from our work in Chapter 3, where the overall RMSE was 0.30 ± 0.13 °C, bias was −0.03 ± 0.19 °C, and 95% of all estimates were within ± 0.63 °C. However, for the GUIDED session the bias of the CT estimator was significantly higher (0.17 ± 0.21 °C), which is why the estimated TWSI bias was also significantly higher. With a positive TWSI bias, the algorithm was weighted to false positives in terms of exceeding the TWSI "safety" goal. Of the five subjects who were guided to stop, three subjects had high estimated TWSIs but much lower observed TWSIs. Using the estimated TWSI, our policy stopped these subjects correctly, but less error would likely have allowed them to continue and complete the 5 miles. For practical work, knowing that there is a positive bias in estimating thermal-work strain, any high estimated TWSI could be used to alert medical personnel to examine individuals more closely. For safety, overestimation of core body temperature is more desirable than underestimation. In our experiment, we did not need to stop anyone during the GUIDED session because their observed CT was too high compared to a lower estimated CT.

Ideally, we would like to automatically identify when the CT to heart rate relationship used by the estimation algorithm is causing systematic bias. Our dynamic Bayesian network model from Chapter 3 utilized additional inputs of heat flux, and accelerometry in order to identify when the CT to heart rate relationship did not provide enough information to correctly estimate additional CT gain. However, the results from this study show no significant differences between point measures of skin temperature and heat flux, making it difficult to identify where the CT to heart rate relationship is behaving differently.

5.7.6 Limitations

One limitation of this study's design was the lack of a direct thermal-work strain state feedback condition to the subjects. This makes comparing time spent above the "safety" threshold difficult as the subjects had no objective way to assess their current TWSI state. However, our data suggest that the thermal sensation scale could have been used as that feedback. Indeed, the maximum thermal scale rating for the UNGUIDED session was 5.1 (between "hot" and "very hot"), while for the GUIDED session the mean maximum rating was 3.0 (between "warm" and "hot"). The mean subject response from the GUIDED session showed that they perceived the pacing guidance as not letting them get "too hot", which met the specific instructions given to subjects prior to the start of the UNGUIDED session. Nevertheless, even if objective feedback were given, it may not be helpful without training or prior knowledge of how to make use of that feedback in an anticipatory manner (Tucker, 2009; Konig et al., 2011).

With almost half of the subjects being guided to stop, it is difficult to broadly generalize the thermo-regulatory efficiencies found in the subjects guided to completion. Further experimentation is necessary where the design allows for completion of the task by all participants. In this type of design direct comparison of the physiology of all subjects between GUIDED and UNGUIDED conditions will be possible.

Additionally, our results can only be applied to "novices". While our participants were fit and often exercised, the particular task combined with the occlusive and insulating clothing made this a very novel task. Only the tri-athlete, who was used to competing in the heat, was able to match the performance of the MDP policy. Training the volunteers on the task would likely have reduced the improvement showed by the MDP policy. However, determining an efficient pacing policy for new and novel tasks may take many bouts of training, even for an experienced athlete.

In hindsight, measuring each participant's VO_2 max (as a measure of fitness) would have helped us to identify if there was a fitness difference between those who were stopped versus those guided to completion. Finally, measures of multiple skin temperature sites would provide more insight into the thermoregulatory mechanisms behind the policy's thermal-work strain efficiencies.

5.8 Conclusions

Our experiment tested whether the combination thermal-work strain state estimation and policy estimation could provide a means to prevent heat injury and manage the longer term effects of thermal-work strain. The goals and thermal-work strain safety limits of a simple one hour exercise were modeled in terms of a reinforcement learning problem described with intuitive rewards and penalties. A physics- and physiology-based thermo-regulatory model was used to estimate probability distributions of human thermal responses across our range of possible actions and states. The rewards and penalties encoded the following three goals: “finish the course”; “don’t get too hot”; and “finish as cool as possible”. The reinforcement learning problem was constructed as a Markov decision process and was solved using dynamic programming.

Our results show that the policy estimation technique was able to guide a majority of subjects to complete the one hour exercise task with significantly lower core body temperatures that translated to physiologically meaningful lower thermal-work strain levels. The remaining subjects were guided to stop, as they were exceeding the MDPs thermal “safety” threshold and stopping provided better overall utility. Our *computational physiology* approach allowed us to discover thermo-regulatory efficiencies that appear to have application beyond the scope of this current scenario. In this work, we successfully demonstrated the real-time management of both acute and chronic thermal-work strain in human subjects. We conclude that this approach shows the potential for use in preventing thermal injury and improving long-term performance of those engaged in thermally stressful work.

Chapter 6

Conclusions

6.1 Conclusion

In this dissertation, we presented computational physiology techniques that were used in a physiological feedback loop to prevent hyperthermia and optimize pacing to take advantage of thermo-regulatory efficiencies. Our method's feedback loop utilizes minute-to-minute measures of heart rate to estimate core body temperature and thermal-work strain health state. Using decision theoretic models, the thermal-work strain health state is used to provide optimized pacing feedback to an individual, preventing hyperthermia and enabling completion of a task with overall lower thermal-work strain.

Previous physiological monitoring approaches for thermal-work strain health state monitoring have been hampered by the difficulties inherent to accurately measuring or estimating core body temperature. Our computational physiology approach demonstrated how formalizing an open physiology research problem into a graphical model allowed us to improve upon current estimation techniques while also providing insight into important internal states and dependencies in the human thermoregulatory system (Chapter 3, Section 3.1). These thermoregulatory system insights enabled us to simplify the model and provide a general core body temperature estimation algorithm based only upon sequential heart rate observations. Using previously collected data, we were able to estimate core body temperature to a similar degree of accuracy as laboratory methods. We also demonstrated that the estimation technique performed similarly for different work rates; across a wide range of environments; and for different clothing ensembles from just shorts and t-shirts to full encapsulation in chemical/biological personal protective equipment (Chapter 3, section 3.2). Finally, we deployed our technique for use in the field as part of a wearable thermal-work strain physiological monitoring system during real-time training missions for two National Guard chemical/biological response teams. During this study, core body temperature was estimated in real-time and used in conjunction with heart rate to estimate the thermal-work strain index (TWSI). Our results found that 95% of all estimates fell within ± 1 TWSI unit of the observed values. The accuracy of the approach was corroborated by focus group feedback that found that all subjects felt that the TWSI provided in real-time was an accurate reflection of how they were feeling (Chapter 3, section 3.3).

Thus, we have shown that a computational physiology approach enabled us to develop a thermal-work strain state estimator that is reasonably accurate across a wide range of settings in both laboratory and field experiments. The approach has better performance compared to previous work, while only using one input. Our approach shows real potential as a practical solution to thermal-work strain monitoring. It can be readily adopted by any device that measures heart rate, and when used in conjunction with the TWSI, can provide accurate estimates of thermal-work strain state.

With an accurate thermal-work strain state estimator, we were able to examine our second problem of developing a method to estimate a policy to provide optimal advice on completing a thermally challenging goal. We focused on the following two questions: 1) is it possible to adequately express the tasks, risks and goals surrounding thermal-work strain management in terms of a simple reinforcement learning problem that would provide a realistic policy; and 2) would any derived policy perform better than the solution provided by the human agents themselves? Using a human thermoregulatory model to simulate a real-world training event, we were able to extract thermal-work strain state transition probabilities necessary for the definition of a Markov decision process (MDP). The tasks, goals, and thermo-regulatory constraints were defined in terms of simple rewards and penalties. Simulated results showed that the derived policy pacing was realistic and matched the pacing profile of those who were better performers in the real-world task. Simulations of physiological response to the training event from observed paces and policy dictated paces found that the simulated agents following our policy finished in a state of lower thermal-work strain (Chapter 4).

Finally, by combining the two approaches of thermal-work strain state estimation and optimal policy estimation, we were able to examine the effectiveness of our approach in real-time with human subjects. We found that our policy was able to meaningfully reduce the overall thermal-work strain over the course of a one-hour exercise. The approach was also able prevent excessive thermal-work strain by stopping individuals who were getting too hot rather than have them complete the task with high and unsafe levels of thermal-work strain. By providing a real-time thermal-work strain feedback loop our computational physiology solution took advantage of thermo-regulatory efficiencies that were present in the physics/physiology thermo-regulatory model. Our approach was able to derive an optimal pacing strategy that was only matched by a tri-athlete who had substantial pacing experience and had previously trained in the heat. For individuals with little or no experience, or for those facing a new task, this approach appears to offer a way to significantly improve thermal-work strain performance.

We conclude that our approach has been able to address both the acute and chronic aspects of thermal-work strain management and that we have successfully developed:

- *A method for the state estimation of the latent human core body temperature from wearable physiological sensors that enables real-time thermal-work strain health state monitoring and heat injury prevention.*
- *Models for policy estimation that provide automated advice to improve thermal-work strain state and performance outcomes over a course of prescribed work.*

We envision that the work in this dissertation will enable practical real-time monitoring systems that can prevent heat injury and improve long-term thermal-work strain state for those in professions requiring physical performance in hot environments.

6.2 Limitations and Future Work

6.2.1 Core Temperature Estimation Algorithm

While our core body temperature estimation technique has proven useful, it does have some limitations. The technique was validated and tested on a fairly homogenous set of subjects. The participants were generally young (early 20s) and fairly fit. For older volunteers, the heart rate to core temperature relationship will likely need to be adjusted, as maximal heart rate reduces with increased age. Similarly, the temporal response of the model will likely need to be adjusted for individuals with substantially different fitness levels. Future work will focus on adapting the model for age and fitness and testing in a larger population, where the specificity and sensitivity can better be determined. Additionally, we also intend to investigate individualizing the model parameters by learning in real-time. Our aim is to increase the accuracy of the technique by individualization and to make the approach more generalizable.

6.2.2 Thermal-Work Strain Performance Optimization

Further work is necessary to examine how direct thermal-work strain state feedback to an individual influences their pacing decisions. In our laboratory study, the human agents only had their own subjective feedback of thermal-work strain state, whereas the policy had an estimate based on direct physiology measures.

Our pacing optimization experiment also focused on a specific task of completing a walk/run exercise within a given time frame. The goals and constraints of the task were structured to stop a participant when they got too hot, but for many tasks, this structure may be too limiting. Instead, in many instances it may be more helpful to change the stopping behavior to allow a maximization of goal completion all the while meeting the thermal-work strain state management constraints. The mechanisms of the thermo-regulatory efficiencies identified in this study require further examination to determine their generalizability to other task configurations.

Although the modeling presented here focused on just pacing, other actions could be incorporated into the reinforcement learning problem such as the following: removing or venting clothing; removing load; or hydrating. Finally, we aim to extend our approach to the management of teams by optimizing team goals across individual team members' pace, rest periods, and shared load carriage.

6.3 Better Health State Estimation, Better Advice, Better Outcomes

We have demonstrated that our *computational physiology* approach was able to obtain better thermal-work strain outcomes for exercising humans over a course of prescribed exercise. The techniques demonstrated here have the potential for use in other aspects of health monitoring. The use of a physiological feedback mechanism for a diabetic could assist in optimizing food intake along with insulin injection to better balance blood sugar highs and lows. For individuals with motor problems, detecting balance instability early may allow better assistance in the rehabilitation process. As the commercial market for wearable monitoring devices continues to grow, so too will the potential for computational techniques for health state and policy estimation. In this market, our methods have the potential for better health state determination, which will allow better and timelier advice, which will improve overall health outcomes.

Bibliography

[1] Abbeel P, Coates A, and Ng AY (2010) Autonomous Helicopter Aerobatics through Apprenticeship Learning. *The International Journal of Robotics Research* 29(13):1608-1639.

[2] Abbiss CR and Laursen PB (2008) Describing and Understanding Pacing Strategies during Athletic Competition. *Sports Med* 38(3):239-252.

[3] Abriat A, Brosset C, Bregigeon M, and Sagui E (2014) *Military Medicine* 179(3):309-314.

[4] American College of Sports Medicine, Franklin BA, Whaley MH, Howley ET, and Balady GJ (2000). ACSM's guidelines for Exercise Testing and Prescription (6th ed.). Lippincott Williams and Wilkins, Philadelphia.

[5] Adams WC, Fox RH, Fry AJ, and MacDonald IC (1975) Thermoregulation during marathon running in cool, moderate and hot environments. *Journal of Applied Physiology* 38(6):1030-1037.

[6] Aleks N, Russell S, Madden MG, Morabito D, Staudenmayer K, Cohen M, and Manley G (2008) Probabilistic detection of short events, with application to critical care monitoring. In *Advances in Neural Information Processing Systems* (pp. 49-56).

[7] Al-Muhaizeem F, Allen U, Komar L, Naser B, Roy L, Stephens D, Read S, Kim C, and Schuh S (2004) Comparison of temporal artery, rectal and esophageal core temperature in children: results of a pilot study. *Pediatr. Child Health* 9(7):461-465.

[8] Amann M (2011) Central and peripheral fatigue: interaction during cycling exercise in humans. *Med. Sci. Sports Exer.* 43(11):2039-2045.

[9] American Society of Heating Refrigerating and Air Conditioning Engineers (ASHRAE) (2001) Thermal comfort. In Fundamentals. ASHRAE, Atlanta (pp. 8.1-8.29).

[10] Anliker U, Ward, JA, Lukowicz P, Troster G, Dolveck F, Baer M, Keita F, Schenker E, Catarsi F, Coluccini L, Belardinelli A, Shklarski D, Alon M, Hirt E, Schmid R, and Vuskovic M (2004) AMON: A Wearable and Multiparameter Medical Monitoring and Alert System. *IEEE Trans Inform Technol Biomed* 8(4):415-427.

[11] Atkinson G, Davison R, Jeukendrup A, and Passfield G (2003) Science and cycling: current knowledge and future directions for research. *Journal of Sports Sciences* 21:767-787.

[12] Banderet LE and Lieberman HR (1989) Treatment with tyrosine, a neurotransmitter precursor, reduces environmental stress in humans. *Brain Res Bull* 22:851-56.

[13] Bassett DR and Strath SJ (2002) Use of pedometers to assess physical activity. In Physical Activity Assessments for Health-Related Research, edited by GJ Welk. Human Kinetics, Champaign (pp. 163-177).

[14] Barnes RB (1967) Determination of body temperature by infrared emission. *J Appl Physiol* 22:1143-1146.

[15] Bellman RE (1957a) Dynamic Programming. Princeton University Press, Princeton.

[16] Bellman RE (1957b) A Markov decision process. *Journal of Mathematical Mechanics* 6:679-684.

[17] Bernard TE, Kenny WL (1994) Rationale for a personal monitor for heat strain. *Am Ind Hyg Assoc J* 55(6): 505-514.

[18] Bertuzzi R, Lima-Silva AE, Pires FO, Damasceno MV, Bueno S, Pasqua LA, and Bishop DJ (2014) Pacing strategy determinants during a 10km running time trial: contributions of perceived effort, physiological, and muscular parameters. *Journal of Strength and Conditioning Research* 28(6):1688-1696.

[19] Bishop CM (2006) Pattern Recognition and Machine Learning. Springer, New York.

[20] Bland JM and Altman DG (1986) Statistical methods for assessing agreement between two methods of clinical measurements. *The Lancet* 1(8476):307-310.

[21] Bland JM and Altman DG (1999) Measuring agreement in method comparison studies. *Statistics Methods in Medical Research* 8:135-160.

[22] Borg GAV (1970) Perceived exertion as an indicator of somatic stress. *Scandinavian Journal of Rehabilitative Medicine* 2:92-98.

[23] Borsotto M, Savell C, Reifman J, Hoyt R, Nunns G, and Crick C (2004) Life-Signs Determination Model for Warfighter Physiological Status Monitoring. NATO Tech. Rept: RTO-MP-HFM-109.

[24] Bouchama A and Knochel JP (2002) Heat Stroke. *N Engl J Med* 346(25):1978-1988.

[25] Braur A, Weyland W, Fritz U, Schuhmann MU, Schmidt JH, and Braun U (1997) Determination of core body temperature. A comparison of esophageal, bladder, and rectal temperature during postoperative rewarming. *Anaesthesist* 46(8):683-688.

[26] Brouha L (1960) Physiology in industry. Ney York: Pergamon Press.

[27] Buller MJ, Hoyt RW, Ames J, Latzka W, Freund B (2005) Enhancing Warfighter Readiness Through Physiologic Situational Awareness – The Warfighter Physiological Status Monitoring – Initial Capability. In *Proceedings of the 11th Conference on Human Computer Interaction*, Las Vegas 2005 (Augmented Cognition).

[28] Buller MJ, Hebert NJ, Tharion WJ, Hoyt RW (2007) Demonstration of Real-Time Physiological Status Monitoring of Encapsulated 1st Civil Support Team-Weapons of Mass Destruction (CST-WMD) Personnel. USARIEM Technical Report No.: T08-01 (ADA473188). United States Army Research Institute of Environmental Medicine. Natick, MA.

[29] Buller MJ, Latzka WA, Yokota M, Tharion WJ, and Moran DS (2008) A real time heat strain risk classifier using heart rate and skin temperature. *Physiological Measurement* 29(12):N79-N85.

[30] Buller MJ, Wallis DC, Karis AJ, Hebert NJ, Cadarette BS, Blanchard LA, Amin MM, DiFilippo JL, Economos D, Hoyt RW, Richter MW (2009) Thermal-work strain during Marine rifle squad operations in Iraq (summer 2008). Technical Report No.: T09-01 (AD B345494). United States Army Research Institute of Environmental Medicine. Natick, MA.

[31] Buller MJ, Tharion WJ, Hoyt RW, and Jenkins OC (2010) Estimation of human internal temperature from wearable physiological sensors. In *Proceedings of the 22nd Conference on Innovative Applications of Artificial Intelligence (IAAI 2010).* 1763-1768.

[32] Buller MJ, Welles AP, Stower J, Desantis C, Margolis L, Karis AJ, Economos D, Hoyt RW, Richter MW (2011) Thermal-work strain during Marine rifle squad operations in Afghanistan (March 2010). Technical Report No.: T11-02 (AD A501301). United States Army Research Institute of Environmental Medicine. Natick, MA.

[33] Buller MJ, Castellani J, Roberts WS, Hoyt RW, and Jenkins OC (2011) Human thermoregulatory system state estimation using non-invasive physiological sensors. In *Conf. Proc. IEEE Eng. Med. Biol. Soc.* 3290-3293.

[34] Buller MJ (2013) Estimation of Human Core Temperature based on Heart Rate System and Method. U.S. Patent Application #14/107920. December 16, 2013.

[35] Buller MJ, Tharion WJ, Cheuvront SN, Montain SJ, Kenefick RW, Castellani J, Latzka WA, Roberts WS, Richter M, Hoyt RW, and Jenkins OC (2013) Estimation of human core temperature from sequential heart rate observations. *Physiological Measurement* 34:781-798.

[36] Buller MJ, Sodomka E, Tharion W, Clements C, Hoyt RW, and Jenkins OC (2013b) Policies to Optimize Work Performance and Thermal Safety in Exercising Humans. In

Proceedings of the 25th Conference on Innovative Applications of Artificial Intelligence (IAAI 2013). 1501-1506.

[37] Burton AC (1935) Human calorimetry. II. The average temperature of the tissue of the body. *J Nutr* 9:261-280.

[38] Byrne C, Lim CL (2007) The ingestible telemetric body core temperature sensor: a review of validity and exercise applications. *Br J Sports Med* 41:126-133.

[39] Carter R, Cheuvront SN, Williams JO, Kolka MA, Stephenson LA, Sawka MN, Amoroso PJ (2005) Epidemiology of hospitalizations and deaths from heat illness in soldiers. *Med Sci Sports Exerc* 37(8): 1338-1344.

[40] Chan APC, Yi W, Wong DP, Yam MCH, Chan DWM (2012) Determining an optimal recovery time for construction rebar workers after working to exhaustion in a hot and humid environment. *Building and Environment* 58:163-171.

[41] Chen KY (2003) The Use of Portable Accelerometers in Predicting Activity Energy Expenditure, Presented at the Institute of Medicine, Committee on Metabolic Monitoring Technologies for Military Field Applications Workshop on Metabolic Monitoring Technologies for Military Field Applications, San Antonio, Texas, USA, Jan. 8-9 (2003).

[42] Chen KY and Bassett DR (2005) The Technology of Accelerometry-Based Activity Monitors: Current and Future. *Med Sci Sports Exerc* 37(11 Suppl): S490-500.

[43] Chertow DS, Kleine C, Edwards JK, Scaini R, Guiliani R, and Sprecher A (2014) Ebola virus disease in west Africa – clinical manifestations and management. *New England Journal of Medicine* 371(22): 2054-57.

[44] Cheung SS (2007) Hyperthermia and voluntary exhaustion: integrating models and future challenges. *Appl Physiol Nutr Metab* 32(2): 808-817.

[45] Cheuvront SN, Haymes EM (2001). Thermoregulation and marathon running: biological and environmental influences. *Sports Med* 31:743-762.

[46] Cheuvront SN, Montain SJ, Goodman DA, Blanchard L, and Sawka MN (2007) Evaluation of the limits to accurate sweat loss prediction during prolonged exercise. *Eur J Appl Physiol* 101(2): 215-224.

[47] Cheuvront SN, Kenefick RW, Montain SJ, and Sawka MN (2010) Mechanisms of aerobic performance impairment with heat stress and dehydration. *J Appl Physiol* 109:1989-1995.

[48] Cheuvront SN (2014) Match maker: How to compare thermoregulatory responses in groups of different body mass and surface area. *J Appl Physiol* 116(9): 1121-1122.

[49] Chi-Wai RK, So-Ning TM, Wing-Kuen KL, Sai-Chuen SH, Ka-Shun PW, and Choi-Ki CW (2011) Can Mobile Virtual Fitness Apps Replace Human Fitness Trainer? In *5th*

International Conference on New Trends in Information Science and Service Science. 56-63.

[50] Clark RP, Mullan BJ, Pugh LGCE, Toy N (1974) Proceedings: heat losses from the moving limbs in running – the pendulum' effect. *J. Physiol.* 240:8P-9P.

[51] Clements C, Buller M, Welles A, Stower J, Desantis C, Richter M, Economous D, and Tharion W (2011) Practical real time assessment of human thermal-work strain. In the 2nd International Congress on Soldiers' Physical Performance, May 4-7, 2011.

[52] Committee on Metabolic Monitoring for Military Field Applications (2004) Rationale for Military interest and Current Capabilities in Monitoring Metabolism. In [National Academies of Science, Monitoring Metabolic Status – Predicting Decrements in Physiology and Cognitive Performance] The National Academies Press, Washington, D.C., Chapter 1, 15-36.

[53] Consolazio CF, Johnson RE, and Pecora LJ (1963) Physiological variability in young men. In Physiological measurements of metabolic functions edited by Consolazio CF, Johnson RE, and Pecora LJ. McGraw Hill, New York, NY, pp 453-480.

[54] Convertino VA, Buller MJ, Van Albert S, and Freund BJ (2010) Physiological Monitoring Combat Casualty Care, Chapter 3-6 in Real-Time Physiological and Psycho-Physiological Status Monitoring. NATO Research and Technology Organization Report: RTO-TR-HFM-132, 77-86, March (2010). Available at: http://www.rta.nato.int/Pubs/RDP.asp?RDP=RTO-TR-HFM-132.

[55] Cox ML, Bennett JB, and Dudley GA (1986) Exercise training-induced alterations of cardiac morphology. *J Appl Physiol* 61(3):926-931.

[56] Coyle EF, Hagberg JM, Hurley BF, Martin WH, Ehsani AA, Holloszy JO (1983) Carbohydrate feeding during prolonged strenuous exercise can delay fatigue. *J Appl Physiol* 55:230-235.

[57] Cramer MN and Jay O. (2014) Selecting the correct exercise intensity for unbiased comparisons of thermoregulatory responses between groups of different mass and surface area. *J Appl Physiol* 116:1123-1132.

[58] Cuddy JS, Buller MJ, Hailes WS, and Ruby BC (2013) Skin temperature and heart rate can be used to estimate physiological strain during exercise in the heat in a cohort of fit and unfit males. *Military Medicine* 178(7):e841-e847.

[59] Cuddy JS, Hailes WS, and Ruby BC (2014) A reduced core to skin temperature gradient, not a critical core temperature, affects aerobic capacity in the heat. *Journal of Thermal Biology* 43:7-12.

[60] Dadashi F, Arami A, Cretten and F, Millet GP, Komar J, Seifert L, and Aminian K (2013) A Hidden Markov Model of the Breaststroke Swimming Temporal Phases Using Wearable Inertial Measurement Units. In *Proceedings of 10th IEEE Body Sensor Networks Conference*.

[61] Dannecker KL, Sazonova NA, Melanson EL, Sazonov ES, and Browning RC (2013) A comparison of energy expenditure estimation of several physical activity monitors. *Medicine and Science in Sports and Exercise* 45(11):2105-2112.

[62] Dempster AP, Laird NM, and Rubin DB (1977) Maximum likelihood from incomplete data via the EM algorithm. *Journal of the Royal Statistical Society Series B (Methodological)* 39(1):1:38.

[63] DeGroot DW, Goodman DA, Montain SJ, and Cheuvront, SN (2008) Validation of the ICDA Model for Predicting Body Core Temperature. *Medicine & Science in Sports & Exercise* 40(5): S367 (Abstract).

[64] De Konig JJ, Foster C, Bakkum A, Kloppenburg S, Thiel C, Joseph T, Cohen J, and Porcari JP (2011) Regulation of pacing strategy during athletic competition. *Plos ONE* 6(1)e15863.

[65] Department of the Army (2006) *Army Regulation 600-9, The Army Weight Control Program*. Washington, D.C. Headquarters Department of the Army.

[66] Dible JH (1970) Napoleon’s Surgeon. William Heinemann Medical Books Ltd, London.

[67] DiRienzo M, Rizzo F, Merrigi P, Castiglioni P, Mazzoleni P, Ferrarin M, and Ferratini M, (2007) MagIC: a Textile System for Vital Signs Monitoring. Advancement in Design and Embedded Intelligence for Daily Life Applications, Conf. Proc. IEEE Med. Biol. Soc. 2007, 3958-61.

[68] Dodd SR, Lancaster GA, Craig JV, Smyth RL, and Williamson PR (2006) In a systematic review, infrared ear thermometry for fever diagnosis in children finds poor sensitivity. *J Clin Epidemiol* 59(4):354-7.

[69] Du Bois D, Du Bois EF (1916) A formula to estimate the approximate surface area if height and weight be known. *Archives of Internal Medicine* 17 (6): 863–71.

[70] Du Bois EF (1948) Fever. Charles C. Thomas, Springfield IL.

[71] Durnin JV and Womersley J (1974) Body fat assessed from total body density and its estimation from skin fold thickness: measurements on 481 men and women aged from 16 to 72 years. *British Journal of Nutrition* 32:77-79, 1974.

[72] Ely BR, Ely MR, Cheuvront SN, Kenefick RW, DeGroot DW, and Montain SJ (2009) Evidence against a 40 °C core temperature threshold for fatigue in humans. *J Appl Physiol* 107:1519-1525.

[73] Ely BR, Cheuvront SN, Kenefick RW, and Sawka MN (2010) Aerobic performance is degraded, despite modest hyperthermia, in hot environments. *Med Sci Sports Exerc* 42(1):135-141.

[74] Epstein Y, Roberts WO, Golan R, Heled Y, Sorkine P, and Halpern P (2015) Sepsis, septic shock, and fatal exertional heat stroke. *Curr Sports Med Rep* 14(1):64-69.

[75] Fahy RF and LeBlanc PR (2006) Firefighter fatalities in the United States – 2005. Fire Analysis and Research Division National Fire Protection Association, Quincy MA.

[76] Fahy RF (2012) U.S. Firefighter Deaths Related to Training, 2001 – 2010. National Fire Protection Association, Quincy, MA.

[77] Fahy RF, LeBlanc PR, and Molis JL (2013) Firefighter Fatalities in the United States – 2012. National Fire Protection Association, Quincy, MA.

[78] Fanger PO (1970) Thermal Comfort. Danish Technical Press, Copenhagen.

[79] Fanger PO (1982) Thermal Comfort. Robert E. Krieger Publishing Company, Malabar, FL.

[80] Fiala D, Lomas KJ, Stohrer M (2001) Computer prediction of human thermoregulatory and temperature responses to a wide range of environmental conditions. *Int J Biometeorol* 45:143-59.

[81] Fick A (1855) On Liquid Diffusion. *The London, Edinburgh, and Dublin Philosophical Magazine and Journal of Science*. 10 – Fourth Series (July-September): 30-39.

[82] Frank A, Belokopytov M, Shapiro Y, and Epstein Y (2001) The cumulative heat strain index – a novel approach to assess the physiological strain induced by exercise heat stress. *Eur J Appl Physiol* 84: 527-532.

[83] Fox RH, Solman AJ, Isaacs R, Fry AJ, and MacDonald IC (1973) A new method for monitoring deep body temperature from the skin surface. *Clin Sci* 44:81-6.

[84] Frank A, Moran D, Epstein Y, Belokopytov M, and Shapiro Y (1996) The estimation of heat tolerance by a new cumulative strain index. In *Environmental Ergonomics: Recent Progress and New Frontiers,* Shapiro Y, Moran D, and Epstein Y (eds.). Freund, London. pp194-197.

[85] Frank A, Belokopytov M, Shapiro Y, Epstein Y (2001) The cumulative heat strain index – a novel approach to assess the physiological strain induced by exercise heat stress. *Eur J Appl Physiol* 84: 527-532.

[86] Fuller FH and Smith PE (1980) The effectiveness of preventive work practices in a hot work shop. In: Dukes-Dobos FN, Henshcel A, eds. Proceedings of a NIOSH workshop on recommended heat stress standards. Cincinnati: U.S. Department of Health and Human

Services, Public Health Service, Centers for Disease Control National Institute for Occupational Safety and Health. Publication Number 81-108:32-45.

[87] Fuller FH and Smith PE (1981) Evaluation of heat stress in a hot workshop by physiological measurements. *Am Ind Hyg Assoc J* 42:32-7.

[88] Gagge AP, Stolwijk JA, Saltin B (1969) Comfort and thermal sensations and associated physiological responses during exercise at various ambient temperatures. *Environ Res* 2:209-229.

[89] Gagnon D and Kenny GP (2012) Does sex have an independent effect on thermoeffector responses during exercise in the heat? *J Physiol* 590:5963-5973.

[90] Ghahramani Z and Hinton GE (1996) Parameter estimation for linear dynamical systems. Technical Report CRG-TR-96-1. University of Toronto.

[91] Givoni B and Goldman RF (1971) Predicting metabolic energy cost. *J Appl Physiol* 30(3):429-433.

[92] Givoni B and Goldman RF (1972) Predicting rectal temperature response to work, environment, and clothing. *J Appl Physiol* 32:812–22.

[93] Gonzalez-Alonzo J, Crandall CG, and Johnson JM (2008) The cardiovascular challenge of exercising in the heat. *J Physiol* 586(1):45-53.

[94] Gotshall RW, Dahl DJ, and Marcus NJ (2001) Evaluation of a Physiological Strain Index for use during intermittent exercise in the heat. Journal of Exercise Physiology 4(3):22-29.

[95] Grossman P (2004) The LifeShirt: A Multi-Function Ambulatory System Monitoring Health, Disease, and Medical Intervention in the Real World. *Stud Health Technol Inform* 108:133-141.

[96] Grubbs FE (1969) Procedures for Detecting Outlying Observations in Samples. *Technometrics* 11(1):1-21.

[97] Gunga HC, Sandsund M, Reinertsen RE, Sattler F, and Koch J (2008) A non-invasive device to continuously determine heat strain in humans. *J Thermal Biology* 33:297-307.

[98] Gunga HC, Werner A, Stahn A, Steinach M, Schlabs T, Koralewski E, Kunz D, Belavy´ DL, Felsenberg D, Sattler F, and Koch J (2009) The Double Sensor—A non-invasive device to continuously monitor core temperature in humans on earth and in space. *Respiratory Physiology & Neurobiology* 169S:S63–S68.

[99] Hall JE (2011) Body temperature regulation and fever. In: Guyton and Hall Textbook of Medical Physiology. Saunders/Elsevier. Philadelphia PA. Chapter 73: 867-877.

[100] Hall JF and Plote JW (1960) Physiological index of strain and body heat storage in hyperthermia. *J Appl Physiol* 15:1027-1030.

[101] Hatch TF (1963) Assessment of heat stress. In: *Temperature: Its Measurement and Control in Science and Industry*, Hardy JD (Ed.) Reinhold, New York pp:307-318.

[102] Havenith G (2001) Individualized model of human thermoregulation for the simulation of heat stress response. *J Appl Physiol* 90:1943-1954.

[103] Hilbel T, Helms TM, Mikus G, Katus HA, and Zugc C (2008) Telemetry in the clinical setting. *Herzschrittmachertherapie & Elektrophysiologie* 19(3):146–64.

[104] Hill OT, Leon L, and McKinnon C (2013) Heat Stroke in Active Duty US Army Soldiers 2000 -2007. Poster, USARIEM, Natick, MA.

[105] Hoey J, von Bertoldi A, Poupart P, and Mihailidis A (2007) Assisting persons with dementia during handwashing using a partially observable Markov decision process. Proceedings of the 5th Conference on Computer Vision Systems (ICVS 2007).

[106] Holmer I, Gavhed DCE, Grahn S, O'Nilsson H (1992) Effect of wind and body movements on clothing insulation – measurements with a moveable thermal manikin. In Proceedings of the 5th International Conference on Environmental Ergonomics.

[107] Horn GP, Blevins S, Fernhall B, and Smith DL (2013) Core temperature and heart rate response to repeated bouts of firefighting activities. *Ergonomics* 56(9):1465-73.

[108] Hoyt RW, Knapik JJ, Lanza JF, Jones BH, and Staab JS (1994) Ambulatory foot contact monitor to estimate metabolic cost of human locomotion. *J Appl Physiol* 76:1818-1822.

[109] Hoyt RW, Buller MJ, Redin MS, Poor RD, Oliver SR, Matthew MT, Latzka WA, Young AJ, Redmond D, and Kearns C (1997) Soldier Physiological Monitoring – Results of Dismounted Battlespace Battle Lab Concept Experimentation Program Field Study. Technical Report No.: T98-6 (AD A332713). United States Army Research Institute of Environmental Medicine. Natick, MA.

[110] Hoyt RW, Young AJ, Matthew WT, Kain JE, and Buller MJ (1997) Warfighter Physiological Status Monitoring (WPSM): Body Core Temperatures During 96 h of Swamp Phase Ranger Training. Technical Report (ADA323018). United States Army Research Institute of Environmental Medicine. Natick, MA.

[111] Hoyt RW, Buller MJ, DeLany JP, Stultz D, Warren K, Hamlet MP, Shantz D, Matthew WT, Tharion WJ, Smith P, and Smith B (2001) Warfighter physiological status monitoring (WPSM): energy balance and thermal status during a 10-day cold weather U.S. Marine Corps Infantry Officer Course field exercise. Technical Report No.: T02-02 (ADA396133). United States Army Research Institute of Environmental Medicine. Natick, MA.

[112] Hoyt RW, Buller MJ, Zdonik S, Kearns C, and Freund B (2002) Physio-Med Web: Real time monitoring of physiological strain index (PSI) of soldiers during an urban training operation. Defense Technical Information Center.

[113] Jazwinski RH (1970) Stochastic Processes and Filtering Theory. Academic Press, New York.

[114] Jarcho S (1967) A Roman experience with heatstroke in 24 B.C. *Bull NY Acad Med* 3:767.

[115] Kalman RE (1960) A new approach to linear filtering and prediction problems. *Journal of Basic Engineering* 82(1): 35–45.

[116] Kark JA, Burr PQ, Wenger CB, Gastaldo E, and Gardner JW (1996) Exertional heat illness in Marine Corps recruit training. *Aviat Space Environ Med* 67(4): 354-360.

[117] Karlsson J and Saltin B (1971) Diet, muscle glycogen and endurance performance. *J Appl Physiol* 31:203-206.

[118] Karter MJ and Molis JL (2014) U.S. Firefighter Injuries—2013. National Fire Protection Association, Quincy, MA.

[119] Kaufman J and Coleman SM (2010) Method and Apparatus for Non-invasively Estimating Body Core Temperature. US Patent Publication. Number: US2010/0280331 A1.

[120] Kenefick RW, Cheuvront SN, Palombo LJ, Ely BR, and Sawka MN (2010) Skin temperature modifies the impact of hypohydration on aerobic performance. *J Appl Physiol* 109:79-86.

[121] Kenefick RW, Cheuvront SN, Ely BR, Palombo LJ, and Sawka MN (2011) DEET insect repellent: effects on thermoregulatory sweating and physiological strain. *Eur J Appl Physiol* 111(12):3061-3068.

[122] Knechtle B, Rust CA, Roseman T, and Martin N (2014) 33 Ironman triathlons in 33 days-a case study. *SpringerPlus* 3:269.

[123] Kolka MA, Quigley MD, Blanchard LA, Toyota DA, and Stephenson LA (1993) Validation of a temperature telemetry system during moderate and strenuous exercise. *J Thermal Biology* 18(4): 203-210.

[124] Kraning KK and Gonzalez RR (1997) A mechanistic computer simulation of human work in heat that accounts for physical and physiological effects of clothing, aerobic fitness, and progressive dehydration. *J Therm Biol* 22(4/5): 331-342.

[125] Lamb KL, Eston RG, and Corns D (1999) Reliability of ratings of perceived exertion during progressive treadmill exercise. *Br J Sports Med* 33(5): 336-339.

[126] Langridge P, Ruzic A, Larsen B, Lord C, and Aisbett B (2012) Assessing the validity of tympanic temperature to predict core temperature of firefighters in different environmental

conditions. Proceedings of Bushfire CRC & AFAC 2012 Conference and Research Forum. Bushfire CRC Perth, Australia.

[127] Laursen PB, Watson G, Abbiss CR, Wall BA, and Nosaka K (2009) Hyperthermic fatigue precedes a rapid reduction in serum sodium in an ironman triathlete: a case report. *Int J Sports Physiol Perf* 4:533-537.

[128] Latzka WA, Sawka MN, Montain SJ, Skrinar GS, Fielding RA, Matott RP, and Pandolf KB (1997) Hyperhydration: thermoregulatory effects during compensable exercise-heat stress. *J Appl Physiol* 83(3): 860-866.

[129] Latzka WA, Sawka MN, Montain SJ, Skrinar GS, Fielding RA, Matott RP, and Pandolf KB (1998) Hyperhydration: tolerance and cardiovascular effects during uncompensable exercise-heat stress. *J Appl Physiol* 84: 1858 –1864.

[130] Lee JK, Nio AQ, Lim CL, Teo EY, and Byrne C (2010) Thermoregulation, pacing and fluid balance during mass participation distance running in a warm humid environment. *Eur J Appl Physiol* 107(5):1519-25.

[131] Lee SMC, Williams WJ and Schneider SM (2000) Core temperature measurement during submaximal exercise: esophageal, rectal, and intestinal temperatures. NASA Center for Aerospace Information Technical Report NASA/TP-2000-210133.

[132] Lefrant JY, Muller L, Coussaye JE, Benbabaali M, Lebris C, Zeitoun N, Mari C, Saissi G, Ripart J, and Eledjam JJ (2003) Temperature measurement in intensive care patients: comparison of urinary bladder, esophageal, rectal, axillary, and inguinal methods versus pulmonary artery core method. *Intensive Care Med* 29:414-418.

[133] Lee DHK (1980) Seventy-five years of search for a heat index. *Environ Res* 22:331-356.

[134] Lim CL, Byrne C, and Lee JKW (2008) Human thermoregulation and measurement of body temperature in exercise and clinical settings. *Annals Academy of Medicine* 37:347-35.

[135] Lindsay P (1936) Kings of Merry England. Ivor Nicholson and Watson Ltd, London.

[136] Long LL and Srinivasan M (2013) Walking, running, and resting under time, distance, and average speed constraints: optimality of walk-run-rest mixtures. *J R Soc Interface* 10:20120980.

[137] Lopez-Matencio P, Alonso J V, Gonzalez-Castano FJ, Sieiro JL, and Alcaraz JJ (2010) Ambient intelligence assistant for running sports based on k-NN classifiers. IEEE 3rd Conference on Human Systems Interactions. 605-611.

[138] Lui B, Cuddy JS, Hailes WS, and Ruby BC (2014) Seasonal heat acclimatization in wildland firefighters. *Journal of Thermal Biology* 45:134-140.

[139] Lurpano J, Sola J, Dasen S, Koller JM, and Chetelat O (2006) Combination of Body Sensor Networks and On-Body Signal Processing Algorithms: the practical case of MyHeart Project, Proc. Int. Workshop on Wearable and Implantable Body Sensor Networks, BSN'06.

[140] McCarthy PW and Heusch AI (2006) The vagaries of ear temperature assessment. *J Med Eng Technol* 30(4):242-51.

[141] McCullom B and Peters OS (1924) A New Electric Telemeter. Technology Papers, National Bureau of Standards No. 247, Vol. 17, January 4, 1924.

[142] McLean JA and Tobin G (1987) Animal and Human Calorimetry. Cambridge University Press, New York.

[143] McNair LM and Droppleman LF (1992) Profile of Mood States Manual. Educational and Industrial Testing Service, San Diego, CA.

[144] Minard D (1961) Prevention of heat casualties in Marine Corps recruits. *Military Medicine* 126: 261-272.

[145] Montain SJ and Coyle EF (1992) Influence of graded dehydration on hyperthermia and cardiovascular drift during exercise. *J Appl Physiol* 73(4): 1340-1350.

[146] Montoye HJ, Kemper HCG, Saris WHM, and Washburn RA (1996) Doubly Labeled Water. In: Measuring Physical Activity and Energy Expenditure. Human Kinetics, Champaign, IL.

[147] Moran DS, Shitzer A, and Pandolf KB (1998) A physiological strain index to evaluate heat stress. *Am J Physiol Regulatory Integrative Comp Physiol* 275:129-134.

[148] Moran DS, Montain SJ, and Pandolf KB (1998) Evaluation of different levels of hydration using a new physiological strain index. *Am J Physiol* 275(3 Pt 2):R854-60.

[149] Moran DS, Shapiro Y, Laor A, Izrael S, and Pandolf KB (1999) Can gender differences during exercise-heat stress be assessed by the physiological strain index? *Am J Physiol* 276(6 pt 2):R1798-R1804.

[150] Moran DS (2000) Stress evaluation by the physiological strain index (PSI). *J Basic Clin Physio Pharmacol* 11(4) 403-23.

[151] Moukabary T (2007) Williem Einthoven (1860-1927): Father of electrocardiography. *Cardiology Journal* 14(3), 316-317.

[152] MSMR (2013) Update: heat injuries, active component, U.S. Armed Forces 2012. MSMR 20(3):17-20.

[153] Murphy KP (2002) Dynamic Bayesian Networks: Representation, Inference and Learning. PhD. Thesis. University of California Berkeley.

[154] Muza SR, Banderet LE, and Cadarette B (2001) Protective uniforms for nuclear, biological and chemical warfare. In Medical Aspects of Harsh Environments eds. K B Pandolf and R E Burr. Office of the Surgeon General, United States Army, Falls Church, VA. Chapter 36, pp1084-1127.

[155] National Guard (2006) "Medical Monitoring Telemetry System." Weapons of Mass Destruction – Civil Support Team. National Working Group Requirement.

[156] Niederman R, Wyss E, Annaheim S, Psikuta A, Davey S, and Rossi RM (2014) Prediction of human core body temperature using non-invasive measurement methods. *Int J Biometeorol* 58:7-15.

[157] Nielsen B (1969) Thermoregulation in rest and exercise. *Acta Physiol Scand Suppl* 323:1-74.

[158] Nielsen B, Hyldig T, and Bidstrup F (2001) Brain activity and fatigue during prolonged exercise in the heat. *Pflugers Arch* 442:41-48.

[159] NIOSH (1986) Occupational Exposure to Hot Environments. National Institute for Occupational Safety and Health, Washington, DC.

[160] O'Brien C, Hoyt RW, Buller MJ, Castellani JW, and Young AJ (1998) Telemetry pill measurement of core temperature in humans during active heating and cooling. *Med Sci Sports Exer* 30, 468-472.

[161] Osais Y, Yu RF, and St-Hilaire M (2010) Optimal management of rechargeable biosensors in temperature-sensitive environments. IEEE 72nd Vehicular Technology Conference Fall (VTC 2010-Fall).

[162] OSHA. 1985. Occupational Safety and Health Guidance Manual for Hazardous Waste Site Activities. Occupational Safety and Health Administration, Washington DC. 8-37 - 8-39.

[163] Pandian PS, Mohanavelu K, Safeer KP, Kotresh TM, Shakunthala DT, Gopal P, Padaki VC (2008) Smart Vest: Wearable multi-parameter remote physiological monitoring system. *Med Eng & Physics* 30:466-477.

[164] Pandolf, KB, Givoni B, and Goldman RF (1977) Predicting energy expenditure while standing and walking very slowly. *J Appl Physiol* 43(4):577-581.

[165] Pandolf KB and Goldman RF (1978) Convergence of Skin and Rectal Temperature as a criterion for heat tolerance. *Aviat Space Environ Med* 49(9):1095-1101.

[166] Pantolopoulos A and Bourbakis N (2008) A Survey on Wearable Biosensor Systems for Health Monitoring. In 30th Annual International IEEE Engineering in Medicine and Biology Society (EMBS) Conference. 4887-4890.

[167] Paradiso R, Loriga G, Taccini N, Gemignani A, Ghelarducci B (2005) WEALTHY—a wearable healthcare system: new frontier on e-textile. *J Telecom Inform Tech*, April, 105-113.

[168] Parkes EA (1864) Manual of Practical Hygiene. John Churchill and Sons, London.

[169] Paroczai R and Kocsis L (2006) Analysis of human walking and running parameters as a function of speed. *Technology and Health Care* 14:251-260.

[170] Penders J, Gyselinckx B, Vullers R, Rousseaux O, Berekovic M, De Nil M, Van Hoof C, Ryckaert J, Yazicioglu RF, Fiorini P, and Leonov V (2007) HUMAN++: Emerging Technology for Body Area Networks. In IFIP International Federation for Information Processing, Volume 249, VLSI-SoC: Research Trends in VLSI and Systems on Chip, eds. De Micheli G, Mir S, Reis R, (Boston: Springer), pp. 377-397.

[171] Porter AMW (2000) The death of a British officer-cadet from heat illness. *Lancet* 355: 569-571.

[172] Potter AW, Santee WR, Clements CM, Brooks KA, and Hoyt RW (2013) Comparative Analysis of Metabolic Cost Equations: A Review. *Journal of Sport and Human Performance* 1(3):34-42.

[173] Qian X and Fan J (2006) Prediction of clothing thermal insulation and moisture vapour resistance of the clothed body walking in wind. *Ann Occup Hyg* 1–10.

[174] Rabiner LR (1989) A tutorial on Hidden Markov Models and Selected Applications in Speech Recognition. *Proceedings of the IEEE* 77(2) 257-286.

[175] Rauch HE, Tung F, and Striebel CT (1965) Maximum likelihood estimates of linear dynamical systems. *AIAA Journal* 3:1445-1450.

[176] Redin SM (1998) Marathon Man. Master Thesis, Department of Electrical Engineering and Computer Science, Media Laboratory, Massachusetts Institute of Technology.

[177] Roberts I and Perner A (2014) Ebola virus disease: clinical care and patient centered research. The *Lancet* 384(9959): 2001-2002.

[178] Robinson S, Robinson DL, Mountjoy RJ, and Bullard RW (1958) Influence of fatigue on the efficacy of men during exhausting runs. *J Appl Physiol* 12(2):197-201.

[179] Robison S, Turrell ES, and Gerking SD (1945) Physiological equivalent conditions of air temperature and humidity. *Am J of Physiol* 143:21-32.

[180] Roelands B, Koning J, Foster C, Hettinga F, and Meesusen R (2013) Neurophysiological Determinants of Theoretical Concepts and Mechanisms Involved in Pacing. *Sports Med* 43:301-311.

[181] Roijers DM, Vamplew P, Whiteson S, Dazeley R (2013) A survey of multi-objective sequential decision-making. *Journal of Artificial Intelligence Research.* 48:67-113.

[182] Romanovsky AA (2007) Thermoregulation: some concepts have changed. Functional architecture of the thermoregulatory system. *American Journal of Physiology: Regulatory, Integrative and Comparative Physiology*. 292:R37-R46.

[183] Rowell LB, Murray JA, Brengelmann GL, and Kraning KK (1969) Human cardiovascular adjustments to rapid changes in skin temperature during exercise. *Circulation Research* 24:711-724.

[184] Rowell LB (1983) Cardiovascular aspects of human thermoregulation. *Circ Res* 52:367-79.

[185] Rowell LB (1986) Human Circulation: Regulation During Physical Stress. Oxford University, New York.

[186] Russell S and Norvig P (2010) Artificial Intelligence A Modern Approach (Third Edition). Prentice Hall, New York NY.

[187] Santee WR and Matthew WT (2012) Evaluation of the thermal environment. In: Friedl KE and Santee WR (Eds). Military Quantitative Physiology: Problems and Concepts in Military Operational Medicine. Borden Institute, Fort Detrick MD. Pp 205-230.

[188] Satava R, Angood PB, Harnett B, Macedonia C, and Merrell R (2000) The Physiological Cipher at Altitude: Telemedicine and Real-Time Monitoring of Climbers on Mount Everest. *Telemedicine Journal and e-Health* 6(3), 303-313.

[189] Sawka MN and Pandolf KB (2002) Physical Exercise in Hot Climates: Physiology, Performance, and Biomedical Issues. In: Pandolf KB and Burr RE (Eds.) Textbooks of Military medicine, Vol. 1. US Army Research Institute of Environment Medicine, Natick, MA, Chapter 3, 3-49.

[190] Sawka MN and Young A J (2006) Physiological systems and their responses to conditions of heat and cold. In: Tipton CM (ed). Advanced Exercise Physiology, American College of Sports Medicine. Lipcot, Williams & Wilkins. New York, NY pp535-63.

[191] Schickele E (1947) Environment and fatal heat stroke. *Military Surgeon* 100:235-256.

[192] Schnayder V, Chen B, Lorincz K, Fulford-Jones TRF, Welsh M (2005) Sensor Networks for Medical Care. Technical Report TR-08-05, Division of Engineering and Applied Sciences, Harvard University. Cambridge, MA.

[193] Sengul G and Baysal U (2012) An extended Kalman filtering approach for the estimation of human head tissue conductivities by using EEG data: a simulation study. *Physiological Measurement* 33: 571-586.

[194] Shaffrath JD and Adams WC (1984) Effects of airflow and work load on cardiovascular drift and skin blood flow. *J Appl Physiol: Respirat Environ Exercise Physiol* 56(5):1411-1417.

[195] Shumway RH, and Stoffer DS (1982) An approach to time series smoothing and forecasting using the EM algorithm. *Journal of Time Series Analysis* 3:253-264.

[196] Smith D L, Manning T S, and Petruzzello S J (2001) Effect of strenuous live-fire drills on cardiovascular and psychological responses of recruit fire fighters. *Ergonomics* 44(3) 244 – 254.

[197] Soule RG, Pandolf KB, Goldman RF (1978) Voluntary march rate as a measure of work output in the heat. *Ergonomics* 21(6): 455-462.

[198] Stacey M, Woods D, Ross D, and Wilson D (2014) Heat illness in military populations: asking the right questions for research. *J R Army Med Corps* 160(2):121-124.

[199] St. Clair-Gibson A and Noakes TD (2004) Evidence for complex system integration and dynamic neural regulation of skeletal muscle recruitment during exercise in humans. *Br J Sports Med* 38:797-806.

[200] Steck LN, Sparrow EM, and Abraham JP (2011) Non-invasive measurement of the human core temperature. *International Journal of Heat and Mass Transfer* 54:975-982.

[201] Steinman AM (1987) Adverse effects of heat and cold on military operations: history and current solutions. *Military Medicine* 152:389-392.

[202] Stubblefield Z, Cleary M, Garvey S, and Eberman (2006) Effects of active hyperthermia on cognitive performance. Proceedings of the Fifth Annual College of Education Research Conference: Section on Allied Health Professionals, vol. 1:25-50.

[203] Sun G, Li L, Li M, and Jiang Q (2011) Hyperthermia impaired pre-attentive processing: an auditory MMN study. *Neuroscience Letters* 502:94-98.

[204] Sutton RS and Barto AG (1998) Reinforcement Learning – An Introduction. MIT Press Cambridge, MA.

[205] Tatbul N, Buller MJ, Hoyt RW, Mullen SP, and Zdonik S (2004) Confidence-based data management for personal area sensor networks. Proceedings of the First Workshop on Data Management of Sensors Networks (DMSN). Toronto, Canada, Aug.

[206] Taylor NAS and Amos D (1997) Insulated Skin Temperature and Cardiac Frequency as Indices of Thermal Strain during Work in Hot Environments. Tech Report No.: DSTO-TR-0590. Aeronautical and Maritime Research Laboratory, Melbourne, Victoria, Australia. pp 150-159.

[207] TBMED 507 (2003) Heat Stress Control and Heat Casualty Management. Department of the Army and Technical Bulletin. Washington DC.

[208] Teunissen LPJ, Klewer J, de Haan A, de Konig JJ, and Daanen HAM (2011) Non-invasive continuous core temperature measurement by zero heat flux. *Physiological Measurement* 32:559-570.

[209] Teunissen LPJ, de Haan A, de Koning JJ, Clairbois HE, and Daanen HAM (2011) Limitations of temperature measurement in the aural canal with an ear mould integrated sensor. *Physiological Measurement* 32: 1403-1416.

[210] Tharion WJ, Shukitt-Hale B, Coffey B, Desai M, Stroman SR, Tulley R, and Lieberman HR (1997) The use of caffeine to enhance cognitive performance reaction time, vigilance, rifle marksmanship, and mood states in sleep deprived Navy SEAL (BUD/S) trainees. Technical Report T89-4 (AD331982). United States Army Research Institute of Environmental Medicine. Natick, MA.

[211] Tharion WJ, Buller MJ, Karis AJ, and Mullen SP (2007) Accountability of a wearable vital signs detection system. Proceedings of the Human Factors and Ergonomics Society 51st Annual Meeting, Santa Monica, CA, 51:1006-1010.

[212] Tharion WJ, Buller MJ, Potter AW, Goetz V, and Hoyt RW (2013a) Acceptability and usability of an ambulatory health monitoring system for use by military personnel. *IIE Transactions on Occupational Ergonomics and Human Factors* 1:203-214.

[213] Tharion WJ, Potter AW, Duhamel CM, Karis AJ, Buller MJ, and Hoyt RW (2013b) Real-time physiological monitoring while encapsulated in personal protective equipment. *J Sport Human Perf* 1(4):14-21.

[214] Toussaint M (2009) Probabilistic inference as a model of planned behavior. *Kunstliche Intelligenz* 3(9):23-29.

[215] Tucker R (2009) The anticipatory regulation of performance: the physiological basis for pacing strategies and the development of a perception-based model of exercise performance. *Br J of Sports Med* 43:392-400.

[216] Ulmer HV (1996) Concept of an extracellular regulation of muscular metabolic rate during heavy exercise in humans by physiological feedback. *Experientia* 52: 416-420.

[217] Waldron M and Highton J (2014) Fatigue and pacing in high-intensity intermittent team sport: an update. *Sports Med* 44(12):1645-1658.

[218] Walter PL (2007) The History of the Accelerometer: 1920s-1996—Prologue and Epilogue, 2006, *Sound & Vibration* 41(11), 84-90.

[219] Welch G and Bishop G (1995) An introduction to the Kalman filter, Technical Report, TR No.: 95-041, Department of Computer Science, University of North Carolina at Chapel Hill.

[220] Welk GJ (2002) Use of accelerometry-based activity monitors to assess physical activity, in Welk, GJ, ed., Physical Activity Assessments for Health-Related Research, Human Kinetics, Champaign, IL, pp. 125-141.

[221] Welk GJ, McClain JJ, Eisenmann JC, and Wickel EE (2007) Field validation of the MTI Actigraph and BodyMedia armband monitor using the IDEEA monitor. *Obesity* 15(4):918-928.

[222] Weyand PG, Smith BR, Schultz NS, Wohlers LM, Puyau MR, and Butte NF (2013) Predicting metabolic rate across walking speed: one fit for all body sizes? *Journal of Applied Physiology* 115(9): 1332-1342.

[223] Wilkinson DM, Carter JM, Richmond VL, Blacker SD and Rayson MP (2008) The effect of cool water ingestion on gastrointestinal pill temperature. *Med Sci Sports Exerc* 40(3): 523-528.

[224] Wilcox WH (1920) The nature, prevention, and treatment of heat hyperpyrexia. *Br Med J* 1:329.

[225] Wright HF and Wilmore JH (1974) Estimation of relative body fat and lean body weight in a United States Marine Corps population. *Aerospace Med* 45: 301-306.

[226] Xu X, Karis AJ, Buller MJ, and Santee WR (2013) Relationship between core temperature, and heat flux during exercise in heat. *European Journal of Applied Physiology*. 113:2381-9.

[227] Yaglou CP and Minard D (1956) Prevention of heat casualties at Marine Corps training centers. Technical Report No.: AD0099920. Harvard School of Public Health, Boston MA

[228] Yaglou CP and Minard D (1957) Control of heat casualties at military training centers. *AMA Archives of Industrial Health* 16(4):302.

[229] Yamakage M, Iwasaki S, and Namiki A (2002) Evaluation of newly developed monitor of deep body temperature. *J Anesth* 16:354-357.

[230] Yokota M, Tharion WJ, Buller MJ, and Hoyt RW (2002) Application of the Physiological Strain Index (PSI) for Evaluation of Simulated Military Activities. Natick, MA. Technical Report No.: M03/15 (ADA408496). United States Army Research Institute of Environmental Medicine. Natick, MA.

[231] Yokota M, Moran DS, Berglund LG, Stephenson LA, and Kolka MA (2005) Noninvasive warning indicator of the "Red Zone" of potential thermal injury and performance

impairment: A pilot study. Proceedings for the 11th International Conference of Environmental Ergonomics. Sweden, Lund University, 514-517.

[232] Yokota M, Berglund L, Cheuvront S, Santee W, Latzka W, Montain S, Kolka M, and Moran D (2008) Thermoregulatory model to predict physiological status from ambient environment and heart rate. *Computers in Biology and Medicine* 38:1187-1193.

[233] Yokota M, Berglund LG, Santee WR, Buller MJ, Karis AJ, Roberts WS, Cuddy JS, Ruby BC, Hoyt RW (2012) Applications of real-time thermoregulatory models to occupational heat stress: validation with military and civilian field studies. *Journal of Strength & Conditioning Research* 26: S37-S44.

[234] Young AJ, Sawka MN Epstein Y, De Ristofano B, and Pandolf KB (1987) Cooling different body surfaces during upper and lower body exercises. *Journal of Applied Physiology* 63: 1218-1223.

[235] Zuntz N, Loewy A, Muller F, and Caspari W (1906) Hohenklima und Bergwanderungen. Deutsches Verlagshaus, Berlin.

[236] Zywietz C (2003) A Brief History of Electrocardiography – Progress through Technology, Biosignal Institute for Biosignal Processing and Systems Research, Hannover, Germany.

Appendix A: Modern Physiological Monitoring Devices

Table A.1: Modern physiological monitoring devices from a market survey by Massachusetts Lincoln Laboratory, under contract to the United States Army Medical Material Development Agency (USAMMDA) Medical Support Systems (MSS) Program Management Office (PMO). Used by permission. Where HR = Heart Rate, BR = Breathing Rate, ST = Skin Temperature, and AC = Accelerometry.

Company	Device	Location	Cost	Life	HR	BR	ST	AC	Other
Orbital		arm			y				
Adidas	miCoach	chest / shirt	$120		y				
AIQ	Bioman	chest / shirt			y				
Athos	Core	chest / shirt	$300	10 hrs.	y	y		y	EMG
Cityzen Sciences	D-shirt	chest / shirt			y				
Hexoskin		chest / shirt	$399	14+ hrs.	y	y		y	
OMSignal	Lifestyle	chest / shirt	$199	30 hrs.	y	y		y	
Qinetiq		chest / shirt			y	y	y	y	
SenseCore	SensePro	chest / shirt	>$1000		y	y	y	y	
Smartex	Wearable Wellness System (WWS)	chest / shirt	TBD	19 hrs.	y	y		y	
SmartLife	HealthVest	chest / shirt			y	y	y		
CSEM	PULSEAR	ear			y				
iriver	ON!	ear	$199		y				
Jabra	Sport Pulse Wireless earphones	ear	$57-$100	240 hrs. standby	?				

LG	HR Earphones	ear	$179.99	4 hrs.	y			y	
Zinc Software	Zen	earlobe		8 hrs.	y				
Withings	PulseO2	fingertip (non continuous)			y				Pulse Ox
Zensorium	Tinke	fingertip (non continuous)			y				
Impact Sports	Epulse 2	forearm	$83.50	6.5 hrs.	y				
Scosche	Rhythm Plus	forearm	$79.99	8 hrs.	y				
Advanced Body Sensing		forehead			y				
Life-Beam	bike helmet, cap	forehead	$229, $99		y			y	
Spree Sports	SmartCap, headband	forehead	$199	8 hrs.	y		y	y	GPS
Breath Research	All-in-One	headset			y	y			Barometer
Adidas	FitSmart	wrist	$199	5 days	y			y	
Adidas	Smart Run Watch	wrist	$400	4-8 hrs.	y			y	GPS
Amiigo	Amiigo wristband	wrist	$179	3 days	y		y	y	SpO2
Angel	Angel	wrist	$159	7 days	y		y	y	SpO2
Apple	Apple Watch	wrist	$349	<1 day	y			y	
Basis	B1	wrist	$149.99	4 days	y		y	y	Sweat
Basis	Peak	wrist	$199.99	4 days	y		y	y	Sweat
Empatica	E3	wrist	$1,000		y		y	y	Skin Conductance
Fitbit	Charge HR	wrist	$220?		y			y	
Fitbit	Surge	wrist	$250		y			y	GPS
Healbe	GoBE	wrist	$299	3 days	y			y	Impedance
HealthStats	BPro	wrist	?	24 hrs.	y				Blood Pressure
MC10		wrist			y			y	

Mio	Alpha	wrist	$198.99	8-10 hrs.	y				
Mio	Link	wrist	$99	8-10 hrs.	y				
Omron	HR-500U	wrist	$149.99		y			y	
Oxitone	Oxitone Watch	wrist			y	y			SpO2, Blood Flow
Samsung	Gear Fit	wrist	$149.00	2-3 days	y			y	Gyroscope
Samsung	SimBand	wrist			y		y		Blood Flow, Blood Pressure, SpO2, CO2
Raytheon	Mednet				y				
Apple	Watch	wrist	$349	?	y			y	
Microsoft	Band	wrist	$199	48 hrs.	y		y	y	Gyroscope, Skin Conductance, UV, Ambient Light

Appendix B: Policy Function for Field Study Simulation

The figures show the policy for 5 minute increments of time, and provide a movement speed for an estimated TWSI and distance completed on the task.

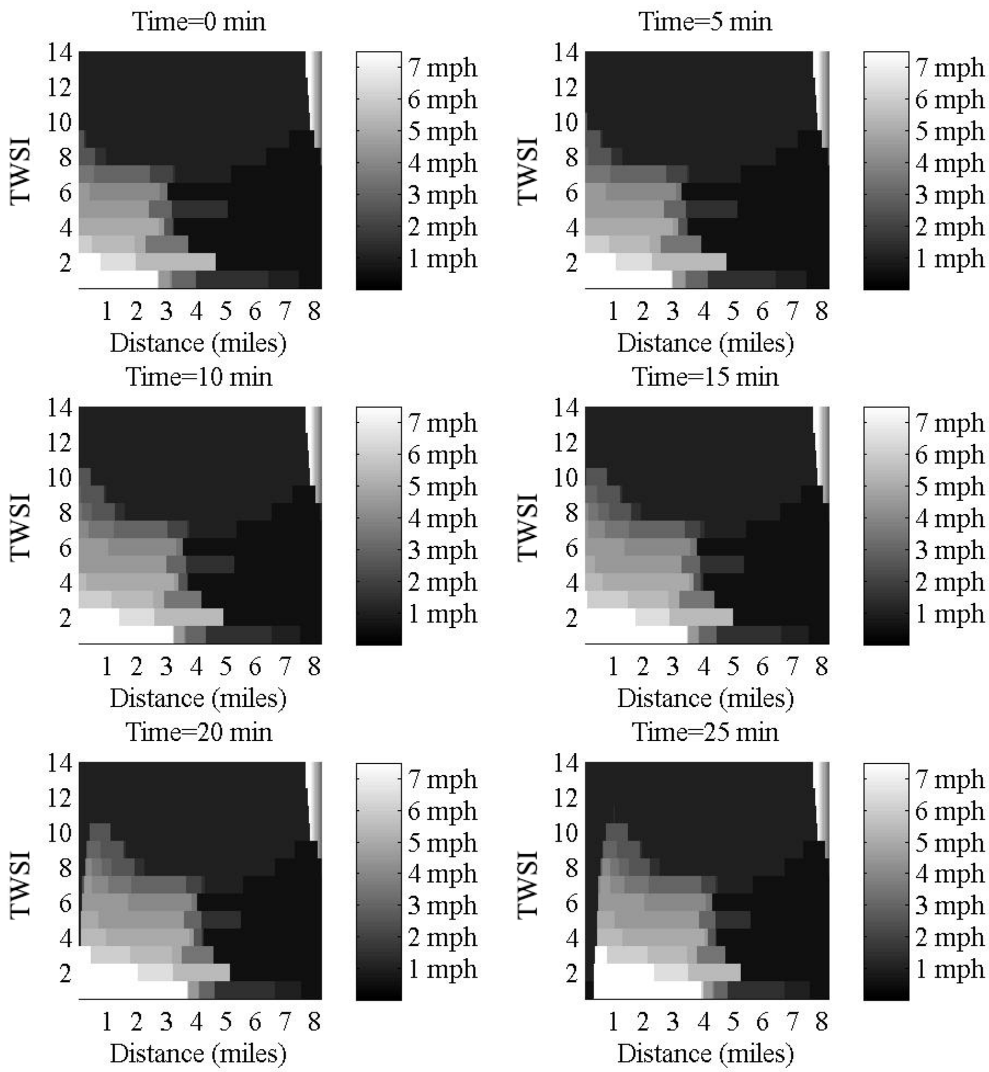

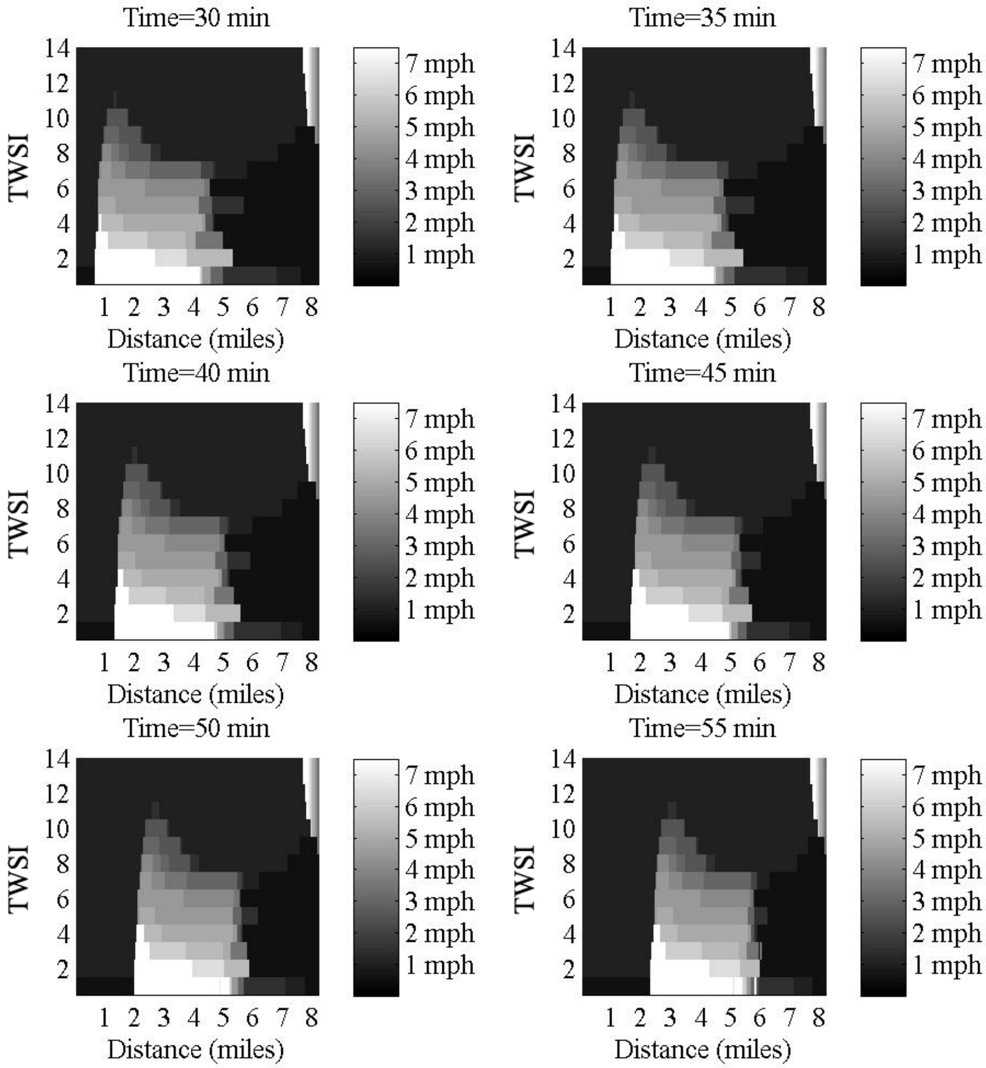
Time=30 min
Time=35 min
Time=40 min
Time=45 min
Time=50 min
Time=55 min
TWSI
Distance (miles)
7 mph
6 mph
5 mph
4 mph
3 mph
2 mph
1 mph

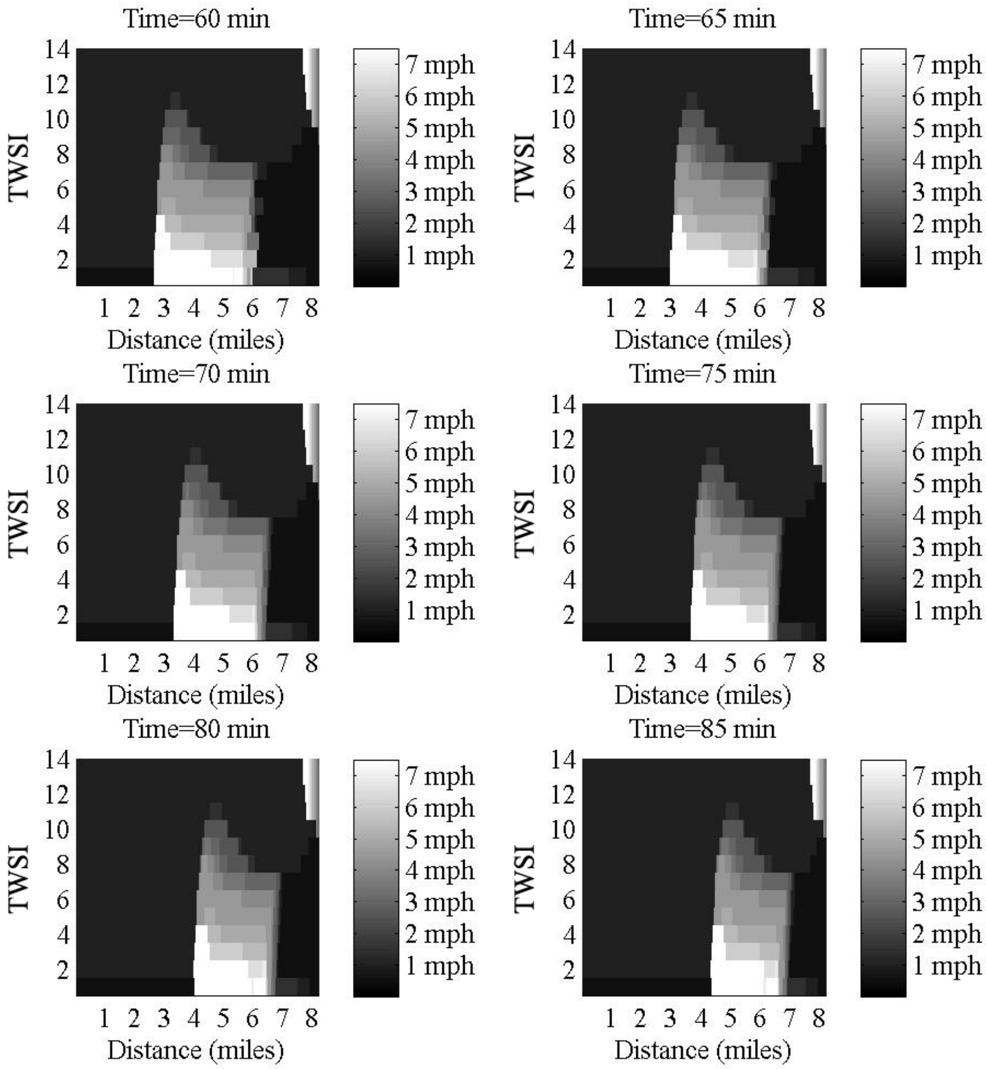
Time=60 min
Time=65 min
Time=70 min
Time=75 min
Time=80 min
Time=85 min
TWSI
Distance (miles)
7 mph
6 mph
5 mph
4 mph
3 mph
2 mph
1 mph

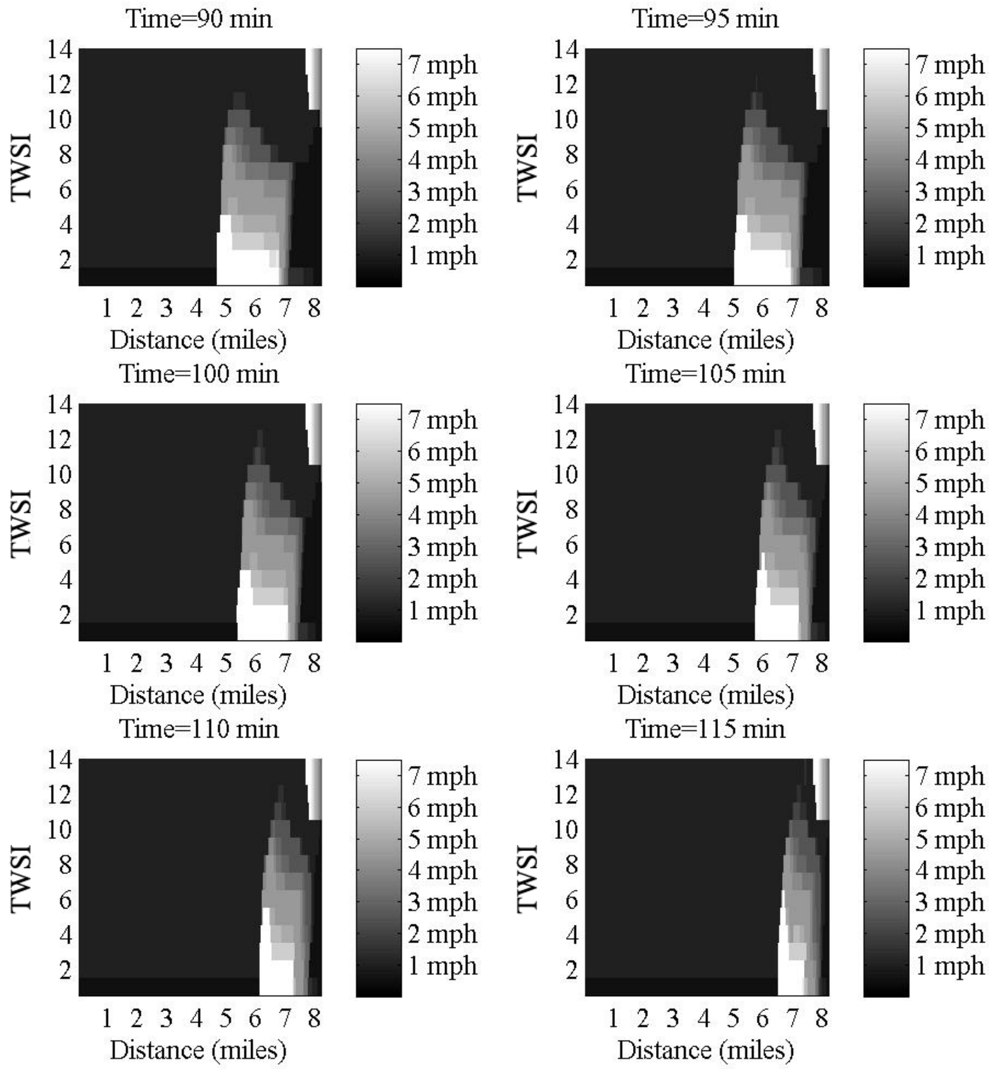
Time=90 min
Time=95 min
Time=100 min
Time=105 min
Time=110 min
Time=115 min
TWSI
14
12
10
8
6
4
2
1 2 3 4 5 6 7 8
Distance (miles)
7 mph
6 mph
5 mph
4 mph
3 mph
2 mph
1 mph

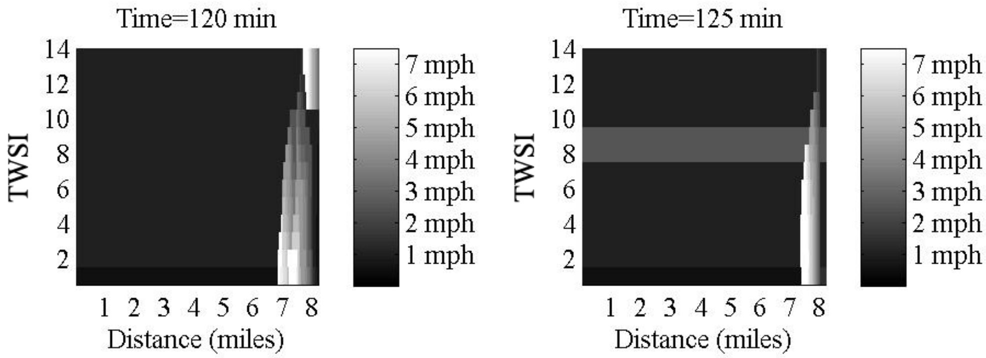
Time=120 min
14
12
10
8
6
4
2
TWSI
1 2 3 4 5 6 7 8
Distance (miles)
7 mph
6 mph
5 mph
4 mph
3 mph
2 mph
1 mph
Time=125 min
14
12
10
8
6
4
2
TWSI
1 2 3 4 5 6 7 8
Distance (miles)
7 mph
6 mph
5 mph
4 mph
3 mph
2 mph
1 mph

Appendix C: Policy Function for Laboratory Study

The figures show the policy for 2 minute increments of time, and provide a movement speed for an estimated TWSI and distance completed on the task.

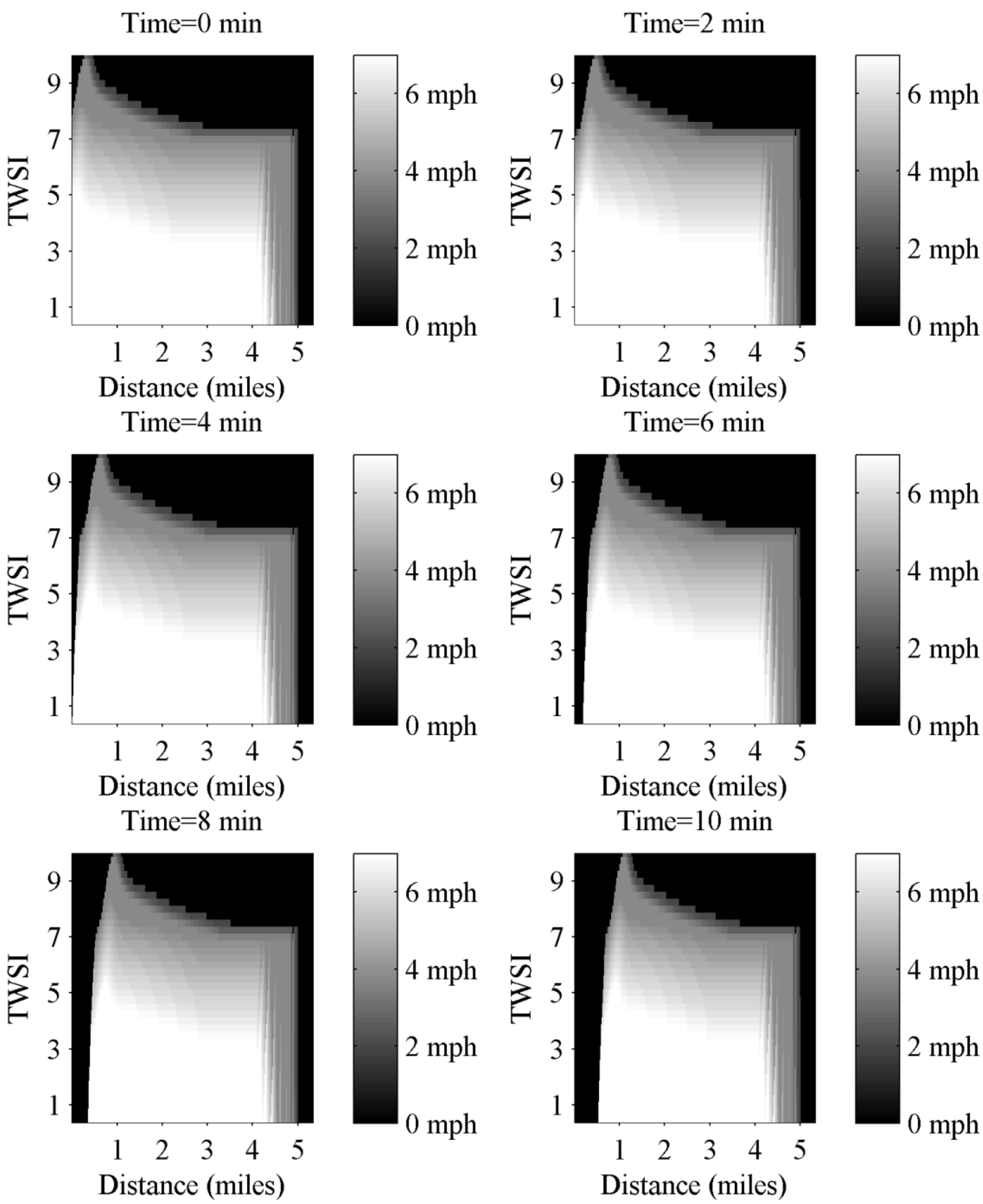

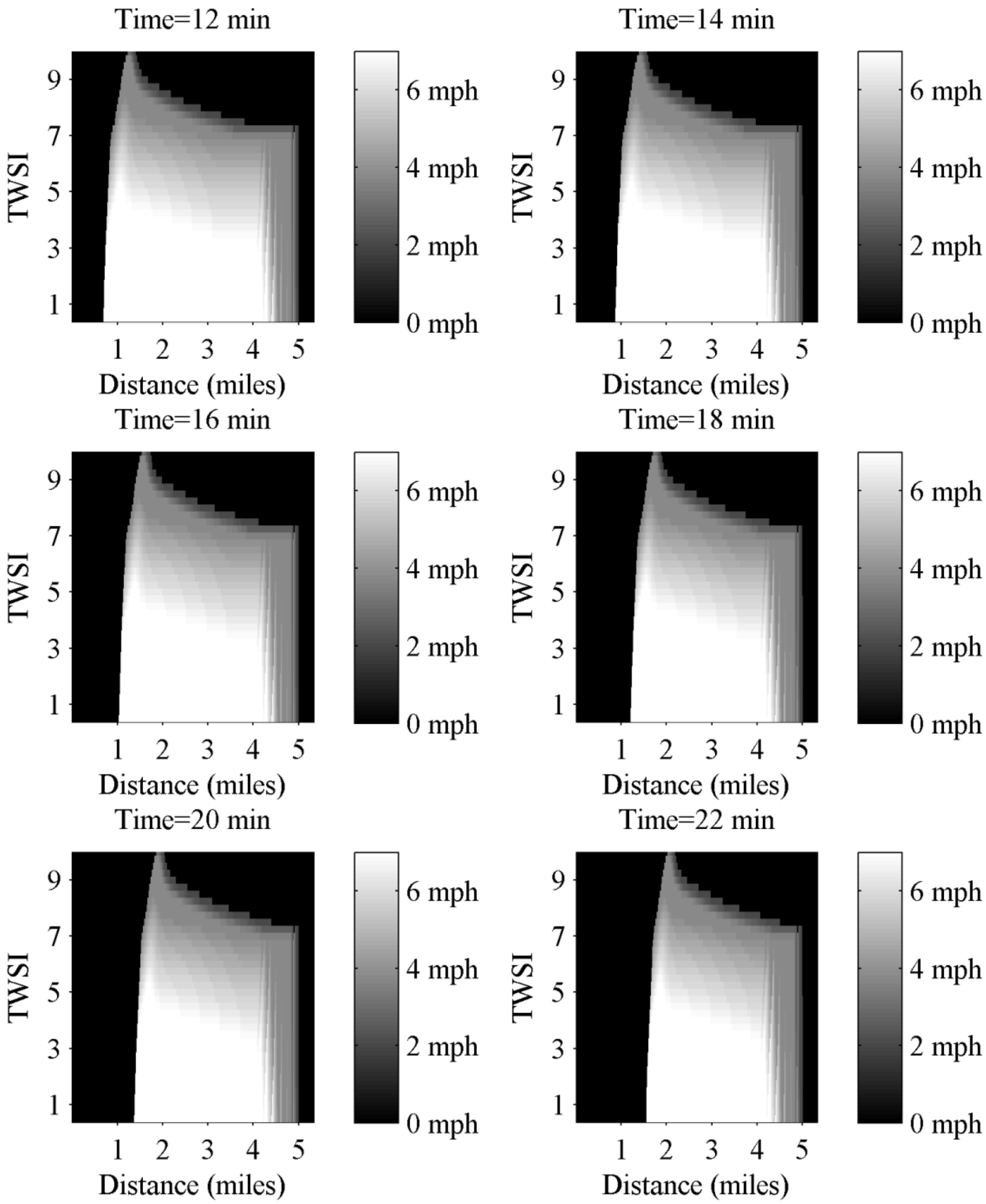
Time=12 min
Time=14 min
Time=16 min
Time=18 min
Time=20 min
Time=22 min
TWSI
Distance (miles)
0 mph
2 mph
4 mph
6 mph

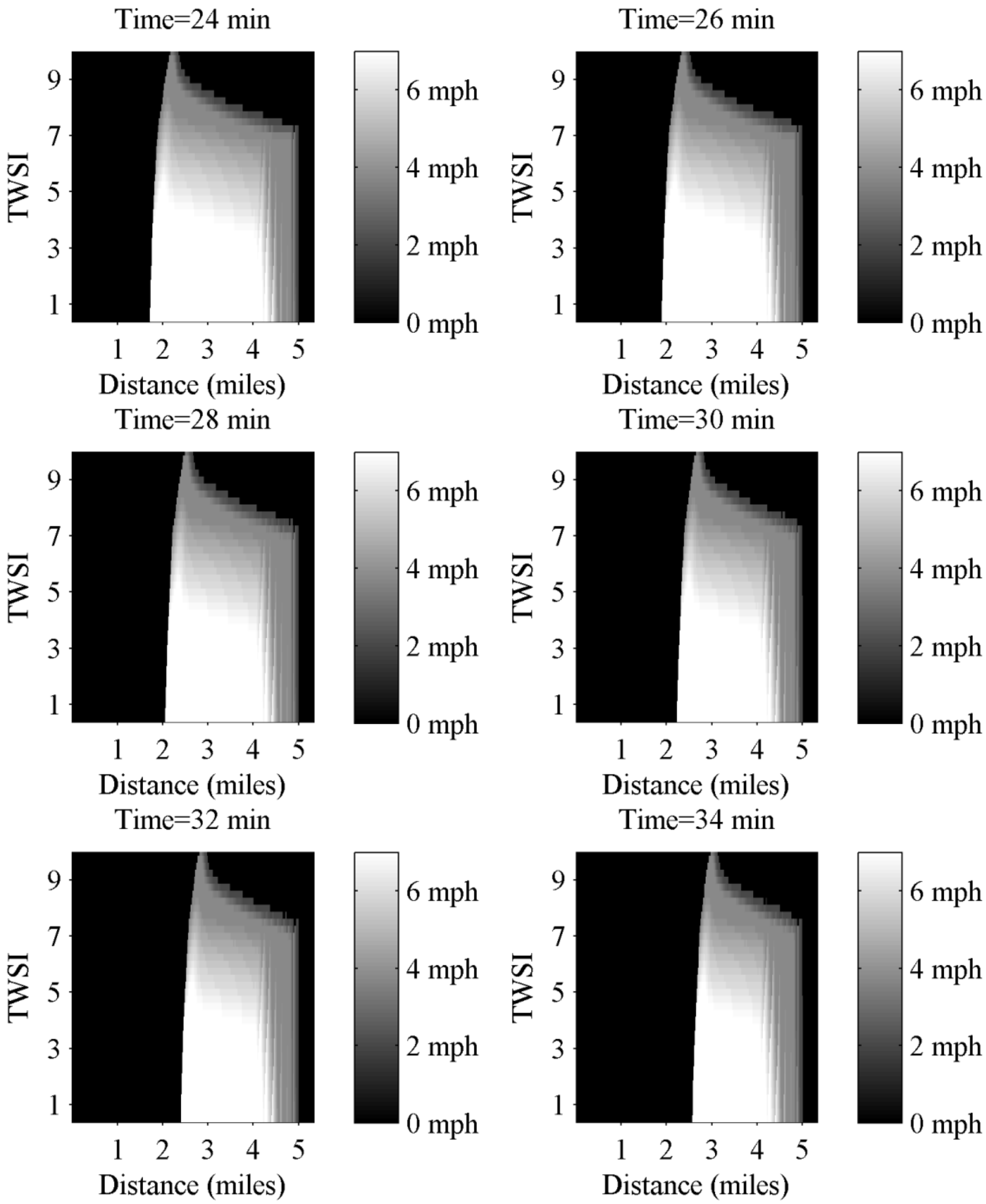
Time=24 min
Time=26 min
Time=28 min
Time=30 min
Time=32 min
Time=34 min
TWSI
Distance (miles)
0 mph
2 mph
4 mph
6 mph

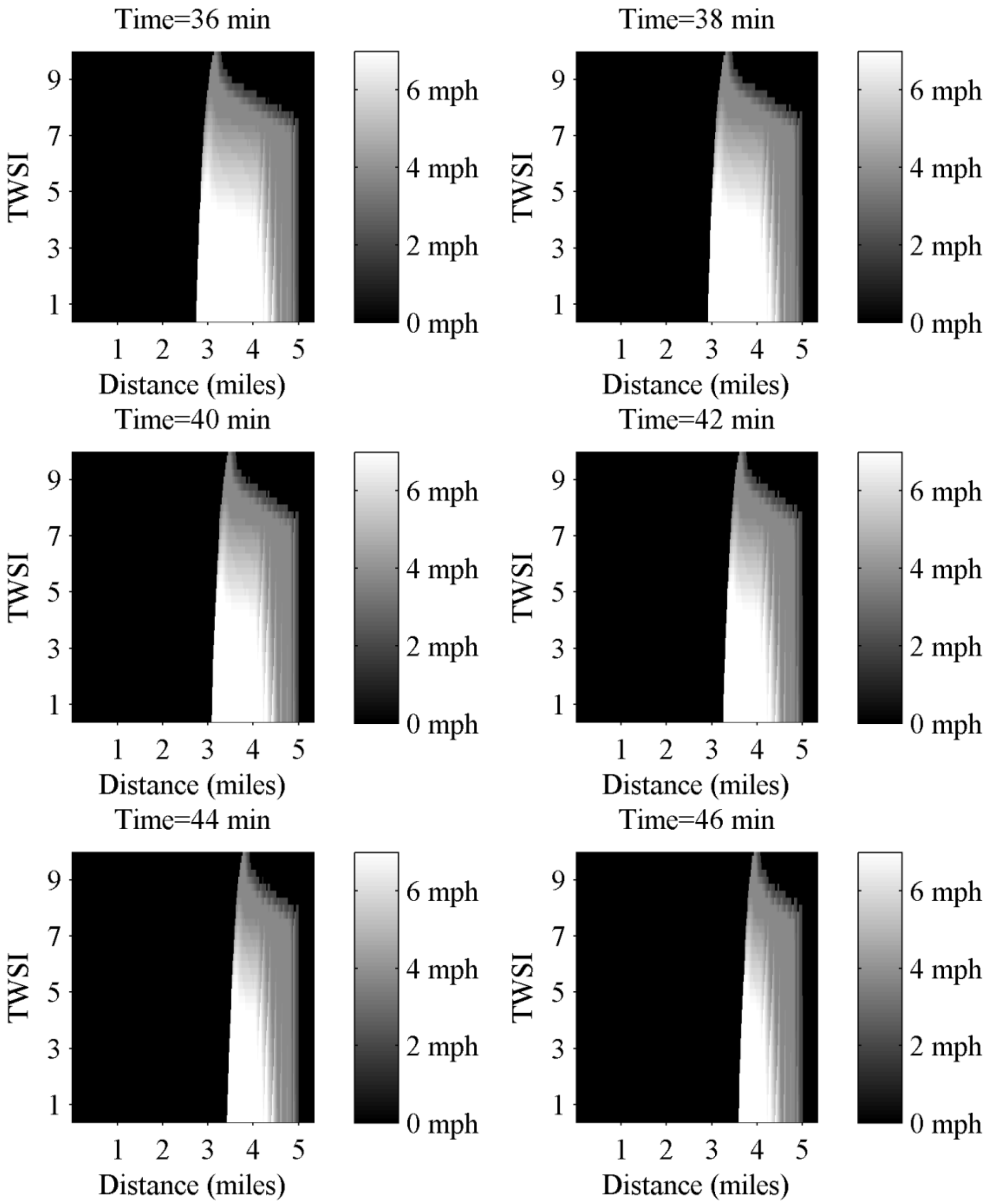
Time=36 min
Time=38 min
Time=40 min
Time=42 min
Time=44 min
Time=46 min
TWSI
Distance (miles)
0 mph
2 mph
4 mph
6 mph

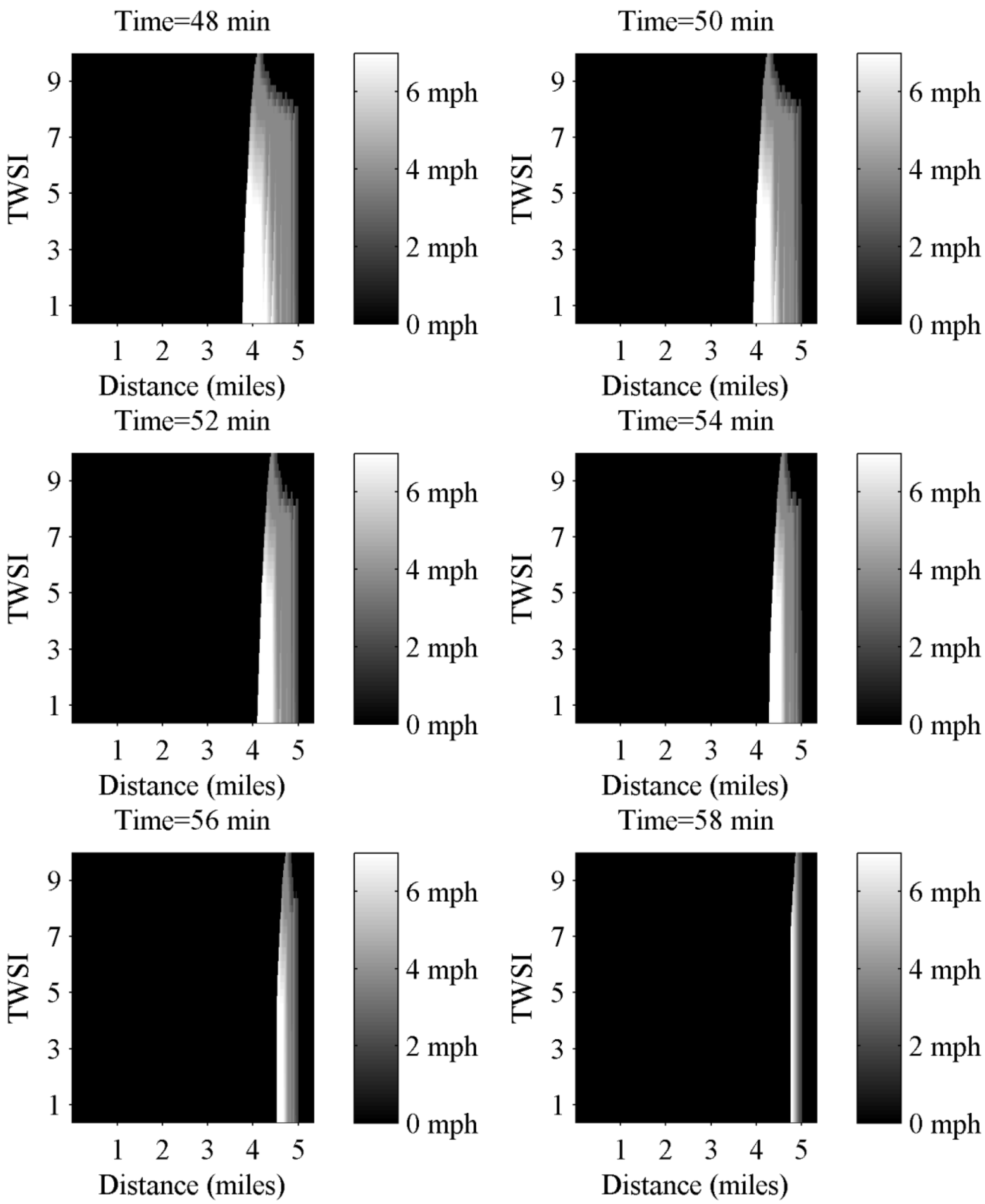
Time=48 min
Time=50 min
Time=52 min
Time=54 min
Time=56 min
Time=58 min
TWSI
Distance (miles)
0 mph
2 mph
4 mph
6 mph